Physical Insight into Novel Lipid Corona Formation and Its Impact on the Interaction with Protein

Ph.D. Thesis

By

AVIJIT MAITY

DEPARTMENT OF CHEMISTRY

INDIAN INSTITUTE OF TECHNOLOGY INDORE

January 2025

Physical Insight into Novel Lipid Corona Formation and Its Impact on the Interaction with Protein

A THESIS

Submitted in partial fulfillment of the
requirements for the award of the degree
of
DOCTOR OF PHILOSOPHY

by
AVIJIT MAITY

DEPARTMENT OF CHEMISTRY
INDIAN INSTITUTE OF TECHNOLOGY INDORE
January 2025

INDIAN INSTITUTE OF TECHNOLOGY INDORE

I hereby certify that the work which is being presented in the thesis entitled **Physical Insight into Novel Lipid Corona Formation and Its Impact on the Interaction with Protein** in the partial fulfillment of the requirements for the award of the degree of **DOCTOR OF PHILOSOPHY** and submitted in the **DEPARTMENT OF CHEMISTRY, Indian Institute of Technology Indore**, is an authentic record of my own work carried out during the time period from **July 2019** to **January 2025** under the supervision of **Prof. ANJAN CHAKRABORTY**, Professor, Department of Chemistry, Indian Institute of Technology Indore.

The matter presented in this thesis has not been submitted by me for the award of any other degree of this or any other institute.

Avijit Maity

AVIJIT MAITY

This is to certify that the above statement made by the candidate is correct to the best of my knowledge.

A Chakraborty

Prof. ANJAN CHAKRABORTY

AVIJIT MAITY has successfully given his Ph.D. Oral Examination held on **16th May, 2025**.

A Chakraborty

Prof. ANJAN CHAKRABORTY

ACKNOWLEDGEMENTS

I sincerely thank all the individuals whose guidance, encouragement, and valuable contributions made this thesis possible. It has been a privilege to receive their support throughout this work.

I would like to express my deepest gratitude to my supervisor, Professor Anjan Chakraborty, for his unwavering support, invaluable guidance, and constant encouragement throughout the course of my thesis work. His extensive knowledge, expertise, and insightful advice have been instrumental in shaping my research and bringing it to completion. His enthusiasm and ideologies have served as a continuous source of inspiration, helping me navigate the challenges of my Ph.D. journey with greater confidence and efficiency. I am especially grateful for his steadfast support during difficult times, which has been invaluable to me. I will always remain indebted to him for his motivation, moral support, and mentorship.

I am thankful to my PSPC members, Prof. Sanjay Kumar Singh and Prof. Tushar Kanti Mukherjee, for their invaluable suggestions and guidance. Their feedback has been helpful in shaping this work. I extend my heartfelt thanks to Professor Suhas Joshi, Director of IIT Indore, and all the faculty members of the Department of Chemistry for their valuable insights and support throughout my thesis journey. I am also grateful to the Sophisticated Instrument Centre (SIC) at IIT Indore for providing access to the necessary research equipment and facilities.

I sincerely extend my heartfelt gratitude to Dr. Ravinder Kumar, Mr. Kinny Pandey, Mr. Ghanshyam Bhavsar, Mr. Tapesh Parihar, Mr. Rahul Shrivas, Mr. Manish Kushwaha, Mrs. Vinita Kothari, Mr. Rameshwar Dohare, Mr. Shouvik Devnath, and Mr. P. K. Parthiban for their invaluable technical support, which was essential for the continuation of my work. Additionally, I would like to acknowledge all the technical and non-technical staff of IIT

Indore for their invaluable assistance and dedicated service throughout this journey.

I sincerely thank Dr. Tridib K. Sarma and his group members for their generous cooperation and support during the DLS experiments. I am also deeply grateful to Prof. Hwankyu Lee for his valuable contributions to the simulation studies in my thesis work. My heartfelt gratitude goes to all my school and college teachers for their years of guidance and teaching, which played a crucial role in helping me reach this stage of my Ph.D. journey. I would like to specifically acknowledge Prof. Tapan Kumar Mandal, Dr. Sankar De, Mr. Chandan Achar, Mr. Samaresh Choudhury, Mr. Subrata Dhara, Mr. Samaresh Hait, Mr. Nimai Hait, Mr. Dipak Kumar Maity, and Mr. Ashutosh Jana for their invaluable influence on my academic growth.

I am thankful to USIEF for awarding me the Fulbright-Nehru Doctoral Fellowship, which allowed me to conduct research in the USA as part of my PhD journey. I am deeply grateful to Prof. Vincent M. Rotello for graciously hosting me in his lab and providing the necessary resources for my research. My heartfelt thanks go to Dr. William Ndugire, Dr. Aarohi Gupta, Mr. Soham Chakraborty, and all the members of the Rotello group for their warm support, constant encouragement, and selfless cooperation during my time in the lab.

I would like to express my gratitude to all the lab members, who are the pillars of our laboratory. I am especially thankful to my seniors, Dr. Soumya Kanti De, Dr. Nishu Kanwa, and Dr. Anupam Das, for their unwavering guidance, support, encouragement, and best wishes. I also extend my heartfelt appreciation to my colleagues, Dr. Debanjan Bagchi, Mr. Saikat Sinha, Mr. Sachin Debnath, Mr. Abhinav Prasad, Ms. Priyanka Nath, Ms. Huma Tabassum, Ms. Kavana M, Ms. Puja Kumari, Mr. Suman Kumar Choudhury, Mr. Naveen Kumar, and Ms. Sheetal Leva, for their selfless cooperation and invaluable assistance in making my work successful.

Additionally, I would like to thank all my fellow researchers at IIT Indore for their support.

Friends are the ones who bring a smile to your face on difficult days and always believe in your potential. I feel incredibly fortunate to have such wonderful people in my life, without whom this journey would have been incomplete. I would like to express my gratitude to Dr. Tapas, Dr. Rishi, Dr. Soumitra, Dr. Sayan, Dr. Mithun, Dr. Sourav, Dr. Argha, Dr. Sayantan, Dr. Amitabha, Dr. Shyama, Dr. Surya, Dr. Bidyut, Dr. Agnideep, Dr. Neha, Dr. Daisy, Dr. Abhiram, Dr. Biju, Dr. Siddarth, Mirajuddin, Dr. Diptendu, Souvik, Dr. Shivendra, Nirmiti, Achena, Aditya, Ravindra, Suryakamal, Tarun, Sagnik, Subha, Anjali, Dondinath, Anika, Tanaya, Subhankar, and Mithu for their encouragement and friendship. A special thanks to Mr. Debanjan Bagchi, Ms. Vidhi Agarwal, and Ms. Amrita Chakraborty for their unwavering support and good wishes in both my personal and professional life.

I would like to express my deepest gratitude to my friends, Mr. Subhadip Maity, Ms. Banashri Dey Mondal, Mr. Kanchan Hait, Mr. Subhankar Dutta, Mr. Rintu Bhowmik, Mr. Dhiman Maity, Mr. Manoj Jana, and Mr. Shibsankar Si, who have stood by my side since childhood and supported me through all the ups and downs of my personal and professional life. I am also sincerely thankful to Ms. Payel Rana for her unwavering belief in me and for helping me grow stronger with each passing day.

Last, but not least, I would finally and with all my heart thank my father, Mr. Asish Maity, and my mother, Mrs. Gitanjali Maity, for their unwavering hard work, selfless love, and unconditional support, which have shaped me into who I am today. I am deeply thankful to my brother, Mr. Arijit Maity, for his constant belief in me, his support, and the endless love he has shown me. I also extend my gratitude to everyone mentioned here and to those whose names I may have unintentionally omitted.

AVIJIT MAITY

Dedicated to My Family, Friends, and Teachers

SYNOPSIS

The coating of proteins and lipids around nanoparticle surfaces is known as the “protein corona” and “lipid corona” respectively. While protein corona formation is well-studied *[1,2]*, the mechanism and stability of lipid corona formation are less understood and have recently attracted attention in nanoscience. Although some studies emphasize the role of electrostatic forces between nanoparticles (NPs) and lipid vesicles in lipid corona formation *[3,4]*, little is known about the specific roles of physicochemical properties of NPs and lipids that influence this process. This thesis uses aromatic amino acid-functionalized NPs as model systems to interact with lipid vesicles based on following the hypothesis. In some virus particles, the capsid, made of protein, encases the viral genome (either DNA or RNA) with lipid membrane wrapping. Given that amino acids are the building blocks of proteins, it is plausible to hypothesize that amino acids could self-assemble on the surface of NPs and potentially attract lipid molecules from membranes to form a lipid coating, or "lipid corona”. The thesis provides a detailed exploration of lipid corona formation, focusing on the influence of lipid (charge, concentration, phase state, chain length, hydrophobicity, and head group area) and NPs properties (surface charge, surface ligands functionalization, and metallic core). Our findings reveal the formation mechanism of lipid corona for the development of potentially smart NPs for various biomedical applications due to their unusual stability against external stimuli. Additionally, we examine how protein molecules interact with different lipid-coated NPs.

Summary of the Thesis Work

The contents of each chapter included in the thesis are discussed as follows:

<u>Chapter 1.</u> Introduction and General Background

This chapter briefly introduces nanoparticle classifications, their applications, limitations, and various model membrane systems that mimic

cellular membranes. It also covers the physicochemical properties of lipid vesicles and explores nanoparticle interactions with lipid vesicles and proteins. Finally, we discuss the motivation and main aim of the research presented in the thesis.

<u>Chapter 2.</u> Interaction of Aromatic Amino Acid-Functionalized Gold Nanoparticles with Lipid Bilayers: Insight into the Emergence of Novel Lipid Corona Formation

This chapter describes the interaction of aromatic amino acid-functionalized gold nanoparticles (Au-AA NPs) with lipid vesicles and the formation of a lipid corona using spectroscopic (steady-state UV-visible and fluorescence) and imaging techniques (CLSM, HR-TEM, and AFM). Different aromatic amino acids (namely phenylalanine, tyrosine, and tryptophan) functionalized gold nanoparticles are synthesized by an *in situ* method where the amino acids act as both reducing and stabilizing agents. Amino acids were selected as ligands for AuNPs because they improve the biocompatibility of the capped nanoparticles and help address key challenges in biomedical applications.The charge and concentration of lipid molecules are varied to understand the nature of the interaction between nanoparticles and lipid vesicles. Our study demonstrates that in the presence of high lipid concentration, Au-AA NPs intrinsically tow the lipid molecules from the lipid vesicles and decorate themselves by lipid molecules leading to unique lipid corona formation. The lipid corona formation is attributed to the strong electrostatic interaction between the Au-AA NPs and lipid bilayer. In contrast, at low lipid concentration, Au-AA NPs undergo lipid-induced aggregation. Lipid-nanoparticle interaction is found to be a time-dependent phenomenon and depends on the surface charge of both the lipid and Au-AA NPs. Our results indicate that the partial lipid coating is an intermediate step of lipid-induced aggregation and lipid corona formation of the Au-AA NPs (**Figure 1**). Significantly, we found that the colloidal property of these lipid-coated nanoparticles (lipid corona) is able to resist extremely harsh conditions e.g. high acidic pH, several repetitive freeze-

thaw cycles, and high salt concentration. The increased stability of Au-AA NPs with a lipid corona presents opportunities to design robust nanomaterials with potential biomedical applications.

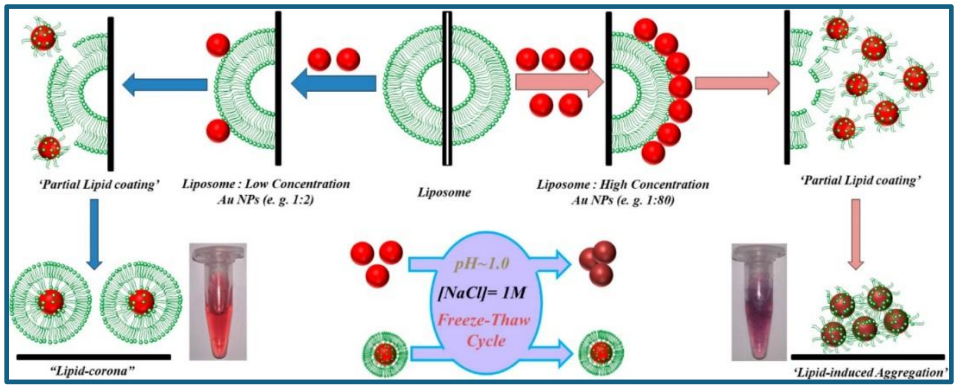

Figure 1. Schematic representation of lipid-induced aggregation and formation of a "stable lipid corona" of the Au-AA NPs through the "partial lipid coating" on the Au-AA NPs surface. Stability of the native Au NPs and lipid-coated Au NPs against external stimuli. Schematics are not drawn to scale.

<u>Chapter 3.</u> Mechanistic Pathway of Lipid Phase-Dependent Lipid Corona Formation on Phenylalanine-Functionalized Gold Nanoparticles: A Combined Experimental and Molecular Dynamics Simulation Study

This chapter examines how lipid properties, including phase state and head group area, influence lipid corona formation and lipid-induced aggregation of phenylalanine-functionalized gold nanoparticles (Au-Phe NPs) at varying lipid concentrations in different media. The zwitterionic lipid vesicles of different phase transition temperatures, namely DOPC (T_m = -20 °C), DLPC (T_m = -1 °C), DMPC (T_m = 23 °C), and DPPC (T_m = 41 °C), are chosen to see the interaction with Au-Phe NPs. Complementing spectroscopic and imaging techniques, coarse-grained molecular dynamics (CGMD) simulations are used to gain molecular insights into lipid-NPs interactions. The study shows that a lipid corona forms at high lipid concentrations for all lipid types, regardless of phase state or head group

area. CGMD simulations reveal that more DPPC molecules are required to form a lipid corona compared to DOPC as DPPC has a smaller head group area than that of DOPC. Lipid phase state, head group area, and buffer medium are crucial in lipid-induced aggregation behavior of Au-Phe NPs. The NPs are found to undergo aggregation at low concentrations of DPPC (ordered state) but remain stable at low DOPC concentrations (liquid-crystalline state). At low lipid concentrations, DOPC forms a complete lipid corona around one individual Au-Phe NPs, while DPPC forms a partial coating around all Au-Phe NPs, leading to aggregation (**Figure 2**). Interestingly, despite their differing phase-transition temperatures, both DLPC and DMPC induce aggregation of Au-Phe NPs at low concentrations of lipid due to their similar head group areas at room temperature. DPPC-coated Au-Phe NPs are found to exhibit more stability than DOPC-coated ones in the freeze-thaw cycles. Based on stability, for the first time, we categorize lipid coronas as "hard lipid corona" and "soft lipid corona".

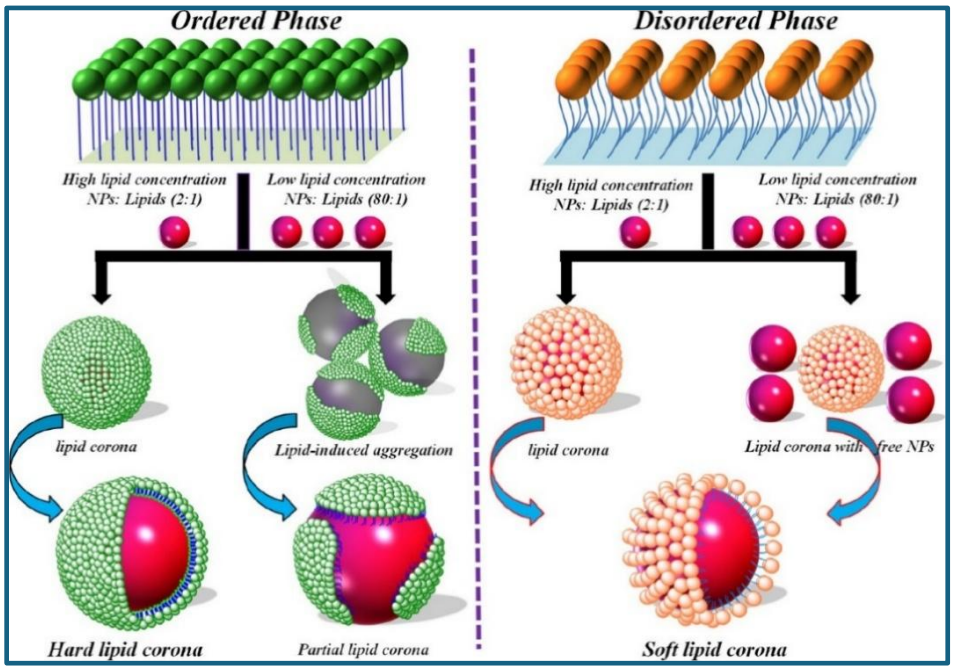

Figure 2. Schematic representation of lipid corona formation and lipid-induced aggregation of Au-Phe NPs at two different concentrations and phase states of the lipid bilayer (ordered and disordered).

<u>Chapter 4.</u> Formation of Lipid Corona on Ag Nanoparticles and Its Impact on Ag^+ Ion Dissolution and Aggregation of Ag Nanoparticles Against External Stimuli

This chapter investigates how the metallic core and surface ligands affect lipid corona formation. For this, tyrosine and tryptophan-functionalized silver nanoparticles (Ag-Tyr and Ag-Trp NPs) are synthesized and then allowed to interact with lipid vesicles of varying surface charges and phase states. We also examine how different zwitterionic and positively charged lipid-coated Ag-Tyr and Ag-Trp NPs resist aggregation of NPs and Ag^+ ion dissolution under external stimuli, including acidic pH, high NaCl concentration, and freeze-thaw cycles. Our results show that lipid corona formation and lipid-induced aggregation mainly depend on surface ligands, regardless of the metallic core. Both gold and silver nanoparticles functionalized with aromatic amino acids interact with lipid vesicles in a similar fashion. The lipid corona significantly imparts the stability of Ag-Tyr and Ag-Trp NPs against external stimuli compared to native Ag NPs (**Figure 3**).

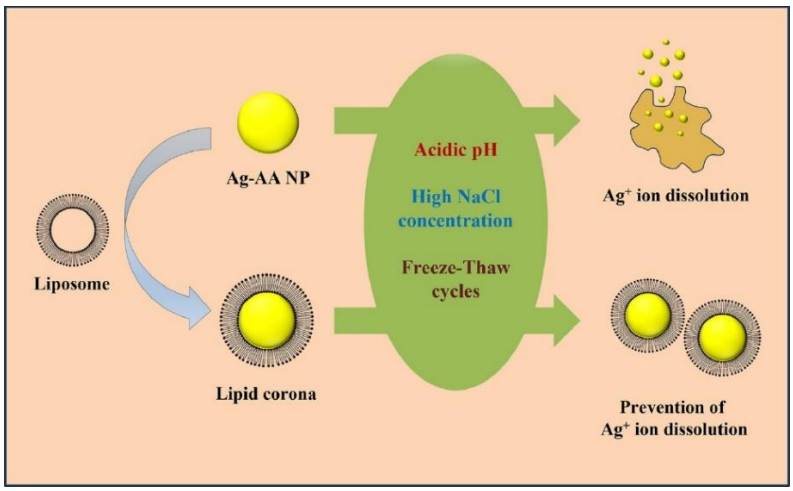

Figure 3. Schematic representation of the stability of the native Ag-AA NPs and lipid-coated Ag-AA NPs against different external stimuli.

Over time, zwitterionic lipid coatings on Ag NPs more effectively prevent aggregation and Ag^+ ion dissolution than positively charged lipid coatings.

The DOPC lipid coated Ag-Tyr NPs is superior to all other lipid coated NPs (Ag-Tyr and Ag-Trp). These findings offer valuable insights for engineering suitable lipid-coated nanoparticles for various biomedical and commercial applications.

<u>Chapter 5.</u> Insight into the Lysozyme-Induced Aggregation of Aromatic Amino Acid-Functionalized Gold Nanoparticles: Impact of the Protein Binding and Lipid Corona on the Aggregation Phenomena

This chapter explores how the bare and lipid coated aromatic amino acids functionalized gold nanoparticles interact with the oppositely charged globular protein in order to understand the impact of lipid corona formation on protein induced nanoparticle aggregation. The aggregation of negatively charged aromatic amino acid (phenylalanine and tyrosine)-functionalized gold nanoparticles (Au-AA NPs) in the presence of positively charged lysozyme protein at different protein concentrations is first investigated and the results are compared with those of conventional citrate-functionalized Au NPs (Au-Cit NPs). Our results reveal distinct aggregation mechanisms for Au-AA NPs at low and high protein concentrations (**Figure 4**).

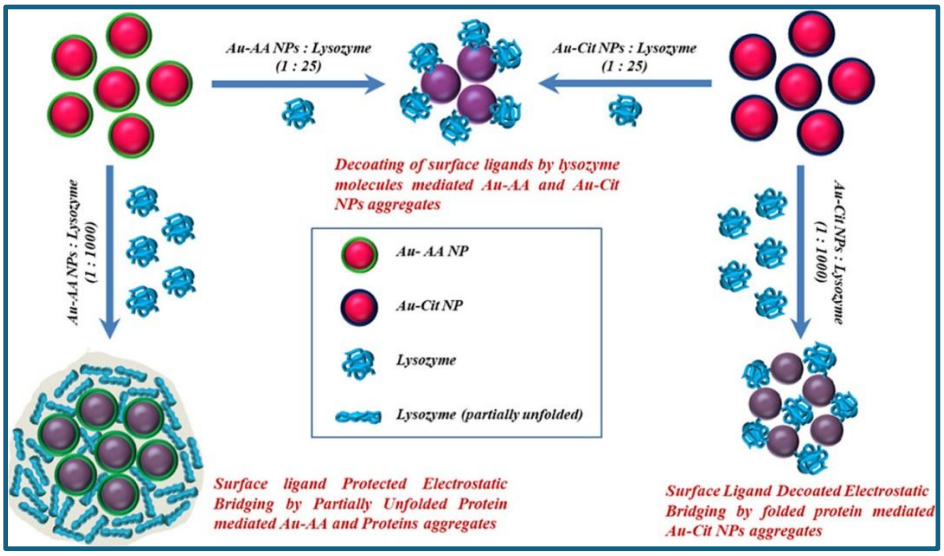

Figure 4. Schematic representation of lysozyme protein-concentration dependent Au-AA and Au-Cit NPs aggregation.

Furthermore, different lipids and proteins bound to the surface of Au-AA NPs have been found to inhibit lysozyme-induced aggregation of the Au-AA NPs. Human serum albumin (HSA) and bovine serum albumin (BSA) are bound to the surfaces of Au-AA and Au-Cit NPs through physisorption. Human serum albumin (HSA)-bound Au-AA and Au-Cit NPs more effectively prevent lysozyme-induced aggregation than bovine serum albumin (BSA)-bound Au-AA and Au-Cit NPs. For the first time, the significant roles of "hard" and "soft" lipid coronas in the aggregation of phenylalanine-functionalized Au NPs in the presence of lysozyme are discussed.

Chapter 6. Materials, Methods, and Instrumentation

In this chapter, the materials used in the thesis works, various protocols regarding the nanoparticle's synthesis, lipid vesicle preparation, nanoparticles/lipid mixture formation, nanoparticles/protein mixture formation and characterization techniques that were used throughout the thesis have been discussed in detail.

Chapter 7. Conclusion and Future Outlook

This thesis provides detailed investigations to the mechanisms of lipid corona formation around aromatic amino acid-functionalized nanoparticles (NPs) and lipid-induced NPs aggregation. It examines how lipid properties (charge, concentration, phase state, chain length, hydrophobicity, and head group area) and NPs properties (surface charge, ligands, and metallic core) influence these interactions. The stability of various lipid-coated NPs under different external conditions and their interactions with proteins are also explored.

As a future prospect, quantifying and understanding the mechanism of cellular uptake of these lipid-coated NPs could guide nano-researchers toward using these robust NPs in catalysis, drug delivery, and photothermal therapy within cellular environments.

References

[1] Wheeler K. E., Chetwynd A. J., Fahy K. M. *et al.* (2021), Environmental Dimensions of the Protein Corona, Nat. Nanotechnol. 16, 617-629 (DOI: 10.1038/s41565-021-00924-1)

[2] Mahmoudi M., Landry M. P., Moore A. *et al.* (2023), The Protein Corona from Nanomedicine to Environmental Science, Nat. Rev. Mater. 8, 422-438 (DOI: 10.1038/s41578-023-00552-2)

[3] Olenick L. L., Troiano J. M., Vartanian A. *et al.* (2018), Lipid Corona Formation from Nanoparticle Interactions with Bilayers, Chem 4, 2709-2723 (DOI: 10.1016/j.chempr.2018.09.018)

[4] Zhang X., Pandiakumar A. K., Hamers R. J. *et al.* (2018), Quantification of Lipid Corona Formation on Colloidal Nanoparticles from Lipid Vesicles, Anal. Chem. 90, 14387-14394 (DOI: 10.1021/acs.analchem.8b03911)

LIST OF PUBLICATIONS

Thesis work:

1. **Avijit Maity**, Soumya Kanti De, Anjan Chakraborty, Interaction of Aromatic Amino Acid-Functionalized Gold Nanoparticles with Lipid Bilayers: Insight into the Emergence of Novel Lipid Corona Formation, J. Phys. Chem. B 2021, 125, 2113-2123 (DOI: 10.1021/acs.jpcb.0c10079) (Impact factor 2.8)

2. **Avijit Maity**, Soumya Kanti De, Debanjan Bagchi, Hwankyu Lee, Anjan Chakraborty, Mechanistic Pathway of Lipid Phase-Dependent Lipid Corona Formation on Phenylalanine-Functionalized Gold Nanoparticles: A Combined Experimental and Molecular Dynamics Simulation Study, J. Phys. Chem. B, 2022, 126, 11, 2241-2255 (DOI: 10.1021/acs.jpcb.2c00356) (Impact factor 2.8)

3. **Avijit Maity**, Priyanka Nath, Debanjan Bagchi, Sachin Debnath, Huma Tabassum, Saikat Sinha, Anjan Chakraborty, Formation of Lipid Corona on Ag Nanoparticles and Its Impact on Ag^{+} Ion Dissolution and Aggregation of Ag Nanoparticles Against External Stimuli, Chemical Physics Impact, 2024, 8, 100445 (DOI: 10.1016/j.chphi.2023.100445) (Impact factor 3.8)

4. **Avijit Maity**, Debanjan Bagchi, Soumya Kanti De, Anjan Chakraborty, Insight into the Lysozyme-Induced Aggregation of Aromatic Amino Acid-Functionalized Gold Nanoparticles: Impact of the Protein Conjugation and Lipid Corona on the Aggregation Phenomena, Langmuir 2023, 39, 14, 4881-4894 (DOI: 10.1021/acs.langmuir.2c03077) (Impact factor 3.7)

Other works:

1. **Avijit Maity**, Debanjan Bagchi, Huma Tabassum, Priyanka Nath, Saikat Sinha, Anjan Chakraborty, Diverse Role of Buffer Mediums and Protein Concentrations to Mediate the Multimodal Interaction of Phenylalanine-

Functionalized Gold Nanoparticle and Lysozyme Protein at Same Nominal pH, J. Phys. Chem. B, 2024, 128, 10625-10635 (DOI: 10.1021/acs.jpcb.4c05463) (Impact factor 2.8)

2. Debanjan Bagchi, **Avijit Maity**, Anjan Chakraborty, Metal Ion-Induced Unusual Stability of the Metastable Vesicle-like Intermediates Evolving during the Self-Assembly of Phenylalanine: Prominent Role of Surface Charge Inversion, J. Phys. Chem. Lett., 2024, 15, 4468-4476 (DOI: 10.1021/acs.jpclett.4c00444) (Impact factor 4.8)

3. Huma Tabassum, **Avijit Maity**, Krishna Singh, Debanjan Bagchi, Abhinav Prasad, Anjan Chakraborty, Effect of Lipid Corona on Phenylalanine-Functionalized Gold Nanoparticles to Develop Stable and Corona-Free Systems, Langmuir 2024, 40, 8, 4531-4543 (DOI: 10.1021/acs.langmuir.4c00019) (Impact factor 3.7)

4. Debanjan Bagchi, **Avijit Maity**, Soumya Kanti De, Anjan Chakraborty, Metal-Ion-Induced Evolution of Phenylalanine Self-Assembly: Structural Polymorphism of Novel Metastable Intermediates, J. Phys. Chem. Lett., 2022, 13, 10409-10417 (DOI: 10.1021/acs.jpclett.2c02882) (Impact factor 4.8)

5. Debanjan Bagchi, **Avijit Maity**, Soumya Kanti De, Anjan Chakraborty, Effect of Metal Ions on the Intrinsic Blue Fluorescence Property and Morphology of Aromatic Amino Acid Self-Assembly, J. Phys. Chem. B, 2021, 125, 12436-12445 (DOI: 10.1021/acs.jpcb.1c07392) (Impact factor 2.8)

6. Soumya Kanti De, **Avijit Maity**, Debanjan Bagchi, Anjan Chakraborty, Lipid phase dependent distinct emission behaviour of hydrophobic carbon dots: C-dot based membrane probes, Chem. Commun., 2021, 57, 9080-9083 (DOI: 10.1039/d1cc01941d) (Impact factor 4.9)

7. Soumya Kanti De, **Avijit Maity**, Anjan Chakraborty, Underlying Mechanisms for the Modulation of Self-Assembly and the Intrinsic Fluorescent Properties of Amino Acid-Functionalized Gold Nanoparticles, Langmuir 2021, 37, 5022-5033 ((DOI: 10.1021/acs.langmuir.1c00431) (Impact factor 3.7)

8. Nishu Kanwa, Soumya Kanti De, **Avijit Maity**, Anjan Chakraborty, Interaction of Aliphatic Amino Acids with Zwitterionic and Charged Lipid Membranes: Hydration and Dehydration Phenomena, Phys. Chem. Chem. Phys., 2020, 22, 3234-3244 (DOI: 10.1039/C9CP06188F) (Impact factor 2.9)

9. Debanjan Bagchi, **Avijit Maity**, Khushwant Saini, Huma Tabassum, Priyanka Nath, Sachin Vishwakarma, Anjan Chakraborty, Visual Monitoring of Biomolecular Self-Assembly Dynamics and Imaging of Protein Aggregates by Distinct Emission of a Unique Hydrophobic Carbon Dot. J. Phys. Chem. Lett., 2025, 16, 3501-3508 (DOI: 10.1021/acs.jpclett.5c00129) (Impact factor 4.8)

TABLE OF CONTENTS

LIST OF FIGURES

LIST OF SCHEMES

LIST OF TABLES

NOMENCLATURE

λ	Wavelength
μ	Micro
π	Pi
L	Liter
V	Volume
M	Molar
N_A	Avogadro's Number
λ	Wavelength
h	hours
%	Percentage
°C	Degree Celsius
ns	Nanosecond
fs	Femtosecond
nM	Nanomolar
mM	Millimolar
μM	Micromolar
mbar	Millibar
nm	Nanometer
μm	Micrometer

K	Kelvin
mL	Milliliter
μL	Microliter
mV	Millivolts
kV	Kilovolts
λ_{ex}	Excitation Wavelength
λ_{em}	Emission Wavelength
a. u.	Arbitrary Unit
min	Minutes
Hz	Hertz
RT	Room Temperature
rpm	Revolutions per minute
ε, σ	Lennard-Jones potential Parameters
T_m	Phase transition temperature
C	Carbon
pH	The negative logarithm of hydronium-ion concentration
pI	Isoelectric Point

ACRONYMS

NPs	Nanoparticles
Au NPs	Gold nanoparticles
Ag NPs	Silver nanoparticles
Au-AA NPs	Aromatic amino acid functionalized gold nanoparticles
Ag-AA NPs	Aromatic amino acid functionalized silver nanoparticles
Au-Phe NPs	Phenylalanine functionalized gold nanoparticles
Au-Tyr NPs	Tyrosine functionalized gold nanoparticles
Au-Trp NPs	Tryptophan functionalized gold nanoparticles
Au-Cit NPs	Citrate functionalized gold nanoparticles
Ag-Tyr NPs	Tyrosine functionalized silver nanoparticles
Ag-Trp NPs	Tryptophan functionalized silver nanoparticles
DOPC	1,2-dioleoyl-sn-glycero-3-phosphocholine
DLPC	1,2-dilauroyl-sn-glycero-3-phosphocholine
DMPC	1,2-dimyristoyl-snglycero-3-phosphocholine
DPPC	1,2-dipalmitoyl-sn-glycero-3-phosphocholine
DMPG	1,2-dimyristoyl-sn-glycero-3-phospho-(1′-rac-glycerol) (sodium salt)
DMTAP	1,2-dimyristoyl-3-trimethylammonium-propane (chloride salt)
Liss Rhod PE	1,2-dimyristoyl-sn-glycero-3-phosphoethanolamine-N-(lissamine rhodamine B sulfonyl) (ammonium salt)

BSA	Bovine Serum Albumin
HSA	Human Serum Albumin
Lyz	Lysozyme
GSH	Glutathione
Phe	Phenylalanine
Tyr	Tyrosine
Trp	Tryptophan
HEPES	4-(2-hydroxyetyl)-1-piperazineethanesulfonic acid
CLSM	Confocal laser scanning microscopy
TEM	Transmission electron microscopy
HR-TEM	High-resolution transmission electron microscopy
AFM	Atomic force microscopy
FESEM	Field Emission Scanning Electron Microscopy
CD	Circular Dichroism
DLS	Dynamic light scattering
SPR	Surface plasmon resonance
CGMD	Coarse-grained molecular dynamics
RDFs	Radial distribution functions
FWHM	Full width half-maximum

$AgNO_3$	Silver nitrate
NaCl	Sodium chloride
NaOH	Sodium hydroxide
O.D.	Optical density
PDI	Polydispersity index
ENPs	Engineered nanoparticles
FDA	Food and Drug Administration
LNPs	Lipid nanoparticles
NLCs	Nanostructured lipid carriers
LMs	Lipid monolayers
SLBs	Supported lipid bilayers
SUVs	Small unilammellar vesicles
LUVs	Large unilammellar vesicles
GUVs	Giant unilammellar vesicles
LDs	Lipid droplets
FLMs	Freestanding lipid membranes
IONs	Iron oxide nanoparticles
MSNs	Mesoporous silica nanoparticles
QDs	Quantum dots

Chapter 1

Introduction and General Background

1.1 Introduction

Nanoscience has given breakthroughs in every sector of scientific domains and nanotechnologies make our life easier in modern days. Nanotechnology applies the nanoscience theory to the practical applications in industry, medicine, and energy *[1,2]*. Furthermore, nanomedicine utilizes nanotechnology to develop medicine *[3]*. Nanoparticles, nanostructured surfaces, and nano analytical techniques are developing in nanomedicine for diagnosis, treatment, and therapy of diseases to improve the human health *[4,5]*. When the engineered nanoparticles (ENPs) come into the vicinity of living systems, the cellular membrane acts as their initial point of contact as a frontier between cell and nanoparticles *[6]*. Cellular membranes are composed of phospholipids, thus the suspended phospholipid vesicles or supported phospholipid bilayer *[7,8]* are often used as models to study the interaction between nanoparticles (NPs) and cell membranes. Also, when nanoparticles come to contact with the biological fluids, several proteins and metabolites (lipid, nucleic acid, amino acid, and carbohydrate etc.) readily adsorb to the surface of the nanoparticles to form the "biomolecular" corona and govern the physicochemical properties of NPs *[9,10]*. Apart from direct intravascular injection (e.g., in medical treatments), the primary exposure route for nanoparticles is via inhalation and they interact with the pulmonary surfactant which consists of ~ 90% lipid-cholesterol and ~ 10% proteins *[11,12]*. Therefore, systematic investigations of the interactions between engineered nanoparticles with lipid vesicles, protein or both is a burgeoning interest among the researchers in the field of nanoscience. All these studies will not only help to understand

the biomolecular interactions with NPs but also pave the way to engineer a new class of nanoparticles for advancing biomedical applications.

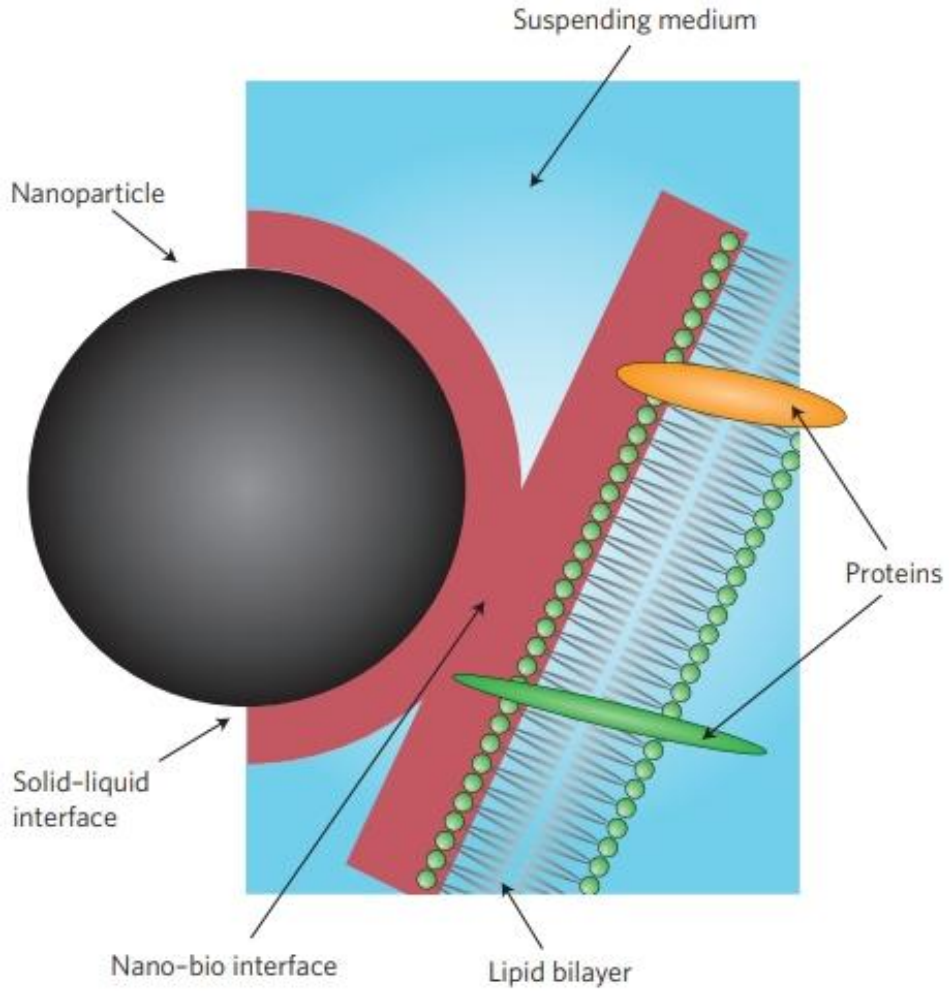

Figure 1.1 *General representation of the interface between a nanoparticle and a lipid bilayer. Figure reproduced with permission from [11] (Copyright 2009, Springer Nature)*

1.2 Nanoparticle's classification and their applications and limitations:

Over the last few decades, we witnessed continuous development in the nanotechnology field. Nanoparticles have profound applications in diagnosis, bio-imaging, and therapeutics field due to their excellent physical

and optical properties through small size, high reactivity, and high surface area *[13]*.

Considering the broader significance of nanoparticles, they can be classified into three different categories: lipid-based nanoparticles, polymeric nanoparticles, and inorganic nanoparticles. In the below, we briefly describe each of the classifications.

1.2.1 Lipid-based nanoparticles:

Lipid-based NPs have several subset structures such as liposomes, lipid nanoparticles (LNPs), and nanostructured lipid carriers (NLCs). Lipid-based NPs are mostly used in delivery systems due to their biocompatibility, formulation simplicity, large payloads of cargo molecules, high bioavailability, and controllable physicochemical properties *[14,15]*. That's why most common FDA-approved nanomedicines are lipid-based NPs *[16]*.

Liposomes are spherical nanoparticles, composed of phospholipids with at least one lipid bilayer surrounding one internal aqueous interior. Liposome can form unilameller and multilamellar vesicles structures which can carry and deliver the hydrophilic, hydrophobic, and lipophilic drug molecules at the target sites of the cell and organelles *[17]*. Also, liposomes can encapsulate different solutes and release them at the specific sites rendering it a prospectus drug delivery system *[18]*. One can easily modulate the liposome size, lipid composition, surface charge, number of lamellae, and surface modifications (anchoring different ligands and polymers during synthesis) which alter the in vitro and in vivo function and stability of liposomes *[19]*. Interestingly, liposomes are readily taken up by the reticuloendothelial system (RES) for clearance, thus limiting the liposome's delivery function in cell. So, Surface modification of liposomes is essential to boost circulation lifespan and delivery effectiveness *[20,21]*.

Lipid nanoparticles (LNPs) are notable subsets of lipid-based NPs with liposome-like structures and are widely used for nucleic acids delivery. However, they differ from conventional liposomes as they possess micellar structure within the particle core and their structure depends on the formulation and synthetic parameters *[22]*. LNPs have become the most promising materials for genetic therapy applications due to their high efficacy to deliver nucleic acids, small size, easy synthesis procedure, and serum tolerance ability *[23,24]*. Basically, lipid nanoparticles are formed with four major components of lipids: cationic or ionizable lipids which can form complex with negatively charged nucleic acids, phospholipid to form particle structure, cholesterol for stability of particles and membrane fusion, and PEGylated lipids to increase the circulation lifetime and serum stability *[25,26]*. Ionizable LNPs are recently preferred for delivery of nucleic acids therapy as they are neutral charged at physiological pH but become protonated in acidic endosomal compartments, helps the LNPs for endosomal escape *[27]*. However, poor drug loading and biodistribution limits the use of LNPs system *[28]*.

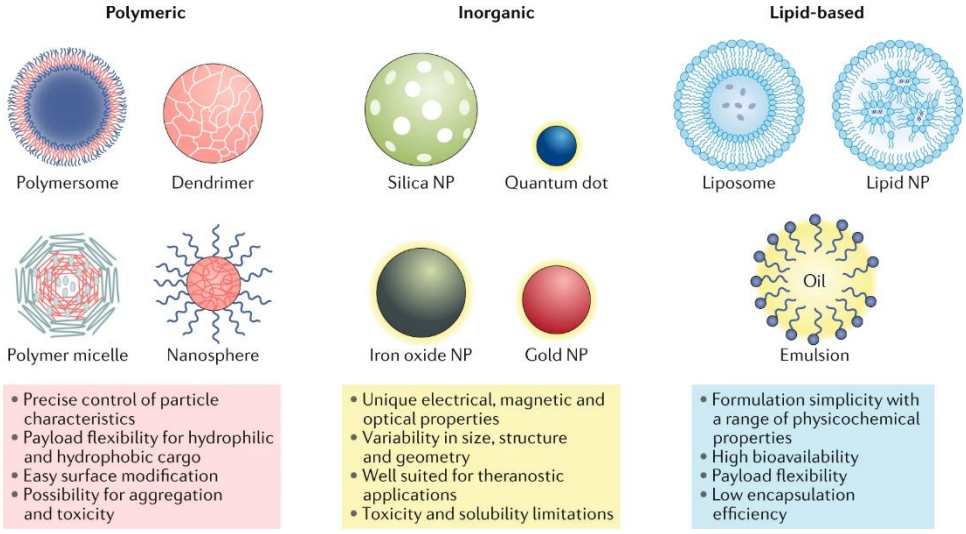

Figure 1.2 *Classes of nanoparticles. Each set of nanoparticles have multiple subsets, some of them are shown here. Each sets advantages and*

disadvantages are also highlighted. Figure reproduced with permission from [29] (Copyright 2020, Springer Nature)

Nanostructured lipid carriers (NLCs) are the alternative of first-generation lipid-based nanoparticles, applied as a drug carrier in vascular aging-related issues *[30,31]*. NLCs are made up of solid and liquid lipids, dispersed in surfactant containing aqueous phases *[32]*. NLCs can be administrated in multiple routes such as intravenous, pulmonary, oral, parental, and topical *[33]*. NLCs have higher drug loading efficiencies and stabilities compared to LNPs *[34]*.

1.2.2 Polymeric nanoparticles:

Polymeric nanoparticles are formed from synthetic or natural materials which can be either monomer or pre-synthesized polymer. Polymeric nanoparticles also have distinct structures, sizes, and characteristics that make them an ideal candidate for drug delivery, cancer therapy, and wound healing *[35-37]*. They are synthesized by different techniques such as nanoprecipitation *[38]*, emulsification *[36]*, microfluidics *[39]*, and ionic gelation *[40]*. Different drug molecules, proteins, polyelectrolytes, small molecules can be incorporated in different parts of NPs: within NPs core, the polymer matrix, chemically conjugated on the polymer, and on the NPs surface. The release of the cargo molecules forms the polymeric nanoparticles can be controlled by modulating the surface charge, stimuli responsivity, composition and stability *[41,42]*.

Based on their different structural properties, polymeric nanoparticles are classified into two categories *[29]*. One is nanocapsules, where the cavities surrounded by the polymeric membrane or shell and other is nanosphere of solid polymer matrix system. Further, the nanocapsules and nanospheres are classified into polymersomes, micelle, and dendrimers.

Polymersomes are a hollow sphere within an aqueous core surrounded by polymer bilayer membrane, made up by the self-assembly of amphiphilic

block copolymers *[43]*. Similar to liposomes, the polymersomes are amphiphilic and locally responsive in nature but exhibit greater stability and cargo retention efficiency *[44]*. Poly(ethylene glycol) (PEG), poly(ethylene oxide) (PEO), and poly(dimethylsiloxane) (PDMS) polymers are mainly used for polymersome formation. Amphiphilic block copolymers can also self-assembled to form nanospheres with hydrophilic core and hydrophobic coating, known as polymeric micelles *[45]*. They can carry diverse small molecules, providing longer circulation time and improved accumulation *[46,47]*. Another class is the dendrimers, a complex highly branched polymeric three-dimensional structure. They consist of several internal repeating units that can carry drugs, nucleic acids, and small molecules *[48,49]*. They often have multiple functional groups on the surface for attaching biomolecules and imaging agents *[50]*. Charged polymers such as poly(ethylenimine) (PEI) and poly(amidoamine) (PAMAM) are mainly used for this purpose.

Overall, polymeric nanoparticles serve as efficient delivery materials since they are biodegradable, water soluble, and biocompatible. The primary downside of employing polymeric nanoparticles is the risk of particle aggregation and cytotoxicity. Although just a few polymeric nanoparticles have been approved by the FDA, many more are now undergoing clinical testing *[16]*.

1.2.3 Inorganic nanoparticles:

Inorganic nanoparticles have unique physical, optical, electrical, and magnetic properties, making them promising candidates for diverse biomedical applications. Iron oxide nanoparticles (IONs), mesoporous silica nanoparticles (MSNs), quantum dots (QDs), and gold nanoparticles (Au NPs) are four different forms of inorganic nanoparticles utilized for drug delivery and imaging *[51,52]*. Various size, structures, and geometries of inorganic NPs are easily formulated using various synthetic methods.

Gold nanoparticles (Au NPs) are extensively researched inorganic nanoparticles that can be synthesized in a variety of sizes and shapes such as nanorods, nanospheres, nanocubes, nanostars, nanoshells, nanoprisms, and nanocages *[53]*. They possess excellent properties such as small size, ease of surface ligand functionalization, biocompatibility, high volume to mass ratio, optical and plasmon characteristics, and low toxicity *[54]*. All these properties make Au NPs ideal candidates for photothermal treatment, drug vehicles, biosensors, and bioimaging *[55,56]*. Furthermore, due to their metallic properties, Au NPs have a variety of catalytic activities, including peroxidase, oxidase, esterase, and superoxide dismutase *[53]*.

Iron oxide NPs (IONs) are another well-studied inorganic nanoparticle, making up the vast majority of FDA-approved inorganic nanomedicines *[57]*. Iron oxide nanoparticles are magnetic and made up of maghemite (Fe_2O_3) or magnetite (Fe_3O_4). The size of these nanoparticles determines their superparamagnetic characteristics. IONs are widely used as contrasting agents, drug vehicles, and thermal-based therapeutics *[58,59]*. Other typical inorganic NPs include mesoporous silica nanoparticles (MSNs), which have large pore volumes and high surface areas for protein and nucleic acid binding sites *[60]*. Their pore sizes, pore volumes, sizes, and shapes are highly controllable, making them an excellent candidate for gene and drugs delivery *[61,62]*. In addition, they are used as biosensors and MRI contrast agents *[63]*. Quantum dots (QDs) are another type of fluorescent inorganic nanoparticles that is commonly employed for *in vitro* and *in vivo* imaging *[64]*.

Inorganic nanoparticles have superior biocompatibility, stability, and a wide range of applications, distinguishing them from organic materials. However, their low solubility and long-term toxicity, particularly from heavy metals, limit their clinical application *[65]*.

1.3 Development of diverse model membrane systems for cellular membrane mimicking:

1.3.1 Importance of model membrane development:

Cell membranes serve as barriers and gatekeepers, partitioning cells by limiting what can flow through them. Cells execute a variety of vital processes across their membranes, including signal reception (plasma membrane) *[66]*, metabolite conversion (adiposome organelle interface) *[67]*, and energy conversion (mitochondrial membrane) *[68]*. Cellular membranes are typically composed of lipids, proteins, and carbohydrates. The primary lipid components are the phospholipids, which form the membrane's bilayer structure and offer a semifluidic environment for proteins and peptides *[69]*. Membrane curvature *[70]*, electrostatic potential *[71,72]*, spatiotemporal distribution of molecules *[73]*, and the presence or absence of certain domains (transient) *[74,75]* all play important roles in membrane chemistry and function. From a molecular perspective, water molecules or membrane hydration are also critical for membrane organization, protein recruitment, maintaining ion gradients, and allowing foreign substances into the cell compartment *[76,77]*. That’s why, in situ real-time tracking and mapping of membrane structure, including hydration, and its function in membrane-modifying mechanisms is essential for understanding the chemistry of living systems. It is a daunting challenge, and such advanced and complex technology has yet to be developed.

1.3.2 Evolution of model membranes:

In general, two main approaches are used to investigate membrane functions: one is top-down and another is bottom-up approaches. In the first approach, dye molecules or nanoparticles are utilized as probes to monitor specific biological activities in living systems *[78,79]*. Using their optical properties, single molecule imaging of membranes is possible in living

systems and can record subsequent images of dynamic membrane processes *[80,81]*. However, this approach fails to deliver any molecular-level information about the membrane interface. On the other hand, the second approach employs considerably simpler model systems to simulate key aspects of cellular membranes, such as lipid monolayers (LMs) and supported lipid bilayers (SLBs) *[82-84]*. Lipid monolayers are single layers of lipid molecules that grow at the air-water interface. Supported lipid bilayers (SLBs) are two-dimensional thin film coatings consisting of a single phospholipid bilayer formed by the fusion of lipid vesicles onto a solid template. Both of the models, together with interface-spectroscopic tools, assist researchers in understanding the fundamentals of membrane interaction with protein, peptides, drugs, nanoparticles, and bio-analytes. These models aid in understanding the role of electrostatics *[85]*, water *[86]*, and membrane complexity *[87]*, however, they cannot give real-time molecular level information on each molecule interaction at the membrane interface.

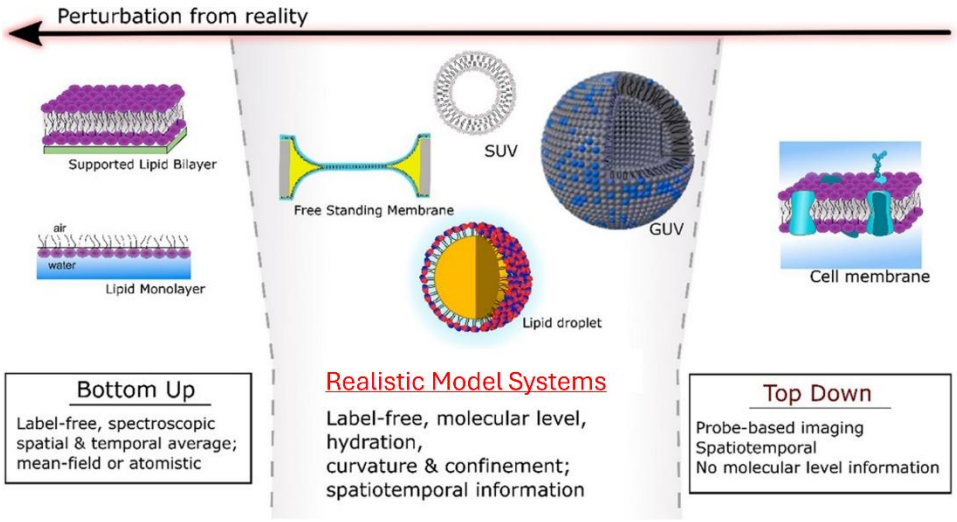

Figure 1.3 *Diverse model membrane systems for understanding the complex biochemistry and physics of membrane interfaces. Figure reproduced with permission from [77] (Copyright 2019, American Chemical Society)*

To overcome this, researchers developed model systems which can bring together both the top-down and bottom-up approach such as liposomes (small and large unilammellar vesicles, SUVs and LUVs as well as giant unilammellar vesicles (GUVs)) *[88]*, lipid droplets (LDs) *[89]*, and freestanding lipid membranes (FLMs) *[73]*. These free-floating membrane systems are more realistic, and both molecular and hydration information is coming out for a better understanding of membrane chemistry and the development of biotechnology.

1.4 Physicochemical properties of liposomes:

The liposome first came to light in 1961 by a British biophysicist, Dr. Alec D. Bangham *[90]*. Liposomes, which means "fat bodies," are spherical vesicle systems containing an aqueous bulk encapsulated by at least one phospholipid bilayer *[91]*. Phospholipids are typically made up of a hydrophilic polar head group and two hydrophobic non-polar tail groups.

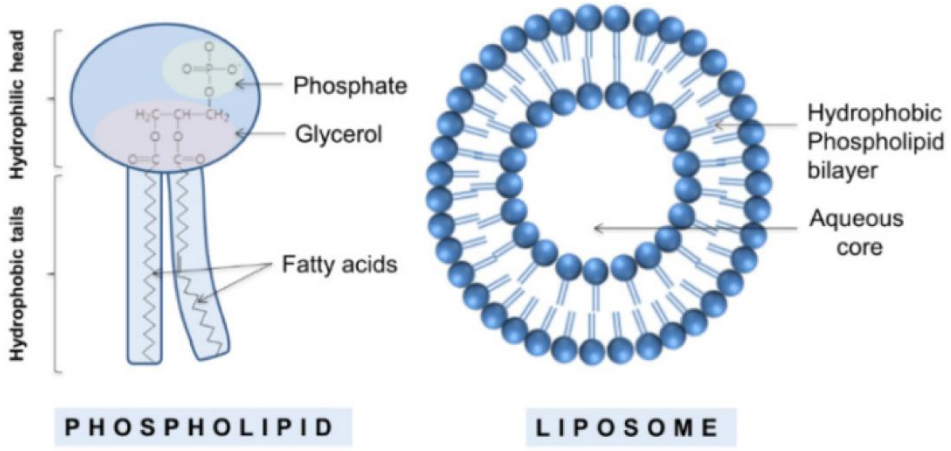

Figure 1.4 *Structure of the phospholipid and liposome [92].*

1.4.1 Head group variation:

The structural and charge diversity of phospholipids comes from the variation in polar head groups such as Phosphatidylcholine (PC), Phosphatidylethanolamine (PE), Phosphatidylserine (PS),

Phosphatidylglycerol (PG), Phosphatidylinositol (PI), Sphingomyelin (SM), and Cardiolipin *[93]*. PC, PE, and SM are neutral (zwitterionic), while PS, PG, PI, and Cardiolipin possess a negative charge (anionic). Along with cholesterol, PC, PE, PS, and SM are the primary phospholipids in mammalian cell plasma membranes *[94]*. In comparison to zwitterionic and negatively charged lipid vesicles, positively charged lipids are extremely rare. However, they serve an important role in the transfer of genetic material into cells by complexing with DNA, mRNA, and siRNA and interacting with the negatively charged plasma membrane *[95,96]*. DOTAP, DMRIE, and DC-Chol are a few typical examples of positively charged lipids. Each of these differently charged lipid head groups has unique physical and chemical properties that determine how liposomes interact with biological membranes *[91]*.

Lipid head groups also affect the shape of the lipid and the stability of lipid bilayers. The chemical structure of the lipid head group, such as charge, size, and polarity together govern the formation of bilayers *[97]*. PC is a typical cylindrical lipid that forms stable lipid bilayers. PE is a conical-shaped lipid with a smaller head group than its tails, which forms inverted micelles and hexagonal phases *[98]*. Liposomes enriched with PE lipid involve in membrane fusion processes. Lysophospholipids (which contain only one fatty acid chain) are inverted conical-shaped lipids with a large polar head group that form micelles rather than bilayers *[99]*.

1.4.2 Tail group variation:

Besides the lipid charge and shape, phase state of the lipid bilayer plays an important role in several membrane processes such as permeability, protein interaction, and membrane fusion *[100,101]*. The phase state of the lipid bilayer is determined by the lipid tail group, temperature, and the presence of other molecules. The lipid bilayer has two extreme phases: the gel-ordered phase and the liquid-disordered phase *[102]*. In the gel-ordered phase, lipid hydrocarbon tails are fully elongated and closely packed,

creating a rigid and less fluid environment. However, in the liquid-disordered phase, the lipid hydrocarbon chains are randomly orientated and less densely packed, making the bilayer more fluid and flexible. The phase state of lipid vesicles is generally defined by the lipid's phase transition temperature (T_m), which varies from one another. Above the phase transition temperature of lipid, lipid bilayer remains in liquid-disordered phase whereas below the T_m of lipid, it remains in gel-ordered phase. In between liquid-disordered and gel-ordered phase, there is ripple phase.

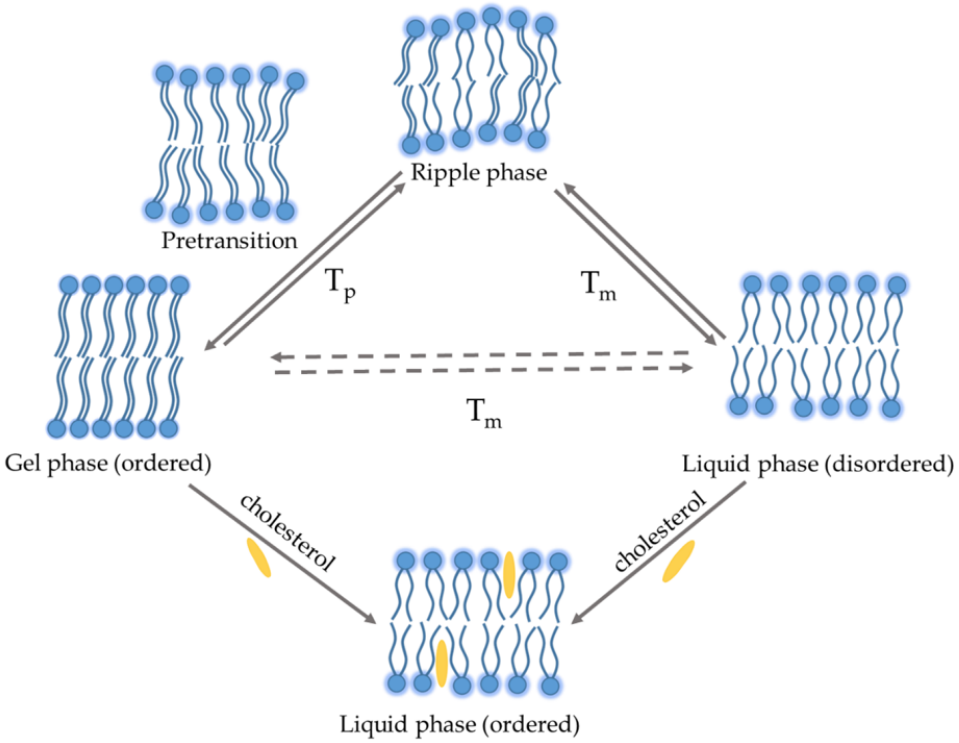

Figure 1.5 *Illustration of thermotropic behaviour of hydrated phospholipid bilayer. T_p: pre-transition temperature, T_m: phase transition temperature [102].*

Several factors affect the phase transition temperature of lipids, including lipid chain length, degree of saturation in the lipid tail group, cis or trans configuration in long fatty acid chains, and cholesterol content *[102-104]*. Longer fatty acid chains raise the T_m of lipids by increasing their *van der Waals* interactions. For example, DLPC (12 C atoms), DMPC (14 C atoms),

DPPC (16 C atoms), and DSPC (18 C atoms) have T_m approximately -2, 24, 41, and 55 °C, respectively. Introducing unsaturation into the fatty acid chain causes bends in the fatty acid tails, resulting in a reduction in the *van der Walls* interaction between lipids and decrease in the T_m of lipid. DOPC has the same 18 carbon atoms as DSPC but has a T_m of -17 °C, which is much lower than DSPC. Cis double bonds in the fatty acid chain have a lower T_m than trans because they cause kinks in the chain and disturb lipid packing. Lipid vesicles in the gel-ordered and liquid-disordered phase states change into a new liquid-ordered phase state upon the addition of cholesterol.

1.4.3 Size and lamellarity variation:

The physicochemical characteristics of liposomes are also influenced by their size and lamellarity (the number of lipid bilayers to form a liposome) *[105,106]*. The size and lamellarity of liposome have a significant impact on its circulatory lifetime, as well as the number of encapsulated drugs and genetic material *[107-109]*. Based on their size and lamellarity of lipid vesicles, they are categorized as unilamellar, multilamellar, and multivesicular vesicles *[110,111]*.

Unilamellar Vesicles (ULVs): These vesicles are made up of a single lipid bilayer that surrounds an aqueous core. Unilamellar Vesicles (UVs) are further classified into three types: small (SUVs), large (LUVs), and giant (GUVs) *[112]*. SUVs, LUVs, and GUVs have diameters of 20-100 nm, 100-1000 nm, and 1-100 µm, respectively. SUVs are often made by sonication or high-pressure extrusion of multilamellar vesicles, as well as the ethanol injection approach. LUVs are formed using the reverse phase evaporation method, freeze-thaw cycles, and extrusion procedures. GUVs are made using electroformation or gentle hydration methods. While GUVs are employed in research pertaining to cell membrane dynamics, permeability, and interactions with proteins or other biological molecules, both SUVs and LUVs are typically used in delivery *[113]*.

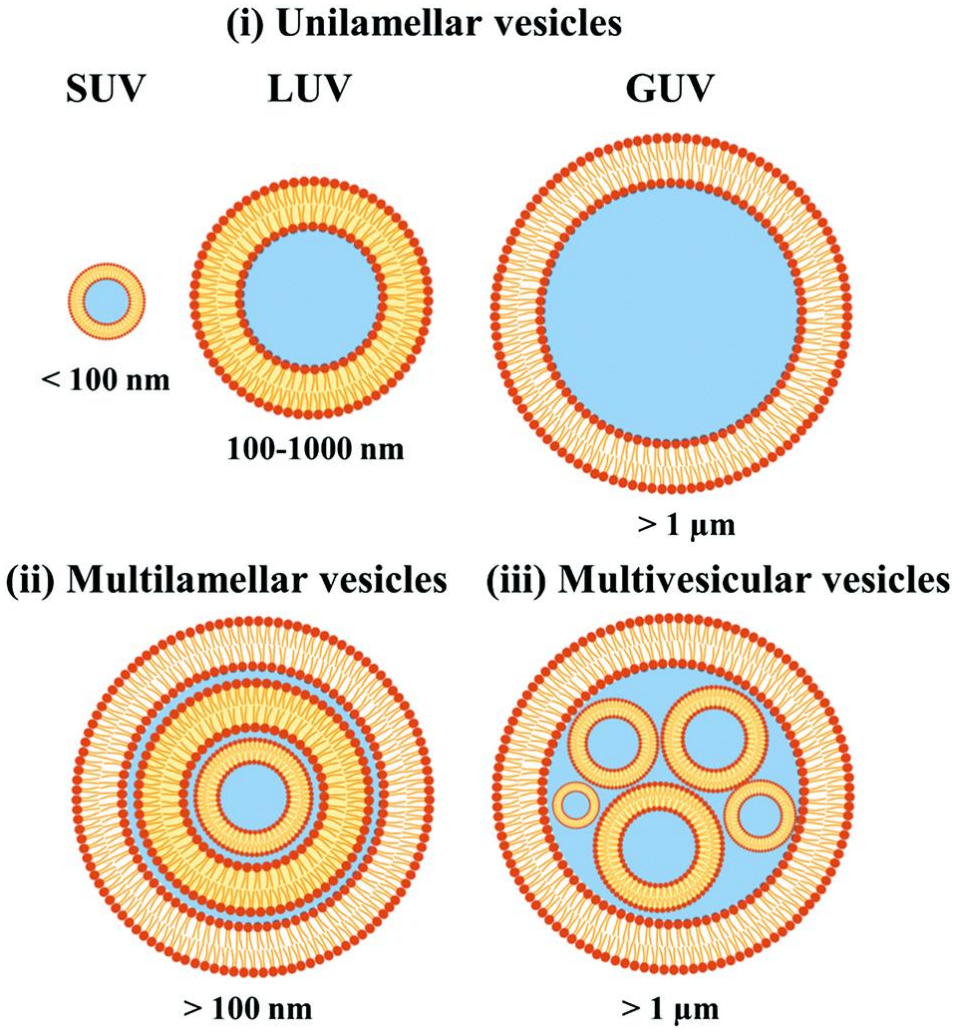

Figure 1.6 *Classification of liposome based on their size and lamellarity. SUV stands for Small Unilamellar Vesicles, LUV denotes Large Unilamellar Vesicles, and GUV represents Giant Unilamellar Vesicles. Figure reproduced with permission from [111] (Copyright 2021, Royal Society of Chemistry)*

Multilamellar Vesicles (MLVs): Multilamellar vesicles are made up of multiple concentric lipid bilayers that surround a series of aqueous compartments, resembling an onion-like structure *[110]*. MLVs have an average size of more than 100 nm and are often prepared using a thin film hydration method.

Multivesicular Vesicles (MVVs): Multiple small vesicles are encased in a larger vesicle to form MVVs *[114]*. MVVs are normally larger than 1 μm and are synthesized using double-emulsion techniques. MVVs are used for the slow and sustained release of encapsulated drugs.

Liposomes are further classed based on their in vivo applications, including conventional liposomes, stealth liposomes, targeted liposomes, and stimuli-responsive (pH, temperature, light, magnetic, and enzyme) liposomes *[108]*.

1.5 Interaction of nanoparticles with liposomes and proteins:

1.5.1 Interaction with liposomes:

Understanding the interaction of engineered nanoparticles with liposomes is important not only from a nano-bio interface perspective *[115]*, but also for building smart hybrid nanostructured complexes *[116]*. The interaction of nanoparticles with liposomes results in functionalization of nanoparticles or incorporation into lipid vesicles *[116]*. These hybrid complexes, which exploit the properties of both liposomes and nanoparticles, have various biomedical applications, including photothermal therapy, bioimaging, stimuli-responsive drug release, and sensing *[117-120]*.

Among the nanomaterials, gold and silver nanoparticles have gained special attention due to their unique optical properties, ease of surface functionalization, tunable size and shape, and large Hamaker constant *[121-123]*. The interaction of these nanoparticles with lipid vesicles is determined by their individual physicochemical properties (size, shape, charge, and hydrophilicity/hydrophobicity) *[124-126]*. Depending on these properties, different kind of assemblies are formed as a result of liposome-NPs interaction: (i) NPs adsorbed on the surface of liposomes, (ii) NPs embedded in the bilayer of liposomes, (iii) NPs encapsulated in the aqueous

core of liposomes, (iv) NPs coated with lipid bilayer of liposome. These four possibilities are summarized in **Figure 1.7.**

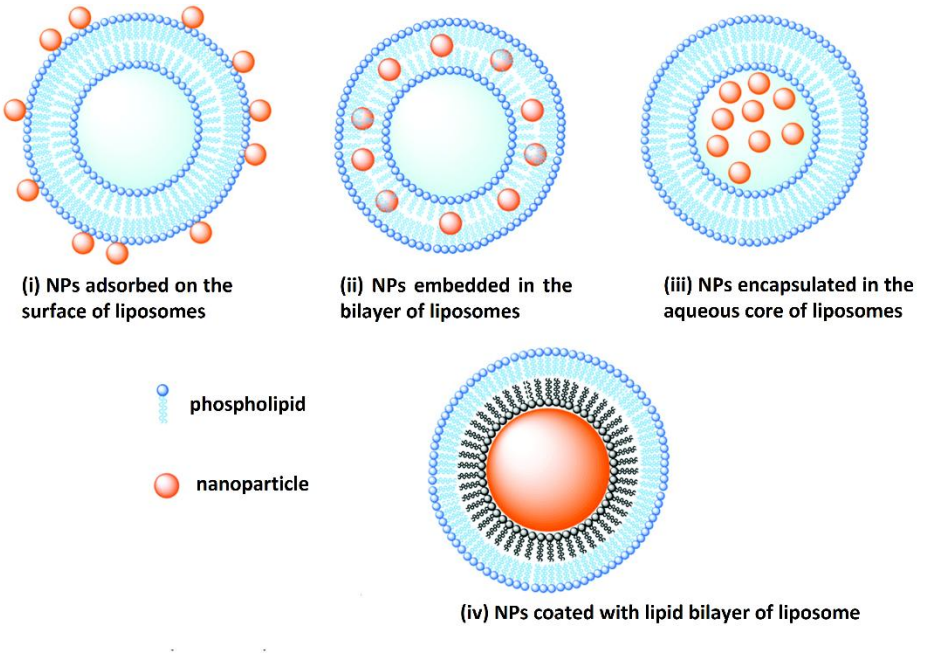

Figure 1.7 *Illustration of nanoparticles interaction with liposomes: (i) NPs adsorb on the surface of liposomes (ii) NPs embedded in the bilayer of liposomes (iii) NPs encapsulated in the aqueous core of liposomes (iv) NPs coated with lipid bilayer of liposome. Figure reproduced with permission from [116] (Copyright 2020, Royal Society of Chemistry)*

(i) NPs adsorbed on the surface of liposomes: Hydrophilic charged nanoparticles are generally known to adsorb on the liposome surface via electrostatic and *Van der Waals* attractive forces. Granick and co-workers first reported that negatively charged carboxyl-modified polystyrene (PS) nanoparticles adsorb on the surface of zwitterionic DLPC liposomes via charge-dipole and non-specific interactions *[127]*. They later observed that negatively charged PS nanoparticles cause local gelation on zwitterionic fluid-phase lipid vesicles, while positively charged PS nanoparticles induce local fluidization of gel-phase liposomes *[128]*. Similarly, citrate-functionalized Au NPs adsorb onto the surface of liquid-phase lipid vesicles and cause local gelation. This gelation thermodynamically favours the

merging of gel-phase regions to minimize liquid/gel interfaces, leading to Au NP aggregation *[129]*. On the other hand, Au-Cit NPs stay adsorbed on gel-phase liposomes with minimal aggregation. The degree of local gelation in zwitterionic lipid vesicles depends on the bulkiness of the Au NPs surface ligand, with the greatest effect seen when the membrane is near its phase transition temperature *[130]*. The stabilization of the liposome surface by surface-bound nanoparticles prevents fusion, overcoming a key limitation of liposomes in biomedical applications *[127]*. Additionally, transient leakage of encapsulated fluorescent calcein occurs during Au NPs adsorption onto fluid liposomes, demonstrating their potential for triggered-release applications *[131,132]*.

In addition to *van der Waals* interactions between charged NPs and zwitterionic liposomes, NPs can also adsorb onto the liposome surface through strong electrostatic interactions between oppositely charged NPs and liposomes. For example, negatively charged mercaptopropionic acid (MPA) functionalized Au NPs adsorb onto positively charged DOTAP phospholipids through electrostatic interactions at neutral pH *[133]*. However, under acidic conditions, the carboxyl groups of the MPA ligands become protonated, causing the Au NPs to detach and leaving the liposomes vulnerable to fusion. Conversely, positively charged chitosan coated Au NPs adsorb onto anionic DOPA phospholipids at acidic pH but detach at physiological pH *[134]*. DOPA is a pH-sensitive phospholipid and becomes protonated at around pH 7.4. These liposome and nanoparticle nanocomposites are used in drug delivery as pH-responsive materials.

Other than electrostatic interactions, carboxyl-modified Au@Ag core-shell nanoparticles can covalently attach to liposomes containing an aminated lipid (DSPE-PEG2000-NH_2) *[135]*. All these liposomes with surface bound nanoparticles have wide applications in drug delivery, photothermal therapy, bioimaging, and biosensors *[136-138]*.

(ii) NPs embedded in the bilayer of liposomes: While surface-bound nanoparticles on liposomes are relatively large and charged, those embedded in the lipid bilayer are small and hydrophobic. The size and loading of nanoparticles in the bilayer can influence membrane thickness, fluidity, and lipid packing.

In 2005, Park et al. embedded 3-4 nm stearylamine-capped Ag NPs into a DPPC bilayer and found that increasing the concentration of NPs increased the bilayer's fluidity above the phase transition temperature of lipid *[139]*. Similar results were observed with Au NPs, suggesting that the surface ligand plays a more important role than the metallic core *[140]*. Furthermore, hydrophobic dodecanethiol-functionalized Ag NPs (around 5.7 nm) were also embedded in the DPPC bilayer, and they increased membrane fluidity both above and below the lipid's phase transition temperature *[141]*. This discrepancy could be due to variations in nanoparticle size or surface ligands. Preiss *et al.* studied the influence of embedded nanoparticle size (2 nm and 4 nm dodecanethiol-capped Ag NPs) on lipid bilayer permeability and phase behaviour using leakage experiments *[142]*. The presence of 4 nm nanoparticles (close to the lipid bilayer thickness) caused more dye leakage compared to 2 nm nanoparticles (smaller than the bilayer thickness), suggesting greater bilayer disruption with the 4 nm NPs. Nanoparticles within the bilayer can form clusters depending on the bilayer's fluidity and the nanoparticle loading concentration. For example, embedded stearylamine-capped AuNPs are dispersed in a gel-phase lipid bilayer but tend to cluster in a fluid-phase lipid bilayer *[143]*.

All these liposomes with bilayer-embedded NPs were prepared by in situ technique using the thin film hydration method. In brief, first, small and hydrophobic nanoparticles were suspended in organic solvents along with dissolved phospholipids. Then, the organic solvents were completely evaporated, leaving a dried film of phospholipids and hydrophobic NPs.

This film was then hydrated to encapsulate the small NPs within the liposome bilayer. The interaction was studied by spectroscopic and imaging techniques. But, the interaction between small hydrophobic nanoparticles and liposomes when simply mixed using *ex situ* techniques is not well understood. While some simulations highlight their interaction behaviour *[144,145]*, experimental results are limited, likely due to the poor solubility of neutral hydrophobic nanoparticles in aqueous solutions. Guo et al., using both theoretical and experimental methods, reported that lipid-covered dodecanethiol-capped gold nanoparticles (Au NPs) smaller than 5 nm can become trapped in the lipid bilayer *[146]*.

To enhance the solubility of small hydrophobic-ligand functionalized Au nanoparticles (NPs), a new class of amphiphilic NPs protected by a binary mixture of hydrophobic and anionic end-functionalized alkanethiol ligands has been developed *[147]*. These monolayer protected amphiphilic Au NPs can insert into and fuse with the hydrophobic core of lipid vesicles without disrupting the lipid bilayer *[148]*. A critical step in the insertion of Au NPs into the lipid bilayer is the hydrophobic interaction between the core of the lipid bilayer and the monolayer of the Au NPs, facilitated by the protrusion of aliphatic lipid chains into the solution *[149]*. The fusion of these Au NPs into the lipid bilayer depends on several factors, including NPs size, the monolayer ligand composition, ligand chemistry (flexibility, hydrophobicity), lipid membrane curvature, lipid charge, phase state of the lipid vesicles, and the ionic strength of the solution *[148,150-153]*. In contrast, Au NPs coated with a single layer of cationic end-functionalized alkanethiol ligands can disrupt cell membranes *[154,155]*, leading to cell death and cytotoxicity. This disruption is influenced by the lipophilicity of the ligands and the charge of the lipids in the membrane *[156,157]*.

(iii) NPs encapsulated in the aqueous core of liposomes: Generally, Au nanoparticles (Au NPs) cannot cross the lipid bilayer of a liposome to reach the aqueous interior due to the high energy barrier of the bilayer's

hydrophobic core. To overcome this, Au NPs often need special surface modifications or external forces. Citrate-coated Au nanoparticles (60 nm in diameter) were encapsulated in the aqueous core of unilamellar liposomes by sonicating preformed Au NPs with multilamellar phospholipid vesicles *[158]*. Furthermore, lipid-covered, dodecanethiol-capped Au NPs larger than 5 nm can insert into the bilayer, form pores, and then move through it *[146]*. Amphiphilic Au NPs with a 1:1 monolayer of 11-mercaptoundecane sulfonate (MUS) and octanethiol (OT) ligands can pass through outer bilayers and interact with inner membranes of multilamellar and multivesicular vesicles without disrupting the membrane *[148]*.

Gold nanoparticles (Au NPs) can be prepared inside the aqueous core of lipid vesicles using other simpler methods. In one method, dried lipid films are rehydrated with a solution of a reducing agent, and then gold precursor ions are added, forming Au NPs within the liposome's core *[159]*. In another method, liposomes are formed in a solution containing both metal ions and a reducing agent, which encapsulates both in the aqueous core, leading to the formation of metal NPs *[160]*. These encapsulated Au NPs within liposomes, have applications in stimuli-triggered drug release, catalysis, and bio-imaging *[161]*.

(iv) NPs coated with lipid bilayer of liposome: An early example of gold nanoparticles (Au NPs) coated with a bilayer of liposomes was introduced by reducing a premixed aqueous solution of an Au precursor and the cationic lipid DDAB *[162]*. These cationic lipid-bilayer-coated Au NPs were later explored for their interaction with DNA, resulting in enhanced stability and improved transfection efficiency *[117]*. However, some studies have shown that lipid-bilayer-coated Au NPs tend to aggregate in biological media with high concentrations of cysteine and glutathione *[163]*. To address this issue, both alkanethiols and phospholipids have been used as capping agents, binding to Au NPs to form hybrid bilayers *[164]*. These hybrid bilayer-coated NPs are susceptible to cyanide etching, which

also depends on the properties of alkanethiols. In 2018, Olenick et al. first reported lipid bilayer coating around Au NPs by simply mixing Au NPs with lipid vesicles and introduced the term “lipid corona” [*165*]. Methods for quantifying the lipid corona on Au NPs from lipid vesicles have also been developed *[166*]**.**

1.5.2 Interaction with proteins:

When nanoparticles (NPs) are exposed to biological media containing thousands of proteins, lipids, carbohydrates, and small metabolites, an adsorption layer quickly forms around the NPs, known as the "protein corona" or “biomolecular corona” *[9,167]*. The adsorbed proteins give the pristine NPs a new biological identity and influence their physicochemical properties *[10,11]*. Key questions about the protein corona, such as its structure (monolayer, bilayer, multilayer) *[168,169]*, the driving forces behind its formation (electrostatic, hydrophobic, hydrogen bonding) *[170,171]*, its time-dependent evolution *[172,173]*, and nature of corona (hard and soft) *[174,175]* are still being explored in the literature.

The interactions between gold nanoparticles (Au NPs) and proteins are influenced by various factors, including size, charge, hydrophobicity, shape, and concentration of NPs and proteins as well as solution pH and ionic strength *[176-180]*. Protein adsorption around NPs can also lead to aggregation and precipitation, which limits their use in biomedical applications. This agglomeration and precipitation of NPs in the presence of proteins can occur due to one or more of the following reasons: surface charge neutralization, protein unfolding after adsorption, protein-mediated bridging, and surface ligand decoating during adsorption *[181-184]*.

To reduce protein corona formation around nanoparticles (NPs) and prevent their aggregation in the presence of proteins, surface properties of NPs are often modified. One popular method is PEGylation, where a hydrophilic polymer layer of polyethylene glycol (PEG) is added to the surface *[185]*.

The molecular weight and density of the PEG coating are crucial in controlling NP-protein interactions, as different nanoparticle sizes have varying surface curvature *[186]*. Zwitterionic coatings on NPs are also effective at repelling proteins *[187]*. With these coatings, proteins interact mainly with the hydrated water layer on the surface rather than directly with the ligands. Polymeric micelles and cylindrical bottle-brush polymers also prevent protein corona formation due to their dense hydrophilic polymer coatings *[188]*. PEGylated or pSarcosinylated liposomes provide some shielding against protein corona formation *[189]*, although typically less effective than polymeric micelles. Nanohydrogels, made from highly polar polymers, are another type of NP that resists protein adsorption on their surface *[190]*.

PEGylation affects the cellular uptake of nanoparticles. Generally, as the PEG content increases, the nanoparticles gain stealth properties, meaning they are better at repelling proteins. However, this also reduces their ability to be taken up by cells *[191]*. Therefore, it's important to strike a balance between enhancing the stealth properties of nanoparticles and maintaining efficient cellular uptake when modifying the surface of nanoparticles with PEG polymers. Despite this challenge, there will always be opportunities for researchers to further develop the protein-repelling capabilities of nanoparticles.

1.6 Motivation and organization of the thesis:

The primary aim of the research presented in this thesis is to explore the emerging field of the "lipid corona" around nanoparticles and its effect on interactions with protein molecules.

It is well-known that during viral budding, the capsid of many viruses pulls lipids from the host cell membrane to form a protective coating. This lipid bilayer gives virus particles enhanced adaptability within our immune system. Therefore, understanding the formation of the novel "lipid corona"

around NPs is of significant interest, not only from virological and biological perspectives but also for the development of smart nanoparticles with lipid bilayer coatings for various biomedical applications. The recent development of membrane-wrapped smart metal nanoparticles, also known as artificial virus nanoparticles (AVNs), mirrors enveloped viruses due to their similar structural concept *[192,193]*.

In virus particles, the capsid, made of protein, encases the viral genome (either DNA or RNA) with lipid membrane wrapping. Since amino acids are the building blocks of proteins, it is reasonable to hypothesize that amino acids could self-assemble on the surface of NPs and will potentially pull the lipid molecules from membranes to form a lipid coating or "lipid corona." This concept of lipid coating will also present exciting possibilities for nanoparticle design in the biomedical field. The following section offers a brief overview of the contents and organization of the thesis.

Chapter 1 begins with a brief introduction to different types of nanoparticles, their applications, and their limitations. It highlights the importance of developing model membranes and traces the evolution of these models. The chapter also covers the physicochemical properties of liposomes, which are used to study their interactions with NPs. Finally, it discusses how various NPs interact with lipid bilayer membranes and proteins, leading to the formation of different NP-biomolecule assemblies.

Chapter 2 explores the interaction between aromatic amino acid-functionalized gold nanoparticles (Au-AA NPs) and lipid vesicles, focusing on the effects of lipid vesicle charge and concentration. The study utilizes various spectroscopic (steady-state UV−visible and fluorescence) and imaging techniques (CLSM, HR-TEM, and AFM). At high lipid concentrations, Au-AA NPs intrinsically pull lipid molecules from the vesicle membrane, forming a distinctive lipid corona around the nanoparticles. In contrast, at low lipid concentrations, Au-AA NPs undergo lipid-induced aggregation. Both the surface charge of the Au-AA NPs and

the lipids play crucial roles in the formation of this lipid corona. The lipid bilayer coating (lipid corona) around the Au-AA NPs provides unusual colloidal stability, protecting the nanoparticles against harsh external conditions such as highly acidic pH, high salt concentrations, and repeated freeze-thaw cycles.

Chapter 3 demonstrates the mechanistic pathway of lipid phase state (sol-gel and liquid crystalline) dependent phenylalanine-functionalized gold nanoparticles (Au-Phe NPs) interaction with lipid vesicles. The study employs both experimental techniques (spectroscopy and microscopy imaging) and coarse-grained molecular dynamics (CGMD) simulations. The main goal is to understand how the lipid phase and the area per lipid head group influence the formation of the lipid corona and lipid-induced aggregation in various media. For the first time, based on the fluidity of lipid at room temperature, lipid corona is classified into two types: "hard lipid corona" and "soft lipid corona". The potential stability of the both the hard corona and soft corona is discussed subsequently.

In Chapter 4, aromatic amino acid-functionalized silver nanoparticles (Ag-AA NPs) are synthesized to investigate how the metallic core and surface ligands affect lipid corona formation. Our results show that both lipid corona formation and lipid-induced aggregation are primarily dependent on the surface ligands of the nanoparticles, regardless of the metallic core. This is evidenced by the fact that aromatic amino acid-functionalized gold and silver nanoparticles exhibit similar interactions with lipid vesicles. By tailoring different charged and phase-state lipid coatings around the Ag-AA NPs, we successfully prevent aggregation, surface oxidation, and Ag^+ ion dissolution under various external stimuli.

Chapter 5 discusses the impact of lipid corona on the protein concentration-dependent aggregation of both Au NPs and proteins during their mutual interactions. We first examine the aggregation behaviour of negatively charged aromatic amino acid (phenylalanine and tyrosine)-functionalized

gold nanoparticles (Au-AA NPs) in the presence of the positively charged globular protein lysozyme at various protein concentrations and compare the results with those of conventional citrate-functionalized Au NPs (Au-Cit NPs). Our findings reveal that the aggregation mechanism of Au-AA NPs is significantly different from that of Au-Cit NPs, as well as under low and high lysozyme concentrations. The "hard lipid corona" around Au-AA NPs is found to be more effective in impeding lysozyme-induced aggregation compared to the "soft lipid corona."

1.7 References:

[1] Malik S., Muhammad K., Waheed Y. (2023), Emerging Applications of Nanotechnology in Healthcare and Medicine, Molecules 28, 6624 (DOI: 10.3390/molecules28186624)

[2] Soni A. K., Jha R. K. (2024), Nanotechnology's Applications and Potential in Various Fields, Cureus 16, e59234 (DOI: 10.7759/cureus.59234)

[3] Bayda S., Adeel M., Tuccinardi T. *et al.* (2019), The History of Nanoscience and Nanotechnology: From Chemical-Physical Applications to Nanomedicine, Molecules 25, 112 (DOI: 10.3390/molecules25010112)

[4] Sim S., Wong N. (2021), Nanotechnology and Its Use in Imaging and Drug Delivery (Review), Biomed. Rep. 14, 42 (DOI: 10.3892/br.2021.1418)

[5] Thwala L. N., Ndlovu S. C., Mpofu K. T. *et al.* (2023), Nanotechnology-Based Diagnostics for Diseases Prevalent in Developing Countries: Current Advances in Point-of-Care Tests, Nanomaterials 13, 1247 (DOI: 10.3390/nano13071247)

[6] Edidin M. (2003), Lipids on the Frontier: A Century of Cell-Membrane Bilayers, Nat. Rev. Mol. Cell Biol. 4, 414-418 (DOI: 10.1038/nrm1102)

[7] Moghadam B. Y., Hou W. -C., Corredor C. *et al.* (2012), Role of Nanoparticle Surface Functionality in the Disruption of Model Cell Membranes, Langmuir 28, 16318-16326 (DOI: 10.1021/la302654s)

[8] Bailey C. M., Kamaloo E., Waterman K. L. *et al.* (2015), Size Dependence of Gold Nanoparticle Interactions with a Supported Lipid Bilayer: A QCM-D Study, Biophys. Chem. 203-204, 51–61 (DOI: 10.1016/j.bpc.2015.05.006)

[9] Monopoli M. P., Åberg C., Salvati A. *et al.* (2012), Biomolecular Coronas Provide the Biological Identity of Nanosized Materials, Nat. Nanotechnol. 7, 779–786 (DOI: 10.1038/nnano.2012.207)

[10] Tenzer S., Docter D., Kuharev J. *et al.* (2013), Rapid Formation of Plasma Protein Corona Critically Affects Nanoparticle Pathophysiology, Nat. Nanotechnol. 8, 772–781 (DOI: 10.1038/nnano.2013.181

[11] Nel A. E., Mädler L., Velegol D. *et al.* (2009), Understanding Biophysicochemical Interactions at the Nano–Bio Interface, Nat. Mater. 8, 543-557 (DOI: 10.1038/nmat2442)

[12] Zuo Y. Y., Veldhuizen R. A. W., Neumann A. W. *et al.* (2008), Current Perspectives in Pulmonary Surfactant - Inhibition, Enhancement and Evaluation, Biochim. Biophys. Acta BBA - Biomembr. 1778, 1947-1977 (DOI: 10.1016/j.bbamem.2008.03.021)

[13] Khan I., Saeed K., Khan I. (2019), Nanoparticles: Properties, Applications and Toxicities, Arab. J. Chem. 12, 908-931 (DOI: 10.1016/j.arabjc.2017.05.011)

[14] Sercombe L., Veerati T., Moheimani F. *et al.* (2015), Advances and Challenges of Liposome Assisted Drug Delivery, Front. Pharmacol. 6, 286 (DOI: 10.3389/fphar.2015.00286)

[15] Yonezawa S., Koide H., Asai T. (2020), Recent Advances in siRNA Delivery Mediated by Lipid-Based Nanoparticles, Adv. Drug Deliv. Rev. 154-155, 64-78 (DOI: 10.1016/j.addr.2020.07.022)

[16] Anselmo A. C., Mitragotri S. (2019), Nanoparticles in the Clinic: An Update, Bioeng. Transl. Med. 4, e10143 (DOI: 10.1002/btm2.10143)

[17] Sarfraz M., Afzal A., Yang T. *et al.* (2018), Development of Dual Drug Loaded Nanosized Liposomal Formulation by A Reengineered Ethanolic Injection Method and Its Pre-Clinical Pharmacokinetic Studies, Pharmaceutics 10, 151 (DOI: 10.3390/pharmaceutics10030151)

[18] Yingchoncharoen P., Kalinowski D. S., Richardson D. R. (2016), Lipid-Based Drug Delivery Systems in Cancer Therapy: What Is Available and What Is Yet to Come, Pharmacol. Rev. 68,701-787 (DOI: 10.1124/pr.115.012070)

[19] Sedighi M., Sieber S., Rahimi F. *et al.* (2019), Rapid Optimization of Liposome Characteristics Using a Combined Microfluidics and Design-of-Experiment Approach, Drug Deliv. Transl. Res. 9, 404-413 (DOI: 10.1007/s13346-018-0587-4)

[20] Fonseca-Santos B., Chorilli M., Palmira Daflon Gremião M. (2015), Nanotechnology-Based Drug Delivery Systems for the Treatment of Alzheimer's Disease, Int. J. Nanomedicine 10, 4981-5003 (DOI: 10.2147/IJN.S87148)

[21] Khalin I., Alyautdin R., Ismail N. M. *et al.* (2014), Nanoscale Drug Delivery Systems and the Blood-Brain Barrier, Int. J. Nanomedicine 9, 795-811 (DOI: 10.2147/IJN.S52236)

[22] Leung A. K. K., Tam Y. Y. C., Chen S. *et al.* (2015), Microfluidic Mixing: A General Method for Encapsulating Macromolecules in Lipid Nanoparticle Systems, J. Phys. Chem. B 119, 8698-8706 (DOI: 10.1021/acs.jpcb.5b02891)

[23] Cheng Q., Wei T., Farbiak L. *et al.* (2020), Selective Organ Targeting (SORT) Nanoparticles for Tissue-Specific mRNA Delivery and CRISPR-Cas Gene Editing, Nat. Nanotechnol. 15, 313-320 (DOI: 10.1038/s41565-020-0669-6)

[24] Berraondo P., Martini P. G. V., Avila M. A. *et al.* (2019), Messenger RNA Therapy for Rare Genetic Metabolic Diseases, Gut 68, 1323-1330 (DOI: 10.1136/gutjnl-2019-318269)

[25] Cheng X., Lee R. J. (2016), The Role of Helper Lipids in Lipid Nanoparticles (LNPs) Designed for Oligonucleotide Delivery, Adv. Drug Deliv. Rev. 99, 129-137 (DOI: 10.1016/j.addr.2016.01.022)

[26] Kulkarni J. A., Witzigmann D., Leung J. *et al.* (2019), On the Role of Helper Lipids in Lipid Nanoparticle Formulations of siRNA, Nanoscale 11, 21733-21739 (DOI: 10.1039/C9NR09347H)

[27] Vhora I., Lalani R., Bhatt, P. *et al.* (2019), Lipid-Nucleic Acid Nanoparticles of Novel Ionizable Lipids for Systemic BMP-9 Gene Delivery to Bone-Marrow Mesenchymal Stem Cells for Osteoinduction, Int. J. Pharm. 563, 324-336 (DOI: 10.1016/j.ijpharm.2019.04.006)

[28] Fenton O. S., Olafson K. N., Pillai P. S. *et al.* (2018), Advances in Biomaterials for Drug Delivery, Adv. Mater. 30, 1705328 (DOI: 10.1002/adma.201705328)

[29] Mitchell M. J., Billingsley M. M., Haley R. M. *et al.* (2021), Engineering Precision Nanoparticles for Drug Delivery, Nat. Rev. Drug Discov. 20, 101-124 (DOI: 10.1038/s41573-020-0090-8)

[30] Müller R. H., Radtke M., Wissing S. A. (2002), Nanostructured Lipid Matrices for Improved Microencapsulation of Drugs, Int. J. Pharm. 242, 121-128 (DOI: 10.1016/S0378-5173(02)00180-1)

[31] Visweswaran G. R. R., Gholizadeh S., Ruiters M. H. J. *et al.* (2015), Targeting Rapamycin to Podocytes Using a Vascular Cell Adhesion Molecule-1 (VCAM-1)-Harnessed SAINT-Based Lipid Carrier System, PLOS ONE 10, e0138870 (DOI: 10.1371/journal.pone.0138870)

[32] Czajkowska-Kośnik A., Szekalska M., Winnicka K. (2019), Nanostructured Lipid Carriers: A Potential Use for Skin Drug Delivery Systems, Pharmacol. Rep. 71, 156-166 (DOI: 10.1016/j.pharep.2018.10.008)

[33] Poonia N., Kharb R., Lather V. *et al.* (2016), Nanostructured Lipid Carriers: Versatile Oral Delivery Vehicle, Future Sci. OA 2, FSO135, (DOI: 10.4155/fsoa-2016-0030)

[34] Beloqui A., Solinís M. Á., Rodríguez-Gascón A. *et al.* (2016), Nanostructured Lipid Carriers: Promising Drug Delivery Systems for Future Clinics, Nanomedicine Nanotechnol. Biol. Med. 12, 143-161 (DOI: 10.1016/j.nano.2015.09.004)

[35] Xiao X., Teng F., Shi C. *et al.* (2022), Polymeric Nanoparticles-Promising Carriers for Cancer Therapy, Front. Bioeng. Biotechnol. 10, 1024143 (DOI: 10.3389/fbioe.2022.1024143)

[36] Zielińska A., Carreiró F., Oliveira A. M. *et al.* (2020), Polymeric Nanoparticles: Production, Characterization, Toxicology and Ecotoxicology, Molecules 25, 3731 (DOI: 10.3390/molecules25163731)

[37] Yu Z., Shen X., Yu H. *et al.* (2023), Smart Polymeric Nanoparticles in Cancer Immunotherapy, Pharmaceutics 15, 775 (DOI: 10.3390/pharmaceutics15030775)

[38] Le Z., Chen Y., Han H. *et al.* (2018), Hydrogen-Bonded Tannic Acid-Based Anticancer Nanoparticle for Enhancement of Oral Chemotherapy, ACS Appl. Mater. Interfaces 10, 42186-42197 (DOI: 10.1021/acsami.8b18979)

[39] Zhang L., Beatty A., Lu L. *et al.* (2020), Microfluidic-Assisted Polymer-Protein Assembly to Fabricate Homogeneous Functional nanoparticles, Mater. Sci. Eng. C 111, 110768 (DOI: 10.1016/j.msec.2020.110768)

[40] He C., Yue H., Xu L. *et al.* (2020), siRNA Release Kinetics from Polymeric Nanoparticles Correlate with RNAi Efficiency and Inflammation Therapy via Oral Delivery, Acta Biomater. 103, 213-222 (DOI: 10.1016/j.actbio.2019.12.005)

[41] Patra J. K., Das G., Fraceto L. F *et al.* (2018), Nano Based Drug Delivery Systems: Recent Developments and Future Prospects, J. Nanobiotechnology 16, 71 (DOI: 10.1186/s12951-018-0392-8)

[42] Volpatti L. R., Matranga M. A., Cortinas A. B. *et al.* (2020), Glucose-Responsive Nanoparticles for Rapid and Extended Self-Regulated Insulin Delivery, ACS Nano 14, 488-497 (DOI: 10.1021/acsnano.9b06395)

[43] Discher D. E., Ahmed F. (2006), POLYMERSOMES, Annu. Rev. Biomed. Eng. 8, 323–341 (DOI: 10.1146/annurev.bioeng.8.061505.095838)

[44] Rideau E., Dimova R., Schwille P. *et al.* Liposomes and Polymersomes: A Comparative Review towards Cell Mimicking, Chem. Soc. Rev. 47, 8572-8610 (DOI: 10.1039/C8CS00162F)

[45] Mahmud A., Xiong X. -B., Aliabadi H. M. *et al.* (2007), Polymeric Micelles for Drug Targeting, J. Drug Target. 15, 553-584 (DOI: 10.1080/10611860701538586)

[46] Deshmukh A. S., Chauhan P. N., Noolvi M. N. *et al.* (2017), Polymeric Micelles: Basic Research to Clinical Practice, Int. J. Pharm. 532, 249-268 (DOI: 10.1016/j.ijpharm.2017.09.005)

[47] Liu X., Li C., Lv J. *et al.* (2020), Glucose and H_2O_2 Dual-Responsive Polymeric Micelles for the Self-Regulated Release of Insulin, ACS Appl. Bio Mater. 3, 1598-1606 (DOI: 10.1021/acsabm.9b01185)

[48] Xu L., Zhang H., Wu Y. (2014), Dendrimer Advances for the Central Nervous System Delivery of Therapeutics, ACS Chem. Neurosci. 5, 2–13 (DOI: 10.1021/cn400182z)

[49] Palmerston Mendes L., Pan J., Torchilin V. (2017), Dendrimers as Nanocarriers for Nucleic Acid and Drug Delivery in Cancer Therapy, Molecules 22, 1401 (DOI: 10.3390/molecules22091401)

[50] Sandoval-Yañez C., Castro Rodriguez C. (2020), Dendrimers: Amazing Platforms for Bioactive Molecule Delivery Systems, Materials 13, 570 (DOI: 10.3390/ma13030570)

[51] Lin Y., Zhang K., Zhang R. *et al.* (2020), Magnetic Nanoparticles Applied in Targeted Therapy and Magnetic Resonance Imaging: Crucial Preparation Parameters, Indispensable Pre-Treatments, Updated Research Advancements and Future Perspectives, J. Mater. Chem. B 8, 5973-5991 (DOI: 10.1039/D0TB00552E)

[52] Matea C., Mocan T., Tabaran F. *et al.* (2017), Quantum Dots in Imaging, Drug Delivery and Sensor Applications, Int. J. Nanomedicine 12, 5421-5431 (DOI: 10.2147/IJN.S138624)

[53] Lou-Franco J., Das B., Elliott C. *et al.* (2021), Gold Nanozymes: From Concept to Biomedical Applications, Nano-Micro Lett. 13, 10 (DOI: 10.1007/s40820-020-00532-z)

[54] Fan J., Cheng Y., Sun M. (2020), Functionalized Gold Nanoparticles: Synthesis, Properties and Biomedical Applications. Chem. Rec. 20, 1474-1504 (DOI: 10.1002/tcr.202000087)

[55] Jahangirian H., Kalantari K., Izadiyan Z. *et al.* (2019), A Review of Small Molecules and Drug Delivery Applications Using Gold and Iron Nanoparticles, Int. J. Nanomedicine 14, 1633-1657 (DOI: 10.2147/IJN.S184723)

[56] Wang J., Potocny A. M., Rosenthal J. *et al.* (2020), Gold Nanoshell-Linear Tetrapyrrole Conjugates for Near Infrared-Activated Dual Photodynamic and Photothermal Therapies, ACS Omega 5, 926-940 (DOI: 10.1021/acsomega.9b04150)

[57] Bobo D., Robinson K. J., Islam J. *et al.* (2016), Nanoparticle-Based Medicines: A Review of FDA-Approved Materials and Clinical Trials to Date, Pharm. Res. 33, 2373-2387 (DOI: 10.1007/s11095-016-1958-5)

[58] Dadfar S. M., Roemhild K., Drude N. I. *et al.* (2019), Iron Oxide Nanoparticles: Diagnostic, Therapeutic and Theranostic Applications, Adv. Drug Deliv. Rev. 138, 302-325 (DOI: 10.1016/j.addr.2019.01.005)

[59] Dadfar S. M., Camozzi D., Darguzyte M. *et al.* (2020), Size-Isolation of Superparamagnetic Iron Oxide Nanoparticles Improves MRI, MPI and Hyperthermia Performance, J. Nanobiotechnology 18, 22 (DOI: 10.1186/s12951-020-0580-1)

[60] Wang Y., Zhao Q., Han N. *et al.* (2015), Mesoporous Silica Nanoparticles in Drug Delivery and Biomedical Applications, Nanomedicine 11, 313-327 (DOI: 10.1016/j.nano.2014.09.014)

[61] Huang K. -W., Hsu F. -F., Qiu J. T. *et al.* (2020), Highly Efficient and Tumor-Selective Nanoparticles for Dual-Targeted Immunogene Therapy against Cancer, Sci. Adv. 6, eaax5032 (DOI: 10.1126/sciadv.aax5032)

[62] Xu C., Nam J., Hong H. *et al.* (2019), Positron Emission Tomography-Guided Photodynamic Therapy with Biodegradable Mesoporous Silica Nanoparticles for Personalized Cancer Immunotherapy, ACS Nano 13, 12148-12161 (DOI: 10.1021/acsnano.9b06691)

[63] Narayan R., Nayak U. Y., Raichur A. M. *et al.* (2018), Mesoporous Silica Nanoparticles: A Comprehensive Review on Synthesis and Recent Advances, Pharmaceutics 10, 118 (DOI: 10.3390/pharmaceutics10030118)

[64] Wagner A. M., Knipe J. M. Orive G. *et al.* (2019), Quantum Dots in Biomedical Applications, Acta Biomater. 94, 44-63 (DOI: 10.1016/j.actbio.2019.05.022)

[65] Manshian B. B., Jiménez J., Himmelreich U. *et al.* (2017), Personalized Medicine and Follow-up of Therapeutic Delivery through Exploitation of Quantum Dot Toxicity, Biomaterials 127, 1-12 (DOI: 10.1016/j.biomaterials.2017.02.039)

[66] Grecco H. E., Schmick M., Bastiaens P. I. H. (2011), Signaling from the Living Plasma Membrane, Cell 144, 897-909 (DOI: 10.1016/j.cell.2011.01.029)

[67] Thiam A. R., Farese Jr R. V., Walther T. C. (2013), The Biophysics and Cell Biology of Lipid Droplets, Nat. Rev. Mol. Cell Biol. 14, 775-786 (DOI: 10.1038/nrm3699)

[68] Rathore S., Berndtsson J., Marin-Buera L. *et al.* (2019), Cryo-EM Structure of the Yeast Respiratory Supercomplex, Nat. Struct. Mol. Biol. 26, 50-57 (DOI: 10.1038/s41594-018-0169-7)

[69] Singer S. J., Nicolson G. L. (1972), The Fluid Mosaic Model of the Structure of Cell Membranes: Cell Membranes Are Viewed as Two-Dimensional Solutions of Oriented Globular Proteins and Lipids, Science 175, 720-731 (DOI: 10.1126/science.175.4023.720)

[70] Jarsch I. K., Daste F., Gallop J. L. (2016), Membrane Curvature in Cell Biology: An Integration of Molecular Mechanisms, J. Cell Biol. 214, 375-387 (DOI: 10.1083/jcb.201604003)

[71] McLaughlin S., Murray D. (2005), Plasma Membrane Phosphoinositide Organization by Protein Electrostatics, Nature 438, 605-611 (DOI: 10.1038/nature04398)

[72] Tarun O. B., Hannesschläger C., Pohl P. *et al.* (2018), Label-Free and Charge-Sensitive Dynamic Imaging of Lipid Membrane Hydration on Millisecond Time Scales, Proc. Natl. Acad. Sci. 115, 4081-4086 (DOI: 10.1073/pnas.1719347115)

[73] Tarun O. B., Eremchev M. Y. Roke S. (2018), Interaction of Oil and Lipids in Freestanding Lipid Bilayer Membranes Studied with Label-Free High-Throughput Wide-Field Second-Harmonic Microscopy, Langmuir 34, 11305-11310 (DOI: 10.1021/acs.langmuir.8b01790)

[74] Eggeling C., Ringemann C., Medda R. *et al.* (2009), Direct Observation of the Nanoscale Dynamics of Membrane Lipids in a Living Cell, Nature 457, 1159-1162 (DOI: 10.1038/nature07596)

[75] De Wit G., Danial J. S. H., Kukura P. *et al.* (2015), Dynamic Label-Free Imaging of Lipid Nanodomains, Proc. Natl. Acad. Sci. 112, 12299-12303 (DOI: 10.1073/pnas.1508483112)

[76] Chattopadhyay M., Krok E., Orlikowska-Rzeznik H. *et al.* (2023), Cooperativity between Sodium Ions and Water Molecules Facilitates Lipid Mobility in Model Cell Membranes, Chem. Sci. 14, 4002-4011 (DOI: 10.1039/D2SC06836B)

[77] Okur H. I., Tarun O. B., Roke S. (2019), Chemistry of Lipid Membranes from Models to Living Systems: A Perspective of Hydration, Surface Potential, Curvature, Confinement and Heterogeneity, J. Am. Chem. Soc. 141, 12168-12181 (DOI: 10.1021/jacs.9b02820)

[78] Veatch S. L., Keller S. L. (2005), Seeing Spots: Complex Phase Behavior in Simple Membranes, Biochim. Biophys. Acta BBA - Mol. Cell Res. 1746, 172-185 (DOI: 10.1016/j.bbamcr.2005.06.010)

[79] Kress A., Wang X., Ranchon H. *et al.* (2013), Mapping the Local Organization of Cell Membranes Using Excitation-Polarization-Resolved Confocal Fluorescence Microscopy, Biophys. J. 105, 127-136 (DOI: 10.1016/j.bpj.2013.05.043)

[80] Shtengel G., Galbraith J. A., Galbraith C. G. *et al.* (2009), Interferometric Fluorescent Super-Resolution Microscopy Resolves 3D Cellular Ultrastructure, Proc. Natl. Acad. Sci. 106, 3125-3130 (DOI: 10.1073/pnas.0813131106)

[81] Nuriya M., Yasui M. (2010), Membrane Potential Dynamics of Axons in Cultured Hippocampal Neurons Probed by Second-Harmonic-Generation Imaging, J. Biomed. Opt. 15, 020503 (DOI: 10.1117/1.3365135)

[82] Roke S., Schins J., Müller M. *et al.* (2003), Vibrational Spectroscopic Investigation of the Phase Diagram of a Biomimetic Lipid Monolayer, Phys. Rev. Lett. 90, 128101 (DOI: 10.1103/PhysRevLett.90.128101)

[83] Mondal J. A., Nihonyanagi S., Yamaguchi S. *et al.* (2012), Three Distinct Water Structures at a Zwitterionic Lipid/Water Interface Revealed by Heterodyne-Detected Vibrational Sum Frequency Generation, J. Am. Chem. Soc. 134, 7842-7850 (DOI: 10.1021/ja300658h)

[84] Richter R. P., Bérat R., Brisson A. R. (2006), Formation of Solid-Supported Lipid Bilayers: An Integrated View, Langmuir 22, 3497-3505 (DOI: 10.1021/la052687c)

[85] Gonella G., Lütgebaucks C., De Beer A. G. F. *et al.* (2016), Second Harmonic and Sum-Frequency Generation from Aqueous Interfaces Is Modulated by Interference, J. Phys. Chem. C 120, 9165-9173 (DOI: 10.1021/acs.jpcc.5b12453)

[86] Singh P. C., Inoue K., Nihonyanagi S. *et al.* (2016), Femtosecond Hydrogen Bond Dynamics of Bulk-like and Bound Water at Positively and

Negatively Charged Lipid Interfaces Revealed by 2D HD-VSFG Spectroscopy, Angew. Chem. Int. Ed. 55, 10621-10625 (DOI: 10.1002/anie.201603676)

[87] Liu J., Conboy J. C. (2004), Direct Measurement of the Transbilayer Movement of Phospholipids by Sum-Frequency Vibrational Spectroscopy, J. Am. Chem. Soc. 126, 8376-8377 (DOI: 10.1021/ja048245p)

[88] Smolentsev N., Lütgebaucks C., Okur H. I. *et al.* (2016), Intermolecular Headgroup Interaction and Hydration as Driving Forces for Lipid Transmembrane Asymmetry, J. Am. Chem. Soc. 138, 4053-4060 (DOI: 10.1021/jacs.5b11776)

[89] Vezočnik V., Hodnik V., Sitar S. *et al.* (2018), Kinetically Stable Triglyceride-Based Nanodroplets and Their Interactions with Lipid-Specific Proteins, Langmuir 34, 8983-8993 (DOI: 10.1021/acs.langmuir.8b02180)

[90] Bangham A. D., Horne R. W. (1964), Negative Staining of Phospholipids and Their Structural Modification by Surface-Active Agents as Observed in the Electron Microscope, J. Mol. Biol. 8, 660-IN10 (DOI: 10.1016/S0022-2836(64)80115-7)

[91] Thapa Magar K., Boafo G. F., Li X. *et al.* (2022), Liposome-Based Delivery of Biological Drugs, Chin. Chem. Lett. 33, 587-596, (DOI: 10.1016/j.cclet.2021.08.020)

[92] Amarandi R. -M., Ibanescu A., Carasevici E. *et al.* (2022), Liposomal-Based Formulations: A Path from Basic Research to Temozolomide Delivery Inside Glioblastoma Tissue, Pharmaceutics 14, 308 (DOI: 10.3390/pharmaceutics14020308)

[93] Bargui R., Solgadi A., Prost B. *et al.* (2021), Phospholipids: Identification and Implication in Muscle Pathophysiology, Int. J. Mol. Sci. 22, 8176 (DOI: 10.3390/ijms22158176)

[94] Cockcroft S. (2021), Mammalian Lipids: Structure, Synthesis and Function, Essays Biochem. 65, 813-845 (DOI: 10.1042/EBC20200067)

[95] Schroeder A., Levins C. G., Cortez C. *et al.* (2010), Lipid-based Nanotherapeutics for siRNA Delivery, J. Intern. Med. 267, 9-21 (DOI: 10.1111/j.1365-2796.2009.02189.x)

[96] Sun D., Lu Z. -R. (2023), Structure and Function of Cationic and Ionizable Lipids for Nucleic Acid Delivery, Pharm. Res. 40, 27-46 (DOI: 10.1007/s11095-022-03460-2)

[97] Dickey A., Faller R. (2008), Examining the Contributions of Lipid Shape and Headgroup Charge on Bilayer Behavior, Biophys. J. 95, 2636-2646 (DOI: 10.1529/biophysj.107.128074)

[98] Rand R. P., Fuller N., Parsegian V. A. *et al.* (1988), Variation in Hydration Forces between Neutral Phospholipid Bilayers: Evidence for Hydration Attraction, Biochemistry 27, 7711-7722 (DOI: 10.1021/bi00420a021)

[99] Leuti A., Fazio D., Fava M. *et al.* (2020), Bioactive Lipids, Inflammation and Chronic Diseases, Adv. Drug Deliv. Rev. 159, 133-169 (DOI: 10.1016/j.addr.2020.06.028)

[100] Lee A. G. (2003), Lipid-Protein Interactions in Biological Membranes: A Structural Perspective, Biochim. Biophys. Acta BBA - Biomembr. 1612, 1-40, (DOI: 10.1016/S0005-2736(03)00056-7)

[101] Jouhet J. (2013), Importance of the Hexagonal Lipid Phase in Biological Membrane Organization, Front. Plant Sci. 4, 494 (DOI: 10.3389/fpls.2013.00494)

[102] Franzé S., Selmin F., Samaritani E. *et al.* (2018), Lyophilization of Liposomal Formulations: Still Necessary, Still Challenging, Pharmaceutics 10, 139 (DOI: 10.3390/pharmaceutics10030139)

[103] Baccouch R., Shi Y., Vernay E. *et al.* (2023), The Impact of Lipid Polyunsaturation on the Physical and Mechanical Properties of Lipid Membranes, Biochim. Biophys. Acta BBA - Biomembr. 1865, 184084 (DOI: 10.1016/j.bbamem.2022.184084)

[104] Manafirad A., Menendez C. A., Perez-Lemus G. R. *et al.* (2023), Structural and Mechanical Response of Two-Component Photoswitchable Lipid Bilayer Vesicles, Langmuir 39, 15932-15941 (DOI: 10.1021/acs.langmuir.3c01764)

[105] Matsuura-Sawada Y., Maeki M., Uno S. *et al.* (2023), Controlling Lamellarity and Physicochemical Properties of Liposomes Prepared Using a Microfluidic Device, Biomater. Sci. 11, 2419-2426 (DOI: 10.1039/D2BM01703B)

[106] Lin C. -M., Li C. -S., Sheng Y. -J. *et al.* (2012), Size-Dependent Properties of Small Unilamellar Vesicles Formed by Model Lipids, Langmuir 28, 689-700 (DOI: 10.1021/la203755v)

[107] Andra V. V. S. N. L., Pammi S. V. N., Bhatraju L. V. K. P. *et al.* (2022), A Comprehensive Review on Novel Liposomal Methodologies, Commercial Formulations, Clinical Trials and Patents, BioNanoScience 12, 274-291 (DOI: 10.1007/s12668-022-00941-x)

[108] Nsairat H., Khater D., Sayed U. *et al.* (2022), Liposomes: Structure, Composition, Types, and Clinical Applications, Heliyon 8, e09394 (DOI: 10.1016/j.heliyon.2022.e09394)

[109] Pattni B. S., Chupin V. V., Torchilin V. P. (2015), New Developments in Liposomal Drug Delivery, Chem. Rev. 115, 10938-10966 (DOI: 10.1021/acs.chemrev.5b00046)

[110] Akbarzadeh A., Rezaei-Sadabady R., Davaran S. *et al.* (2013), Liposome: Classification, Preparation, and Applications, Nanoscale Res. Lett. 8, 102 (DOI: 10.1186/1556-276X-8-102)

[111] Jash A., Ubeyitogullari A., Rizvi S. S. H. (2021), Liposomes for Oral Delivery of Protein and Peptide-Based Therapeutics: Challenges, Formulation Strategies, and Advances, J. Mater. Chem. B 9, 4773-4792 (DOI: 10.1039/D1TB00126D)

[112] Lombardo D., Kiselev M. A. (2022), Methods of Liposomes Preparation: Formation and Control Factors of Versatile Nanocarriers for Biomedical and Nanomedicine Application, Pharmaceutics 14, 543 (DOI: 10.3390/pharmaceutics14030543)

[113] Lu Y., Allegri G., Huskens J. (2022), Vesicle-Based Artificial Cells: Materials, Construction Methods and Applications, Mater. Horiz. 9, 892-907 (DOI: 10.1039/D1MH01431E)

[114] Giuliano C. B., Cvjetan N., Ayache J. *et al.* (2021), Multivesicular Vesicles: Preparation and Applications, ChemSystemsChem 3, e2000049 (DOI: 10.1002/syst.202000049)

[115] Villanueva-Flores F., Castro-Lugo A., Ramírez O. T. *et al.* (2020), Understanding Cellular Interactions with Nanomaterials: Towards a Rational Design of Medical Nanodevices, Nanotechnology 31, 132002 (DOI: 10.1088/1361-6528/ab5bc8)

[116] Vargas K. M., Shon Y. -S. (2019), Hybrid Lipid–Nanoparticle Complexes for Biomedical Applications, J. Mater. Chem. B 7, 695-708 (DOI: 10.1039/C8TB03084G)

[117] Li P., Li D., Zhang L. *et al.* (2008), Cationic Lipid Bilayer Coated Gold Nanoparticles-Mediated Transfection of Mammalian Cells, Biomaterials 29, 3617-3624 (DOI: 10.1016/j.biomaterials.2008.05.020)

[118] Thamphiwatana S., Gao W., Pornpattananangkul D. *et al.* (2014), Phospholipase A2-Responsive Antibiotic Delivery via Nanoparticle-Stabilized Liposomes for the Treatment of Bacterial Infection, J Mater Chem B 2, 8201-8207 (10.1039/C4TB01110D)

[119] Rengan A. K., Jagtap M., De A. *et al.* (2014), Multifunctional Gold Coated Thermo-Sensitive Liposomes for Multimodal Imaging and Photo-Thermal Therapy of Breast Cancer Cells, Nanoscale 6, 916-923 (DOI: 10.1039/C3NR04448C)

[120] Bhuvana M., Dharuman V. (2014), Tethering of Spherical DOTAP Liposome Gold Nanoparticles on Cysteamine Monolayer for Sensitive Label Free Electrochemical Detection of DNA and Transfection, The Analyst 139, 2467-2475 (DOI: 10.1039/C4AN00017J)

[121] Pasparakis G. (2022), Recent Developments in the Use of Gold and Silver Nanoparticles in Biomedicine, WIREs Nanomedicine Nanobiotechnology 14, e1817 (DOI: 10.1002/wnan.1817)

[122] Kang H., Buchman J. T., Rodriguez R. S. *et al.* (2019), Stabilization of Silver and Gold Nanoparticles: Preservation and Improvement of Plasmonic Functionalities, Chem. Rev. 119, 664-699 (DOI: 10.1021/acs.chemrev.8b00341)

[123] Alberti G., Zanoni C., Magnaghi L. R. *et al.* (2021), Gold and Silver Nanoparticle-Based Colorimetric Sensors: New Trends and Applications, Chemosensors 9, 305 (DOI: 10.3390/chemosensors9110305)

[124] Martin C. S., Maximino M. D., Martins J. F. V. A. *et al.* (2024), Exploring the Effects of Silver, Silica-Coated Silver, and Gold Nanoparticles on Lipid Vesicles: Insights from LUVs and GUVs, J. Mol. Liq. 406, 125081 (DOI: 10.1016/j.molliq.2024.125081)

[125] Contini C., Hindley J. W., Macdonald T. J. *et al.* (2020), Size Dependency of Gold Nanoparticles Interacting with Model Membranes, Commun. Chem. 3, 130 (DOI: 10.1038/s42004-020-00377-y)

[126] Mendozza M., Caselli L., Salvatore A. *et al.* (2019), Nanoparticles and Organized Lipid Assemblies: From Interaction to Design of Hybrid Soft Devices, Soft Matter 15, 8951-8970 (DOI: 10.1039/C9SM01601E)

[127] Zhang L., Granick S. (2006), How to Stabilize Phospholipid Liposomes (Using Nanoparticles), Nano Lett. 6, 694-698 (DOI: 10.1021/nl052455y)

[128] Wang B., Zhang L., Bae S. C. *et al.* (2008), Nanoparticle-Induced Surface Reconstruction of Phospholipid Membranes, Proc. Natl. Acad. Sci. 105, 18171-18175 (DOI: 10.1073/pnas.0807296105)

[129] Wang F., Curry D. E., Liu J. (2015), Driving Adsorbed Gold Nanoparticle Assembly by Merging Lipid Gel/Fluid Interfaces, Langmuir 31, 13271-13274 (DOI: 10.1021/acs.langmuir.5b03606)

[130] Kanwa N., Patnaik A., De S. K. *et al.* (2019), Effect of Surface Ligand and Temperature on Lipid Vesicle–Gold Nanoparticle Interaction: A Spectroscopic Investigation, Langmuir 35, 1008-1020 (DOI: 10.1021/acs.langmuir.8b03673)

[131] Liu Y., Liu J. (2016), Adsorption of Nanoceria by Phosphocholine Liposomes, Langmuir 32, 13276-13283 (DOI: 10.1021/acs.langmuir.6b03342)

[132] Liu J. (2016), Interfacing Zwitterionic Liposomes with Inorganic Nanomaterials: Surface Forces, Membrane Integrity, and Applications, Langmuir 32, 4393-4404 (DOI: 10.1021/acs.langmuir.6b00493)

[133] Pornpattananangkul D., Olson S., Aryal S. *et al.* (2010), Stimuli-Responsive Liposome Fusion Mediated by Gold Nanoparticles, ACS Nano 4, 1935-1942 (DOI: 10.1021/nn9018587)

[134] Thamphiwatana S., Fu V., Zhu J. *et al.* (2013), Nanoparticle-Stabilized Liposomes for pH-Responsive Gastric Drug Delivery, Langmuir 29, 12228-12233 (DOI: 10.1021/la402695c)

[135] Zhu D., Wang Z., Zong S. *et al.* (2018), Investigating the Intracellular Behaviors of Liposomal Nanohybrids via SERS: Insights into the Influence

of Metal Nanoparticles, Theranostics 8, 941-954 (DOI: 10.7150/thno.21173)

[136] Pornpattananangkul D., Zhang L., Olson S. *et al.* (2011), Bacterial Toxin-Triggered Drug Release from Gold Nanoparticle-Stabilized Liposomes for the Treatment of Bacterial Infection, J. Am. Chem. Soc. 133, 4132-4139 (DOI: 10.1021/ja111110e)

[137] Rengan A. K., Bukhari A. B., Pradhan A. *et al.* (2015), In Vivo Analysis of Biodegradable Liposome Gold Nanoparticles as Efficient Agents for Photothermal Therapy of Cancer, Nano Lett. 15, 842-848 (DOI:10.1021/nl5045378)

[138] Bhuvana M., Dharuman V. (2016), Influence of Alkane Chain Lengths and Head Groups on Tethering of Liposome–Gold Nanoparticle on Gold Surface for Electrochemical DNA Sensing and Gene Delivery, Sens. Actuators B Chem. 223, 157-165 (DOI: 10.1016/j.snb.2015.09.031)

[139] Park S. -H., Oh S. -G., Mun J. -Y. *et al.* (2005), Effects of Silver Nanoparticles on the Fluidity of Bilayer in Phospholipid Liposome, Colloids Surf. B Biointerfaces 44, 117-122 (DOI: 10.1016/j.colsurfb.2005.06.002)

[140] Park S. -H., Oh S. -G., Mun J. -Y. *et al.* (2006), Loading of Gold Nanoparticles inside the DPPC Bilayers of Liposome and Their Effects on Membrane Fluidities, Colloids Surf. B Biointerfaces 48, 112-118 (DOI: 10.1016/j.colsurfb.2006.01.006)

[141] Bothun G. D. (2008), Hydrophobic Silver Nanoparticles Trapped in Lipid Bilayers: Size Distribution, Bilayer Phase Behavior, and Optical Properties, J. Nanobiotechnology 6, 13 (DOI: 10.1186/1477-3155-6-13)

[142] Preiss M. R., Hart A., Kitchens C. *et al.* (2017), Hydrophobic Nanoparticles Modify the Thermal Release Behavior of Liposomes, J. Phys. Chem. B 121, 5040-5047 (DOI: 10.1021/acs.jpcb.7b01702)

[143] Von White G., Chen, Y., Roder-Hanna J. *et al.* (2012), Structural and Thermal Analysis of Lipid Vesicles Encapsulating Hydrophobic Gold Nanoparticles, ACS Nano 6, 4678-4685, (DOI: 10.1021/nn2042016)

[144] Su C. -F., Merlitz H., Rabbel H. *et al.* (2017), Nanoparticles of Various Degrees of Hydrophobicity Interacting with Lipid Membranes, J. Phys. Chem. Lett. 8, 4069-4076 (DOI: 10.1021/acs.jpclett.7b01888)

[145] Lin X., Li Y., Gu N. (2010), Nanoparticle's Size Effect on Its Translocation Across a Lipid Bilayer: A Molecular Dynamics Simulation, J. Comput. Theor. Nanosci. 7, 269-276 (DOI: 10.1166/jctn.2010.1358)

[146] Guo Y., Terazzi E., Seemann R. *et al.* (2016), Direct Proof of Spontaneous Translocation of Lipid-Covered Hydrophobic Nanoparticles through a Phospholipid Bilayer, Sci. Adv. 2, e1600261 (DOI: 10.1126/sciadv.1600261)

[147] Verma A., Uzun O., Hu Y. *et al.* (2008), Surface-Structure-Regulated Cell-Membrane Penetration by Monolayer-Protected Nanoparticles, Nat. Mater. 7, 588-595 (DOI: 10.1038/nmat2202)

[148] Van Lehn R. C., Atukorale P. U., Carney R. P. *et al.* (2013), Effect of Particle Diameter and Surface Composition on the Spontaneous Fusion of Monolayer-Protected Gold Nanoparticles with Lipid Bilayers, Nano Lett. 13, 4060-4067 (DOI: 10.1021/nl401365n)

[149] Van Lehn R. C., Ricci M., Silva P. H. J. *et al.* (2014), Lipid Tail Protrusions Mediate the Insertion of Nanoparticles into Model Cell Membranes, Nat. Commun. 5, 4482 (DOI: 10.1038/ncomms5482)

[150] Van Lehn R. C., Alexander-Katz A. (2014), Free Energy Change for Insertion of Charged, Monolayer-Protected Nanoparticles into Lipid Bilayers, Soft Matter 10, 648-658 (DOI: 10.1039/C3SM52329B)

[151] Van Lehn R. C., Alexander-Katz A. (2014), Fusion of Ligand-Coated Nanoparticles with Lipid Bilayers: Effect of Ligand Flexibility, J. Phys. Chem. A 118, 5848-5856 (DOI: 10.1021/jp411662c)

[152] Van Lehn R. C., Alexander-Katz A. (2015), Pathway for Insertion of Amphiphilic Nanoparticles into Defect-Free Lipid Bilayers from Atomistic Molecular Dynamics Simulations, Soft Matter 11, 3165-3175 (DOI: 10.1039/C5SM00287G)

[153] Atukorale P. U., Guven Z. P., Bekdemir A. *et al.* (2018), Structure–Property Relationships of Amphiphilic Nanoparticles That Penetrate or Fuse Lipid Membranes, Bioconjug. Chem. 29, 1131-1140, (DOI: 10.1021/acs.bioconjchem.7b00777)

[154] Leroueil P. R., Berry S. A., Duthie K. *et al.* (2008), Wide Varieties of Cationic Nanoparticles Induce Defects in Supported Lipid Bilayers, Nano Lett. 8, 420-424 (DOI: 10.1021/nl0722929)

[155] Zuraw-Weston S., Wood D. A., Torres I. K. *et al.* (2019), Nanoparticles Binding to Lipid Membranes: From Vesicle-Based Gels to Vesicle Tubulation and Destruction, Nanoscale 11, 18464-18474 (DOI: 10.1039/C9NR06570A)

[156] Lochbaum C. A., Chew A. K., Zhang X. *et al.* (2021), Lipophilicity of Cationic Ligands Promotes Irreversible Adsorption of Nanoparticles to Lipid Bilayers, ACS Nano 15, 6562-6572 (DOI: 10.1021/acsnano.0c09732)

[157] Huang-Zhu C. A., Sheavly J. K., Chew A. K. *et al.* (2024), Ligand Lipophilicity Determines Molecular Mechanisms of Nanoparticle Adsorption to Lipid Bilayers, ACS Nano 18, 6424-6437 (DOI: 10.1021/acsnano.3c11854)

[158] Ip S., MacLaughlin C. M., Gunari N. *et al.* (2011), Phospholipid Membrane Encapsulation of Nanoparticles for Surface-Enhanced Raman Scattering, Langmuir 27, 7024-7033 (DOI: 10.1021/la200212c)

[159] Lee J. -H., Shin Y., Lee W. *et al.* (2016), General and Programmable Synthesis of Hybrid Liposome/Metal Nanoparticles, Sci. Adv. 2, e1601838 (DOI: 10.1126/sciadv.1601838)

[160] Genç R., Clergeaud G., Ortiz M. *et al.* (2011), Green Synthesis of Gold Nanoparticles Using Glycerol-Incorporated Nanosized Liposomes, Langmuir 27, 10894-10900 (DOI: 10.1021/la201771s)

[161] Lajunen T., Viitala L., Kontturi L. -S. *et al.* (2015), Light Induced Cytosolic Drug Delivery from Liposomes with Gold Nanoparticles, J. Controlled Release 203, 85-98 (DOI: 10.1016/j.jconrel.2015.02.028)

[162] Zhang L., Sun X., Song Y. *et al.* (2006), Didodecyldimethylammonium Bromide Lipid Bilayer-Protected Gold Nanoparticles: Synthesis, Characterization, and Self-Assembly, Langmuir 22, 2838-2843 (DOI: 10.1021/la052822l)

[163] Wang M., Petersen N. O. (2015), Characterization of Phospholipid-Encapsulated Gold Nanoparticles: A Versatile Platform to Study Drug Delivery and Cellular Uptake Mechanisms, Can. J. Chem. 93, 265-271 (DOI: 10.1139/cjc-2014-0280)

[164] Sitaula S., Mackiewicz M. R., Reed S. M. (2008), Gold Nanoparticles Become Stable to Cyanide Etch When Coated with Hybrid Lipid Bilayers, Chem. Commun. 26, 3013 (DOI: 10.1039/b801525b)

[165] Olenick L. L., Troiano J. M., Vartanian A. *et al.* (2018), Lipid Corona Formation from Nanoparticle Interactions with Bilayers, Chem 4, 2709-2723 (DOI: 10.1016/j.chempr.2018.09.018)

[166] Zhang X., Pandiakumar A. K., Hamers R. J. *et al.* (2018), Quantification of Lipid Corona Formation on Colloidal Nanoparticles from Lipid Vesicles, Anal. Chem. 90, 14387-14394 (DOI: 10.1021/acs.analchem.8b03911)

[167] Chetwynd A. J., Lynch I. (2020), The Rise of the Nanomaterial Metabolite Corona, and Emergence of the Complete Corona, Environ. Sci. Nano 7, 1041-1060 (DOI: 10.1039/C9EN00938H)

[168] Zhang Y., Wu J. L. Y., Lazarovits J. *et al.* (2020), An Analysis of the Binding Function and Structural Organization of the Protein Corona, J. Am. Chem. Soc. 142, 8827-8836 (DOI: 10.1021/jacs.0c01853)

[169] Sheibani S., Basu K., Farnudi A. *et al.* (2021), Nanoscale Characterization of the Biomolecular Corona by Cryo-Electron Microscopy, Cryo-Electron Tomography, and Image Simulation, Nat. Commun. 12, 573 (DOI: 10.1038/s41467-020-20884-9)

[170] Wheeler K. E., Chetwynd A. J., Fahy K. M. *et al.* (2021), Environmental Dimensions of the Protein Corona, Nat. Nanotechnol. 16, 617-629 (DOI: 10.1038/s41565-021-00924-1)

[171] Gupta A., Ndugire W., Hirschbiegel C.-M. *et al.* (2023), Interfacing Nanomaterials with Biology through Ligand Engineering, Acc. Chem. Res. 56, 2151-2169 (DOI: 10.1021/acs.accounts.3c00255)

[172] Casals E., Pfaller T., Duschl A. *et al.* (2010), Time Evolution of the Nanoparticle Protein Corona, ACS Nano 4, 3623-3632 (DOI: 10.1021/nn901372t)

[173] Lyu K., Chen H., Gao J. *et al.* (2022), Protein Desorption Kinetics Depends on the Timescale of Observation, Biomacromolecules 23, 4709-4717 (DOI: 10.1021/acs.biomac.2c00917)

[174] Kihara S., Van Der Heijden N. J., Seal C. K. *et al.* (2019), Soft and Hard Interactions between Polystyrene Nanoplastics and Human Serum Albumin Protein Corona, Bioconjug. Chem. 30, 1067-1076 (DOI: 10.1021/acs.bioconjchem.9b00015)

[175] Lee H. (2023), Differences in Protein Distribution, Conformation, and Dynamics in Hard and Soft Coronas: Dependence on Protein and Particle Electrostatics, Phys. Chem. Chem. Phys. 25, 7496-7507 (DOI: 10.1039/D2CP05936C)

[176] Piella J., Bastús N. G., Puntes V. (2017), Size-Dependent Protein–Nanoparticle Interactions in Citrate-Stabilized Gold Nanoparticles: The Emergence of the Protein Corona, Bioconjug. Chem. 28, 88-97 (DOI: 10.1021/acs.bioconjchem.6b00575)

[177] Wang G., Wang W., Shangguan E. *et al.* (2020), Effects of Gold Nanoparticle Morphologies on Interactions with Proteins, Mater. Sci. Eng. C 111, 110830 (DOI: 10.1016/j.msec.2020.110830)

[178] Wang A., Perera Y. R., Davidson M. B. *et al.* (2016), Electrostatic Interactions and Protein Competition Reveal a Dynamic Surface in Gold Nanoparticle-Protein Adsorption, J. Phys. Chem. C 120, 24231-24239 (DOI: 10.1021/acs.jpcc.6b08469)

[179] Cedervall T., Lynch I., Lindman S. *et al.* (2007), Understanding the Nanoparticle–Protein Corona Using Methods to Quantify Exchange Rates and Affinities of Proteins for Nanoparticles, Proc. Natl. Acad. Sci. 104, 2050–2055 (DOI: 10.1073/pnas.0608582104)

[180] Okyem S., Awotunde O., Ogunlusi T. *et al.* (2021), Probing the Mechanism of Antibody-Triggered Aggregation of Gold Nanoparticles, Langmuir 37, 2993-3000 (DOI: 10.1021/acs.langmuir.1c00100)

[181] Johnston B. D., Kreyling W. G., Pfeiffer C. *et al.* (2017), Colloidal Stability and Surface Chemistry Are Key Factors for the Composition of the Protein Corona of Inorganic Gold Nanoparticles, Adv. Funct. Mater. 27, 1701956 (DOI: 10.1002/adfm.201701956)

[182] Dominguez-Medina S., Kisley L., Tauzin L. J. *et al.* (2016), Adsorption and Unfolding of a Single Protein Triggers Nanoparticle Aggregation, ACS Nano 10, 2103-2112 (DOI: 10.1021/acsnano.5b06439)

[183] Cukalevski R., Ferreira S. A., Dunning C. J. *et al.* (2015), IgG and Fibrinogen Driven Nanoparticle Aggregation, Nano Res. 8, 2733-2743 (DOI: 10.1007/s12274-015-0780-4)

[184] Neupane S., Pan Y., Takalkar S. *et al.* (2017), Probing the Aggregation Mechanism of Gold Nanoparticles Triggered by a Globular Protein, J. Phys. Chem. C 121, 1377-1386 (DOI: 10.1021/acs.jpcc.6b11963)

[185] Wattendorf U., Merkle H. P. (2008), PEGylation as a Tool for the Biomedical Engineering of Surface Modified Microparticles, J. Pharm. Sci. 97, 4655-4669 (DOI: 10.1002/jps.21350)

[186] Pelaz B., Del Pino P., Maffre P. *et al.* (2015), Surface Functionalization of Nanoparticles with Polyethylene Glycol: Effects on Protein Adsorption and Cellular Uptake, ACS Nano 9, 6996-7008 (DOI: 10.1021/acsnano.5b01326)

[187] Ashraf, S., Park J., Bichelberger M. A. *et al.* (2016), Zwitterionic Surface Coating of Quantum Dots Reduces Protein Adsorption and Cellular Uptake, Nanoscale 8, 17794-17800 (DOI: 10.1039/C6NR05805A)

[188] Alberg I., Kramer S., Schinnerer M. *et al.* (2020), Polymeric Nanoparticles with Neglectable Protein Corona, Small 16, 1907574 (DOI: 10.1002/smll.201907574)

[189] Bleher S., Buck J., Muhl C. *et al.* (2019), Poly(Sarcosine) Surface Modification Imparts Stealth-Like Properties to Liposomes, Small 15, 1904716 (DOI: 10.1002/smll.201904716)

[190] Huppertsberg A., Leps C., Alberg I. *et al.* (2022), Squaric Ester-Based Nanogels Induce No Distinct Protein Corona but Entrap Plasma Proteins into Their Porous Hydrogel Network, Macromol. Rapid Commun. 43, 2200318 (DOI: 10.1002/marc.202200318)

[191] Pozzi D., Colapicchioni V., Caracciolo G. *et al.* (2014), Effect of Polyethyleneglycol (PEG) Chain Length on the Bio–Nano-Interactions between PEGylated Lipid Nanoparticles and Biological Fluids: From Nanostructure to Uptake in Cancer Cells, Nanoscale 6, 2782 (DOI: 10.1039/c3nr05559k)

[192] Yu X., Feizpour A., Ramirez N. -G. P. *et al.* (2014), Glycosphingolipid-Functionalized Nanoparticles Recapitulate CD169-Dependent HIV-1 Uptake and Trafficking in Dendritic Cells, Nat. Commun. 5, 4136 (DOI: 10.1038/ncomms5136)

[193] Xu F., Bandara A., Akiyama H. *et al.* (2018), Membrane-Wrapped Nanoparticles Probe Divergent Roles of GM3 and Phosphatidylserine in Lipid-Mediated Viral Entry Pathways, Proc. Natl. Acad. Sci. 115, E9041-E9050 (DOI: 10.1073/pnas.1804292115)

Chapter 2

Interaction of Aromatic Amino Acid-Functionalized Gold Nanoparticles with Lipid Bilayers: Insight into the Emergence of Novel Lipid Corona Formation

2.1 Introduction

At the age of the 21st century, the use of engineered nanoparticles has been extended in the interdisciplinary area of nanotechnology and bioscience owing to their numerous biomedical application such as drug delivery, bioimaging, biosensing, and so forth *[1-4]*. As the application of nanomaterials is increasing day by day in medicinal research, there has been burgeoning interest to study the interaction of the engineered nanomaterials with living cells. When the nanomaterial comes to the vicinity of the living systems, the membrane acts as their initial point of contact and appears as the frontier between the cell and the nanoparticles *[5]*. Both the interaction and cytotoxicity of the nanoparticles are often governed by physicochemical factors of nanoparticles such as size, surface charge density, and hydrophobicity *[6-11]*. Among the diverse nanomaterials, gold nanoparticles (Au NPs) are most promising to study the intracellular processes because of their ability to show distance-dependent color to visualize the aggregation of Au NPs *[12,13]*, easily variable surface chemistry by varying surface ligands *[14-16]*, and large Hamaker constant rendering strong van der Waals interactions *[17,18]*.The frequently models used to study the interaction of the cellular membranes with Au NPs are suspended lipid vesicles and supported lipid bilayers. The suspended lipid vesicles are best suited for intracellular organelles because suspended lipid vesicles impart high lipid concentration to study nanoparticle binding, lipid

phase behavior, and membrane permeabilization using spectroscopic and cryogenic transmission electron microscopy (cryo-TEM) techniques *[18-20]*.

Theoretical studies demonstrated that neutral or hydrophobic nanoparticles can engulf into cell membranes causing membrane swelling. On the other hand, charged or hydrophilic nanoparticles can pull a large number of phospholipids away from the membrane resulting in "pore" or "hole" formation *[6,7]*. As nanoparticles drag phospholipid molecules from the membrane [6], there is a possibility of the formation of lipid coating around the nanoparticle. The layer of lipid molecules around the nanoparticles is described as "lipid corona" and is just beginning to emerge in the literature *[21-29]*. Most convenient anionic citrate functionalized Au NPs (Au-Cit NPs) do not form lipid corona upon interaction with zwitterionic and negatively charged lipid vesicles *[18,19,29]*. Our group previously established that anionic Au-Cit NPs interact strongly and stabilizes the zwitterionic lipid membrane *[19]*. Recently, it was reported that small and weakly adsorbed citrate on the Au NPs surface can be replaced by the lipid molecules, and the Au-Cit NPs typically aggregated into an ordered monolayer in the lipid bilayers *[30,31]*. On the other hand, anionic polystyrene functionalized gold nanoparticles, depending on their size, concentration, and ionic strength of the medium, adsorb to the zwitterionic supported lipid bilayer (SLB) surface and drag lipids from the SLBs to the surface of nanoparticles *[32]*. Depending upon zwitterionic and negatively charged lipid concentration, cationic poly(allylamine) hydrochloride (PAH) functionalized gold nanoparticles form patchy lipid layer on the Au NP's surface and undergo lipid-induced aggregation *[28,29,33]*. Dragging of the lipid molecules from lipid bilayer by the Au NPs is a common phenomenon in the above-mentioned studies. However, the impact of lipid coating (i.e., lipid corona) on the stability of Au NPs remains elusive. Besides all of these experimental shreds of evidence, some computer simulation studies also propose the possibility of lipid corona between certain lipids and

nanoparticles, although the role of specific functionalization (nature of ligands) or charge or size of the NPs remains controversial *[34-36]*. In this context, it is of utmost interest to investigate the possible mechanism and enlightenment into the intrinsic stability of the lipid corona. Therefore, to replicate our interest we used the single aromatic amino acids' functionalized-gold nanoparticles to study the interaction of nanoparticles with the lipid membrane and possibly the lipid corona formation. In order to investigate the interaction between the lipid vesicles and Au-AA NPs, we employed spectroscopic techniques (steady-state UV-visible and fluorescence) and state of the art imaging techniques such as confocal laser scanning microscopy (CLSM), high-resolution transmission electron microscopy (HR-TEM), and atomic force microscopy (AFM). We varied the charge and concentration of the lipid molecules to understand the nature of the interaction between nanoparticles and the vesicles. We also investigated the influence of the lipid corona formation on the colloidal stability of the nanoparticles against external stimuli like pH, ionic strength, and repetitive freeze-thaw cycles.

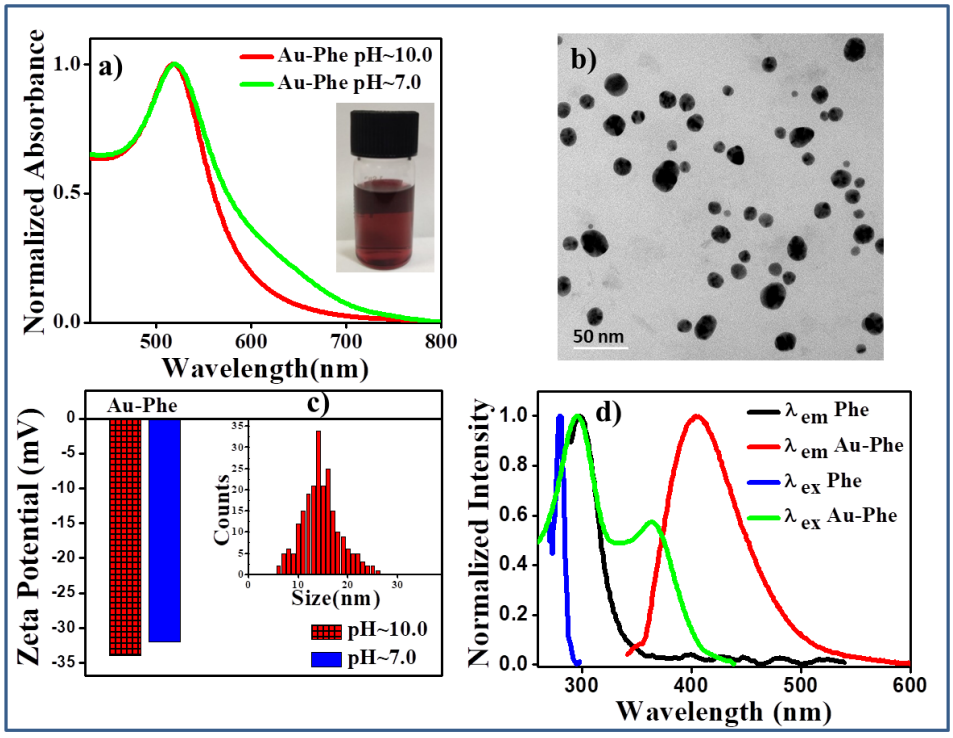

Figure 2.1 *(a) UV-Visible spectra, (b) TEM imaging, (c) zeta potential measurement (inset shows the TEM histogram data) and (d) normalized fluorescence excitation and emission spectra of blank phenylalanine (Phe) and phenylalanine functionalized Au NPs (Au-Phe NPs).*

2.2 Results and Discussion

2.2.1 Synthesis and characterization of the aromatic amino acid functionalized gold nanoparticles (Au-AA NPs):

We synthesized different aromatic amino acids (namely phenylalanine, tyrosine, and tryptophan) functionalized gold nanoparticles following an in situ method where the amino acids acted as both reducing and stabilizing agents (Experimental Methods). We purposefully avoided the replacement of citrate from Au-Cit by amino acid because this method may lead to the partial replacement of citrate and make Au-AA NPs unstable *[37]*.

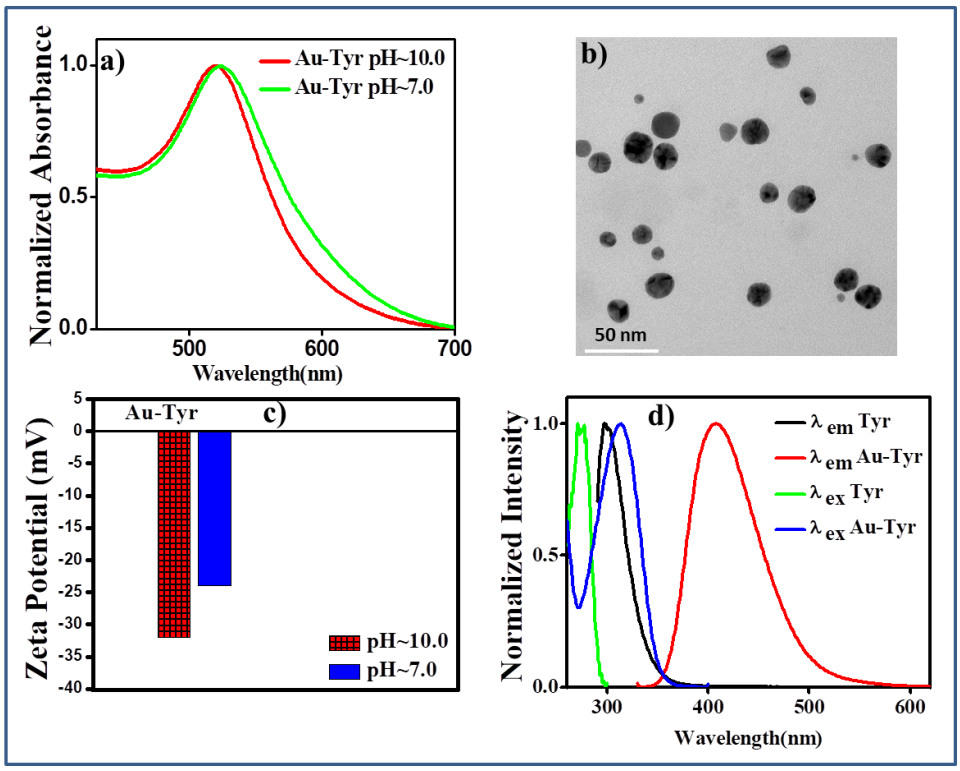

Figure 2.2 *(a) UV-Visible spectra, (b) TEM imaging, (c) zeta potential measurement and (d) normalized fluorescence excitation and emission spectra of blank tyrosine (Tyr) and tyrosine functionalized Au NPs (Au-Tyr NPs).*

The formation of aromatic amino acid functionalized colloidal Au NPs (Au-AA NPs) was confirmed by the appearance of surface plasmon resonance (SPR) band from the UV-Visible spectra at reaction conditions, that is pH ~ 10, and the colloidal property of Au-AA NPs remained stable even at pH ~ 7 (**Figure 2.1a, 2.2a, and 2.3a**). The TEM images (**Figure 2.1b, 2.2b, and 2.3b**) and the corresponding histogram data (**inset of Figure 2.1c**) revealed that nanoparticles had a core diameter around 12-15 nm with uniform size distribution.

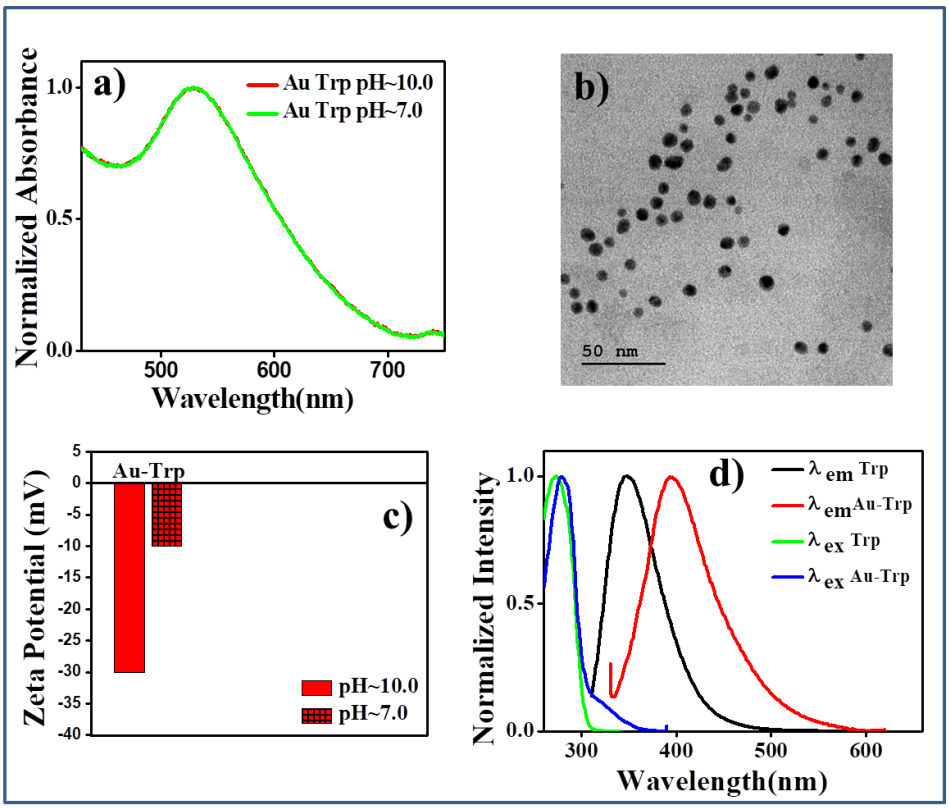

Figure 2.3 *(a) UV-Visible spectra, (b) TEM imaging, (c) zeta potential measurement and (d) normalized fluorescence excitation and emission spectra of blank tryptophan (Trp) and tryptophan functionalized Au NPs (Au-Trp NPs).*

The negative zeta potential for the Au-AA NPs at pH ~ 10 and pH ~ 7 (**Figure 2.1c, 2.2c, and 2.3c**) indicated that the $-COO^-$ group of the amino acids was likely exposed toward the bulk. All of the Au-AA NPs exhibited similar zeta potential at pH ~ 10, however, the surface charge for the Au-

Phe (-32 mV) and Au-Tyr NPs (-24 mV) was higher compared to that for Au-Trp NPs (-10 mV) at pH ~ 7. The excitation and emission spectra of Au-AA NPs and blank amino acids were shown in **Figure 2.1d, 2.2d, and 2.3d** which indicated that the excitation and the emission property of the Au-AA NPs exhibited significant differences from the blank amino acids.

2.2.2 Interaction of the aromatic amino acid functionalized gold nanoparticles with different charged lipid bilayers:

To investigate the interaction of Au-AA NPs with lipid vesicles, we varied the surface charge of the lipid vesicles from pure zwitterionic DMPC to positively charged DMPC/DMTAP (70/30) and negatively charged DMPC/DMPG (70/30) lipid mixture at physiological pH. The fixed concentration of Au-AA NPs (20 nM) solution was incubated overnight with different concentrations (0.0125-0.40 mM) of lipid vesicles at room temperature (25 °C) to achieve the equilibrium for all the experiments. The nanoparticles-lipid vesicles interactions were monitored through UV-Visible and fluorescence spectroscopy as a function of the number ratio of the Au-AA NPs/vesicles (**Table 2.1, and experimental methods**) *[29,38]*.

Concentration of Au-AA NPs (nM)	Number of Au-AA NPs /mL	Concentration of lipid (mM)	N_{tot}	N_{lipo}	number ratio of Au-AA NPs : liposomes
20	6.023×10^{12}	0.4	97,389.01	2.469×10^{12}	2: 1
20	6.023×10^{12}	0.2	97,389.01	1.236×10^{12}	5: 1
20	6.023×10^{12}	0.1	97,389.01	6.184×10^{11}	10: 1
20	6.023×10^{12}	0.05	97,389.01	3.092×10^{11}	20: 1
20	6.023×10^{12}	0.025	97,389.01	1.546×10^{11}	40:1
20	6.023×10^{12}	0.0125	97,389.01	7.730×10^{10}	80:1

Table 2.1 *Calculation of the number ratio of Au-AA NPs: liposomes. Where N_{tot} is the total number of lipid molecules per liposome and N_{lipo} is the total number of liposomes per mL for a known concentration of lipids*.

It was observed that upon interaction with the low concentration (0.0125 mM) of zwitterionic DMPC lipid vesicles [i.e., Au-Phe NPs/DMPC (80:1)], Au-Phe NPs underwent visual aggregation (color change along with

sedimentation, **Figure 2.4a**) with a new broadened peak that appeared at a longer wavelength ranging between 547 to 650 nm (**Figure 2.4b**).

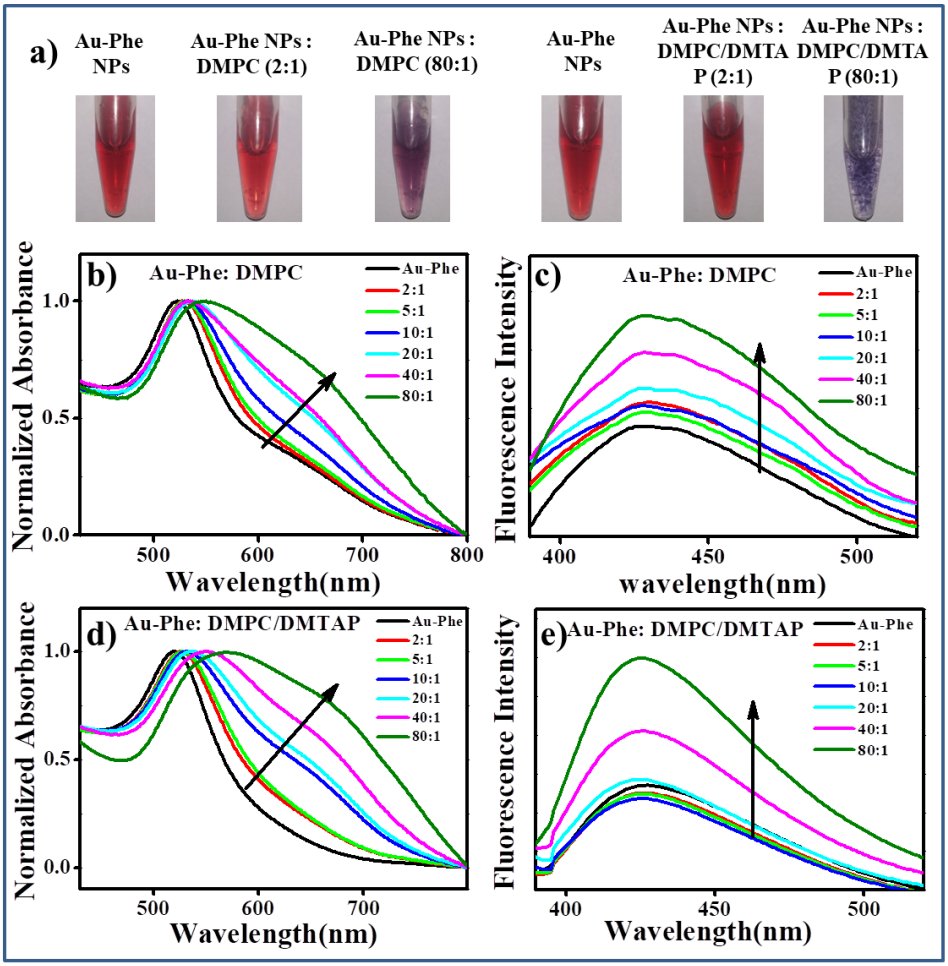

Figure 2.4 *(a) Photograph of Au-Phe NPs mixed with various concentrations of DMPC and DMPC/DMTAP liposomes. Normalized UV-Visible and steady-state fluorescence spectra of the variation of Au-Phe NPs/liposome in zwitterionic DMPC (b, c) and positively charged DMPC/DMTAP (d, e) lipid vesicles.*

On the other hand, when nanoparticles were incubated with higher concentration (0.4 mM) of zwitterionic lipid vesicles [i.e., Au-Phe NPs/DMPC (2:1)], we did not observe any visual aggregation of Au-Phe NPs (**Figure 2.4a**). However, the UV-Visible spectra of the Au-Phe NPs in the presence of high lipid concentration showed a slight red-shifted (~5 nm) SPR peak (**Figure 2.5**). Thus, we concluded that at low zwitterionic lipid concentration, Au-Phe NPs undergo lipid-induced aggregation whereas at

high lipid concentration, NPs were stable. The steady-state fluorescence data also revealed that there is a successive enhancement of fluorescence intensity as a function of nanoparticle aggregation (**Figure 2.4c**). The increment in the fluorescence intensity could be attributed to the increase in the local concentration followed by aggregation-induced emission of the amino acid upon the aggregation of nanoparticles.

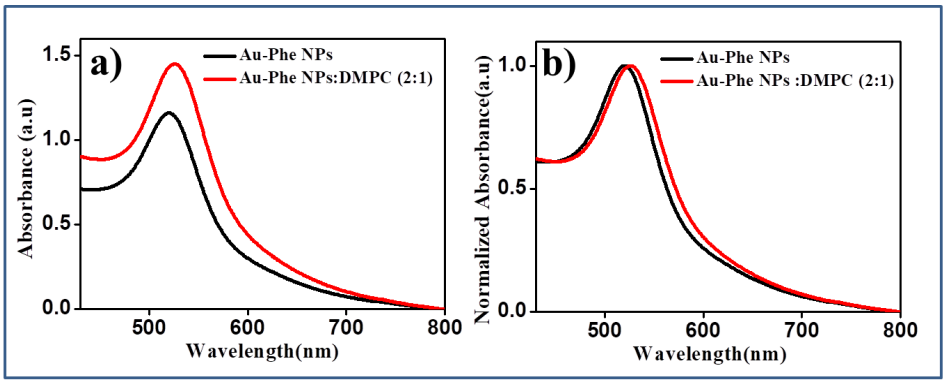

Figure 2.5 *UV-Visible absorbance (a) and Normalized UV-Visible absorbance (b) spectra of Au-Phe NPs in the absence and presence of high DMPC lipid concentration [Au-Phe NPs: DMPC(2:1)].*

Next, we varied the surface charge of liposomes by introducing the positively charged and negatively charged lipid vesicles in order to understand the underlying mechanism of the interaction between Au-Phe NPs and lipid vesicles. For the low concentration of positively charged lipid vesicles (DMPC/DMTAP), we observed a rapid and much more prominent aggregation than zwitterionic lipid vesicles (**Figure 2.4d, e**) indicating the interaction between Au-Phe NPs and lipid membrane was primarily governed by electrostatic force. This conclusion was further supported by the fact that Au-Phe NPs did not undergo aggregation at any concentration of negatively charged lipid vesicles (DMPC/DMPG) despite the prolonged incubation (**Figure 2.6a, b**).

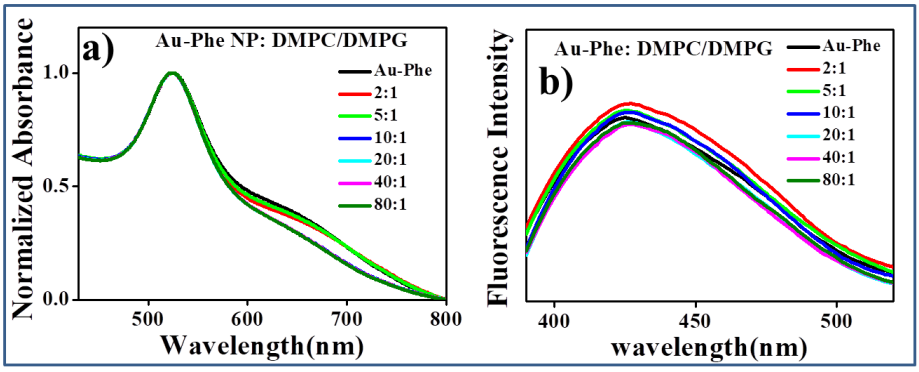

Figure 2.6 *Normalized UV-Visible (a) and Steady-state fluorescence spectra (b) of the variation of number ratio of the Au-Phe NP: liposome in negatively charged (DMPC/DMPG) lipid vesicles.*

The time-dependent aggregation of the Au-Phe NPs revealed that in the presence of zwitterionic DMPC vesicles, Au-Phe NPs slowly underwent aggregation within 4 h at very low [Au-Phe NPs/DMPC (80:1)] to moderate concentration [Au-Phe NPs/DMPC (20:1)] of lipid vesicles, while NPs were fairly stable over a period of 15 days (data not shown) at high concentration of lipid vesicles [Au-Phe NPs/DMPC (2:1)] (**Figure 2.7a, b**). On the other hand, aggregation was found to be instantaneous when a low concentration of positively charged vesicles (DMPC/DMTAP, 7/3) was added to the Au-Phe NPs. Surprisingly, despite the strong electrostatic interactions we did not observe any lipid-induced aggregation at the high concentration of lipid irrespective of their charge and incubation time.

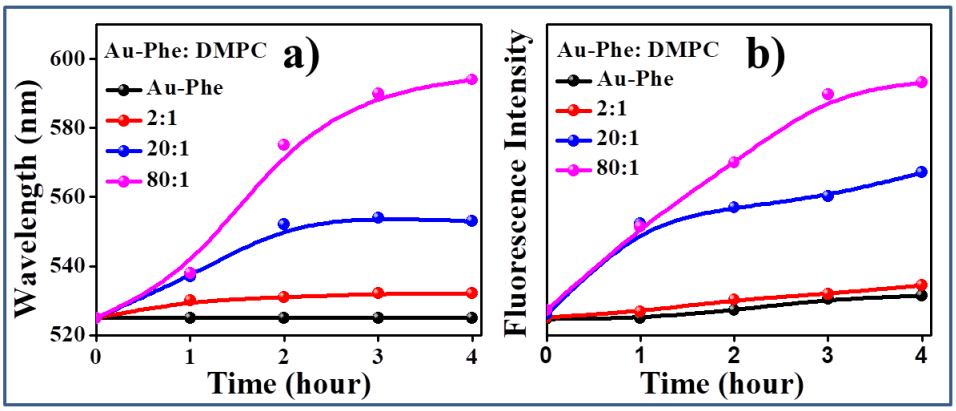

Figure 2.7 *a) UV-Visible and (b) steady-state fluorescence measurements of the time dependent aggregation of Au-Phe NPs at different number ratio of the Au-Phe NPs: liposome.*

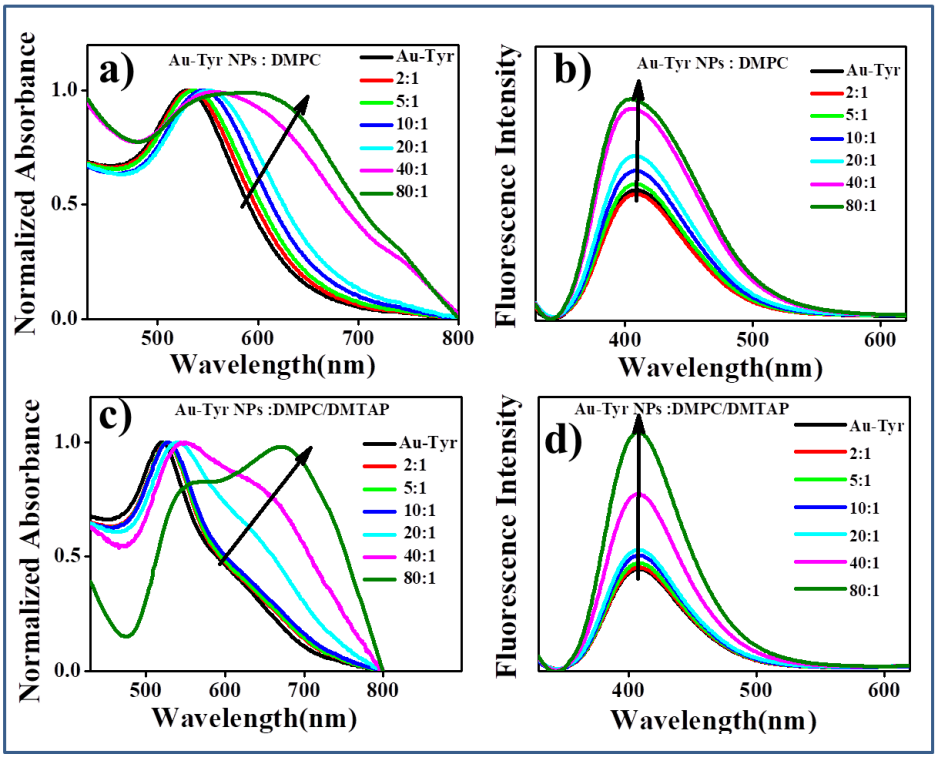

Figure 2.8 *Normalized UV-Visible and steady-state fluorescence spectra of the variation of number ratio of Au-Tyr NPs: liposome in (a, b) zwitterionic DMPC and (c, d) positively charged DMPC/DMTAP lipid vesicles.*

We observed similar phenomena in the case of Au-Tyr NPs upon interaction with the zwitterionic and positive charged lipid vesicles (**Figure 2.8a-d**). However, the Au-Trp NPs did not undergo aggregation either at any concentration of DMPC vesicles (**Figure 2.9a**). Interestingly, in the case of positively charged lipid vesicles, the Au-Trp NPs underwent instantaneous aggregation at low lipid concentration [Au-Trp NPs-DMPC/DMTAP (80:1)] whereas they were resistant toward aggregation at high lipid concentration [Au-Trp NPs-DMPC/DMTAP (2:1)] (**Figure 2.9c**). Similar to other Au-AA NPs, the Au-Trp NPs did not offer any interaction towards negatively charged DMPC/DMPG lipid vesicles (**Figure 2.9b**). Therefore, the three main features that emerge here are the following: (i) All of the

three Au-AA NPs undergo instantaneous aggregation at positively charged low lipid concentration. However, they are very much stable in the high concentration of lipid for several days. (ii) All of the three nanoparticles except Au-Trp NPs undergo slow aggregation in low to moderate concentration of zwitterionic lipid. However, they are stable at a higher concentration of lipid. (iii) The nanoparticles do not show any interaction with a negatively charged lipid. Thus, one can infer that the primary interaction between lipid vesicles and the nanoparticles is electrostatic in nature. As the zeta potential of nanoparticles is negative, the interaction is likely to take place through terminal COO^- of amino acid and charged head NR_3^+ group of the DMPC and DMPC/DMTAP. The lower surface charge of Au-Trp NPs compared to other Au-AA NPs at physiological pH may be responsible for nonaggregation behaviour at low concentration of zwitterionic DMPC lipid vesicles.

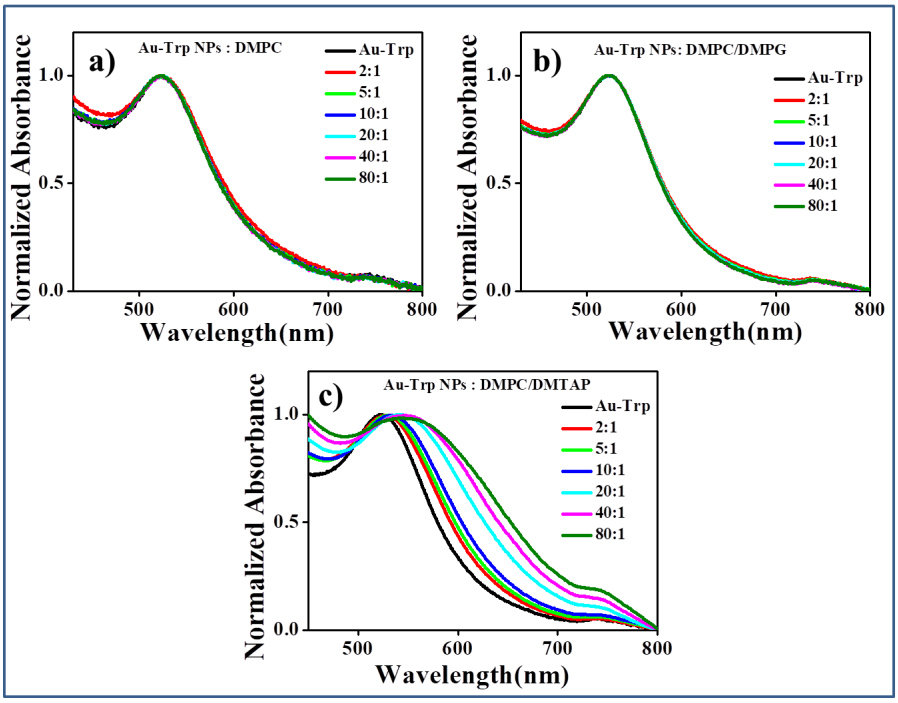

Figure 2.9 *Normalized UV-Visible spectrum in the variation of number ratio of Au-Trp NPs: liposome in (a) zwitterionic DMPC, (b) negatively charged DMPC/DMPG, and (c) positively charged DMPC/DMTAP lipid vesicles.*

2.2.3 Microscopic investigation for the stability of Au NPs at high and low lipid concentration:

Although it was evident that the Au-AA NPs underwent aggregation at low lipid concentration of zwitterionic and positively charged lipid vesicles (except Au-Trp NPs in DMPC), the spectroscopic data were not conclusive about the origin of stability and the location of the Au NPs in the presence of high lipid concentration. It also remained unclear whether the Au-AA NPs form aggregates on the liposome surface without rupturing membrane *[18]* or formed aggregates by dragging out the lipid from the lipid bilayer *[28]*. We therefore put our best effort to capture the microscopic images to account for the stability of Au NPs at high and low lipid concentration. As mentioned earlier, we took the help of three different imaging techniques (i) CLSM, (ii) HR-TEM, and (iii) AFM. As the cationic lipids brought about instantaneous aggregation to all of the Au-AA NPs, in order to capture presentable images, we focused on the DMPC-Au-AA NPs system where the aggregation was relatively much slower and can be controlled.

We started with CLSM images which revealed the morphological changes of the Au-Phe NPs at different lipid concentration. We used a fluorescent lipid probe Liss RhodPE to monitor the susceptibility of the lipid vesicles into the nanoparticle-vesicle suspensions. **Figure 2.10a-d** represented the formation of blank spherical zwitterionic lipid vesicles (DMPC) of size around 800-900 nm. We found the spherical structure of the vesicles remained almost intact at high lipid concentration [Au-Phe NPs/DMPC (2:1)] (**Figure 2.10e-h**). The faint blue signal from the inside of the few vesicles indicated that a few Au-Phe NPs were surrounded by the lipid molecules along with the presence of some elongated fibril structure which may be due to the partial replacement of phenylalanine (vide infra). However, we did not find a significant aggregation of the Au-Phe NPs in this concentration of lipid, and this observation corroborated well with the conclusion from absorption spectra (**Figure 2.4b**).

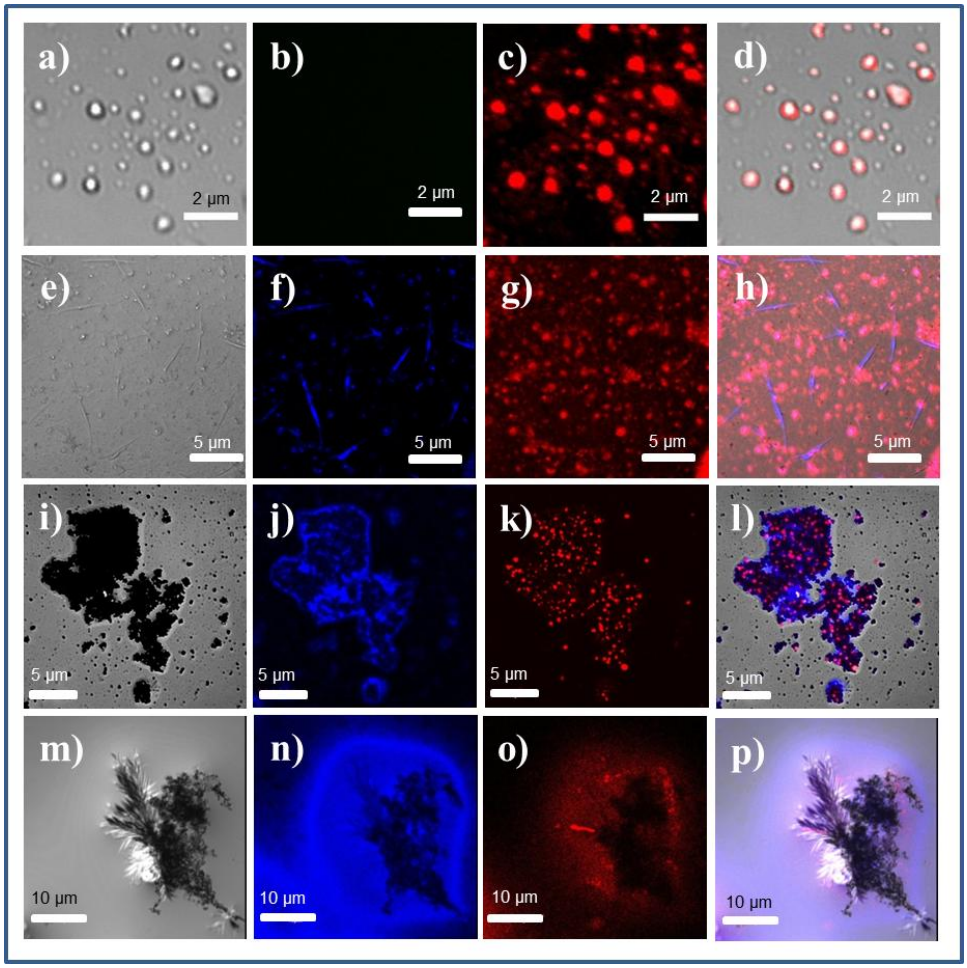

Figure 2.10 *Confocal laser scanning microscopy images of Au-Phe NPs in the presence and absence of various concentration of zwitterionic (DMPC) and positively charged (DMPC/DMTAP) lipid vesicles using the emission of Au-Phe NPs (410-460 nm) and Liss Rhod PE (570-610 nm). Bright-field, fluorescence (blue and red) and merged images for DMPC tagged with Liss Rhod PE (a-d) as a control, Au-Phe NPs/DMPC [2:1] (e-h), Au-Phe NPs/DMPC [80:1] (i-l), and Au-Phe NPs-DMPC/DMTAP [80:1] (m-p).*

On the other hand, at a low lipid concentration of DMPC [Au-Phe NPs/DMPC (80:1)], the microsized aggregates of Au-Phe NPs along with the lipid molecules were found (**Figure 2.10i-l**). The time-dependent CLSM imaging study was also performed to account for the aggregation mechanism of the Au-Phe NPs in the presence of low concentration of zwitterionic DMPC lipid vesicles. The overnight incubation of Au-Phe NPs with low concentration of DMPC lipid lead to the large aggregates of the Au-Phe NPs indicating complete lipid-induced aggregation of Au-Phe NPs,

however, the time-dependent imaging (after 2 h) revealed very small aggregates of the Au-Phe NPs along with some lipid vesicles (**Figure 2.11a-d**). The time-dependent CLSM images suggest that at the low concentration, the Au-Phe NPs first formed small aggregates along with lipid molecules and then formed larger lipid-induced aggregates of Au-Phe NPs.

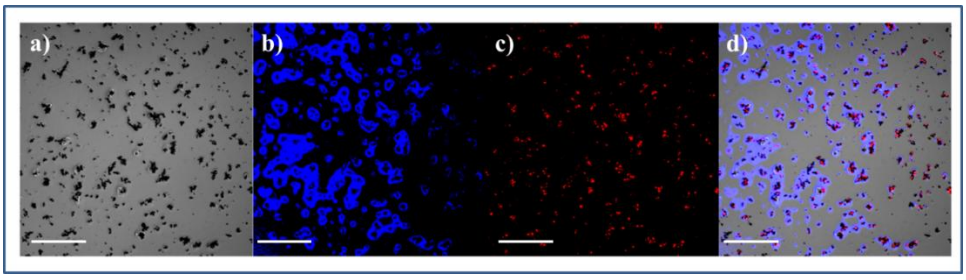

Figure 2.11 *Time-dependent CLSM imaging (after 2 hours) of Au-Phe NPs in presence of low concentration of DMPC lipid vesicles. (a) Bright field, (b) fluorescence (blue and red), and merged images for Au-Phe NP: DMPC (80:1). Scale bar is 5 µm.*

A similar observation was found with the low concentration of positively charged lipid vesicles [Au-Phe NPs-DMPC/DMTAP (80:1)] (**Figure 2.10m-p**). This aggregation behavior was in accordance with the recent report of Olenick and co-workers who reported that positively charged polymer (PAH) wrapped gold nanoparticles also showed sub- or supermicron size aggregates in the presence of negatively charged lipid vesicles *[28]*. In addition to the rapid formation of sub- or supermicron size aggregates (visual aggregation) of Au-Phe NPs, we also observed some of the prominent fibril structure of Phe as shown in **Figure 2.10m-p**. Aromatic amino acids have the excellent ability to form amyloid-like fibril structure *[39]*. In our previous study, we also observed that phenylalanine molecule can self-assemble into fibril structure even in the presence of lipid vesicles *[40]*. So, the appearance of fibril structure indicated that the strong electrostatic interaction between Au-Phe NPs and positively charged bilayer may influence the lipid molecules to replace the large number of phenylalanine molecules which self-assemble into fibril structure. The negligible presence of fibril structure in the case of zwitterionic lipid

vesicles indicated that the DMPC vesicles were less likely to replace the Phe molecules from the Au-Phe NPs surface. The CLSM images of tyrosine-functionalized gold nanoparticles at low lipid concentration of neutral and positively charged lipid vesicles were shown in **Figure 2.12a-h** which also confirmed the sub- or supermicron aggregates of the Au NPs. Although CLSM images established the lipid-induced aggregation, we were unable to get insight into the location of the Au NPs in lipid bilayer at high lipid concentration.

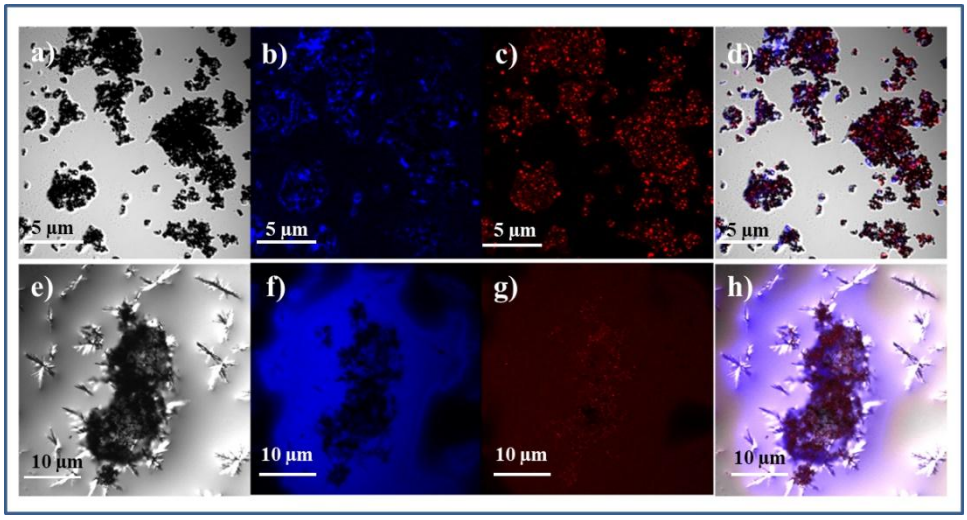

Figure 2.12 *Confocal laser scanning microscopy images of Au-Tyr NPs in presence of low concentration of zwitterionic DMPC and positively charged DMPC/DMTAP lipid vesicles using the emission of Au-Tyr NPs (410-460 nm) and Liss Rhod PE (570-610 nm). Bright field, fluorescence (blue and red), and merged images for the number ratio of Au-Tyr NPs: DMPC (80:1) (a-d), Au- Tyr NPs: DMPC/DMTAP (80:1) (e-h).*

Therefore, we took the help of HR-TEM imaging to get a conclusive view of the morphology of Au-Phe NPs in the presence of high and low lipid concentration. The HR-TEM images revealed that gold nanoparticles in the presence of a low concentration of DMPC lipid vesicles [Au-Phe NPs/DMPC (80:1)] underwent aggregation as shown in the **Figure 2.13c** which has a close resemblance to corresponding CLSM image. Interestingly, the enlarged TEM image (**Figure 2.13d or 2.14**) revealed that unlike bare Au-Phe NPs (**Figure 2.13a, b**), there is a partial or thin lipid

coating all around the nanoparticle at low concentration of DMPC lipid vesicles. However, in the presence of a high concentration of DMPC lipid vesicles [Au-Phe NPs/DMPC (2:1)], we found a much thicker and more prominent lipid coating all around the colloidal stable Au-Phe NPs (**Figure 2.13e, f**). It is well-known that the thickness of a lipid bilayer is about 4.5 nm. However, the measured lipid layered thickness for Figure **2.13e** ranges from 1.6 to 2.4 nm and for **Figure 2.13f** ranges from 3.5 to 4.9 nm, indicating a variable thickness of lipid over the NP's surface.

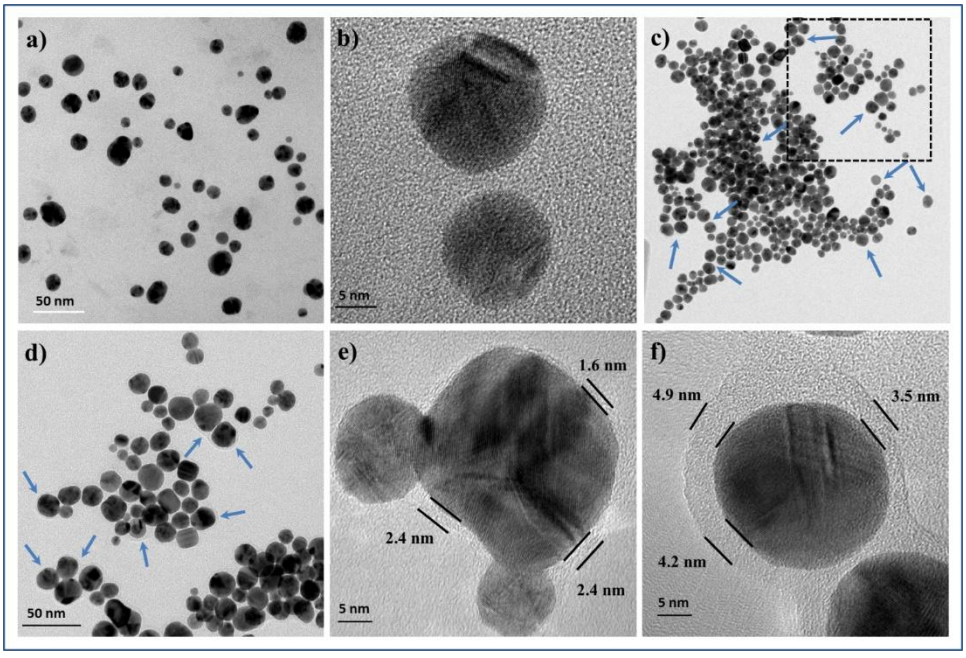

Figure 2.13 *HR-TEM images of the bare Au-Phe NPs (a, b), lipid-induced aggregation of the Au-Phe NPs (c, d), and panel d is the enlarged image of panel c in the presence of low DMPC lipid concentration ([Au-Phe NPs/DMPC (80:1)]) and the formation of lipid corona in the presence of high DMPC lipid concentration ([Au-Phe NPs/DMPC (2:1)]) (e, f). We manually draw the lines to indicate the thickness of the lipid coating around the Au-Phe NPs.*

Further AFM imaging was used to gain a deeper insight into the structural aspects of the Au-Phe NPs after interaction with zwitterionic (DMPC) lipid vesicles. This technique was applied on native Au-Phe NPs and Au-Phe NPs incubated with a high and low concentration of DMPC lipid vesicles.

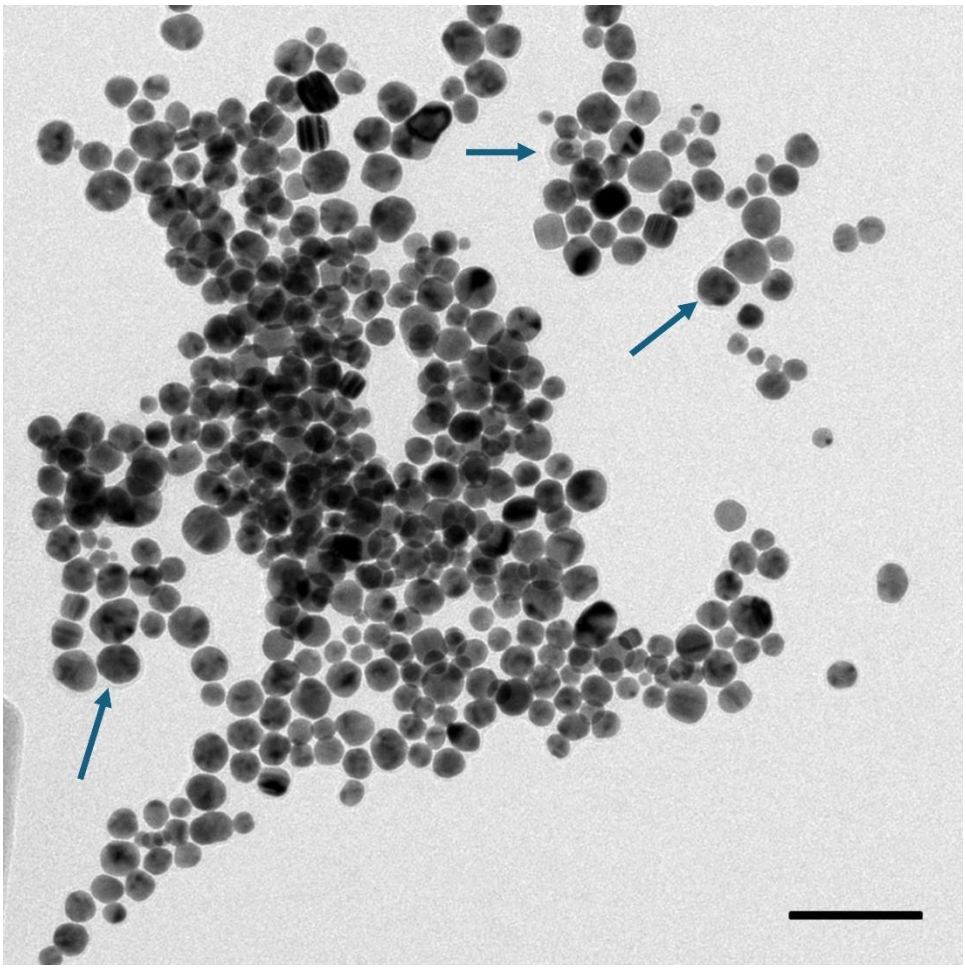

Figure 2.14 *HR-TEM image of Au-Phe NPs in presence of low concentration of DMPC lipid vesicles. This image is also provided in figure 2.13c. Here, we present the same image for a clearer view of lipid coating (blue arrow) on the surface of the nanoparticles. The scale bar is 50 nm.*

Cross-section analysis of the AFM image revealed that the native Au-Phe NPs showed a single-humped peak with a core diameter of 10-14 nm (**Figure 2.15**). This observation is in accordance with the size obtained from the TEM image. Careful examination of the surface of the Au-Phe NPs in the presence of high concentration of zwitterionic (DMPC) lipid vesicles showed that the Au-Phe NPs were coated by the lipid bilayer (**Figure 2.16a, c**). The cross-section analysis of the AFM imaging revealed the presence of three humped peaks of the lipid-coated Au-Phe NPs with the diameter of 10-16 nm which corresponds to Au-Phe NPs and 4-8 nm corresponding to

lipid bilayer thickness respectively (**Figure 2.16b, d**). Therefore, we believe that in the presence of lipid vesicles, the Au-Phe NPs have the intrinsic ability to form a lipid layer around themselves, and this layer of lipid around the Au NPs was referred to as a lipid corona *[28, 29]*.

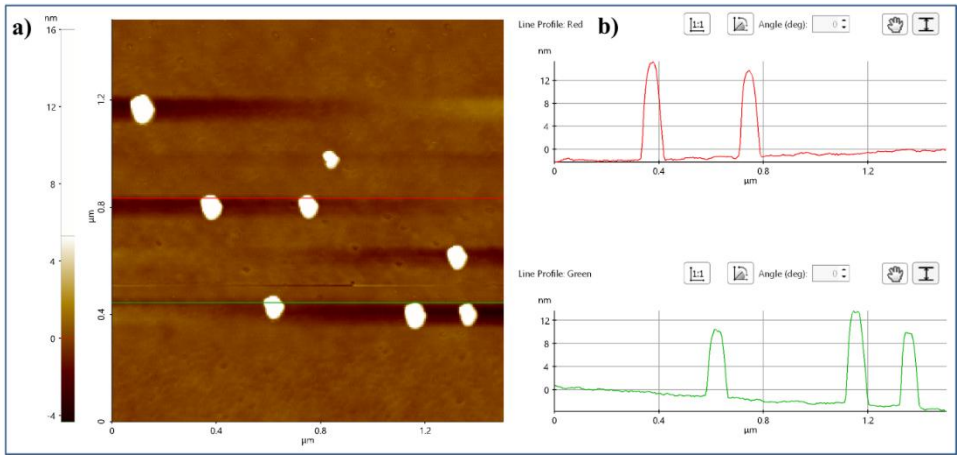

Figure 2.15 *Atomic force microscopy imaging (a) and corresponding cross-section area analysis (b) of the blank Au-Phe NPs.*

The HR-TEM analysis (**Figure 2.13**) and AFM images (**Figure 2.16 and 2.17**) indicated that in the presence of high lipid concentration, NPs can form a lipid corona of higher thickness all over the surface, whereas in the presence of low lipid concentration, NPs were partially coated by the monolayer. Interestingly, we observed that the available lipid concentration to the Au NPs can significantly influence the thickness of the lipid layer. In the presence of high lipid concentration, it is possible that Au NPs are preferably coated with a lipid "bilayer" or multilayer (≥4.5 nm); however, in some cases we found a thickness of a monolayer (~2.4 nm) over the Au NPs surface. The variable thickness of lipid over the surface of nanoparticles (at high lipid concentration) and the presence of lipids on the aggregated nanoparticles (at low lipid concentration) lead us to conclude that partial lipid coating over the NP's surface is an intermediate step toward the lipid-induced aggregation at low lipid concentration and a lipid corona formation at high lipid concentration.

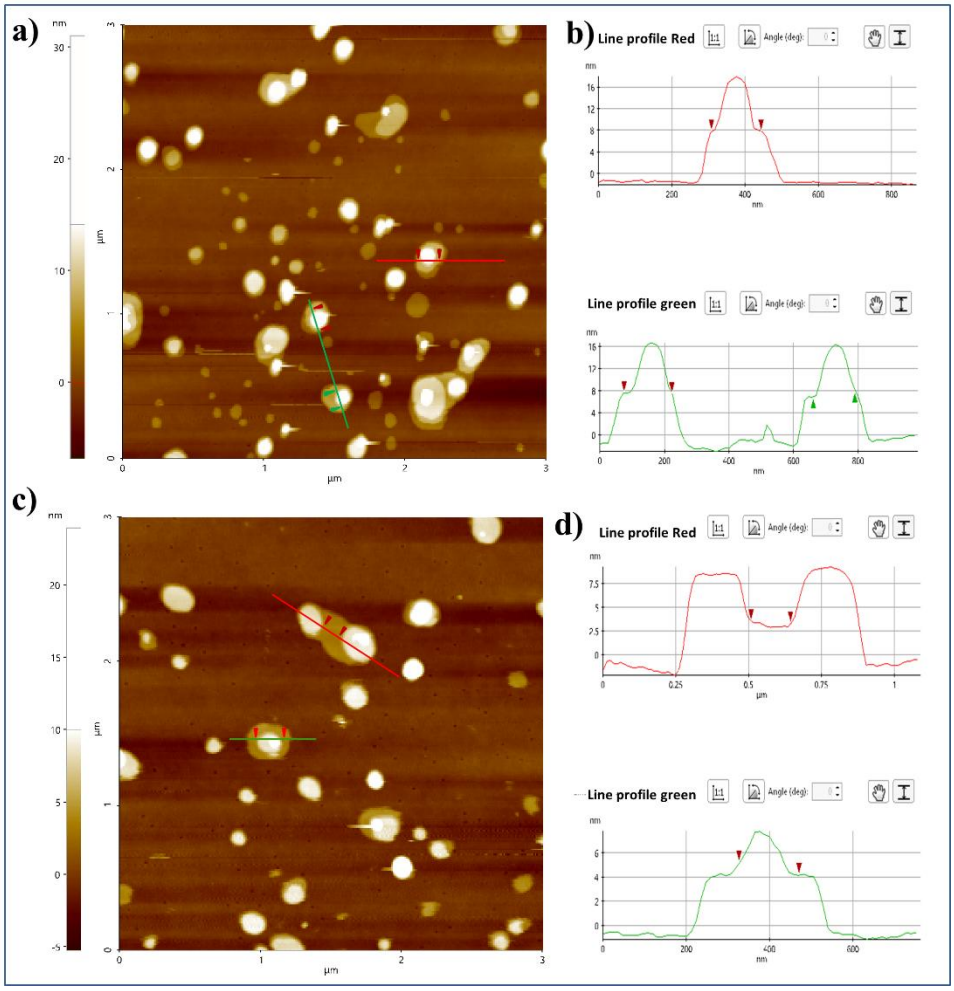

Figure 2.16 *AFM imaging (a, c) and corresponding cross-section area analysis (b, d) of the Au-Phe NPs in the presence of high DMPC lipid concentration [Au-Phe NPs/DMPC (2:1)].*

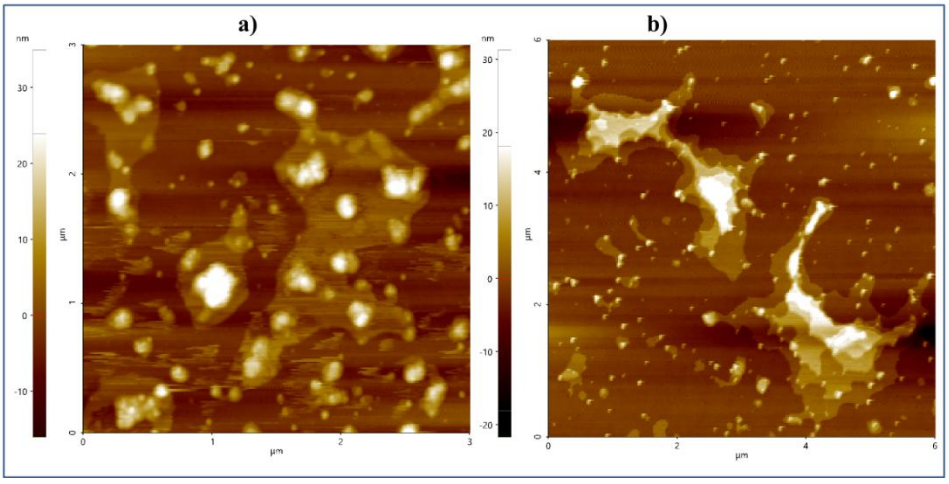

Figure 2.17 *Atomic force microscopy imaging (a, b) of the Au-Phe NPs in presence of low DMPC lipid concentration [Au-Phe NPs: DMPC (80:1)].*

One important question which needs to be addressed is whether the lipid molecules replace the surface ligands of the NPs? The CLSM imaging study revealed that at high lipid concentration where the lipid-coated nanoparticle or lipid corona is well-formed, we did not find a significant presence of fiber structure indicating that at high lipid concentration the lipid molecules do not replace the surface ligands. However, the appearance of fiber structure in the case of low DMPC and DMPC/DMTAP indicates that the replacement of surface ligand completely depends on the electrostatic interaction which pulls out the amino acids from the nanoparticles.

2.2.4 Stability of lipid corona against external stimuli:

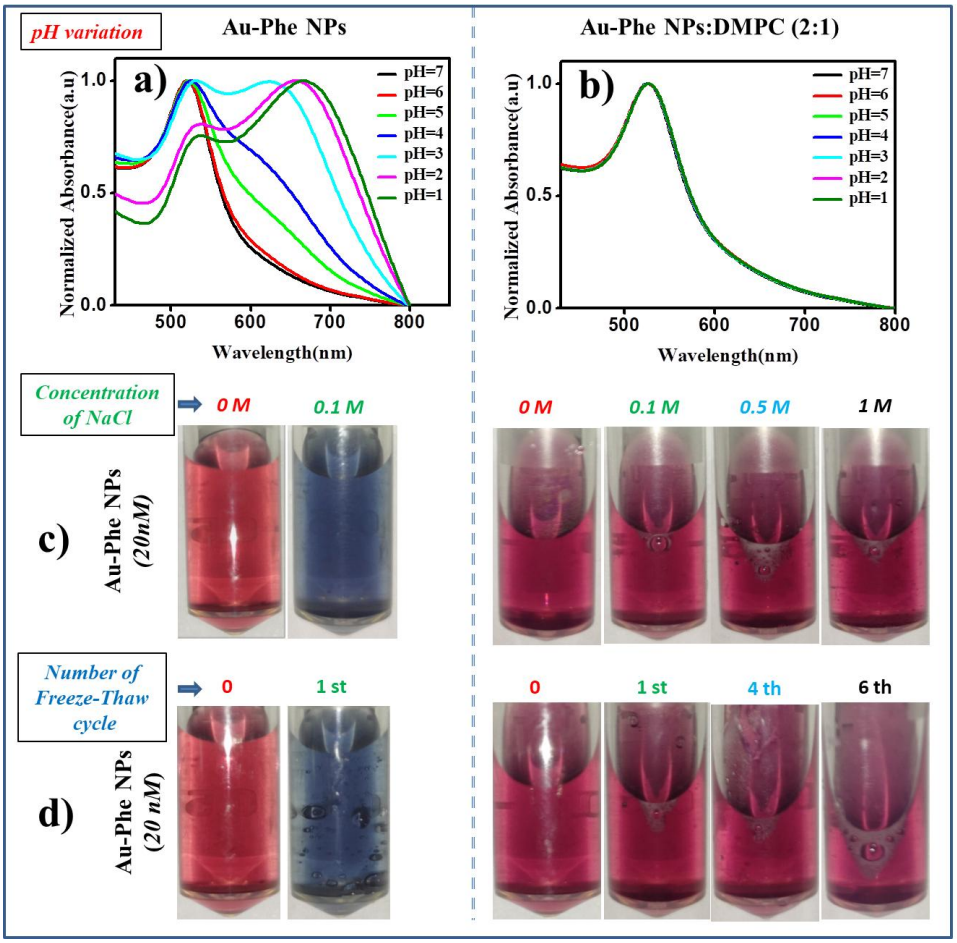

Figure 2.18 *Normalized UV-Visible spectra of (a) blank Au-Phe NPs and (b) Au-Phe NPs in the presence of high concentration of DMPC lipid vesicles against pH variation. Photograph of Au-Phe NPs in the absence and presence of high concentration DMPC lipid vesicles against (c) NaCl concentration and (d) repetitive freeze-thaw cycles.*

The lipid coating or corona formation may impact the stability of the nanoparticles against external stimuli. Therefore, we were interested in the stability of the lipid-coated Au-AA NPs over native Au-AA NPs against external stimuli (pH, salt, and freeze-thaw) which may help to use them in broad biomedical applications. We first studied the pH-dependent response of the Au-Phe NPs in the presence of high lipid concentration [Au-AA NPs/lipid (2:1)] and compared with that of native Au-Phe NPs. The native Au-Phe NPs at physiological pH were found to undergo instantaneous aggregation with the decrease in pH. The UV-Visible spectra of the bare Au-Phe NPs showed that at reduced pH, a new broadened peak appeared in the near-infrared region (at 650-730 nm) along with the primary SPR peak indicating the aggregation of bare Au-Phe NPs (**Figure 2.18a**). However, the same NPs in the presence of high lipid concentration [Au-Phe NPs/lipid (2:1)] were stable as evident from UV-Visible spectra which revealed no spectral SPR peak shift even at very low pH (∼1.0) (**Figure 2.18b**). Interestingly, Murphy et al. previously showed that the lipid "bilayer" coated PAH-Au NPs were highly stable against aggregation over a large pH range compared to their native Au NPs *[33]* which is accordance with our results. After investigating the effect of pH, we were keen to study the stability of the Au-Phe NPs at high lipid concentration compared to the native Au-Phe NPs against salt concentration and freeze-thaw cycle. We observed that the bare Au-Phe underwent instantaneous aggregation at 0.1 M NaCl, whereas in the presence of high lipid (DMPC) concentration Au-Phe NPs remained stable even at 1 M NaCl (**Figure 2.18c**). Previously, Murphy et al. reported that the lipid-coated L-PAH Au NPs (formed by the electrostatic interaction between zwitterionic lipid and PAH Au NPs) did not undergo aggregation when AuNPs are immersed into high salt cell

media *[41]*. Apart from this, the bare Au-Phe NPs are unstable and undergo aggregation against a single freeze-thaw cycle, whereas the same nanoparticles were stable after successive six freeze-thaw cycles in high lipid concentration (**Figure 2.18d**). Thus unusual stability of NPs in the presence of a lipid over a larger pH range, salt, and the freeze-thaw cycle may stem from the fact that NPs are coated by the lipid bilayer which provides additional stability to the NPs.

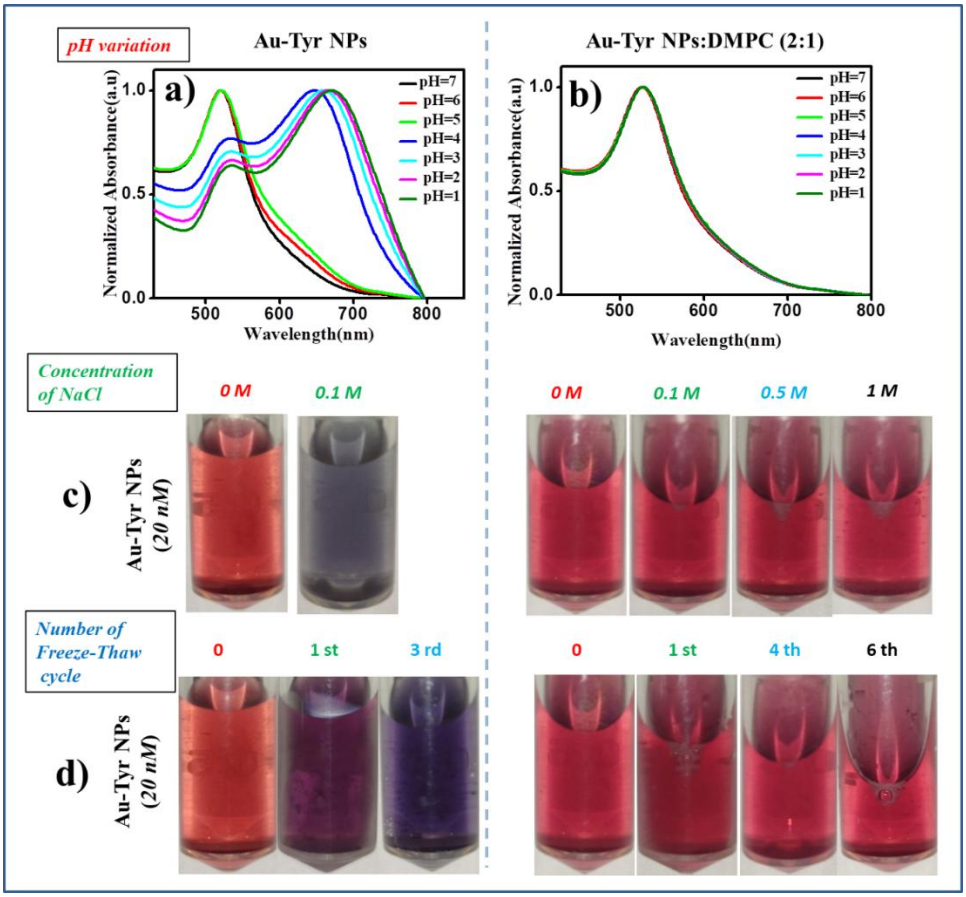

Figure 2.19 *Normalized UV-Visible spectra of a) blank Au-Tyr NPs and b) Au-Tyr NPs in presence of high concentration [Au-Tyr NPs: DMPC (2:1)] of DMPC lipid vesicles against pH variation. Photograph of Au-Tyr NPs in absence and presence of high concentration DMPC lipid vesicles against (c) NaCl concentration and (d) repetitive freeze-thaw cycles.*

Similarly, the lipid-coated Au-Tyr NPs also showed similar stability against external stimuli like lipid-coated Au-Phe NPs than bare Au NPs (**Figure 2.19a-d**). The drastic stability difference between the lipid-coated Au-Phe

and Au-Tyr NPs compared to their blank NPs against pH, salt concentration, and freeze-thaw cycle depicts the significance of the lipid corona formation. Interestingly, the lipid-coated Au-Trp NPs were slightly more stable than bare Au-Trp NPs but less stable than lipid-coated Au-Phe and Au-Tyr NPs against pH and salt (**Figure 2.20a-c**). However, we could not draw any conclusion for Au-Trp NPs from the freeze-thaw cycle as the bare Au-Trp NPs are also stable even after six freeze-thaw cycles (**Figure 2.20d**).

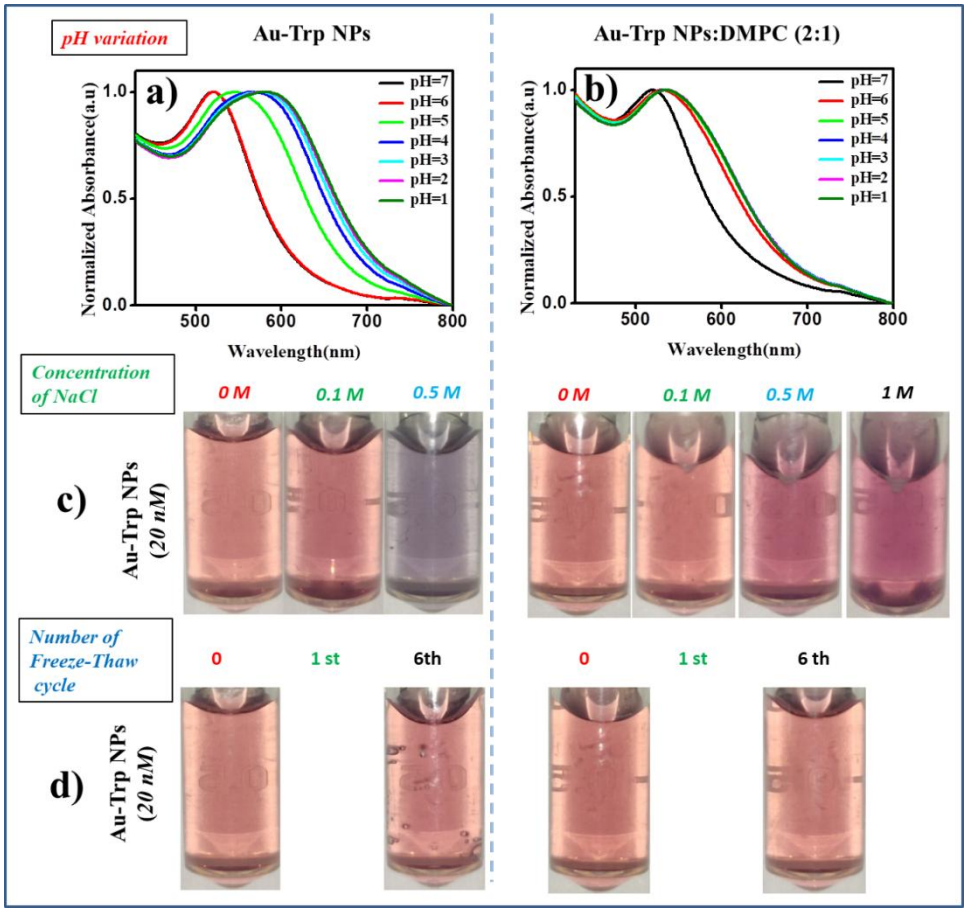

Figure 2.20 *Normalized UV-Visible spectra of a) blank Au-Trp NPs and b) Au-Trp NPs in presence of high concentration [Au-Trp NPs: DMPC (2:1)] of DMPC lipid vesicles against pH variation. Photograph of Au-Trp NPs in absence and presence of high concentration DMPC lipid vesicles against (c) NaCl concentration and (d) repetitive freeze-thaw cycles.*

This discrepancy for the tryptophan-functionalized gold nanoparticles again supports our earlier conjecture that the electrostatic interaction plays a key role for coating the nanoparticles by the lipid molecules. As the zeta

potential of the Au-Trp NPs is much lower at pH ~ 7, the electrostatic interaction between the Au-Trp NPs with zwitterionic lipid vesicles is much weaker than between other nanoparticles and lipid molecules and thus the probability of dragging the lipid molecule from lipid vesicles by the Au-Trp NPs is less. Therefore, the lipid/Au-Trp NP system does not provide so much extra stability as compared to either of the lipid/Au-Phe or lipid/Au-Tyr NPs system.

2.2.5 Mechanistic pathway of lipid corona and lipid-induced aggregates formation:

From all of our above experiments and their corresponding analysis, we draw a mechanistic pathway for the interaction between the lipid vesicles and Au-AA NPs as a function of lipid concentration (at constant Au-AA NPs concentration). It is straightforward that irrespective of gold/lipid concentration, Au NPs first adsorb on the lipid vesicles through electrostatic interaction by the positively charged headgroup ($-NR_3^+$) of the lipid and negatively charged $-COO^-$ group of Au NPs. At low lipid concentration, when the number of nanoparticles is much higher compared to the number of lipid vesicles, the large numbers of Au NPs adsorb on the lipid bilayer thus disrupt the lipid bilayer by increasing the threshold tension on the bilayer [32]. In this process, the Au NPs possibly drag the lipid molecules away from the membrane and form a partial or incomplete coating (because of less availability of lipid) of lipid molecules around the Au NPs surface, and here NPs act as the supportive surface for the lipid molecules. As the number of lipid vesicles is reduced (because of disruption of lipid vesicles by NPs) during the formation of a partial coating, the partially lipid-coated Au NPs start to undergo aggregation through the hydrophobic interaction between the tails of lipid molecules with another "partially lipid-coated" AuNP and show visible lipid-induced aggregation. We have depicted the aggregation process in **Scheme 2.1** (red accent arrow). However, when the number of nanoparticles is almost equal or lesser than the number of lipid

vesicles, the Au NPs do not undergo aggregation despite strong electrostatic interaction. In this case, initially the NPs also form a partial coating of lipid molecules through the electrostatic interaction (same as low lipid concentration). However, in order to sequester the hydrophobic tail from water, these partially lipid-coated NPs drag more numbers of lipid molecules from the lipid vesicles as there are plenty of lipid vesicles. Thus, in this way a second lipid layer associates to form the "bilayer" around the NPs, and this provides better colloidal stability than bare NPs against external stimuli (**Scheme 2.1**, blue accent arrow).

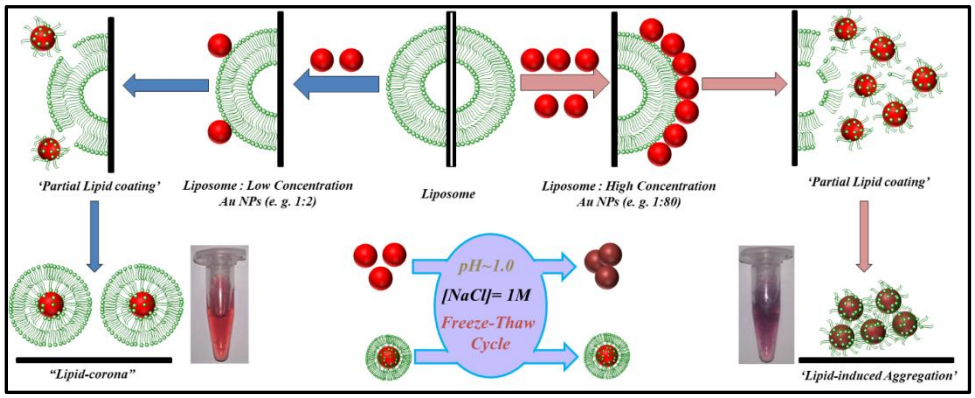

Scheme 2.1 *Schematic representation of the formation of lipid-induced aggregation and "stable lipid corona" of the Au-AA NPs through the "partial lipid coating" on the Au-AA NPs surface. Stability of the native Au NPs and lipid coated Au NPs against the external stimuli. Schematics are not drawn to scale.*

2.3 Conclusion

In summary, we observe that the novel lipid corona formation is an intrinsic property of the aromatic amino acid functionalized gold nanoparticles. The lipid corona formation is attributed to the strong electrostatic interaction between the Au-AA NPs and the lipid bilayer followed by subsequent dragging of the lipid molecules by the nanoparticles. At relatively low lipid concentration, because of insufficient availability of lipids NPs form a "partial lipid corona" which further leads to the lipid-induced aggregation of the nanoparticles. However, we found that in the presence of very high

lipid concentration the “partial lipid corona” converted into the lipid corona which imparts stability to the nanoparticles against harsh external influences like change in pH, ionic strength, and repetitive freeze-thaw cycles. The microscopic analysis also indicates that the “partial lipid corona” is one of the intermediate steps for the lipid-induced aggregation. Because of their significant stability, the lipid-coated Au-AA NPs can be used as a future prospective in biomedical application. Understanding of the mechanism and the formation of lipid corona on the Au NPs surface and lipid-induced aggregation of the Au NPs can help to engineer a nanomaterial for numerous potential applications with low cytotoxicity.

2.4 References

[1] Ghosh P., Han G., De M. *et al.* (2008), Gold Nanoparticles in Delivery Applications, Adv. Drug Deliv. Rev. 60, 1307−1315 (DOI: 10.1016/j.addr.2008.03.016)

[2] Murphy C. J., Gole A. M., Stone J. W. *et al.* (2008), Gold Nanoparticles in Biology: Beyond Toxicity to Cellular Imaging, Acc. Chem. Res. 41, 1721−1730 (DOI: 10.1021/ar800035u)

[3] Saha K., Agasti S. S., Kim C. *et al.* (2012), Gold Nanoparticles in Chemical and Biological Sensing, Chem. Rev. 112, 2739−2779 (DOI: 10.1021/cr2001178)

[4] Kim D. Y., Kim M., Shinde S. *et al.* (2019), Temperature Dependent Synthesis of Tryptophan-Functionalized Gold Nanoparticles and Their Application in Imaging Human Neuronal Cells, ACS Sustain. Chem. Eng. 5, 7678-7689 (DOI: 10.1021/acssuschemeng.7b01101)

[5] Edidin M. (2003), Lipids on the Frontier: a Century of Cell-Membrane Bilayers, Nat. Rev. Mol. Cell Biol. 4, 414-418 (DOI: 10.1038/nrm1102)

[6] Ginzburg V. V., Balijepalli S. (2007), Modeling the Thermodynamics of the Interaction of Nanoparticles with Cell Membranes, Nano Lett. 7, 3716-3722 (DOI: 10.1021/nl072053l)

[7] Roiter Y., Ornatska M., Rammohan A. R. *et al.* (2008), Interaction of Nanoparticles with Lipid Membrane, *Nano Lett. 8*, 941-944 (DOI: 10.1021/nl080080l)

[8] Mendozza M., Caselli L., Salvatore A. (2019), Nanoparticles and Organized Lipid Assemblies: from Interaction to Design of Hybrid Soft Devices, Soft Matter 15, 8951-8970 (DOI: 10.1039/C9SM01601E)

[9] Contini C., Hindley J. W., Macdonald T. J. *et al. (2020),* Size Dependency of Gold Nanoparticles Interacting with Model Membranes, Commun. Chem. 3, 1-12 (DOI: 10.1038/s42004-020-00377-y)

[10] Lunnoo T., Assawakhajornsak J., Puangmali T. (2019), In Silico Study of Gold Nanoparticle Uptake into a Mammalian Cell: Interplay of Size, Shape, Surface Charge, and Aggregation, J. Phys. Chem. C 123, 3801-3810 (DOI: 10.1021/acs.jpcc.8b07616)

[11] Sun S., Huang Y., Zhou C. *et al.* (2018), Effect of Hydrophobicity on Nano-Bio Interactions of Zwitterionic Luminescent Gold Nanoparticles at the Cellular Level, Bioconjugate Chem. 29, 1841-1846 (DOI: 10.1021/acs.bioconjchem.8b00202)

[12] Iarossi M., Schiattarella C., Rea I. *et al.* (2018), Colorimetric Immunosensor by Aggregation of Photochemically Functionalized Gold Nanoparticles, ACS Omega 3, 3805-3812 (DOI: 10.1021/acsomega.8b00265)

[13] Wang X., Gogol P., Cambril E. *et al.* (2012), Near- and Far-Field Effects on the Plasmon Coupling in Gold Nanoparticle Arrays, J. Phys. Chem. C 116, 24741-24747 (DOI: 10.1021/jp306292r)

[14] Piella J., Bastus N. G., Puntes V. (2016), Size-Controlled Synthesis of Sub-10-nanometer Citrate-Stabilized Gold Nanoparticles and Related Optical Properties, Chem. Mater. 28, 1066−1075 (DOI: 10.1021/acs.chemmater.5b04406)

[15] Gao J., Huang X., Liu H. *et al.* (2012), Colloidal Stability of Gold Nanoparticles Modified with Thiol Compounds: Bioconjugation and Application in Cancer Cell Imaging, Langmuir 28, 4464−4471 (DOI: 10.1021/la204289k)

[16] Gupta A., Moyano D.F., Parnsubsakul A. *et al.* (2016), Ultrastable and Biofunctionalizable Gold Nanoparticles, ACS Appl. Mater. Interfaces 8, 14096-14101 (DOI: 10.1021/acsami.6b02548)

[17] Rance G. A., Marsh D. H., Bourne S. J. *et al.* (2010), Van der Waals Interactions between Nanotubes and Nanoparticles for Controlled Assembly of Composite Nanostructures, ACS Nano 4, 4920-4928 (DOI: 10.1021/nn101287u)

[18] Wang F., Liu J. (2015), Self-Healable and Reversible Liposome Leakage by Citrate-Capped Gold Nanoparticles: Probing the Initial Adsorption/Desorption Induced Lipid Phase Transition, Nanoscale 7, 15599-15604 (DOI: 10.1039/C5NR04805B)

[19] Kanwa N., Patnaik A., De S. K. *et al.* (2019), Effect of Surface Ligand and Temperature on Lipid Vesicle–Gold Nanoparticle Interaction: A Spectroscopic Investigation, Langmuir 35, 1008-1020 (DOI: 10.1021/acs.langmuir.8b03673)

[20] Chen K. L., Bothun G. D. (2014), Nanoparticles Meet Cell Membranes: Probing Nonspecific Interactions using Model Membranes, Environ. Sci. Technol. 48, 873-880 (DOI: 10.1021/es403864v)

[21] Kapralov A.A., Feng W.H., Amoscato A.A. *et al.* (2012), Adsorption of Surfactant Lipids by Single-Walled Carbon Nanotubes in Mouse Lung upon Pharyngeal Aspiration, ACS Nano 6, 4147-4156 (DOI: 10.1021/nn300626q)

[22] Bahrami A.H., Raatz M., Agudo-Canalejo J. *et al.* (2014), Wrapping of Nanoparticles by Membranes, Adv. Colloid Interface Sci. 208, 214-224 (DOI: 10.1016/j.cis.2014.02.012)

[23] Zhang S., Gao H., Bao G. (2015), Physical Principles of Nanoparticle Cellular Endocytosis, ACS Nano 9, 8655-8671 (DOI: 10.1021/acsnano.5b03184)

[24] Raesch S.S., Tenzer S., Storck W. *et al.* (2015), Proteomic and Lipidomic Analysis of Nanoparticle Corona upon Contact with Lung Surfactant Reveals Differences in Protein, but Not Lipid Composition, ACS Nano 9, 11872-11885 (DOI: 10.1021/acsnano.5b04215)

[25] Yu X., Feizpour A., Ramirez N.G.P. *et al.* (2014), Glycosphingolipid-Functionalized Nanoparticles Recapitulate CD169-Dependent HIV-1 Uptake and Trafficking in Dendritic Cells, Nat. Commun. 5, 4136 (DOI: 10.1038/ncomms5136)

[26] Xu F., Reiser M., Yu X. *et al.* (2016), Lipid-Mediated Targeting with Membrane-Wrapped Nanoparticles in the Presence of Corona Formation, ACS Nano 10, 1189-1200 (DOI: 10.1021/acsnano.5b06501)

[27] Xu F., Bandara A., Akiyama H. *et al.* (2018), Membrane-Wrapped Nanoparticles Probe Divergent Roles of GM3 and Phosphatidylserine in Lipid-Mediated Viral Entry Pathways, Proc. Natl. Acad. Sci. U.S.A. 115, E9041-E9050 (DOI: 10.1073/pnas.1804292115)

[28] Olenick L. L., Troiano J. M., Vartanian A. *et al.* (2018), Lipid Corona Formation from Nanoparticle Interactions with Bilayers, Chem 4, 2709-2723 (DOI: 10.1016/j.chempr.2018.09.018)

[29] Zhang X., Pandiakumar A. K., Hamers R. J. *et al.* (2018), Quantification of Lipid Corona Formation on Colloidal Nanoparticles from Lipid Vesicles, Anal. Chem. 90, 14387-14394 (DOI: 10.1021/acs.analchem.8b03911)

[30] Wang X., Wang X., Bai X. *et al.* (2018), Nanoparticle Ligand Exchange and Its Effects at the Nanoparticle–Cell Membrane Interface, Nano Lett. 19, 8-18 (DOI: 10.1021/acs.nanolett.8b02638)

[31] Montis C., Caselli L., Valle F. *et al.* (2020), Shedding Light on Membrane-Templated Clustering of Gold Nanoparticles, J. Colloid Interface Sci. 573, 204-214 (DOI: 10.1016/j.jcis.2020.03.123)

[32] Jing B., Zhu Y. (2011), Disruption of Supported Lipid Bilayers by Semihydrophobic Nanoparticles, J. Am. Chem. Soc. 133, 10983-10989 (DOI: 10.1021/ja2040305)

[33] Yang J. A., Murphy C. J. (2012), Evidence for Patchy Lipid Layers on Gold Nanoparticle Surfaces, Langmuir 28, 5404-5416 (DOI: 10.1021/la300325p)

[34] Hu M., Stanzione F., Sum A. K. *et al.* (2015), Design Principles for Nanoparticles Enveloped by a Polymer-Tethered Lipid Membrane, ACS Nano 9, 9942-9954 (DOI: 10.1021/acsnano.5b03439)

[35] Van Lehn R. C., Alexander-Katz A. (2013), Structure of Mixed-Monolayer-Protected Nanoparticles in Aqueous Salt Solution from Atomistic Molecular Dynamics Simulations, J. Phys. Chem. C 117, 20104-20115 (DOI: 10.1021/jp406035e)

[36] Van Lehn R.C., Ricci M., Silva P.H. *et al.* (2014), Lipid Tail Protrusions Mediate the Insertion of Nanoparticles into Model Cell Membranes, Nat. Commun. 5, 4482 (DOI: 10.1038/ncomms5482)

[37] Sethi M., Knecht M. R. (2009), Experimental Studies on the Interactions between Au Nanoparticles and Amino Acids: Bio-Based Formation of Branched Linear Chains, ACS Appl. Mater. Interfaces 1, 1270-1278 (DOI: 10.1021/am900157m)

[38] Das A., Adhikari C., Chakraborty A. (2016), Lipoplex-Mediated Deintercalation of Doxorubicin from Calf Thymus DNA–Doxorubicin Complex, Langmuir 32, 8889-8899 (DOI: 10.1021/acs.langmuir.6b01860)

[39] Shaham-Niv S., Adler-Abramovich L., Schnaider L. *et al.* (2015), Extension of the Generic Amyloid Hypothesis to Nonproteinaceous Metabolite Assemblies, Sci. Adv 1, e1500137 (DOI: 10.1126/sciadv.1500137)

[40] De S. K., Chakraborty A. (2019), Interaction of Monomeric and Self-Assembled Aromatic Amino Acids with Model Membranes: Self-Reproduction Phenomena, Chem. Commun. 55, 15109-15112 (DOI: 10.1039/C9CC08495A)

[41] Yang J. A., Lohse S. E., Murphy C. J. (2014), Tuning Cellular Response to Nanoparticles via Surface Chemistry and Aggregation, Small 10, 1642-1651 (DOI: 10.1002/smll.201302835)

Chapter 3

Mechanistic Pathway of Lipid Phase Dependent Lipid Corona Formation on Phenylalanine Functionalized Gold Nanoparticles: a Combined Experimental and Molecular Dynamics Simulation Study

3.1 Introduction

Understanding the interactions between nanoparticles (NPs) and biomolecules is of utmost importance for advancing biomedical applications such as NP-based drug and gene delivery, bio-imaging, bio-sensing, and tissue engineering *[1-4]*. Upon contact with biological systems, the surface of NPs rapidly adsorbs biomolecules to minimize large surface free energy *[5-9]*. Therefore, *in vivo*, instead of bare NPs, the physicochemical properties of adsorbed biomolecules determine the biological identity of nanomaterials and influence their uptake by cells and organisms *[10-14]*. The NP-biomolecule complex is often referred to as a "biomolecular corona" [14] has two major components: proteins and metabolites. The protein corona has been extensively studied in nano-bio research over past decade while the metabolite corona has been mostly overlooked to date. Phospholipids are one type of metabolites found mainly at high concentrations in cell membrane and lung surfactants, considered as the first metabolites to be encountered by nanomaterial *[15]*. The lipid (metabolite) corona has been given special attention in recent times *[15-25]*. It is well known that other than intravascular injection, NPs migrate to respiratory system through inhalation and interact with the pulmonary surfactant lining layer of alveoli *[6,14]*. The pulmonary surfactants are

composed of ~ 90% lipids -cholesterol and ~ 10% proteins *[26]*. As the nanoparticles interact with pulmonary surfactants, both protein and lipid molecules are found around the nanoparticles *[27-30]*. However, the surface potential of the monolayer counterparts of lipid bilayer is less *[31]*, so it is not well understood whether the lipid corona forms in a more generalized case of lipid bilayer.

Recently, a few studies reported the possible factors responsible for lipid corona formation on different surface-functionalized nanoparticles *[22,23, 32-35]*. Olenick and co-workers first analyzed the mechanism of lipid corona formation upon the interaction of cationic poly (allylamine) hydrochloride (PAH) functionalized gold nanoparticles (Au NPs) with zwitterionic and negatively charged supported and suspended lipid bilayers *[22]*. They reported that electrostatic interaction was crucial for lipid corona formation. Murphy and co-workers quantified the degree of lipid-binding to the PAH-Au NPs and MTAB-Au NPs (16-mercaptohexadecyltrimethylammonium bromide functionalized gold nanoparticles) and aggregation of the NPs *[23]*. The same PAH-Au NPs could undergo either lipid-corona formation or aggregation depending on the concentration of lipid used *[16,22,23]*. Apart from electrostatic interaction, hydrophobic interaction as well as size of the nanoparticles also played a significant role in formation of lipid and protein corona *[30,35-36]*. Recent work from our laboratory reported that lipid corona formation and lipid-induced aggregation predominantly depended on available lipid concentration to Au NPs and surface charge of both NPs and lipids *[37]*. We reported that aromatic amino acid functionalized gold NPs in presence of an inadequate amount of lipid underwent partial corona formation followed by lipid-induced aggregation. However, these NPs readily formed lipid corona at high lipid concentrations. Most of the literature reported different factors such as surface charges of both NPs and lipids and surface hydrophobicity of NPs as the primary driving forces for lipid corona formation. However, till now, the effect of different properties of lipids *e.g.*

lipid phase state, chain length hydrophobicity, and area per lipid head group in lipid corona formation and lipid-induced aggregation remain enigmatic in literature.

In this context, for the first time, we have investigated phase-dependent interaction of phenylalanine-functionalized gold nanoparticles by using different zwitterionic phospholipid membranes to find out plausible mechanistic pathway for the formation of lipid corona and lipid-induced aggregation. The zwitterionic lipid vesicles, namely, 1,2-dioleoyl-sn-glycero-3-phosphocholine (DOPC, T_m = -20 °C), 1,2- dilauroyl-sn-glycero-3-phosphocholine (DLPC, T_m = -1 °C), 1,2-dimyristoyl-sn-glycero-3-phosphocholine (DMPC, T_m = 23 °C), and 1,2-dipalmitoyl-sn-glycero-3-phosphocholine (DPPC, T_m = 41 °C) are selected because of wide difference in their phase transition temperatures (T_m). At room temperature (RT), DOPC and DLPC lipid bilayer remain in liquid-crystalline phase, DPPC in sol-gel phase, and DMPC near sol-gel to liquid-crystalline phase. The lipid-nanoparticles interaction and possible lipid corona formation are studied by varying the concentration of lipid in buffer medium, and in the presence of cholesterol for biological relevance. Using different spectroscopic (*e.g.* UV-Visible, steady-state fluorescence) and imaging techniques such as confocal laser scanning microscopy (CLSM), high-resolution transmission electron microscopy (HR-TEM), and atomic force microscopy (AFM), we have studied the influence of lipid properties (phase state, area per lipid head group) on lipid corona formation and lipid-induced aggregation. Subsequently, we have employed coarse-grained molecular dynamics (CGMD) simulation study to gain a deeper insight into the molecular-level understanding of lipid-nanoparticles interaction. The CGMD simulation studies have provided valuable insight into the mechanistic pathway of formation of lipid-phase dependent lipid corona and lipid-induced aggregation. Finally, the effect of the phase state of the lipid on the formation of “hard” and “soft” lipid corona has been discussed with the help of freeze-thaw cycles.

3.2 Results

3.2.1 Synthesis and characterization of the Au-Phe NPs:

We synthesized phenylalanine functionalized gold nanoparticles (Au-Phe NPs) using a method previously reported by our group, in which phenylalanine acts as both a reducing and stabilizing agent *[38]*. The formation of well-dispersed and colloidal Au-Phe NPs was confirmed by UV-Visible spectra, revealed a characteristic surface plasmon resonance (SPR) band for Au NPs in both neutral (pH~7.0) and alkaline (pH~10.0) reaction conditions (**Figure 3.1a**).

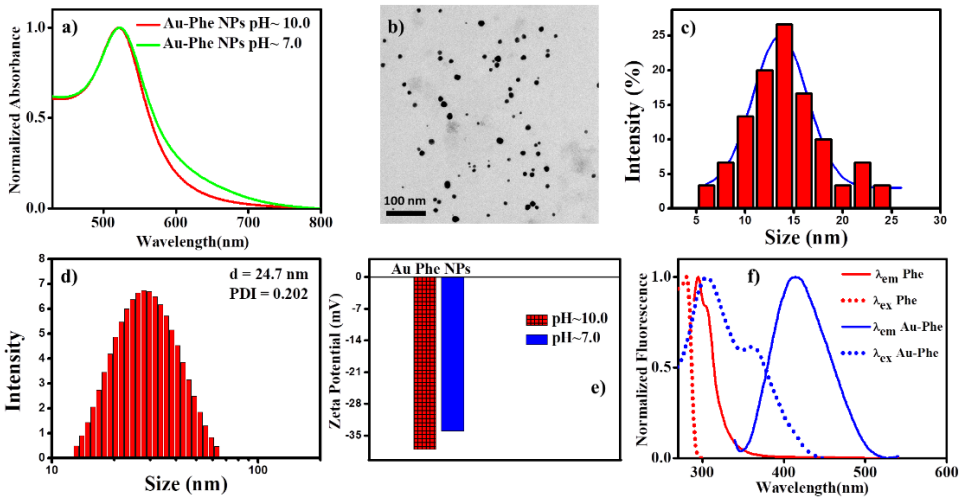

Figure 3.1 *Characterization of the Au-Phe NPs. UV-Visible spectra (a), HR-TEM imaging (b), Particle size distribution histogram using TEM imaging (c), DLS measurement (d), zeta potential measurement of the Au-Phe NPs (e), and normalized fluorescence excitation and emission spectra of blank phenylalanine (Phe) and phenylalanine functionalized Au NPs (Au-Phe NPs) (f).*

The average radius (r_c) of Au- Phe NPs was found ~ 6 ± 1 nm based on HR-TEM analysis (**Figure 3.1b, c**). However, dynamic light scattering (DLS) measurements revealed that the Au-Phe NPs had a hydrodynamic radius (r_h) of ~12 ± 1 nm (**Figure 3.1d)**. The discrepancy in size between two measurements is attributed to the fact that DLS measurement estimated the overall size of nanoparticles (pristine Au NPs along with ligand and

solvated water molecules). The amino acid (Phe) coating, surrounding the Au-Phe NPs is not observable in TEM micrographs. Therefore, difference between r_h and r_c determines the thickness of the surface coverage by surface ligands *[39-40]*. Thus we concluded that phenylalanine molecule may form a thick coating of around 6 nm during the formation of Au-Phe NPs. The zeta potential of Au-Phe NPs in neutral (pH~7) and alkaline medium (pH~10) was -34 mV and -38 mV, respectively, which implies that the COO^- are oriented towards bulk solution (**Figure 3.1e)**. The distinct fluorescence property of Au-Phe NPs from blank amino acids was attributed to the clusterization of the Phe molecules on Au-NPs surface *[38]* (**Figure 3.1f)**.

3.2.2 Phase-dependent interaction between Au-Phe NPs and lipid bilayer:

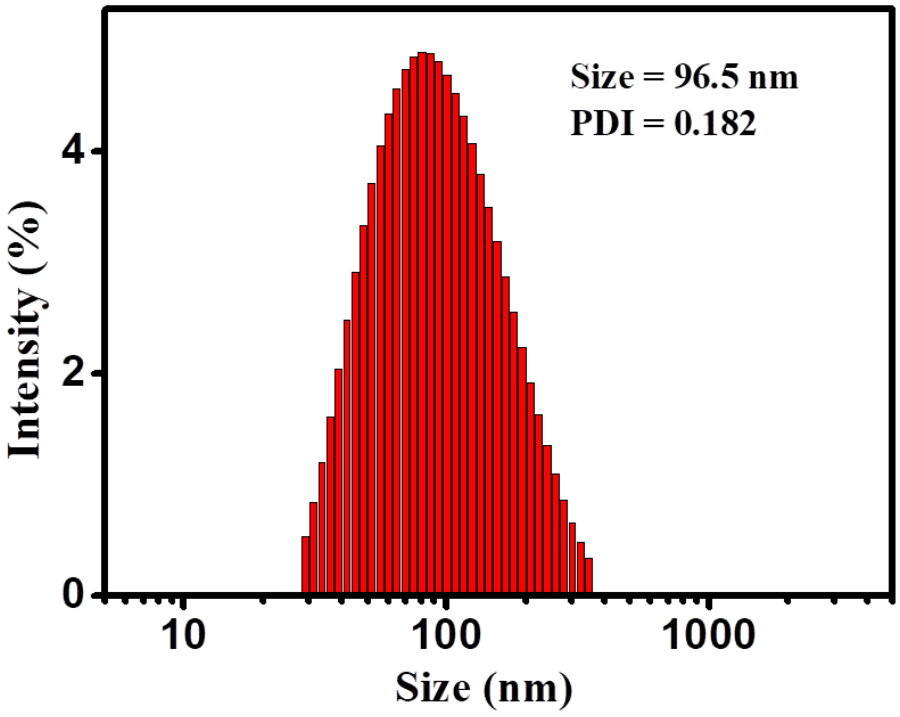

Figure 3.2 *Size distribution histogram of DMPC lipid vesicle.*

To investigate the phase-sensitivity of lipid corona and lipid-induced aggregation, the fixed concentration of Au-Phe NPs (20 nM) was incubated with high (0.4 mM) and low (0.0125 mM) concentrations of four different lipids (DOPC, DLPC, DMPC, and DPPC) in HEPES buffer at pH ~ 7.0 (I = 10 mM) at room temperature (25 °C) for 24 h to achieve the equilibrium. The size of the prepared lipid vesicles is ~ 96.5 nm (**Figure 3.2**).

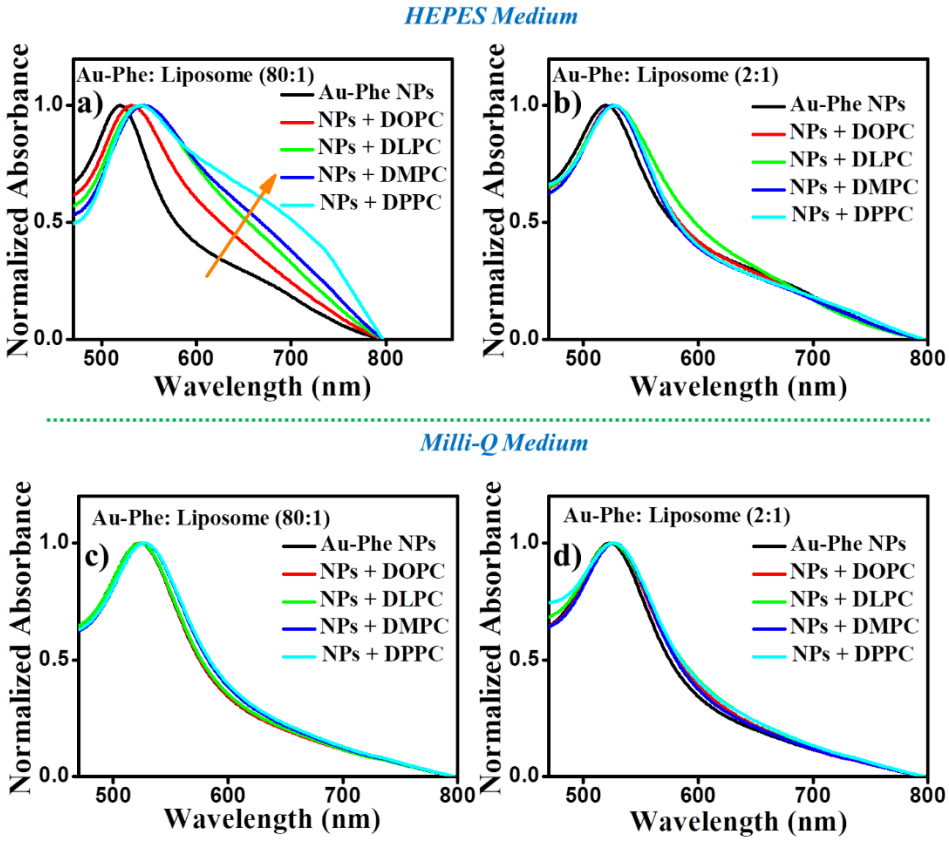

Figure 3.3 *UV-Visible spectra of blank Au-Phe NPs in the presence of low concentration (a, c) and high concentration (b, d) of DOPC, DLPC, DMPC, and DPPC lipid vesicles in HEPES buffer (a, b) and Milli-Q (c, d).*

It was observed that Au-Phe NPs underwent aggregation with respect to blank Au-Phe NPs at a low lipid concentration (0.0125 mM) of DLPC, DMPC and DPPC lipid vesicles [Au-Phe NP/DLPC or DMPC or DPPC (80:1)]. The UV-Visible spectra revealed that a new broadened peak at a higher wavelength along with the shift in the SPR peak (**Figure 3.3a**).

However, discrimination was observed at low lipid concentration of DOPC vesicles [Au-Phe NP/DOPC (80:1)], the SPR peak of Au-Phe NPs was found to be slightly red-shifted (~8 nm) with no significant broadened peak at higher wavelength (**Figure 3.3a**). The naked Au-Phe NPs also remained stable in only HEPES buffer after the incubation for 24 h. Interestingly, at high lipid concentration (0.4 mM) of DOPC, DLPC, DMPC, and DPPC vesicles [Au-Phe NP/liposome (2:1)], the Au-Phe NPs were highly stable. The UV-Visible spectra showed the SPR peak of the Au-Phe NPs were slightly red shifted (~ 5 nm) in presence of all lipid vesicles (**Figure 3.3b**).

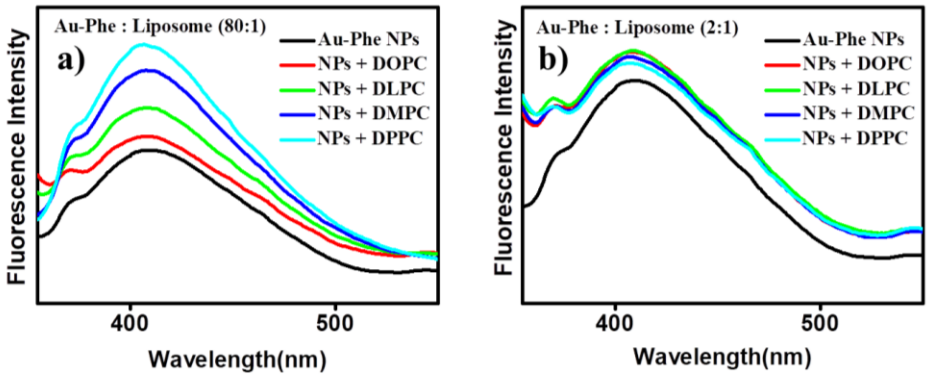

Figure 3.4 *Steady-state fluorescence spectra of the Au-Phe NPs in the presence of DOPC, DLPC, DMPC, and DPPC lipid vesicles in low (a) and high (b) lipid concentration. The excitation wavelength for Au-Phe NPs and Au-Phe NPs/lipid system is 330 nm and the emission wavelength is 424 nm.*

The fluorescence spectra revealed that there was no significant increment in the fluorescence intensity of Au-Phe NPs at a high lipid concentration of the lipid vesicles (DOPC, DLPC, DMPC, and DPPC) (**Figure 3.4b**). On the other hand, at a low concentration of lipid vesicles, the fluorescence intensity of the Au-Phe NPs increased with the aggregation of Au-Phe NPs (DLPC<DMPC<DPPC but not for DOPC) (**Figure 3.4a**). The increment in the fluorescence intensity is attributed to the increase in the local concentration followed by aggregation-induced emission of the amino acid upon the aggregation of nanoparticles *[37]*. The time-dependent UV-Visible spectra (**Figure 3.5**) showed that the rate of aggregation was faster

in DPPC than DMPC and DLPC. It should be noted that there is some aggregation for DOPC, as well.

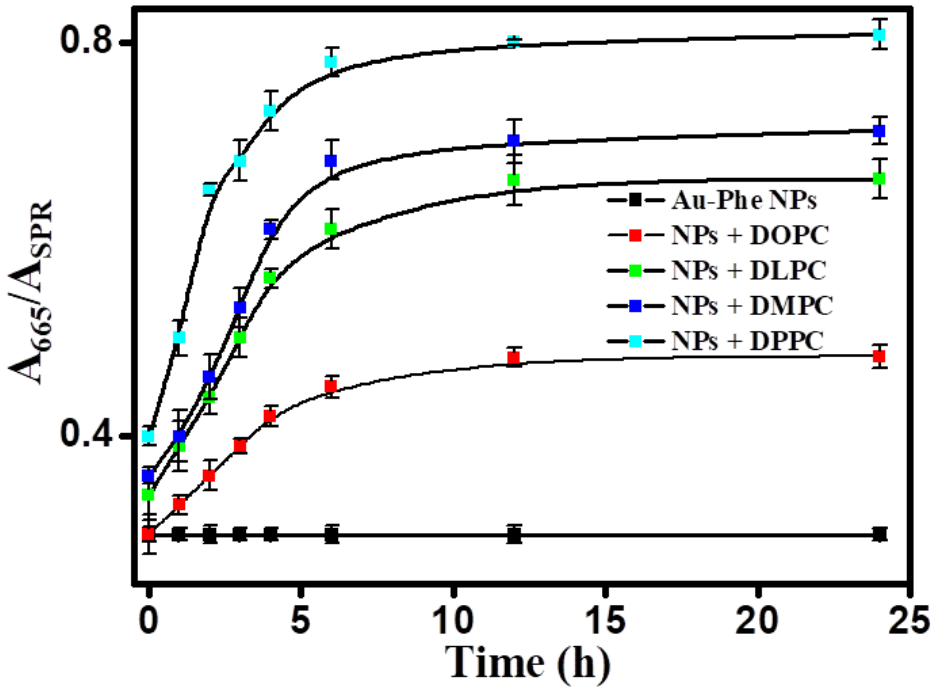

Figure 3.5 *Time-dependent aggregation of the Au-Phe NPs in low concentration [Au-Phe NPs: lipid (80:1)] of DOPC, DLPC, DMPC and DPPC lipid vesicles through UV-Visible absorption spectra.*

Cholesterol is an essential component of cell membranes and the presence of cholesterol affects the phase state of lipid membrane. DPPC lipid bilayer with 5% cholesterol remains in sol-gel phase, and with 40% cholesterol shifts the phase state to liquid-crystalline phase *[41]*. In presence of the high concentration of DPPC lipid bilayer with 5% and 40% cholesterol, the Au-Phe NPs were stable (**Figure 3.6b**). But, at a low concentration of DPPC lipid bilayer with 5% cholesterol (gel phase), the Au-Phe NPs underwent aggregation, whereas, in the presence of 40% cholesterol (liquid phase), Au-Phe NPs were stable (**Figure 3.6a**).

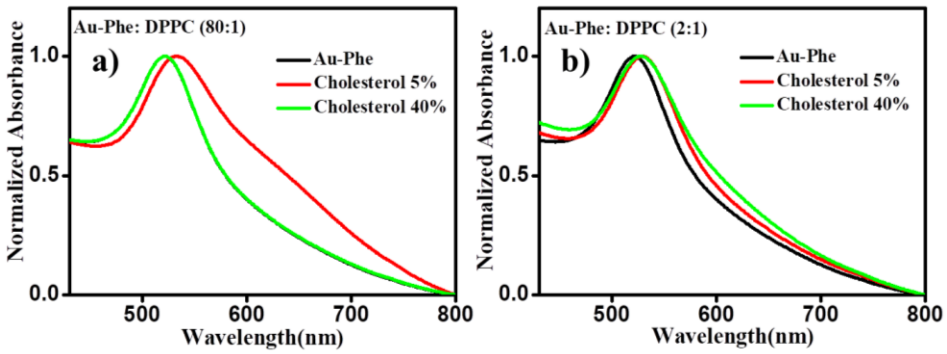

Figure 3.6 *UV-Visible absorption spectra of the Au-Phe NPs in low (a) [Au-Phe NPs: DPPC (80:1)] and high (b) [Au-Phe NPs: DPPC (2:1)] DPPC lipid concentration in presence of 5 % and 40 % cholesterol.*

In order to investigate the effect of medium, we further conducted all the experiments in Milli-Q water (**Figure 3.3c, d**). Similar to the HEPES medium, the UV-Visible spectra revealed that the SPR peak of the Au-Phe NPs was slightly red shifted (~ 5 nm) at a high concentration of all lipids (**Figure 3.3d**). Interestingly, unlike in HEPES buffer medium, the Au-Phe NPs did not undergo aggregation at a low concentration of lipid vesicles in Milli-Q water (**Figure 3.3a, c**). The SPR peak of Au-Phe NPs was shifted ~ 5 nm at low concentration of DMPC and DPPC lipid vesicles (**Figure 3.3c**). This observation indicates that the buffer medium of the solution plays a crucial role in the aggregation of Au-Phe NPs at a low lipid concentration.

3.2.3 Microscopic study of the lipid-induced aggregation and lipid corona formation:

We employed different state of the art of imaging techniques e. g. CLSM, HR-TEM, and AFM to visualize above phenomena microscopically. We particularly studied the aggregation of Au-Phe NPs at a low concentration of lipid vesicles in both buffer and Milli-Q medium by CLSM. The blank lipid vesicles with a size around 900-1000 nm were observed in CLSM imaging as presented in **Figure 3.7a-d**. The micro-sized aggregates of Au-Phe NPs along with the lipid vesicles were found at a low concentration of

DPPC lipid vesicles [Au-Phe NPs/ DPPC (80:1)] in HEPES buffer medium (**Figure 3.7e-h)**. Interestingly, at a low concentration of DOPC lipid vesicles [Au-Phe NPs/ DOPC (80:1)], we did not observe any micro-sized aggregates of Au-Phe NPs (**Figure 3.7i-l)**.

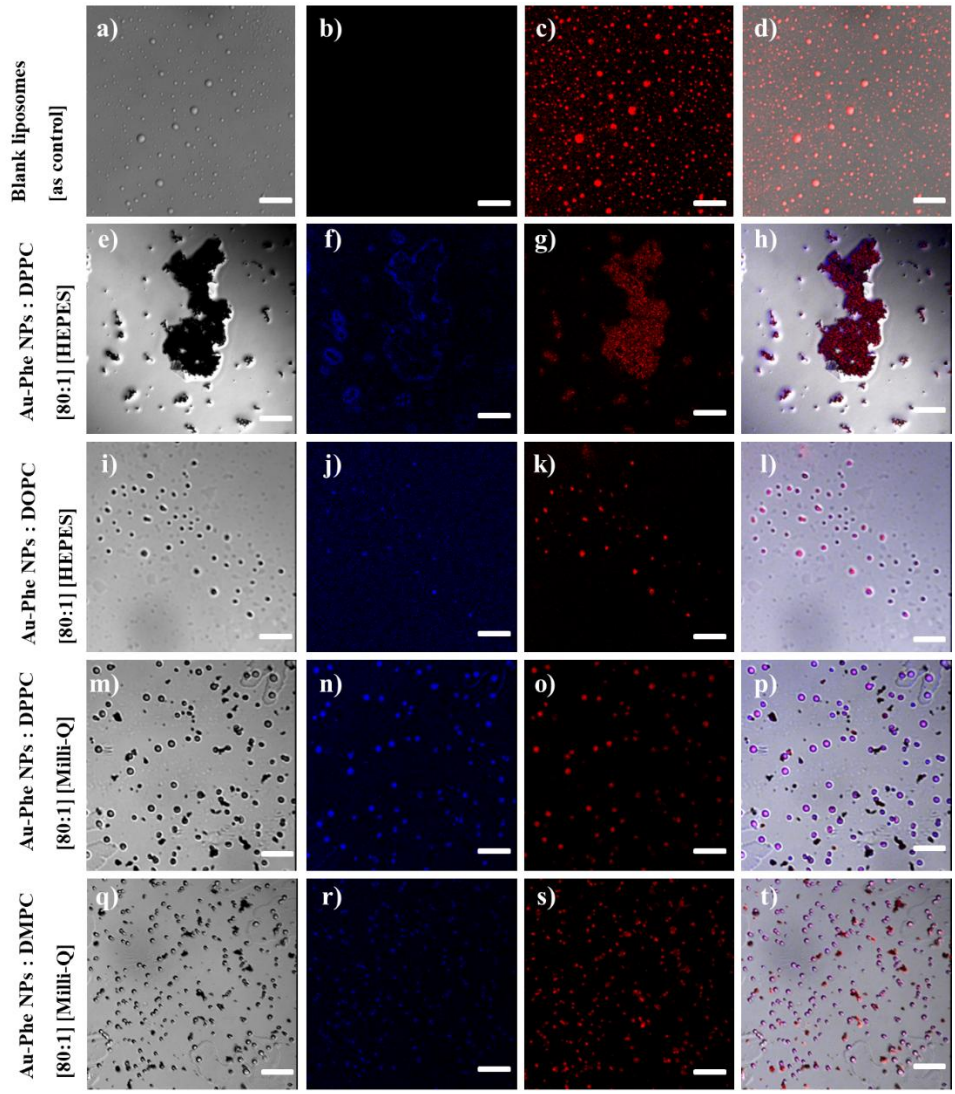

Figure 3.7 *Confocal laser scanning microscopy images of Au-Phe NPs in presence of low concentration of zwitterionic DOPC, DPPC lipid vesicles in HEPES buffer and DPPC, DMPC in Milli-Q medium using the emission of Au-Phe NPs (410-460 nm) and Liss Rhod PE (570-610 nm). Bright field, fluorescence (blue and red), and merged images for lipid tagged with Liss Rhod PE (a-d) as a control, Au-Phe NPs : DPPC [80:1] [HEPES] (e-h) , Au-Phe NPs : DOPC [80:1] [HEPES] (i-l) , Au-Phe NPs : DPPC[80:1] [Milli-Q] (m-p), and Au-Phe NPs : DMPC[80:1] [Milli-Q]. Scale bar is 2 µm.*

However, in Milli-Q medium, the Au-Phe NPs at low concentration of DPPC lipid vesicles [Au-Phe NPs/ DPPC (80:1)] did not form any sub or super micron aggregates (**Figure 3.7m-p)**. Similarly, at the low concentration of DMPC lipid vesicles in Milli-Q medium [Au-Phe NPs/ DMPC (80:1)], the Au-Phe NPs were as stable as in case of DPPC lipid vesicles (**Figure 3.7q-t)**. This observation for the DMPC lipid vesicles is different from our previous report in HEPES medium *[37]*. The colocalization of the blue fluorescence of Au-Phe NPs and red fluorescence from Liss Rhod PE in lipid vesicles indicates that both the NPs and the lipid vesicles coalesce with each other which indicates the formation of lipid vesicle coating around the nanoparticles. Interestingly, we did not find any fibrillar structure for all of the above cases, confirming that the zwitterionic lipid molecules did not replace the surface ligands.

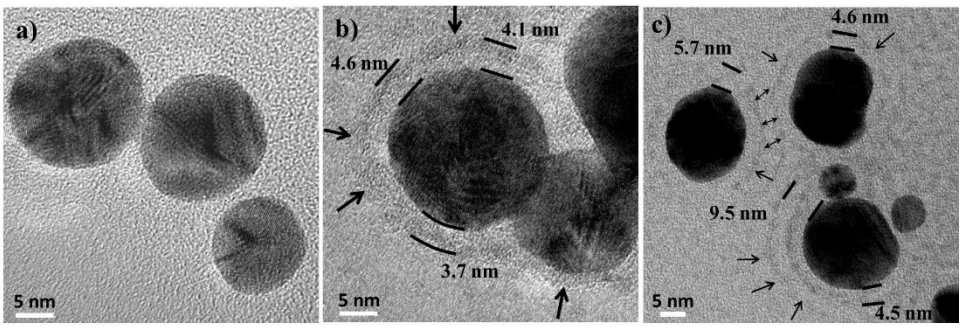

Figure 3.8 *HR-TEM images of the bare Au-Phe NPs (a), Au-Phe NPs in the presence of high lipid concentration [Au-Phe NPs: lipid (2:1)] of DLPC (b) and DPPC (c) lipid vesicles. The arrow indicates the coating of lipid around Au-Phe NPs. Scale bars = 5 nm.*

Next, we were keen to capture the HR-TEM imaging of Au-Phe NPs in presence of different phase states of lipid vesicles. It is worth mentioning that the drying and processing steps can greatly alter the thickness of lipid bilayer *[16]*. Moreover, for smaller particles, it is challenging to get an exact coating. Further, the presence of two double bonds in the tail group of DOPC bilayer needs the staining to visualize lipid in TEM imaging *[16]*. Therefore, instead of taking DOPC, we had chosen DLPC lipid which remains in the disordered phase (T_m = -1 °C) at RT for imaging purpose.

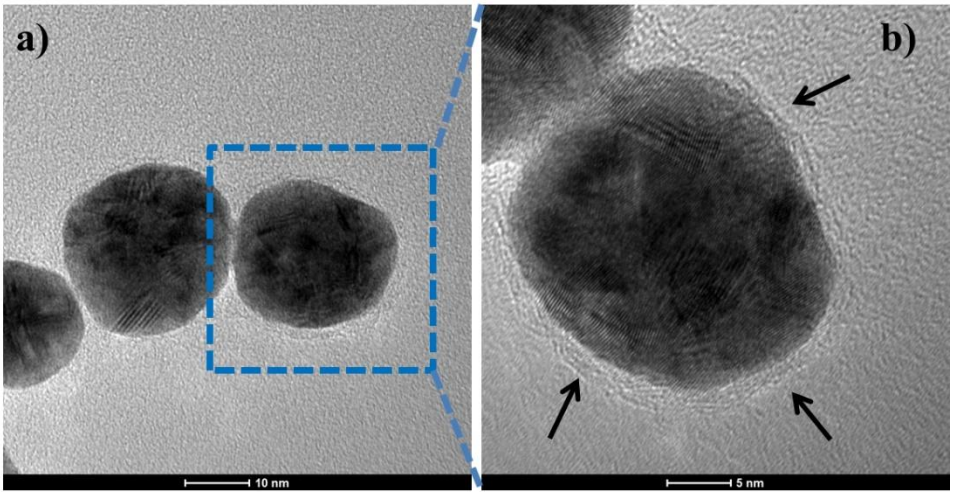

Figure 3.9 *HR-TEM imaging (a-b) of Au-Phe NPs at high lipid concentration of DLPC lipid vesicles [Au-Phe NPs: DLPC (2:1)].*

The HR-TEM images (**Figure 3.8a-c**) revealed that unlike bare Au-Phe NPs (no coating), there was a thick lipid coating (4.1 nm for DLPC and 4.9 nm for DPPC) around Au-Phe NPs in presence of a high concentration of DLPC and DPPC lipid vesicles [Au-Phe NPs/ DLPC or DPPC (2:1)]. **Figure 3.9a-b** provided additional detail on the lipid coating around Au-Phe NPs, in presence of high concentration of DLPC lipid vesicles. The expected thickness of lipid bilayer is about 4.5 nm while the measured thickness of DLPC lipid around Au-Phe NPs in **Figure 3.8b** is ~ 4.1 nm and for **Figure 3.9b** is 2.2 nm. Previously Murphy and co-workers reported that the drying and processing steps can greatly alter the thickness of lipid bilayer *[16]*.

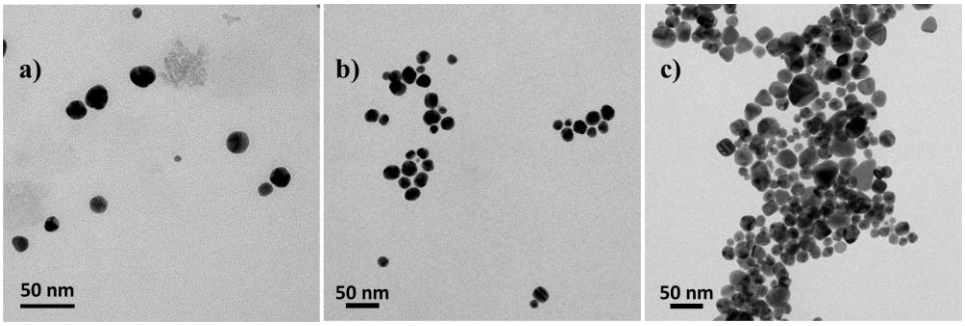

Figure 3.10 *HR-TEM images (a-c) of bare Au-Phe NPs (a) and in the presence of low concentration [Au-Phe NPs: lipid (80:1)] of DOPC (b) and DPPC (c) lipid vesicles. The bare Au-Phe NPs (a) image (Scale bar = 50 nm) was the enlarged image of figure 3.1b (Scale bar = 100 nm).*

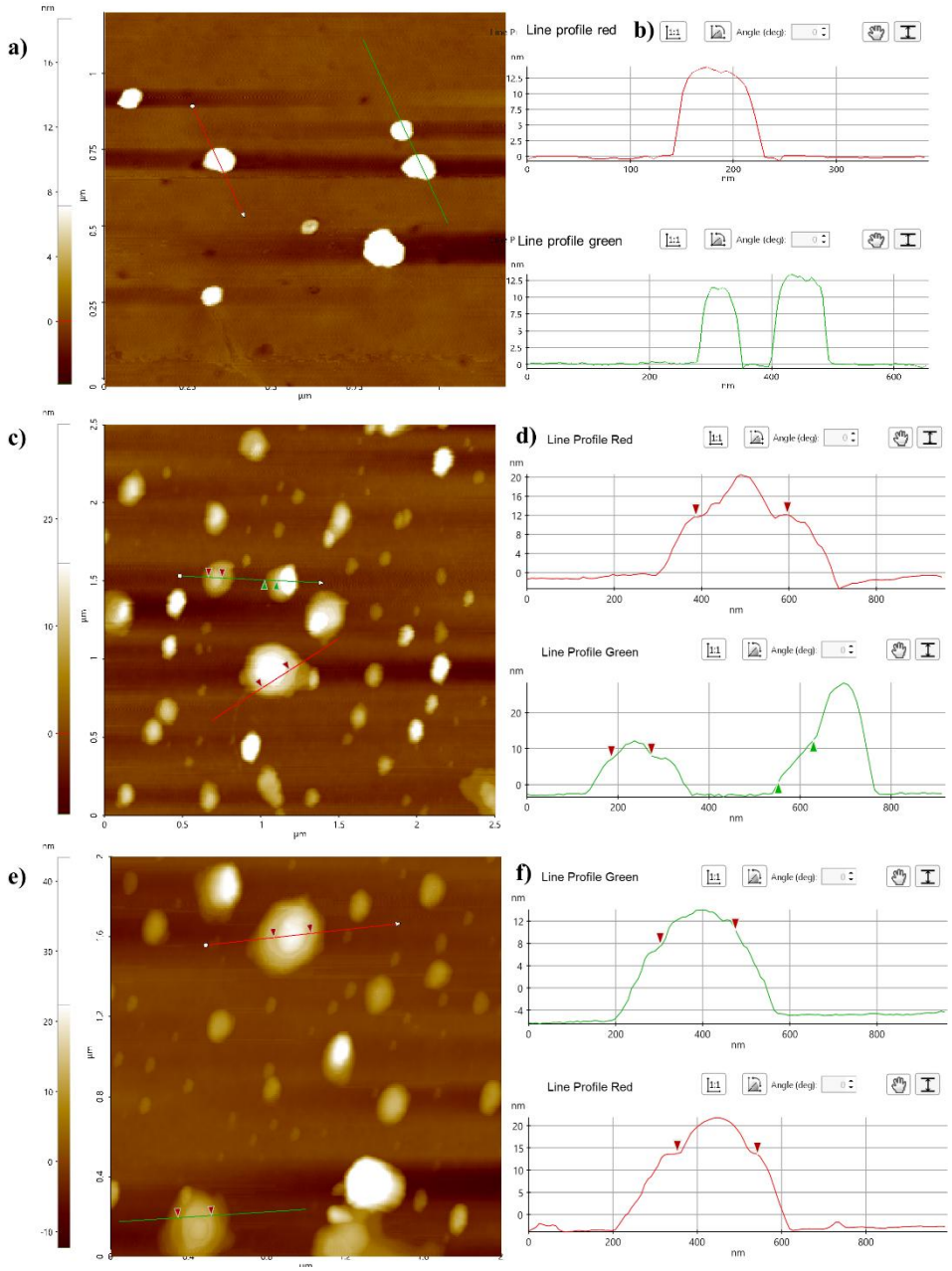

Figure 3.11 *AFM imaging (a, c, e) and corresponding cross-section area analysis (b, d, f) of the blank Au-Phe NPs as control (a-b) and in the presence of high concentration [Au-Phe NPs/lipid (2:1)] of DOPC (c-d) and DPPC (e-f) lipid vesicles.*

Furthermore, at a low concentration of DPPC lipid vesicles [Au-Phe NPs/ DPPC (80:1)] in buffer medium, the Au-Phe NPs formed aggregated structure (**Figure 3.10c**) compared to that of blank Au-Phe NPs (**Figure 3.10a**). But, for low concentration of DOPC lipid vesicle [Au-Phe NPs/ DOPC (80:1)], less aggregation (**Figure 3.10b**) of Au-Phe NPs was

observed compared to DPPC. We had chosen DOPC lipid vesicles instead of DLPC at low lipid concentration because the Au-Phe NPs underwent less aggregation at low concentration of DOPC lipid vesicles (**Figure 3.3a**).

Further, the AFM images confirmed lipid bilayer coating around the Au-Phe NPs in presence of a high concentration of DOPC and DPPC lipid vesicles in buffer medium (**Figure 3.11c-f**). The cross-section analysis of the AFM imaging revealed the presence of three humped peaks of the lipid bilayer-coated Au-Phe NPs with the diameter of 12-20 nm which corresponds to Au-Phe NPs and 5-10 nm corresponding to lipid bilayer thickness respectively. The cross-section analysis of AFM image of bare Au-Phe NPs (as control) showed a single humped peak with a core diameter of 12-14 nm (**Figure 3.11a-b**).

3.2.4 Molecular dynamics simulations: lipid corona formation and lipid-induced aggregation

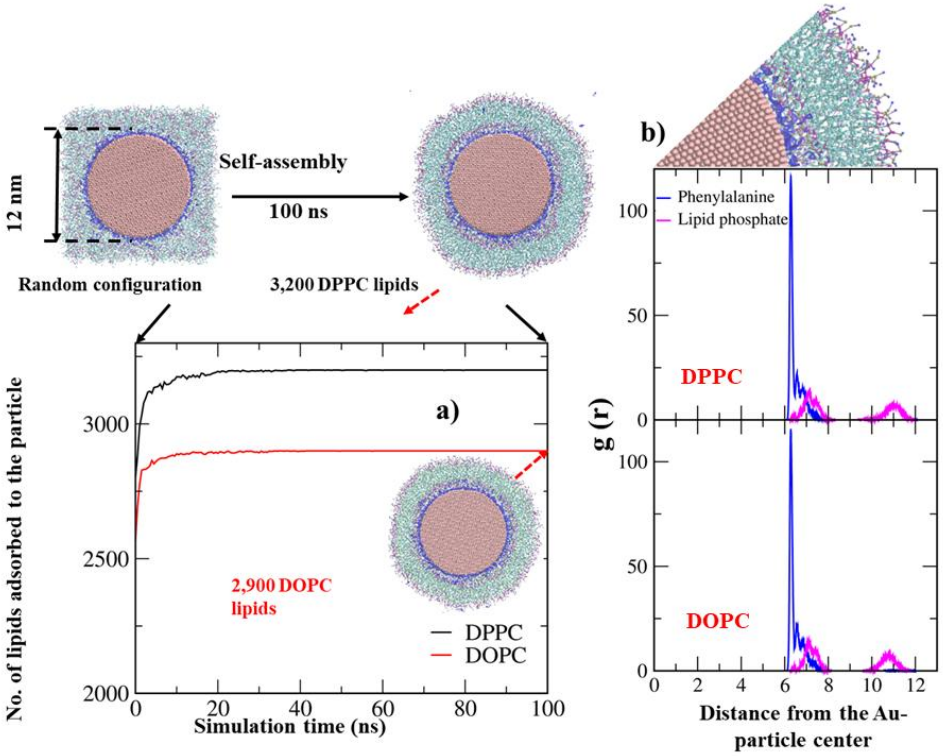

Figure 3.12 *a) Number of DPPC and DOPC lipids adsorbed to the Au-Phe particle as a function of simulation time. Snapshots at the beginning (0 ns) and at the end (100 ns) of simulations are shown, where Au, Phe, lipid heads and tails were colored in pink, blue, purple, and light blue, respectively. Water molecules were omitted for clarity. The images were created using Visual Molecular Dynamics [42]. b) Radial distribution functions (RDFs) of phenylalanine and lipid phosphates with respect to the particle center.*

To interpret these experimental results at nearly atomic resolution, self-assembly of the 12 nm sized spherical Au-Phe particle and phospholipids was simulated at high and low lipid concentrations. We first simulated mixtures of a single Au-Phe particle and ~3,000 lipids that represent the high lipid concentration, showing that both DPPC and DOPC lipids spontaneously self-assemble to liposomes encapsulating the Au-Phe particle (**Figure 3.12a**), as observed in the experimental observation of lipid corona. In **Figure 3.12a**, DPPC and DOPC liposomes respectively consist of 3,200 and 2,900 lipids, showing more lipids for DPPC liposome than for DOPC liposome. Note that, the simulated temperature of 293 K is between the phase-transition temperatures of DPPC and DOPC bilayers, and hence DPPC and DOPC bilayers are respectively in the Sol-gel (order) and liquid-crystalline (disorder) phases, indicating that more DPPC lipids are required to form lipid corona than DOPC lipids are, as observed in **Figure 3.12a**.

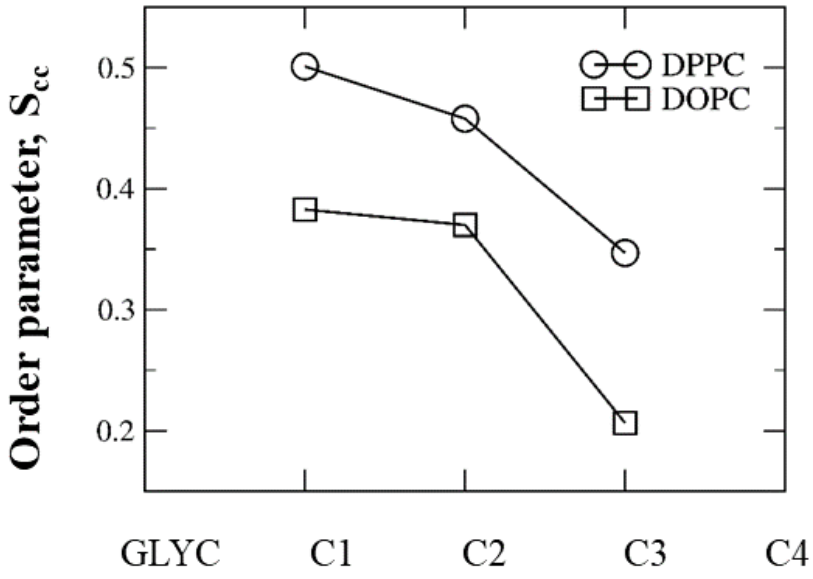

Figure 3.13 *Order parameters of coarse-grained (CG) lipid tails with respect to the surface normal of the liposome. GLYC designates the bead for glycerol in lipids, and C1 through C4 are beads for the tails.*

In **Figure 3.13**, DOPC tails were more disordered than DPPC tails, clearly showing a difference in the ordered state of DPPC and DOPC lipid bilayer. This conformation of lipid corona was further confirmed by calculating radial distribution functions (RDFs) of phenylalanine and lipid phosphates with respect to the particle center. In **Figure 3.12b**, there was a sharp RDF peak for phenylalanine at ~ 6.3 nm, indicating a phenylalanine layer on the particle surface. In particular, two RDF peaks were observed for lipid phosphates, indicating the formation of lipid bilayer. We also employed molecular dynamics simulation for bare Au NPs surface with DOPC and DPPC lipid molecules to study the role of the Phe molecules self-assembly on Au-NPs surface. The final snapshots showed that lipids bind to the particle surface because of hydrophobic interaction but do not form complete liposomes or bilayer shape (**Figure 3.14**). They formed more likely irregular aggregation around the Au-particle surface. Hydrophobic Au particles were wrapped by the hydrophobic tail of lipids, leading to the irregular arrangement of lipids.

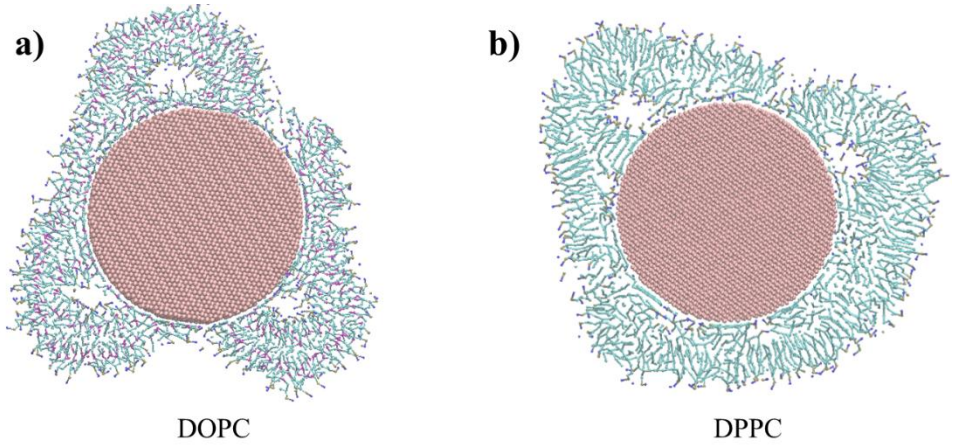

Figure 3.14 *Final snapshots (100 ns) of the simulation of the bare Au NPs with (a) DOPC and (b) DPPC lipid vesicles.*

To understand the experimental result regarding lipid-induced aggregation of Au-Phe particles at low lipid concentrations, the self-assembly of eight Au-Phe particles and lipids was also simulated. Note that 2,900~3,200 lipids per particle were simulated for lipid corona formation at the high lipid concentration as mentioned above, while 500 lipids per particle were simulated for the lipid-induced aggregation at the low lipid concentration. Mixtures of eight Au-Phe particles, which were initially positioned with a distance of 2.5 nm between neighbouring particles, and 4,000 lipids (500 lipids per particle), were simulated, showing that DPPC and DOPC lipids self-assemble to membranes around Au-Phe particles, although their conformations differ.

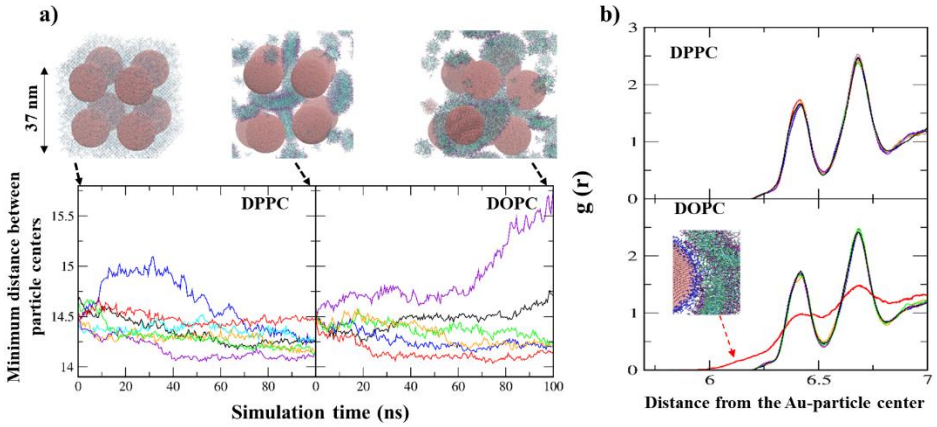

Figure 3.15 *a) Minimum distances between each particle and its neighbouring particle centers as a function of time. Since there are eight Au-Phe particles, values for each particle are represented in different colors. Initial (0 ns) and final (100 ns) snapshots of simulations are shown, where phenylalanine and water molecules are omitted for clarity. (b) RDFs of water with respect to each particle center. Since there are eight Au-Phe particles for each simulation, eight peaks are shown for each lipid system*.

In **Figure 3.15a**, from the model, we observed that DPPC lipids self-assemble to partial bilayer and bicelles, while DOPC lipids predominantly form liposomes that encapsulate fully only one particle. In **Figure 3.15a**, we could also observed that minimum distances between particles interacting with DPPC lipids reach steady-state values below 14.5 nm,

while those values between particles interacting with DOPC lipids drastically increased above 14.5 nm. To further examine these assembled structures, RDFs of water were calculated with respect to each particle center. **Figure 3.15b** showed that there are eight sharp peaks for DPPC, while for DOPC there was a peak that was much lower than the other seven sharp peaks. These indicated that all eight Au-Phe particles mixed with DPPC are somewhat exposed to water, but one of Au-Phe particles mixed with DOPC was much less exposed to water than the other seven particles mixed with DOPC, implying that only a few Au-Phe particles can be fully covered by disordered DOPC lipids rather than by ordered DPPC lipids. Note that differences in methodology, system size and concentration of simulation and experiment preclude quantitative comparison between the two. For example, the CG model did not have partial charges on water, and hence electrostatic interactions were screened implicitly by assuming a uniform relative dielectric constant ($\varepsilon = 15$), which might make it difficult to distinguish the effects of Milli-Q and buffer mediums. However, our simulations clearly showed a partial coverage of Au-Phe NPs by DPPC lipids at the low lipid concentration, which was not directly observed by experiments but may help explain the mechanism of particle aggregation in the buffer medium.

3.2.5 Hard and soft lipid corona: insight into the stability of the NPs:

The stability of nanomaterials is of utmost importance for their broad biomedical applications. Therefore, we were interested to study the stability of lipid corona of different zwitterionic lipid bilayer coated Au-Phe NPs (DOPC/Au-Phe and DPPC/Au-Phe NPs) against external stimuli. We already mentioned that the lipid corona for DOPC/Au-Phe and DPPC/Au-Phe NPs systems were formed at high concentration of DOPC and DPPC respectively [Au-Phe NPs/lipid (2:1)]. The pH-dependent stability of both lipid bilayer coated Au-Phe NPs and native Au-Phe NPs was studied via UV-Visible spectroscopy. The UV-Visible spectra of bare Au-Phe NPs

showed that with the decrease in pH, a new broadened peak appeared at near-infrared region (at 664-708 nm), indicating the aggregation of Au-Phe NPs **(Figure 3.16a)**.

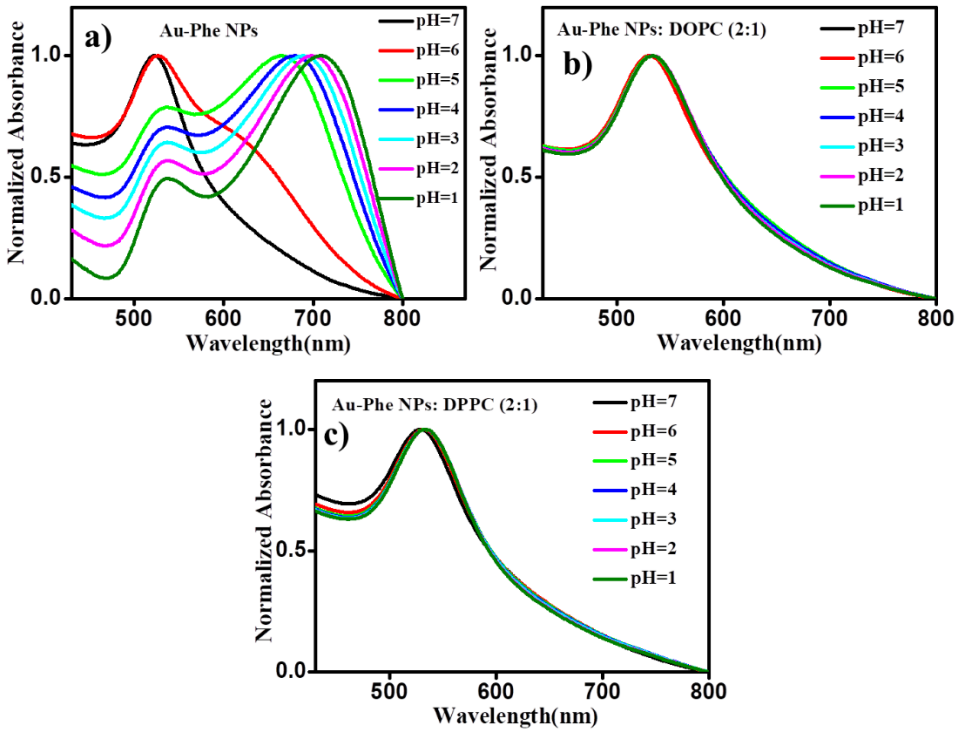

Figure 3.16 *UV-Visible absorption spectra of the (a) native Au-Phe NPs, (b) Au-Phe NPs: DOPC (2:1), and (c) Au-Phe NPs: DPPC (2:1) against the pH variation (from 7 to 1).*

However, the DOPC/Au-Phe and DPPC/Au-Phe at high lipid concentration [Au-Phe NPs/lipid (2:1)] remained stable at very low pH (pH~1.0), as confirmed from the unchanged spectral shift in UV-Visible spectra of Au-Phe NPs **(Figure 3.16b, c)**. This result suggests that any lipid-bilayer coating around the Au-Phe NPs (lipid corona) imparts additional stability to Au-Phe NPs against low pH aggregation. Next, we investigated the effect of salt concentration on the stability of lipid bilayer coated Au-Phe NPs and native Au-Phe NPs. The result showed that native Au-Phe NPs undergo aggregation in presence of 0.1 M NaCl, whereas both the DOPC/Au-Phe and DPPC/Au-Phe NPs were stable at a high salt concentration (1 M NaCl)

(Figure 3.17a-c). This observation again indicates that lipid corona around NPs also prevents their aggregation in high salt media *[43]*.

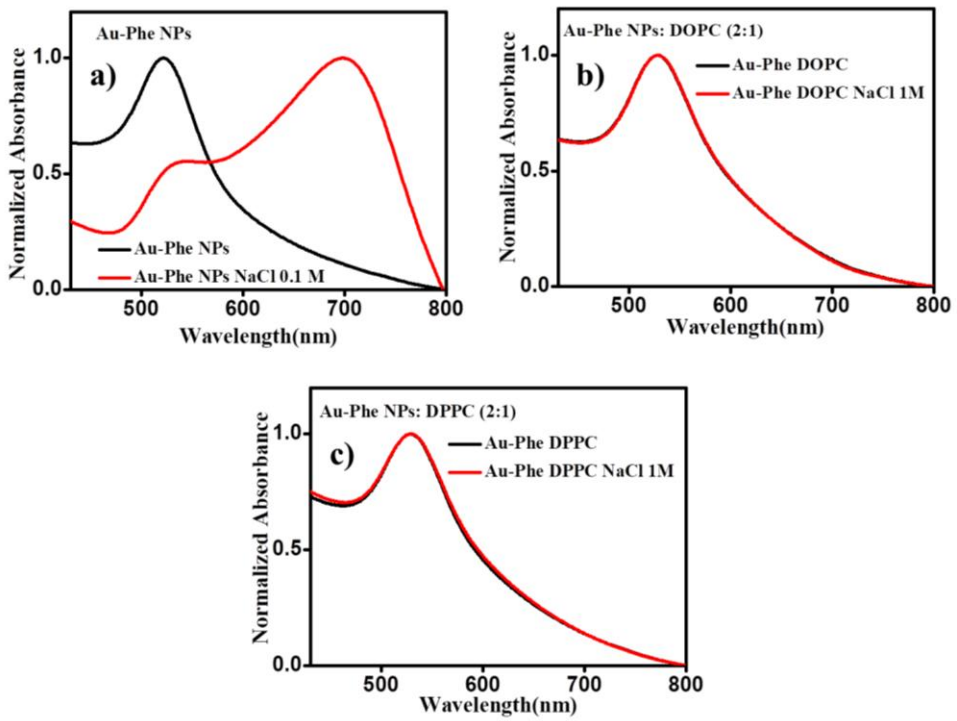

Figure 3.17 *UV-Visible absorption spectra of the (a) native Au-Phe NPs against 0.1M NaCl salt concentration, (b) Au-Phe NPs: DOPC (2:1), and (c) Au-Phe NPs: DPPC (2:1) against 1 M NaCl salt concentration.*

The stability of NPs against the freeze-thaw cycle is worth studying because NPs need freeze-thawed for long time preservation and storage of biological samples. But, this process often has some limitations such as disruption of cell membranes and aggregation of the Au NPs. So, we were keen to investigate the stability of bare Au-Phe, DOPC/Au-Phe, and DPPC/Au-Phe NPs systems against freeze-thaw cycles. We adopted two different freezing protocols to study the stability of lipid corona around the Au-Phe NPs. One protocol was to freeze the samples in liquid nitrogen (-196 °C) followed by thawing at RT and in another protocol, the sample was to be frozen in the refrigerator at -12 °C and then thawed at RT. In both cases, the bare Au-Phe NPs undergo aggregation after one freeze-thaw cycle (**Figure 3.18a, d)**. In case of lipid bilayer coated Au-Phe NPs, when both the DOPC/Au-Phe and

DPPC/Au-Phe systems were frozen in liquid nitrogen and thawed at RT, DOPC/Au-Phe system started to undergo aggregation with the successive freeze-thaw cycles (**Figure 3.18b)**, however, the DPPC/Au-Phe system remained stable against this (**Figure 3.18c)**. Interestingly, when the DOPC/Au-Phe and DPPC/Au-Phe systems were frozen in the refrigerator (-12 °C) and thawed in RT, both the systems were found to be stable against successive freeze-thaw cycles (**Figure 3.18 e, f)**.

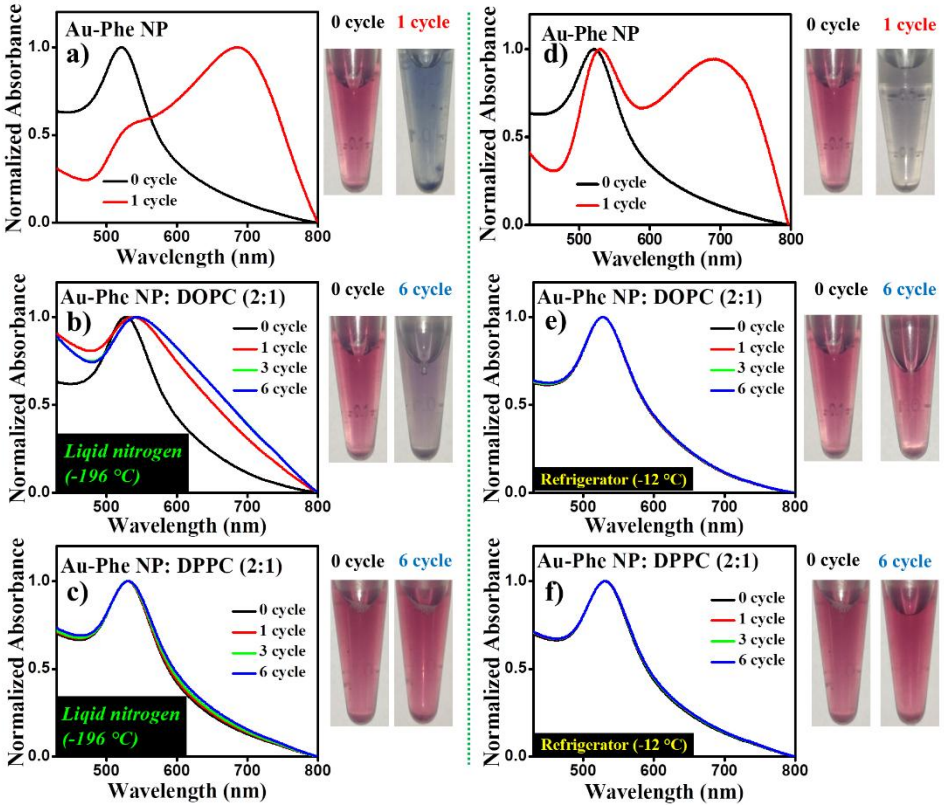

Figure 3.18 *Photograph and UV-Visible spectra of blank Au-Phe NPs in the absence (a, d) and presence of DOPC (b, e) and DPPC (c, f) lipid vesicles against freeze-thaw cycles in liquid nitrogen (-196 °C) (a-c) and refrigerator (-12 °C) (d-f) respectively.*

This observation can be explained in the following way. The freezing process removes hydrogen-bonded water from the lipid head group region and thus increase head group packing by enhancing the van der Waals interaction between lipid bilayer *[44].* As a result, the lipid bilayer undergo phase transition (from liquid-crystalline to sol-gel phase). Then, the lipid

bilayer is rehydrated upon thawing and undergoes reverse phase transition (from sol-gel to liquid-crystalline phase). In this process, disruption of the lipid bilayer takes place and the Au NPs aggregate due to the decrease in the repulsion. For the case of DOPC/Au-Phe, DOPC lipid bilayer remains in liquid-crystalline phase at RT. The freezing process of DOPC/Au-Phe system in liquid nitrogen caused the phase transition of DOPC lipid bilayer from liquid-crystalline to sol-gel phase and vice versa upon thawing at RT. These processes lead to the disruption of the lipid bilayer and aggregation of Au-Phe NPs. However, when the same DOPC/Au-Phe system was frozen in refrigerator (-12 °C), no phase transition was occurred in the lipid bilayer, resulting in stable Au-Phe NPs. On the other hand, for DPPC/Au-Phe system, DPPC remains in sol-gel phase owing to the high phase transition temperature (41 °C). When the DPPC/Au-Phe system was frozen either in liquid nitrogen or refrigerator and subsequently thawed at RT, no phase transition and reverse phase transition occurred as the DPPC bilayer remained in sol-gel phase in both conditions. So, we observe stable lipid corona in case of DPPC lipid-coated Au-Phe NPs against any kind of freeze-thaw cycle. From all these observations, one may infer that DOPC lipid forms leaky lipid bilayer and DPPC forms hard lipid bilayer around the Au-Phe NPs. We propose that DOPC lipid-coated Au-Phe NPs form “soft lipid corona” and DPPC lipid-coated Au-Phe NPs form “hard lipid corona”. It should be noted that the formation mechanisms of 'hard' and 'soft' protein and lipid corona differ substantially while for the proteins have been discussed in literature but not for lipid. The other possibility that should be considered is that excess lipid molecules also may give extra stability against freeze-thaw cycles. To rule out this possibility, we centrifuged the Au-Phe NPs and lipid mixture to remove excess lipids and performed similar experiments. The results showed that there were no significant differences in results between centrifuged and non-centrifuged Au-Phe NPs/lipid systems **(Figure 3.19a, b)**. We thus conclude that excess lipids

present in systems have no effect on the stability of Au-Phe NPs against freeze-thaw cycles.

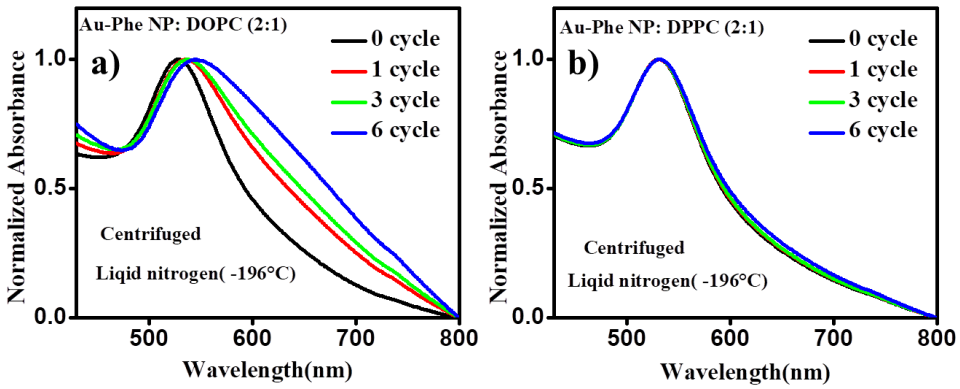

Figure 3.19 *UV-Visible spectra of the Au-Phe NPs in presence of DOPC (a) and DPPC (b) lipid vesicles [Au-Phe NPs: lipid (2:1)] against freeze-thaw cycles in liquid nitrogen (-196 °C) after the centrifugation of the mixture.*

3.3 Discussions

After analyzing all the experimental and molecular dynamics simulation results, we draw a possible mechanistic pathway of lipid phase and area per lipid head group dependent lipid corona formation and lipid-induced aggregation of Au-Phe NPs. It is well-known that rigid DPPC lipid bilayer is more tensed than fluid DOPC lipid bilayer and surface area per lipid head group of the DPPC is lesser than that of DOPC lipid vesicles. **Figure 3.20** showed a negative zeta potential for all the lipid vesicles (in the range of -2 mV to -8 mV) *[45-47]*. The Au-Phe NPs first adsorb to all the lipid bilayers irrespective of the phase states through electrostatic interaction between positively charged NR_3^+ group of lipid and the negatively charged COO^- group of the Au-Phe NPs. Although electrostatic interaction facilitates the membrane area (A_1) to contact Au-Phe NPs, it is unable to determine the number of Au NPs (N) adsorbed on surface of bilayers. Two possibilities emerge in this case: the first is that a small number of nanoparticles can be fully covered with lipid bilayer. The second one is that a large number of nanoparticles can be partially covered with a lipid bilayer.

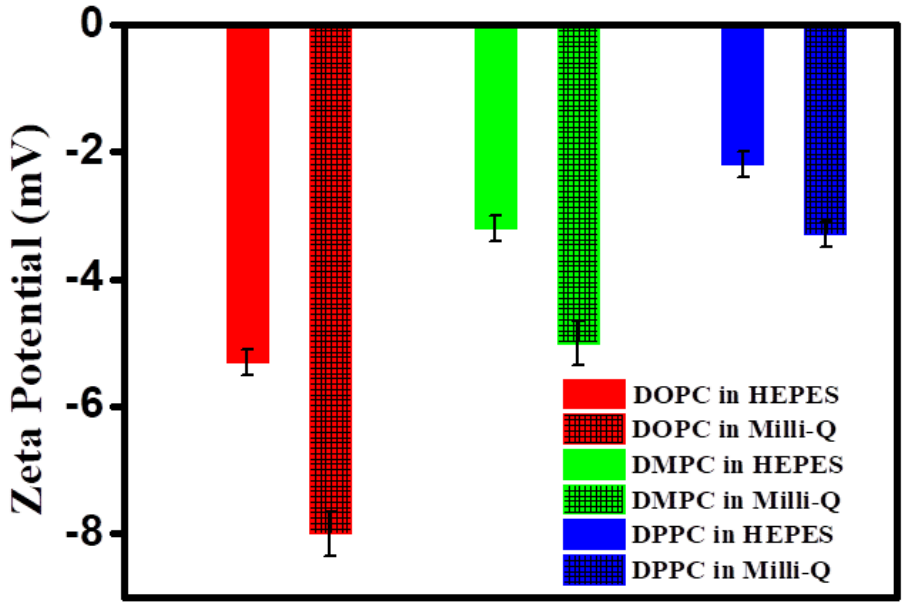

Figure 3.20 *Zeta potential measurements of DOPC, DMPC, and DPPC lipid vesicles in buffer and Milli-Q medium.*

At the high lipid concentration [Au-Phe NPs: lipid (2:1)] of both the liquid-crystalline and sol-gel lipid bilayer i.e. when the number of nanoparticles is almost equal to that of the number of lipid vesicles, the Au-Phe NPs are fully wrapped by lipid bilayer. Our HR-TEM imaging (**Figure 3.8b, c**), AFM imaging (**Figure 3.11c-f**), and simultaneously Molecular dynamics simulation (**Figure 3.12a, b**) results establish that the Au-Phe NPs are fully covered with the lipid bilayer of both sol-gel and liquid-crystalline states. So, the Au-Phe NPs are stable at high lipid concentration of all lipid vesicles. The observation is in accordance with UV-Visible spectra (**Figure 3.3b, d**). On the other hand, at low concentration of lipid vesicles [Au-Phe NPs: lipid (80:1)] i.e. when the number of nanoparticles is higher than that of lipid vesicles, the number of nanoparticles to be adsorbed on the vesicle surface completely depends on the phase state (tensed or not) and area per lipid head group of the lipid bilayer. For a tensed lipid bilayer (DPPC) which area per lipid head group is also less, rupturing of the lipid vesicles is required to wrap more than an infinitesimal area of each Au NPs *[48]*. Thus a large number of Au NPs is needed to reach the total adhering area.

The required large number of adsorbed nanoparticles increases the threshold tension of the bilayer and disrupts the lipid vesicles. In this process, all of the nanoparticles are partially coated by lipid bilayers and undergo aggregation to produce sub or super micron sized aggregates. But in presence of a low concentration of the fluid DOPC lipid vesicles [Au-Phe NPs: DOPC (80:1)] which area per lipid head group is large, the number of nanoparticles adsorb on the vesicle surface is self-limited *[48]*. This implies that among 80 nanoparticles per lipid vesicles, only a few nanoparticles are adsorbed on the vesicle surface while others remain in solution. Because of the adsorption of lesser number of nanoparticles on the vesicle surface, all of the excess surface area of the vesicle is not used. So, because of availability of the excess vesicle surface area, complete wrapping of the lipid bilayer around some of Au-Phe NPs is observed. We have depicted the mechanism in **Scheme 1**.

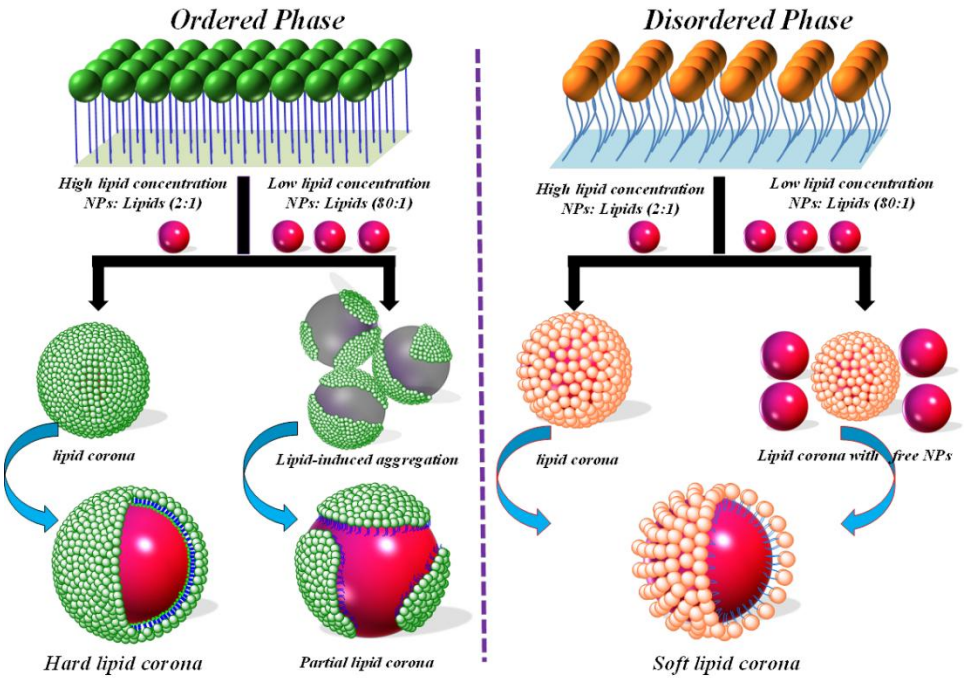

Scheme 3.1 Schematic representation of lipid corona formation and lipid-induced aggregation of Au-Phe NPs in two different concentrations and phase states of lipid bilayer (ordered and disordered). The ordered phase of the lipids is tightly packed and has a smaller area per lipid head group compared to the disordered phase of the lipid. In both ordered

and disordered phase state of lipid, the Au-Phe NPs are fully covered with lipid vesicles at high lipid concentration, forming the lipid corona. At a low lipid concentration, the Au-Phe NPs undergo lipid-induced aggregation through partial lipid corona in the ordered phase of the lipid membrane. In the disordered phase of the lipid (DOPC), a few nanoparticles are fully covered whereas other remains unwrapped. However, in the disordered phase of the bilayer , the Au-Phe NPs formed "soft lipid corona", whereas, in the ordered phase, the Au-Phe NPs form "hard lipid corona". For a better and clear representation of the soft lipid corona, the head groups of the lipids are slightly far from each other. Schematics are not drawn to scale.

The CLSM images also confirm that at a low concentration of DOPC lipid vesicles (**Figure 3.7i-l**), few nanoparticles are coated by vesicles while others remain unwrapped. On the other hand, for the DPPC lipid vesicles (**Figure 3.7e-h**), a large number of the Au-Phe NPs form aggregated structure along with lipid vesicles. Our HR-TEM imaging result also show that the Au-Phe NPs form large aggregated structure (**Figure 3.10c**) in case of DPPC whereas less aggregated structure (**Figure 3.10b**) is present in case of DOPC lipid vesicles. Apart from the CLSM and HR-TEM imaging, the computer simulation results also strengthen the proposed mechanism. At a low concentration of the lipid, DOPC lipid molecules form well-defined lipid bilayer around one Au-Phe NPs while the others did not, whereas for DPPC, all the Au-Phe NPs are partially covered with the lipid bilayer (**Figure 3.15a, b**). This is the possible reason for the unusual stability of Au-Phe NPs in liquid-crystalline DOPC lipid vesicles and aggregation in the sol-gel DPPC lipid vesicles at a low lipid concentration which corroborates well with UV-Visible spectra (**Figure 3.3a**). Interestingly, the Au-Phe NPs also undergo aggregation at low concentration of DLPC lipid vesicles which remains liquid-crystalline phase at room temperature (RT). This discrepancy can be explained by the area per lipid head group of DLPC lipid. The experimental measurements of the area per lipid head group of DLPC and DMPC lipid vesicles are 0.687 nm^2 and 0.67 nm^2 respectively at RT which are less than that of DOPC lipid vesicles (0.82 nm^2) *[49]*. As the area per lipid head group of the DLPC and DMPC lipid is comparable at

RT, the Au-Phe NPs undergo aggregation at low concentration of both lipid vesicles inspite of having wide difference in their phase transition temperatures.

After discussing the phase dependent stability of Au-Phe NPs, we suggest a possible explanation for the larger stability of the Au-Phe NPs in Milli-Q medium, compared to buffer medium, at low concentration of vesicles (DPPC and DMPC). We propose that both in the buffer and Milli-Q medium, partial lipid bilayer coating around the nanoparticles takes place. The partial lipid bilayer coated Au-Phe NPs gain stability through mutual repulsive interaction. The membrane coated Au-Phe NPs remain stable when the membrane surface charge is very low (almost neutral) due to the repulsive interaction *[50]*. So, in presence of zwitterionic lipid vesicles (DPPC and DMPC) in Milli-Q, the Au-Phe NPs are coated by lipid bilayer and stable (without aggregation), which was further confirmed from CLSM images (**Figure 3.7m-p and 3.7q-t**). But in presence of the buffer medium, the repulsive interaction between the partial lipid bilayer coated Au-Phe NPs is screened and they start to undergo aggregation to form sub or super micron aggregates (**Figure 3.7e-h**).

3.4 Conclusions

In summary, we found that interaction of phenylalanine functionalized gold nanoparticles with the lipid bilayer of different phase states results in either lipid-induced aggregation or corona formation depending upon phase state, area per lipid head group and concentration of the lipid bilayer. The high lipid concentration of DPPC, DMPC, DLPC, and DOPC leads to corona formation, imparting extra stability towards nanoparticles. The Au-Phe NPs undergo aggregation at low lipid concentration of DPPC, which remains in the ordered state. In contrast, Au-Phe NPs are stable at a low lipid concentration of DOPC, which remain in the liquid crystalline phase. Interestingly, the Au-Phe NPs undergo aggregation at low concentration of

both DLPC and DMPC lipid vesicles inspite of having wide difference in their phase transition temperatures due to the comparable area per lipid head group of both lipid vesicles at RT. The CGMD simulation study indicates that the higher number of lipid molecules is essential for forming lipid corona for the DPPC compared to that for DOPC as the lipid head group of DPPC is smaller than that of DOPC. At a low lipid concentration, DOPC lipid molecules potentially form the lipid corona around one Au-Phe NPs, whereas DPPC molecules form partial coating around all Au-Phe NPs, which leads to the aggregation of NPs. We found that DPPC lipid coated Au-Phe NPs are more stable than DOPC lipid coated Au-Phe NPs against freeze-thaw cycles offers a concept of a "hard and soft lipid corona". In a corollary, the lipid coated nanoparticles or lipid corona is a promising candidate for numerous biomedical applications. A study on the formation mechanism of lipid corona and its impact on stability may help us to use it as artificial virus nanoparticles (AVNs), therapeutic agents.

3.5 References

[1] Ghosh P., Han G., De M. *et al.* (2008), Gold Nanoparticles in Delivery Applications, Adv. Drug Delivery Rev. 60, 1307−1315 (DOI: 10.1016/j.addr.2008.03.016)

[2] Murphy C. J., Gole A. M., Stone J. W. *et al.* (2008), Gold Nanoparticles in Biology: Beyond Toxicity to Cellular Imaging, Acc. Chem. Res. 41, 1721−1730 (DOI: 10.1021/ar800035u)

[3] Saha K., Agasti S. S., Kim C. *et al.* (2012), Gold Nanoparticles in Chemical and Biological Sensing, Chem. Rev. 112, 2739−2779 (DOI: 10.1021/cr2001178)

[4] Kim D. Y., Kim M., Shinde S. *et al.* (2017), Temperature Dependent Synthesis of Tryptophan Functionalized Gold Nanoparticles and Their

Application in Imaging Human Neuronal Cells, ACS Sustainable Chem. Eng. 5, 7678−7689 (DOI: 10.1021/acssuschemeng.7b01101)

[5] Cedervall T., Lynch I., Lindman S. *et al.* (2007), Understanding the Nanoparticle–Protein Corona Using Methods to Quantify Exchange Rates and Affinities of Proteins for Nanoparticles, Proc. Natl. Acad. Sci. U.S.A. 104, 2050-2055 (DOI: 10.1073/pnas.0608582104)

[6] Nel A.E., Mädler L., Velegol D. *et al.* (2009), Understanding Biophysicochemical Interactions at the Nano–Bio Interface, Nat. Mater. 8, 543-557 (DOI: 10.1038/nmat2442)

[7] Lynch I., Dawson K. A. (2008), Protein-Nanoparticle Interactions, Nano Today 3, 40-47 (DOI: 10.1016/s1748-0132(08)70014-8)

[8] Tenzer S., Docter D., Rosfa S. *et al.* (2011), Nanoparticle Size is a Critical Physicochemical Determinant of the Human Blood Plasma Corona: a Comprehensive Quantitative Proteomic Analysis, ACS Nano 5, 7155-7167 (DOI: 10.1021/nn201950e)

[9] Ge C., Du J., Zhao L. *et al.* (2011), Binding of Blood Proteins to Carbon Nanotubes Reduces Cytotoxicity, Proc. Natl. Acad. Sci. U.S.A. 108, 16968-16973 (DOI: 10.1073/pnas.1105270108)

[10] Aggarwal P., Hall J.B., McLeland C.B. *et al.* (2009), Nanoparticle Interaction with Plasma Proteins as It Relates to Particle Biodistribution, Biocompatibility and Therapeutic Efficacy, Adv. Drug Deliv. Rev. 61, 428-437 (DOI: 10.1016/j.addr.2009.03.009)

[11] Walczyk D., Bombelli F.B., Monopoli M.P. *et al.* (2010), What the Cell “Sees” in Bionanoscience, J. Am. Chem. Soc. 132, 5761-5768 (DOI: 10.1021/ja910675v)

[12] Deng Z. J., Liang M., Monteiro M. *et al.* (2011), Nanoparticle-Induced Unfolding of Fibrinogen Promotes Mac-1 Receptor Activation and Inflammation, Nat. Nanotechnol. 6, 39-44 (DOI: 10.1038/nnano.2010.250)

[13] Walkey C. D., Chan W. C. (2012), Understanding and Controlling the Interaction of Nanomaterials with Proteins in a Physiological Environment, Chem. Soc. Rev. 41, 2780-2799 (DOI: 10.1039/c1cs15233e)

[14] Monopoli M. P., Åberg C., Salvati A. *et al.* (2012), Biomolecular Coronas Provide the Biological Identity of Nanosized Materials, Nat. Nanotechnol. 7, 779-786 (DOI: 10.1038/nnano.2012.207)

[15] Chetwynd A. J., Lynch I. (2020), The Rise of the Nanomaterial Metabolite Corona, and Emergence of the Complete Corona, Environ. Sci.: Nano 7, 1041−1060 (DOI: 10.1039/c9en00938h)

[16] Yang J. A., Murphy C. J. (2012), Evidence for Patchy Lipid Layers on Gold Nanoparticle Surfaces, Langmuir 28, 5404-5416 (DOI: 10.1021/la300325p)

[17] Bahrami A. H., Raatz M., Agudo-Canalejo J. *et al.* (2014), Wrapping of Nanoparticles by Membranes, Adv. Colloid Interface Sci. 208, 214-224 (DOI: 10.1016/j.cis.2014.02.012)

[18] Zhang S., Gao H., Bao G. (2015), Physical Principles of Nanoparticle Cellular Endocytosis, ACS Nano 9, 8655-8671 (DOI: 10.1021/acsnano.5b03184)

[19] Yu X., Feizpour A., Ramirez N. G. P. *et al.* (2014), Glycosphingolipid-Functionalized Nanoparticles Recapitulate CD169-Dependent HIV-1 Uptake and Trafficking in Dendritic Cells, Nat. Commun. 5, 4136 (DOI: 10.1038/ncomms5136)

[20] Xu F., Reiser M., Yu X. *et al.* (2016), Lipid-Mediated Targeting with Membrane-Wrapped Nanoparticles in the Presence of Corona Formation, ACS Nano 10, 1189-1200 (DOI: 10.1021/acsnano.5b06501)

[21] Xu F., Bandara A., Akiyama H. *et al.* (2018), Membrane-Wrapped Nanoparticles Probe Divergent Roles of GM3 and Phosphatidylserine in Lipid-Mediated Viral Entry Pathways, Proc. Natl. Acad. Sci. U.S.A. 115, E9041-E9050 (DOI: 10.1073/pnas.1804292115)

[22] Olenick L. L., Troiano J. M., Vartanian A. *et al.* (2018), Lipid Corona Formation from Nanoparticle Interactions with Bilayers, Chem 4, 2709-2723 (DOI: 10.1016/j.chempr.2018.09.018)

[23] Zhang X., Pandiakumar A. K., Hamers R. J. *et al.* (2018), Quantification of Lipid Corona Formation on Colloidal Nanoparticles from Lipid Vesicles, Anal. Chem. 90, 14387-14394 (DOI: 10.1021/acs.analchem.8b03911)

[24] Mendozza M., Caselli L., Salvatore A. *et al.* (2019), Nanoparticles and Organized Lipid Assemblies: from Interaction to Design of Hybrid Soft Devices, Soft Matter 15, 8951−8970 (DOI: 10.1039/c9sm01601e)

[25] Zuraw-Weston S., Wood D. A., Torres I. K. *et al.* (2019), Nanoparticles Binding to Lipid Membranes: from Vesicle-Based Gels to Vesicle Tubulation and Destruction, Nanoscale 11, 18464−18474 (DOI: 10.1039/c9nr06570a)

[26] Zuo Y. Y., Veldhuizen R. A., Neumann A. W. *et al.* (2008), Current Perspectives in Pulmonary Surfactant-Inhibition, Enhancement and Evaluation, Biochim. Biophys. Acta 1778, 1947–1977 (DOI: 10.1016/j.bbamem.2008.03.021)

[27] Kapralov A. A., Feng W. H., Amoscato A. A. *et al.* (2012), Adsorption of Surfactant Lipids by Single-Walled Carbon Nanotubes in Mouse Lung

upon Pharyngeal Aspiration, ACS Nano 6, 4147-4156 (DOI: 10.1021/nn300626q)

[28] Hu G., Jiao B., Shi X. *et al.* (2013), Physicochemical Properties of Nanoparticles Regulate Translocation across Pulmonary Surfactant Monolayer and Formation of Lipoprotein Corona, ACS Nano 7, 10525−10533 (DOI: 10.1021/nn4054683)

[29] Raesch S. S., Tenzer S., Storck W. *et al.* (2015), Proteomic and Lipidomic Analysis of Nanoparticle Corona upon Contact with Lung Surfactant Reveals Differences in Protein, but not Lipid Composition, ACS Nano 9, 11872-11885 (DOI: 10.1021/acsnano.5b04215)

[30] Hu Q., Bai X., Hu G. *et al.* (2017), Unveiling the Molecular Structure of Pulmonary Surfactant Corona on Nanoparticles, ACS Nano 11, 6832−6842 (DOI: 10.1021/acsnano.7b01873)

[31] Casper C. B., Verreault D., Adams E. M. *et al.* (2016), Surface Potential of DPPC Monolayers on Concentrated Aqueous Salt Solutions, J. Phys. Chem. B 120, 2043-2052 (DOI: 10.1021/acs.jpcb.5b10483)

[32] Hu M., Stanzione F., Sum A. K. *et al.* (2015), Design Principles for Nanoparticles Enveloped by a Polymer-Tethered Lipid Membrane, ACS Nano 9, 9942-9954 (DOI: 10.1021/acsnano.5b03439)

[33] Van Lehn R. C., Alexander-Katz A. (2013), Structure of Mixed-Monolayer-Protected Nanoparticles in Aqueous Salt Solution from Atomistic Molecular Dynamics Simulations, J. Phys. Chem. C 117, 20104-20115 (DOI: 10.1021/jp406035e)

[34] Van Lehn R. C., Ricci M., Silva P.H. *et al.* (2014), Lipid Tail Protrusions Mediate the Insertion of Nanoparticles into Model Cell Membranes, Nat. Commun. 5, 4482 (DOI: 10.1038/ncomms5482)

[35] Mandal T., Konduru N. V., Ramazani A., *et al.* (2018), Effect of Surface Charge and Hydrophobicity on Phospholipid-Nanoparticle Corona Formation: A Molecular Dynamics Simulation Study, Colloid Interface Sci. Commun. 25, 7−11 (DOI: 10.1016/j.colcom.2018.04.008)

[36] Lima T., Bernfur K., Vilanova M. *et al.* (2020), Understanding the Lipid and Protein Corona Formation on Different Sized Polymeric Nanoparticles, Sci. Rep. 10, 1129 (DOI: 10.1038/s41598-020-57943-6)

[37] Maity A., De S. K., Chakraborty A. (2021), Interaction of Aromatic Amino Acid-Functionalized Gold Nanoparticles with Lipid Bilayers: Insight into the Emergence of Novel Lipid Corona Formation, J. Phys. Chem. B 125, 2113–2123 (DOI: 10.1021/acs.jpcb.0c10079)

[38] De S. K., Maity A., Chakraborty A. (2021), Underlying Mechanisms for the Modulation of Self-Assembly and the Intrinsic Fluorescent Properties of Amino Acid-Functionalized Gold Nanoparticles, Langmuir 37, 5022–5033 (DOI: 10.1021/acs.langmuir.1c00431)

[39] Bothun G. D., Ganji N., Khan I. *et al.* (2017), Anionic and Cationic Silver Nanoparticle Binding Restructures Net-Anionic PC/ PG Monolayers with Saturated or Unsaturated Lipids, Langmuir 33, 353-360 (DOI: 10.1021/acs.langmuir.6b02003)

[40] Ganji N., Khan I. A., Bothun G. D. (2018), Surface Activity of Poly (ethylene glycol)-Coated Silver Nanoparticles in the Presence of a Lipid Monolayer, Langmuir 34, 2039−2045 (DOI: 10.1021/acs.langmuir.7b03743)

[41] Sugikawa K., Matsuo K., Ikeda A. (2018), Suppression of Gold Nanoparticle Aggregation on Lipid Membranes using Nanosized Liposomes to Increase Steric Hindrance, Langmuir 35, 229-236 (DOI: 10.1021/acs.langmuir.8b03550)

[42] Humphrey W., Dalke A., Schulten K. (1996), VMD: Visual Molecular Dynamics, J. Mol. Graph. 14, 33-38 (DOI: 10.1016/0263-7855(96)00018-5)

[43] Yang J. A., Lohse S. E., Murphy C. J. (2014), Tuning Cellular Response to Nanoparticles via Surface Chemistry and Aggregation, Small 10, 1642-1651 (DOI: 10.1002/smll.201302835)

[44] Zhang L., Li P., Li D. *et al.* (2008), Effect of Freeze Thawing on Lipid Bilayer-Protected Gold Nanoparticles, Langmuir 24, 3407−3411 (DOI: 10.1021/la703737q)

[45] Nandi S., Pyne A., Ghosh M. *et al.* (2020), Antagonist Effects of L-Phenylalanine and the Enantiomeric Mixture Containing D-Phenylalanine on Phospholipid Vesicle Membrane, Langmuir 36, 2459-2473 (DOI: 10.1021/acs.langmuir.9b03543)

[46] Nandi S., Layek S., Nandi P. K. *et al.* (2021), Self-Assembly of Artificial Sweetener Aspartame Adversely Affects Phospholipid Membranes: Plausible Reason for Its Deleterious Effects, Chem. Commun. 57, 10532-10535 (DOI: 10.1039/d1cc04482f)

[47] De S. K., Kanwa N., Ahamed M. *et al.* (2018), Spectroscopic Evidence for Hydration and Dehydration of Lipid Bilayers upon Interaction with Metal Ions: a New Physical Insight, Phys. Chem. Chem. Phys. 20, 14796-14807 (DOI: 10.1039/c8cp01774c)

[48] Ramos L., Lubensky T. C., Dan N. *et al.* (1999), Surfactant-Mediated Two-Dimensional Crystallization of Colloidal Crystals, Science 286, 2325−2328 (DOI: 10.1126/science.286.5448.2325)

[49] Poger D., Mark A. E. (2010), On the Validation of Molecular Dynamics Simulations of Saturated and cis-Monounsaturated Phosphatidylcholine Lipid Bilayers: A Comparison with Experiment, J. Chem. Theory Comput. 6, 325-336 (DOI: 10.1021/ct900487a)

[50] Petrova A. B., Herold C., Petrov E. P. (2017), Conformations and Membrane-Driven Self-Organization of Rodlike fd Virus Particles on Freestanding Lipid Membranes, Soft Matter 13, 7172−7187 (DOI: 10.1039/c7sm00829e)

Chapter 4

Formation of Lipid Corona on Ag Nanoparticles and Its Impact on Ag^+ Ion Dissolution and Aggregation of Ag Nanoparticles against External Stimuli

4.1 Introduction

The coating of lipid molecules around nanoparticles (NPs) is known as "lipid corona" emerged in the literature in 2018 *[1,2]*. During the budding of virus, virus particles have the ability to drag the lipid molecules from the host cell membrane to form lipid corona that protects virus from environment *[3,4]*. Similarly, when nanoparticles come near the vicinity to the cell membrane, there is a possibility of the formation of lipid corona which may affect the bio physico-chemical properties of original NPs *[5-18]*. The underlying mechanism of formation of lipid corona around the gold nanoparticles (Au NPs) has just been established in the literature. The properties of both Au NPs (size, shape, surface charge, hydrophobicity) and lipids (phase-state, area per lipid head group, hydrophobicity, and surface charge) play crucial roles in the formation of lipid corona *[1,2,19-22]*. While lipid corona of gold nanoparticles have been well established, there is no such report of formation of lipid corona around the other metallic nanoparticles like silver nanoparticles (Ag NPs). So, there exists huge research gap regarding the dependency of the nature of metallic core in lipid corona formation. Moreover, the question arises whether the lipid corona formation depends only on the surface ligands of the nanoparticle surface (independent of metallic core e.g. Au, Ag etc.) or the metallic core also plays a significant role in the formation of lipid corona.

It is important to note that both the commercial and biological applications of Ag NPs are limited due to the Ag NPs agglomeration, surface oxidation

of NPs, Ag^+ ions release and dissolution which influences the toxicity of Ag NPs *[23-28]*. It is well-known that physicochemical properties of Ag NPs like size, surface charge, shape, surface coatings play significant roles on the NPs toxicity, long-term stability, and interaction with biomolecules *[29-40]*. The surface oxidation and Ag^+ ion dissolution also affects the size and shape of the NPs (optical and light scattering property changes) which restricts the Ag NPs based imaging applications *[41,42]*. Different strategies have been adopted to prevent the Ag NPs surface oxidation and aggregation such as coating with polyvinylpyrrolidone (PVP) *[31]*, polyethylene glycol (PEG) polymer *[43-46]*, thiolated PEG *[47]*, lipids *[48-49]* as well as hybrid gold or silica core-shell *[50-51]*. Although inorganic surface layer better protects the inner Ag NPs core from surface oxidation than organic surface layer, the synthesis of inorganic surface layer is complicated. Also, the coating of polymer, thiolated ligands around the Ag NPs surface induces toxicity. So, there is an opportunity to form a biocompatible system which will impart stability to the Ag NPs and prevent surface oxidation against external stimuli. The lipid corona around Ag NPs can be a better alternative system to overcome all of the above-mentioned issues.

In this context, some of our recent reports on lipid corona are really intriguing. Our group first reported novel lipid corona formation around aromatic amino acid functionalized gold nanoparticles (Au-AA NPs) *[20,22]*. The study revealed that at high lipid concentration, the Au-AA NPs form lipid corona whereas the Au-AA NPs undergo agglomeration at low lipid concentration which also depends on the surface charge of both Au-AA NPs and lipid. The influence of lipid phase state in formation of lipid corona and lipid-induced aggregation was also investigated *[22]*. For first time, the lipid corona was categorized as “hard” and “soft” lipid corona depending on the phase transition temperature of lipids. The lipid corona was found to provide stability towards the Au NPs against different external stimuli. All of these results motivate us to study the corona formation of

aromatic amino acids functionalized silver nanoparticles (Ag-AA NPs) using different surface charged and phase state lipid vesicles. The main objective of the present study to investigate if the metallic core of nanoparticle has any role in forming the lipid corona. The zwitterionic phospholipids having wide difference in their phase transition temperature (T_m), namely, 1,2-dioleoyl-sn-glycero3-phosphocholine (DOPC, T_m = - 20 °C), 1,2-dimyristoyl-sn-glycero-3-phosphocholine (DMPC, T_m = 23 °C), and 1,2-dipalmitoyl-sn-glycero-3-phosphocholine (DPPC, T_m = 41 °C) and negatively charged 1,2-dimyristoylsn-glycero-3-phospho-(1′-rac-glycerol) (sodium salt) (DMPG), positively charged 1,2-dimyristoyl-3-trimethylammonium-propane (chloride salt) (DMTAP) lipids were chosen for this purpose. Next, we studied the behaviour of lipid coated Ag-AA NP to understand whether lipid coated Ag-AA NPs can prevent the surface oxidation, aggregation, and dissolution of metallic core against external stimuli like pH, high salt concentration, and freeze thaw cycles. Our results showed that surface ligands present on the nanoparticles surface play important part in lipid corona formation rather than metallic core. The lipid corona around Ag-AA NPs brings long term stability of the NPs and protects the Ag NPs from surface oxidation and Ag^+ ions release.

4.2 Results and Discussion

4.2.1 Optimization and characterization of aromatic amino acid functionalized silver nanoparticles (Ag-AA NPs):

At first, we optimized the reaction conditions to synthesize the smaller size silver nanoparticles using aromatic amino acids by in situ method. For this, we have varied the concentration of aromatic amino acids (0.5 and 1 mM) and NaOH (2-10 mM) by keeping the silver nitrate ($AgNO_3$) concentration fixed. The results have been summarized in **Figure 4.1, Table 4.1 and 4.2**. We found that the optimized reaction concentration of aromatic amino acids (tyrosine and tryptophan), NaOH, and $AgNO_3$ were 1, 10, and 0.75 mM

respectively for synthesizing smaller size silver nanoparticles. The SPR peak of the Ag-Tyr and Ag-Trp NPs in this concentrations range appeared at shorter wavelength (407 nm) along with less full width half-maximum (FWHM) of the SPR peak (**Figure 4.1**).

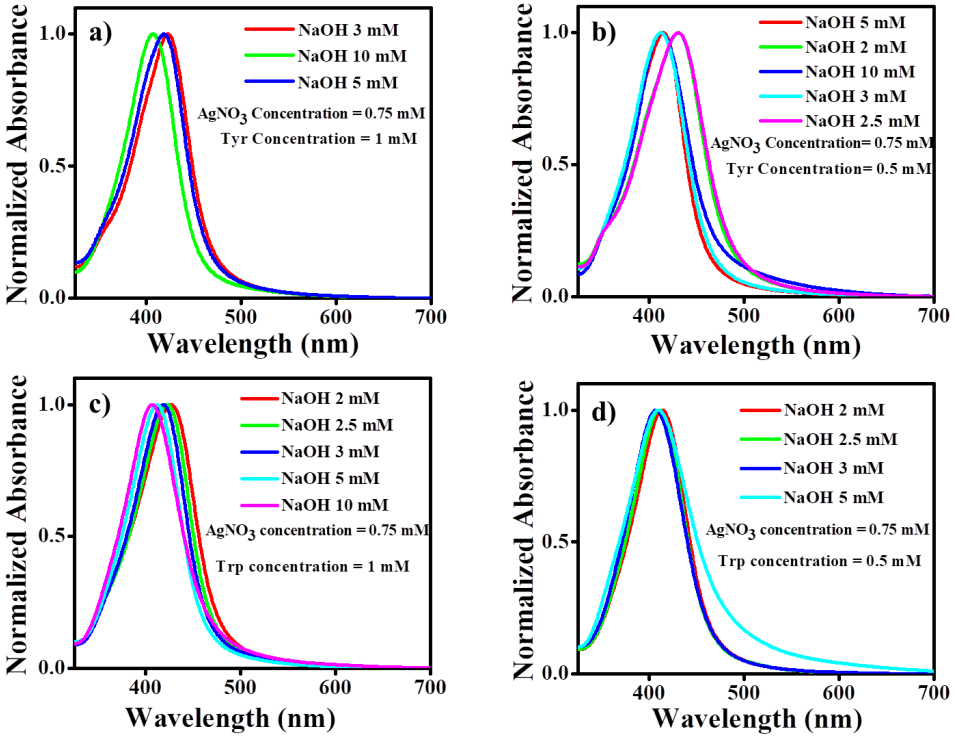

Figure 4.1 *Normalized UV-Visible spectra of Ag-Tyr (a, b) and Ag-Trp NPs (c, d) at a fixed concentration of $AgNO_3$ (0.75 mM) and Tyr and Trp concentration (1 mM and 0.5 mM) in various concentration of NaOH.*

Tyr concentration (mM)	NaOH concentration (mM)	SPR peak (nm)	FWHM
1	3	423	66
1	5	418	67
1	10	407	63
0.5	2	431	78
0.5	2.5	430	78
0.5	3	419	70
0.5	5	415	64
0.5	10	412	69
1	3	423	66

Table 4.1 *Optimization table for the concentration of tyrosine and NaOH to synthesize silver nanoparticles*

Trp concentration (mM)	NaOH concentration (mM)	SPR peak (nm)	FWHM
1	2	427	74
1	2.5	422	70
1	3	418	65
1	5	411	65
1	10	407	69
0.5	2	413	68
0.5	2.5	410	66
0.5	3	407	70
0.5	5	409	84

Table 4.2 *Optimization table for the concentration of tryptophan and NaOH to synthesize silver nanoparticles*

Noteworthy that we could not synthesize the stable phenylalanine functionalized silver nanoparticles in all these concentration range (data not shown) as phenylalanine is much weaker reducing agent than tyrosine and tryptophan. The successful synthesis of stable silver nanoparticles was first confirmed visually as the colourless solution was turned into yellow colour after the addition of amino acids and NaOH to the $AgNO_3$ solution (**Figure 4.2a**). Both the Ag-Tyr and Ag-Trp NPs displayed a strong absorption SPR maximum peak at 407 nm (**Figure 4.2b**). The FWHM was found to be 63 and 69 nm for Ag-Tyr and Ag-Trp NPs respectively. This difference of the FWHM is attributed to the slight better dispersity of Ag-Tyr NPs than Ag-Trp NPs. From the DLS measurements, the hydrodynamic diameter of Ag-Tyr and Ag-Trp NPs was calculated 44.1 ± 0.6 and 34.9 ± 0.4 nm respectively (**Figure 4.2c**). The HR-TEM imaging was then employed to estimate the size of the Ag NPs. TEM analysis revealed that Ag-Tyr and Ag-Trp NPs were spherical, and the average size of the NPs were ~ 22 and ~ 24 nm respectively (**Figure 4.2d, e**). The discrepancy in size of the DLS and TEM analysis might arise due the surface ligands (amino acids) coating and solvated water molecules around the Ag NPs. The surface charge of the

Ag-AA NPs was measured at physiological pH by zeta potential measurements. The zeta potential value of Ag-Tyr and Ag-Trp NPs at physiological pH was - 42 and -10 mV respectively (**Figure 4.2f**).

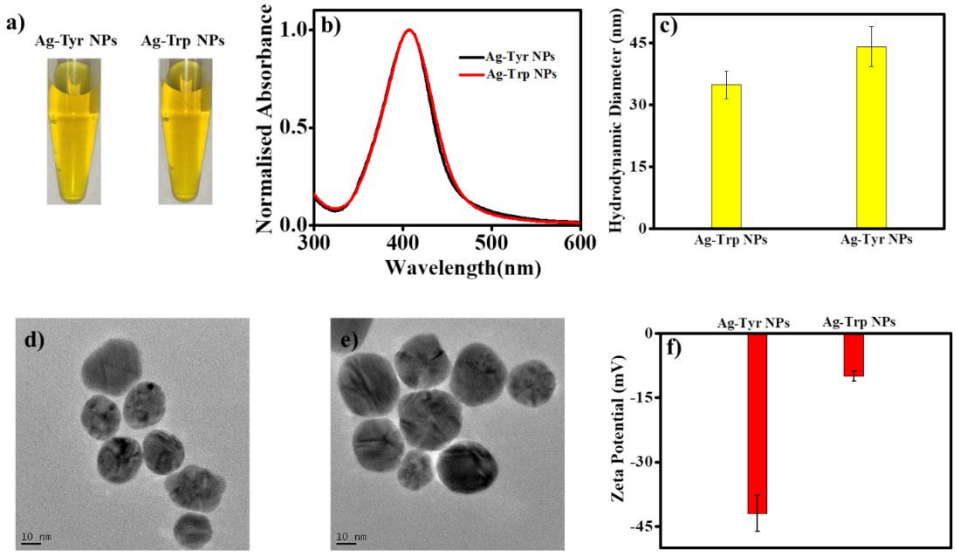

Figure 4.2 *Photograph (a), UV-Visible spectra (b), DLS data (c) of Ag-Tyr and Ag-Trp NPs at physiological pH, TEM images of Ag-Tyr (d) and Ag-Trp (e) NPs, and zeta potential of Ag-Tyr and Ag-Trp NPs at physiological pH.*

It is well reported that oxygen containing ligands prefer to bind on the Ag NPs surface and semiquinone moiety of the oxidised tyrosine is the binding site for the Ag NPs *[52]*. This results in the high negative zeta potential for the Ag-Tyr NPs as most of COO^- functional groups are oriented towards bulk. On the other hand, kynurenine moiety of the oxidized tryptophan binds on the Ag NPs surface *[53]*. Chen et al. reported both the carboxylate and amino groups of tryptophan are the preferential binding site to the Ag NPs by using Surface-Enhanced Raman Scattering (SERS) spectroscopy *[54]*. As the COO^- functional group binds to the Ag NPs surface, the zeta potential of the Ag-Trp NPs is less negative than Ag-Tyr NPs.

4.2.2 Interaction of Ag-Tyr and Ag-Trp NPs with lipid vesicles:

To investigate the lipid corona formation around Ag-Tyr and Ag-Trp NPs and lipid-induced aggregation, we have varied the number ratio of the

number of NPs to the number of lipid vesicles per mL. For this, we added required concentration of lipid to a fixed concentration of Ag NPs (20 nM) to get the desired ratio listed on **Table 4.3**. The concentration of the Ag NPs was calculated by using the previously reported method *[55]* (see Experimental Methods for detailed calculation). The number of lipid vesicles per mL for different concentration of lipid was estimated following our previous methodology [*20*,*22*].

Concentration of Ag-Tyr and Ag-Trp NPs (nM)	Number of Ag-Tyr and Ag-Trp NPs /mL	Concentration of lipid (mM)	N_{tot}	N_{lipo}	number ratio of Ag-Tyr and Ag-Trp NPs: liposomes
20	6.023×10^{12}	0.8	97,389.01	4.938×10^{12}	1:1
20	6.023×10^{12}	0.4	97,389.01	2.469×10^{12}	2:1
20	6.023×10^{12}	0.2	97,389.01	1.236×10^{12}	5:1
20	6.023×10^{12}	0.1	97,389.01	6.184×10^{11}	10:1
20	6.023×10^{12}	0.05	97,389.01	3.092×10^{11}	20:1
20	6.023×10^{12}	0.025	97,389.01	1.546×10^{11}	40:1
20	6.023×10^{12}	0.0125	97,389.01	7.730×10^{10}	80:1

Table 4.3 *Calculation of the number ratio of Ag-Tyr and Ag-Trp NPs: liposomes. Where N_{tot} is the total number of lipid molecules per lipid vesicles and N_{lipo} is the total number of lipid vesicles per mL for a known concentration of lipids.*

The zwitterionic lipid vesicles of widely different phase transition temperature namely DOPC (T_m = -20 °C), DMPC (T_m = 23 °C), and DPPC (T_m = 41 °C) along with charged lipids namely positively charged DMPC/DMTAP and negatively charged DMPC/DMPG were used to investigate the interaction of these lipids with Ag-Tyr and Ag-Trp NPs. The interaction of Ag NPs and lipid vesicles was primarily monitored by UV-Visible spectroscopy. Our results showed that both the Ag-Tyr and Ag-Trp NPs did not interact with negatively charged DMPC/DMPG lipid vesicles as both the Ag NPs are negatively charged (**Figure 4.3a, b**).

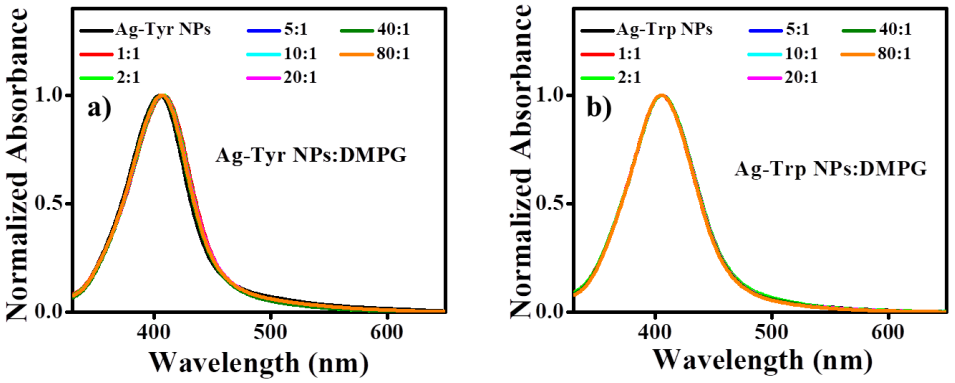

Figure 4.3 *Normalized UV-Visible absorption spectra of Ag-Tyr (a) and Ag-Trp (b) NPs in different number ratio of Ag NPs: DMPC/DMPG lipid vesicles.*

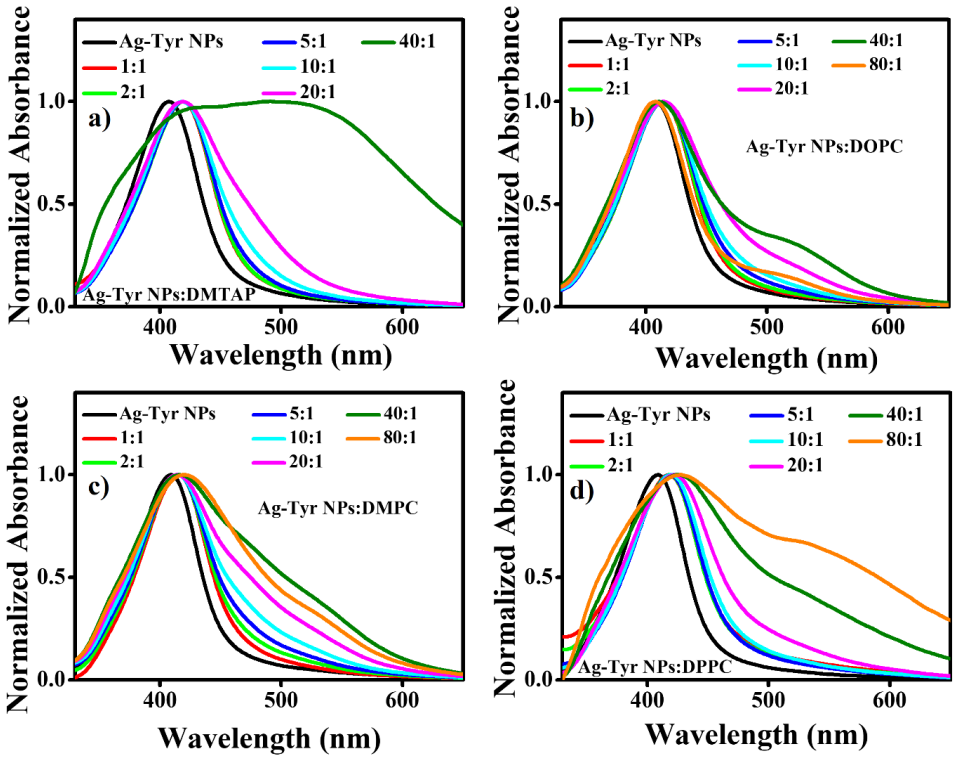

Figure 4.4 *Normalized UV-Visible absorption spectra of Ag-Tyr NPs (a-d) in different number ratio of Ag-Tyr NPs: DMPC/DMTAP (a), Ag-Tyr NPs: DOPC (b), Ag-Tyr NPs: DMPC (c), and Ag-Tyr NPs: DPPC (d) lipid vesicles.*

But, Ag-Tyr and Ag-Trp NPs interacted strongly with the positively charged DMPC/DMTAP lipid vesicles. The UV-Visible spectra showed that at low concentration of positively charged lipid vesicles

(DMPC/DMTAP) [Ag NPs: DMPC/DMTAP (20:1-80:1)], the Ag-Tyr and Ag-Trp NPs underwent rapid aggregation whereas the Ag NPs remained stable at high lipid concentration [Ag NPs: DMPC/DMTAP (1:1-5:1)] (**Figure 4.4a, 4.5a, 4.6a, and 4.7a**). The SPR peak of Ag-Tyr and Ag-Trp NPs shifted ~ 7-9 nm along with the increase in the absorbance than the native Ag NPs at high lipid concentration [Ag NPs: DMPC/DMTAP (1:1-2:1)] suggesting the possible lipid corona formation around the Ag NPs (**Figure 4.5a and 4.7a)**. Interestingly, at low lipid concentration [Ag NPs: DMPC/DMTAP (40:1-80:1)], the SPR peak of Ag-Tyr and Ag-Trp NPs shifted to the longer wavelength along with the sharp decrement in absorbance value of Ag NPs, implying the possible aggregation and subsequent Ag^{+} ion dissolution of Ag NPs (**Figure 4.4a, 4.5a, 4.6a, and 4.7a**).

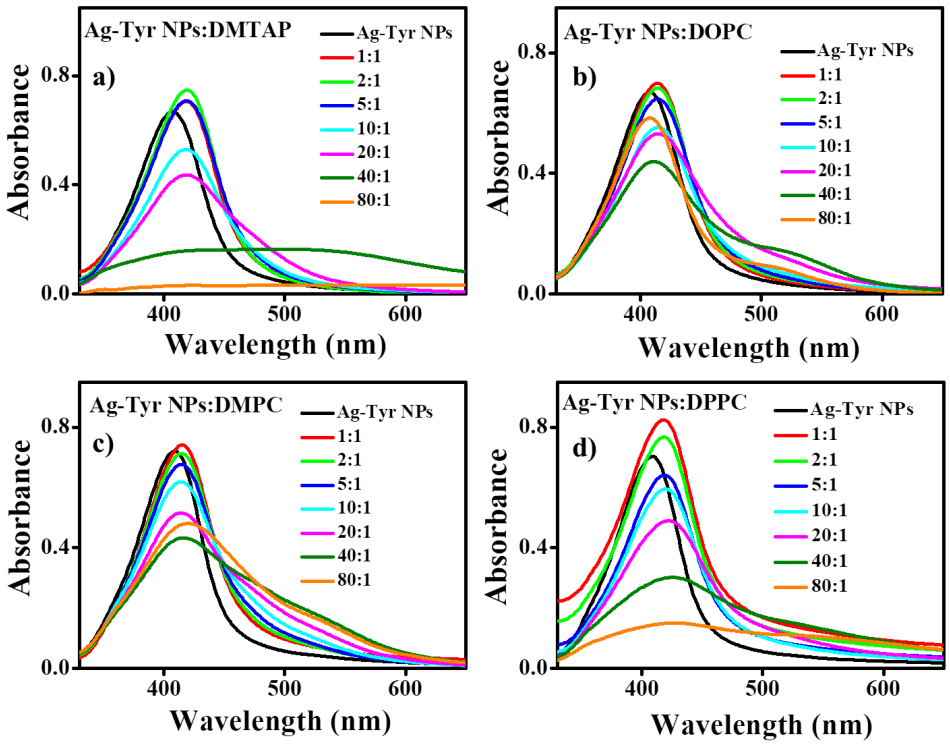

Figure 4.5 *UV-Visible absorption spectra of Ag-Tyr NPs (a-d) in different number ratio of Ag-Tyr NPs: DMPC/DMTAP (a), Ag-Tyr NPs: DOPC (b), Ag-Tyr NPs: DMPC (c), and Ag-Tyr NPs: DPPC (d) lipid vesicles.*

The Ag-Tyr NPs, owing to more negative surface charge, interact strongly with the positively charged lipid vesicles than Ag-Trp NPs. So, decrement in absorbance for Ag-Tyr NPs is more than Ag-Trp NPs at low lipid concentration [Ag NPs: DMPC/DMTAP (80:1)] (**Figure 4.5a and 4.7a)**. These results suggest that the interaction of Ag-AA NPs and lipid vesicles is mainly governed by electrostatic interaction.

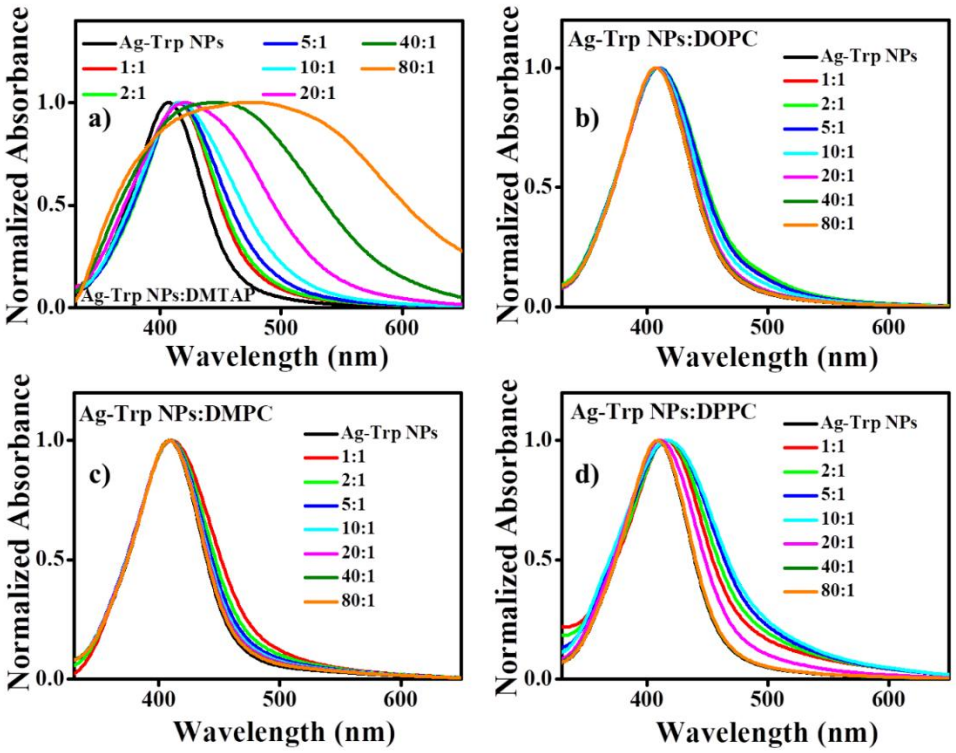

Figure 4.6 *Normalized UV-Visible absorption spectra of Ag-Trp NPs (a-d) in different number ratio of Ag-Trp NPs: DMPC/DMTAP (a), Ag-Trp NPs: DOPC (b), Ag-Trp NPs: DMPC (c), and Ag-Trp NPs: DPPC (d) lipid vesicles.*

Next, we investigated the interaction of Ag-Tyr and Ag-Trp NPs with neutrally charged lipid vesicles of different phase transition temperature. At 30 °C, DOPC and DMPC will be in liquid-crystalline phase and DPPC will be in sol-gel phase. The normalized UV-Visible spectra revealed that the Ag-Tyr NPs underwent aggregation at low concentration of [Ag-Tyr NPs: DOPC or DMPC or DPPC (40:1-80:1)] all these three lipid vesicles as a new peak appeared at longer wavelength (500-600 nm) along with the

presence of primary SPR peak (**Figure 4.4b, c, d**). Interestingly, the extent of aggregation of Ag-Tyr NPs in presence of DPPC lipid vesicles was the maximum and the order was DPPC>DMPC>DOPC (**Figure 4.4b, c, d and 4.5b, c, d)**. However, at high lipid concentration of all these lipid vesicles [Ag-Tyr NPs: DOPC or DMPC or DPPC (1:1-2:1)], the SPR peak was red shifted to ~ 6-9 nm which indicates the formation of lipid corona irrespective of phase state of lipid vesicles (**Figure 4.4b, c, d**).

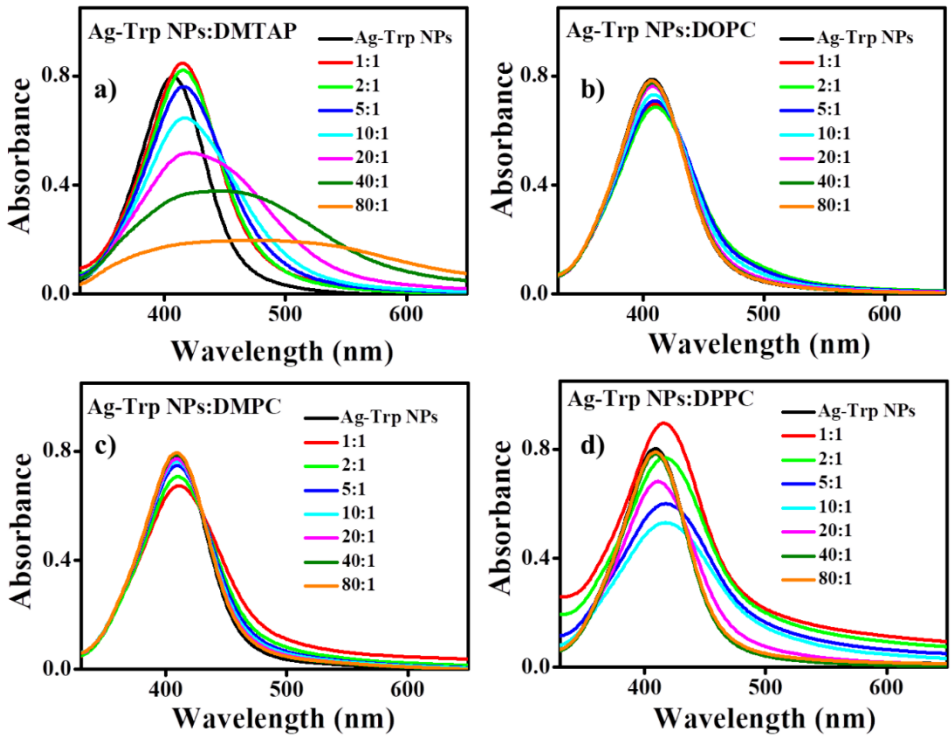

Figure 4.7 *UV-Visible absorption spectra of Ag-Trp NPs (a-d) in different number ratio of Ag-Trp NPs: DMPC/DMTAP (a), Ag-Trp NPs: DOPC (b), Ag-Trp NPs: DMPC (c), and Ag-Trp NPs: DPPC (d) lipid vesicles.*

On contrary, the Ag-Trp NPs did not interact at all at low concentration [Ag-Trp NPs: DOPC or DMPC or DPPC (40:1-80:1)] of any zwitterionic lipid vesicles as the SPR peak of the Ag-Trp NPs remain unchanged (**Figure 4.6b, c, d and 4.7b, c, d**). But, the SPR peak of the Ag-Trp NPs was shifted ~ 3 nm for DOPC and DMPC and ~ 7 nm for DPPC lipid vesicles at high lipid concentration [Ag-Trp NPs: DOPC or DMPC or DPPC (1:1-2:1)]

(**Figure 4.6b, c, d)**. This observation indicates that DPPC lipid may be more effective in formation of lipid corona around Ag-Trp NPs rather than DOPC and DMPC. The slight shift in the SPR peak of Ag-Trp NPs in presence of DOPC and DMPC also suggests partial lipid coating may be formed around Ag-Trp NPs.

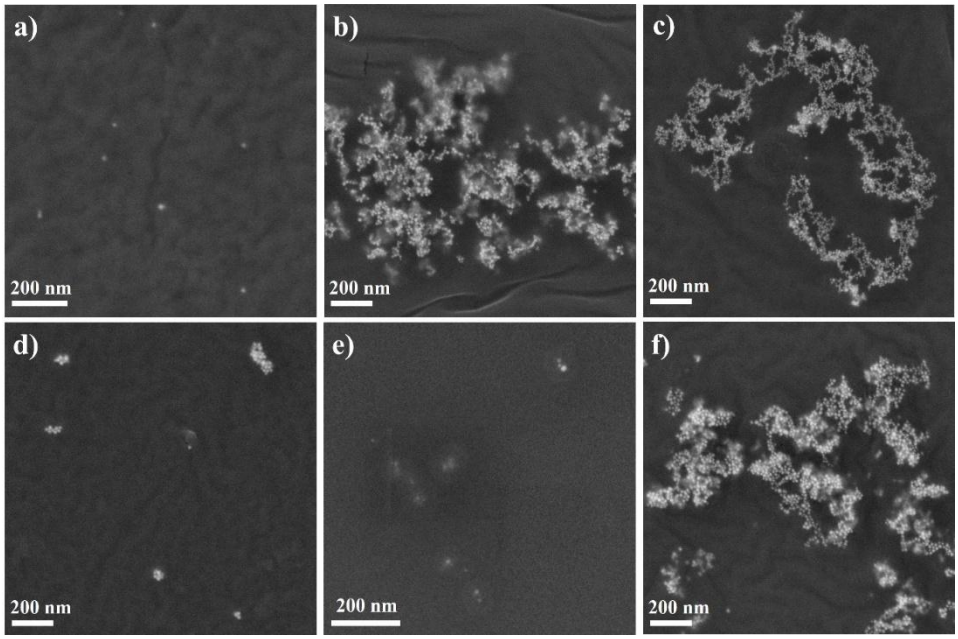

Figure 4.8 *Field Emission Scanning Electron Microscopy (FESEM) images of Ag-Tyr (a-c) and Ag-Trp NPs (d-f) as control (a, d), in presence of low concentration of neutral DMPC lipid vesicles [Ag NPs: DMPC (40:1)] (b, e) and positively charged DMPC/DMTAP lipid vesicles [Ag NPs: DMPC/DMTAP (40:1)] (c, f) respectively. Scale bar = 200 nm.*

After the spectroscopic investigation, we studied the morphology of Ag NPs aggregation using Field Emission Scanning Electron Microscopy (FESEM). Both the blank Ag-Tyr and Ag-Trp NPs showed the dispersed spherical morphology of Ag NPs with minimal aggregation (**Figure 4.8a, d)**. But, in presence of low concentration of neutral DMPC lipid vesicles [Ag NPs: DMPC (40:1)], the Ag-Tyr NPs formed aggregated structure whereas the Ag-Trp NPs remained non-aggregated (**Figure 4.8b, e).** These results corroborate well with our spectroscopic findings that the Ag-Tyr NPs interact strongly than the Ag-Trp NPs and underwent aggregation in

presence of low concentration of neutral charged lipid vesicles. However, both the Ag-Tyr and Ag-Trp NPs formed aggregated structures at low concentration of positively charged DMPC/DMTAP lipid vesicles [Ag NPs: DMPC/DMTAP (40:1)] (**Figure 4.8c, f**).

We can now compare the lipid corona of Ag NPs with that of Au NPs. We previously investigated the interaction of aromatic amino acid functionalized gold nanoparticles (Au-AA NPs) with differently charged lipid vesicles *[20]*. We reported that both the phenylalanine and tyrosine functionalized gold nanoparticles (Au-Phe and Au-Tyr NPs) interact strongly with zwitterionic and positively charged lipid vesicles. At high lipid concentration, the Au-AA NPs formed lipid corona whereas at low lipid concentration, they underwent lipid-induced aggregation [20]. Tryptophan functionalized gold nanoparticles (Au-Trp NPs) did not interact with zwitterionic DMPC lipid vesicles rather it interacted with positively charged lipid vesicles [20]. All of these three Au NPs did not interact at all with negatively charged lipid vesicles. At high zwitterionic lipid concentration, the Au-Phe NPs formed lipid corona irrespective of the phase state of lipid vesicles. However, the sol-gel state of lipid vesicles (DPPC) induced more aggregation than liquid crystalline state lipid vesicles (DOPC) at low lipid concentration [22]. Similar observations were obtained in case of Ag-Tyr and Ag-Trp NPs as discussed before. At high lipid concentration i.e. when the number of Ag NPs and lipid vesicles are almost same [Ag NPs: lipid (2:1)], the Ag NPs are fully coated by lipid bilayer as there are plenty of lipid vesicles. So, the Ag NPs remain stable at high lipid concentration due to the full coating of lipid bilayers. However, at lower lipid concentration i.e. when the number of Ag NPs are much higher than the number of lipid vesicles [Ag NPs: lipid (40:1 - 80:1)], the Ag NPs are partially coated with lipid bilayer because of the less availability of lipid vesicles. The partially lipid coated Ag NPs come closer and triggers the aggregation of the NPs. Thus we can conclude that surface ligands rather than metallic core solely have significant effect on lipid corona and lipid-

induced aggregates formation of nanoparticles at different lipid concentration.

4.2.3 Stability of different zwitterionic and positively charged lipid coated Ag-Tyr and Ag-Trp NPs in presence of different external stimuli:

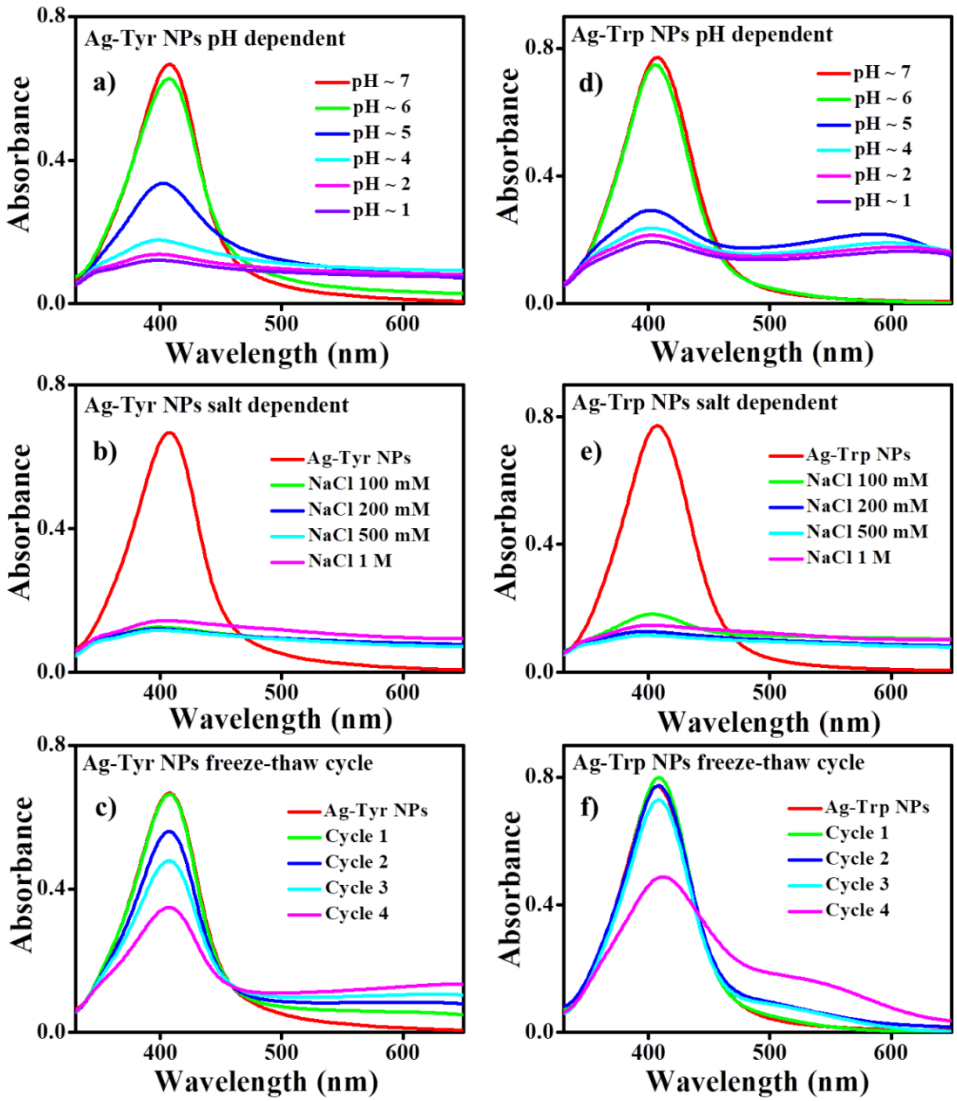

Figure 4.9 *UV-Visible absorption spectra of Ag-Tyr (a-c) and Ag-Trp NPs (b-f) against acidic pH (a, d), high NaCl salt concentration (b, e) and repetitive freeze-thaw cycles (c, f).*

At first, we studied the stability of native Ag-Tyr and Ag-Trp NPs against different external stimuli i.e. acidic pH, high salt concentration, and freeze-thaw cycles. The UV-Visible spectra revealed that the absorbance of SPR peak of both Ag-Tyr and Ag-Trp NPs significantly reduced at acidic pH (5 to 1) and high salt concentration (100 mM to 1 M NaCl) suggesting dissolution of Ag^+ ion from Ag NPs (**Figure 4.9a, b, d, e**). Stability against freeze-thaw cycle is more relevant from biological standpoint view as the nanoparticles have to pass through several repetitive freeze-thaw cycle for long term preservation for biological studies. In the present investigation, we observed that the Ag-Tyr NPs underwent Ag^+ ion dissolution as the solution become colourless and absorbance of SPR peak decreased predominantly after several freeze-thaw cycles (**Figure 4.9c**). But for Ag-Trp NPs, the aggregation of Ag-Trp NPs took place as evident from the secondary SPR peak that developed along with the primary SPR peak, and the colour changed (not colourless) (**Figure 4.9f**). This observation indicates that the native Ag-Trp NPs are more stable than Ag-Tyr NPs against successive freeze-thaw cycles. Both the Ag^+ ion dissolution from Ag NPs and the aggregation of Ag NPs induces toxicity to the Ag NPs. So, it is utmost interest to prevent the Ag^+ ion dissolution and the aggregation of Ag NPs. For these purposes, different surface charged and phase state lipid corona (coating around the Ag NPs) could be a potential candidate. Herein, we are particularly interested to compare the degree of stability induced by different lipids (DOPC, DMPC, DPPC, and DMPC/DMTAP) when they form corona around Ag-Tyr and Ag-Trp NPs.

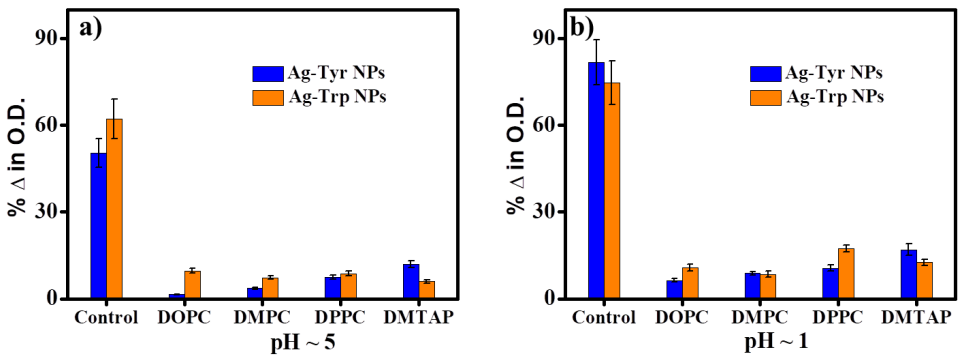

Figure 4.10 *Percentage of decrement of O.D. for Ag-Tyr and Ag-Trp NPs as control and after DOPC, DMPC, DPPC, and DMPC/DMTAP lipid coating at pH ~5 (a) and pH ~ 1 (b).*

To study the effect of acidic pH on the stability of the different lipid coated Ag-Tyr and Ag-Trp NPs over native Ag NPs, we conducted the experiment at two different pH: one was pH ~ 5 to simulate lysosomal fluid and tumour microenvironments of the cell where Ag NPs reside and another was extreme pH (pH ~1). From UV-Visible spectra, we estimated percentage of the decrement in O.D. which reveals the surface oxidation and Ag^+ ion dissolution from Ag NPs. We witnessed a noticeable decrement in O.D. at pH ~5, for the both Ag-Tyr and Ag-Trp NPs (50.45 % for Ag-Tyr and 62.1 % for Ag-Trp NPs), indicating significant Ag^+ ion dissolution. However, the percentage of decrement of O.D. at pH ~ 5 was very less in case of all lipid coated Ag-Tyr and Ag-Trp NPs which is shown in **Table 4.4**. Similar trend in prevention of surface oxidation and Ag^+ ion dissolution was obtained in case of lipids coated Ag-Tyr and Ag-Trp NPs at extreme acidic pH (pH ~1) (**Table 4.5**). However, the percentage of decrement in O.D. value was slightly higher compared to pH ~5 (**Figure 4.10a, b**). The stability of the lipid coated Ag-Tyr and Ag-Trp NPs against acidic pH compared to native Ag NPs demonstrates the usefulness of lipid corona to impede the Ag^+ ion dissolution and the present data indicates that DOPC lipid coated Ag-Tyr NPs stood best among all.

	Control (%)	DOPC (%)	DMPC (%)	DPPC (%)	DMPC/DMTAP (%)
Ag-Tyr NPs	50.45	1.54	3.6	7.49	12
Ag-Trp NPs	62.1	9.67	7.3	8.74	5.97

Table 4.4 *Percentage of decrement of O.D. for Ag-Tyr and Ag-Trp NPs as control and after DOPC, DMPC, DPPC, and DMPC/DMTAP lipid coating at pH ~ 5.*

	Control (%)	DOPC (%)	DMPC (%)	DPPC (%)	DMPC/DMTAP (%)
Ag-Tyr NPs	81.77	6.32	8.79	10.57	16.97
Ag-Trp NPs	74.7	10.68	8.47	17.34	12.63

Table 4.5 *Percentage of decrement of O.D. for Ag-Tyr and Ag-Trp NPs as control and after DOPC, DMPC, DPPC, and DMPC/DMTAP lipid coating at pH ~ 1.*

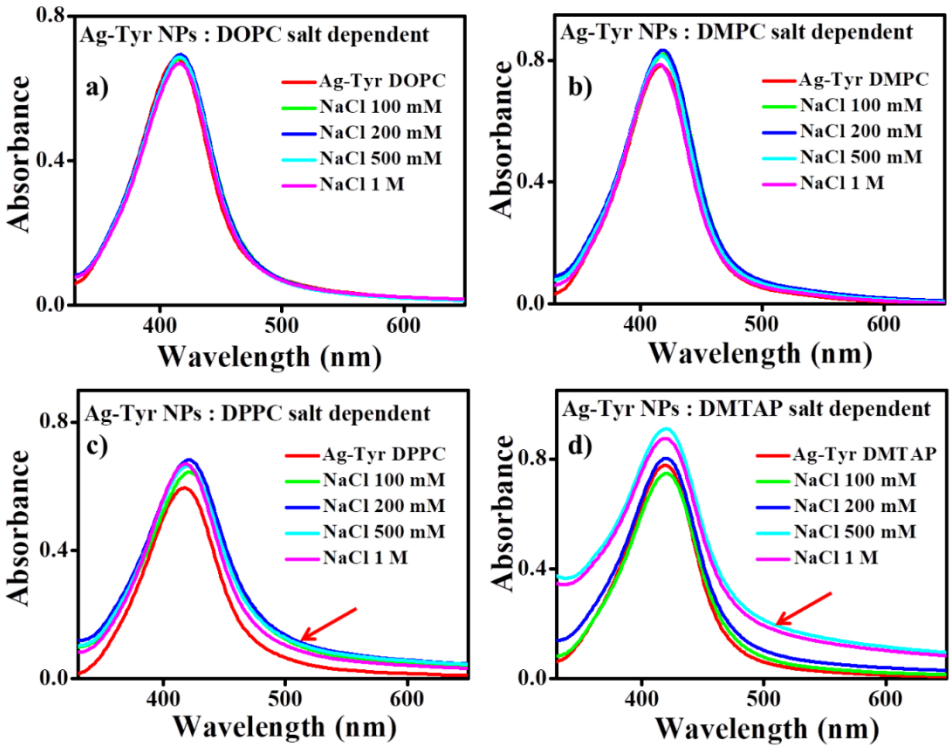

Figure 4.11 *UV-Visible absorption spectra of DOPC (a), DMPC (b), DPPC (c), and DMPC/DMTAP (d) lipid coated Ag-Tyr NPs against high NaCl salt concentration (100 mM - 1M).*

We further investigated the stability of lipid coated Ag-Tyr and Ag-Trp NPs against high NaCl concentration (100 mM - 1 M). The UV-Visible spectra revealed that unlike native Ag-Tyr and Ag-Trp NPs, the O.D. value of lipid coated Ag NPs did not decrease rather it increased more than that of bare Ag NPs (**Figure 4.11a-d and 4.12a-d**). The increment was much more in case of both DPPC and DMTAP lipid coated Ag NPs at high salt concentration (500 mM -1 M) which may be due the adsorption of

negatively charged Cl^- to the more positive charge of phospholipid choline head group (NR_3^+ group) (**Figure 4.11c-d and 4.12c-d**). As a result of that, the dissolution of Ag^+ ion did not happen but the broadening of the SPR peak (red arrow) indicates the slight aggregation of the Ag NPs. The aggregation could be attributed to the decrement of the surface charge of the lipid coated Ag NPs after the adsorption of negatively charged chloride ion. The aggregation is more prominent in case of DPPC and DMTAP lipid coated Ag-Trp NPs (**Figure 4.12c-d**) (as the secondary peak generated at longer wavelength) than DPPC and DMTAP lipid coated Ag-Tyr NPs (no secondary peak generation but only peak broadening) (**Figure 4.11c-d**). The observation is attributed to lower the surface charge of Ag-Trp NPs than that of Ag-Tyr NPs.

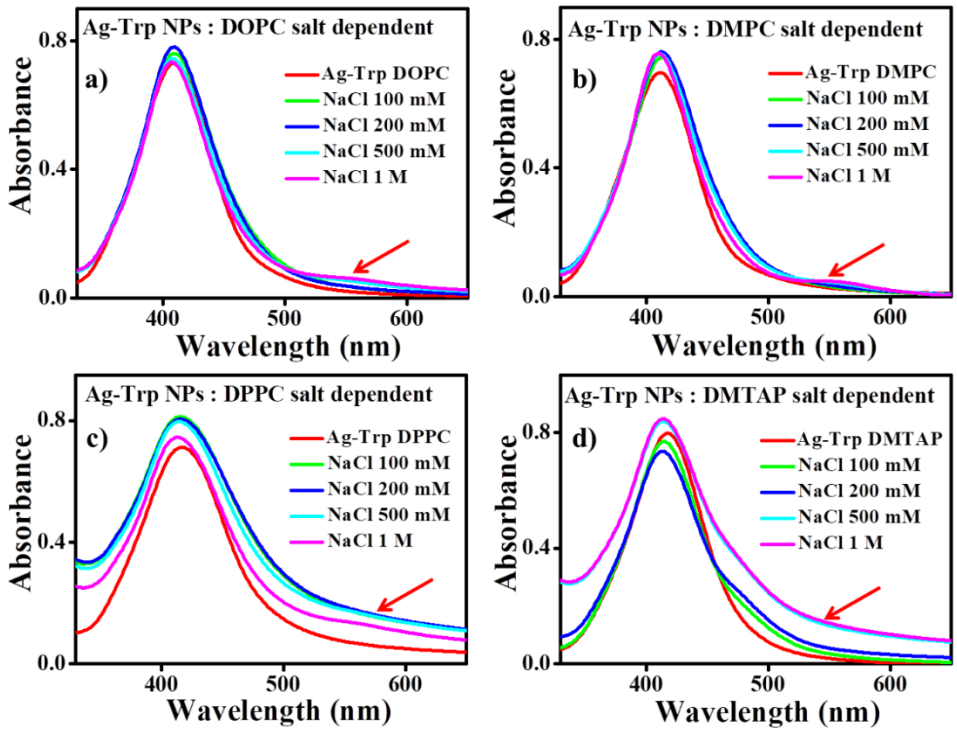

Figure 4.12 *UV-Visible absorption spectra of DOPC (a), DMPC (b), DPPC (c), and DMPC/DMTAP (d) lipid coated Ag-Trp NPs against high NaCl salt concentration (100 mM – 1 M).*

Interestingly, both DOPC and DMPC lipid coated Ag-Tyr NPs were more stable than DOPC and DMPC lipid coated Ag-Trp NPs (secondary peak

generated at high NaCl concentration) (**Figure 4.11a-b and 4.12a-b**). We assume that the partial coverage of lipid around Ag-Trp NPs in presence of DOPC and DMPC lipid vesicles may be possible factor for the lesser stability of the lipid coated Ag-Trp NPs. Therefore, we summarize that the lipid corona prevents the Ag^+ ion dissolution in all lipids coated Ag NPs but failed to stabilize the Ag NPs in some cases in presence of high NaCl concentration.

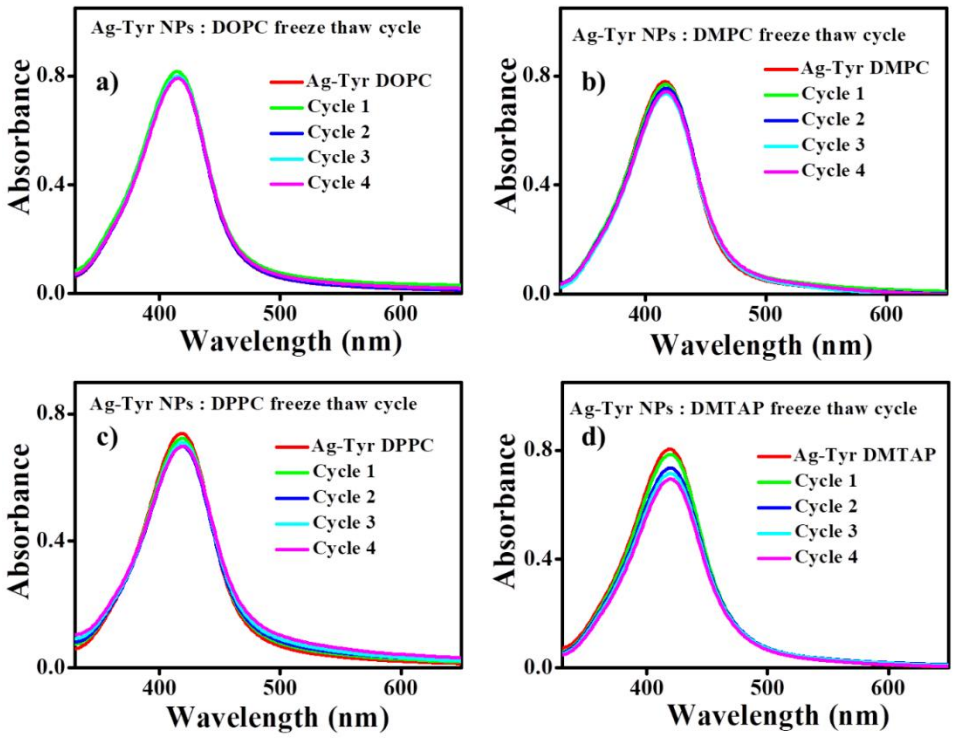

Figure 4.13 *UV-Visible absorption spectra of DOPC (a), DMPC (b), DPPC (c), and DMPC/DMTAP (d) lipid coated Ag-Tyr NPs against freeze-thaw cycles.*

Next, we were interested to study the stability of the lipid coated Ag-Tyr and Ag-Trp NPs (lipid corona) against freeze thaw cycles (**Figure 4.13a-d and 4.14a-d**). Unlike the Ag^+ ion dissolution in case of native Ag-Tyr NPs (percentage of decrement of O.D. was 50 %), all lipids coated Ag-Tyr NPs regained stability against four successive freeze-thaw cycles. The decrement in percentage of O.D. for DMPC/DMTAP lipid coated Ag-Tyr NPs (13.6%) is more than that of DOPC (0.5 %), DMPC (4.6 %), and DPPC

(4.53 %) lipid coated Ag-Tyr NPs (**Figure 4.13a-d**). On the contrary, in case of Ag-Trp NPs, both the DOPC and DMPC lipid coated Ag NPs underwent aggregation (O.D value decreases along with a new broadened peak at longer wavelength) (**Figure 4.14a, b**) although the aggregation is lesser than the native Ag-Trp NPs. This observation proves that Ag-Trp NPs is not fully covered by lipid molecules in presence of DOPC and DMPC lipid vesicles. Both the DPPC and DMPC/DMTAP lipid coated Ag-Trp NPs did not undergo aggregation against four successive freeze-thaw cycles (no new peak generation at longer wavelength) (**Figure 4.14c-d**). However, the percentage of O.D. decrement in case of DMPC/DMTAP lipid coated Ag-Trp NPs (11.2 %) was more compared to DPPC lipid coated Ag-Trp NPs (5.4 %) (**Figure 4.14c-d**). All of these findings led us to a conclusion that zwitterionic lipid coated Ag NPs are more superior than positively charged lipid coated Ag NPs against all these external stimuli. Another important observation is that DOPC lipid coated Ag-Tyr NPs is much worthier among all the zwitterionic lipid coated Ag-Tyr NPs against all these harsh external stimuli.

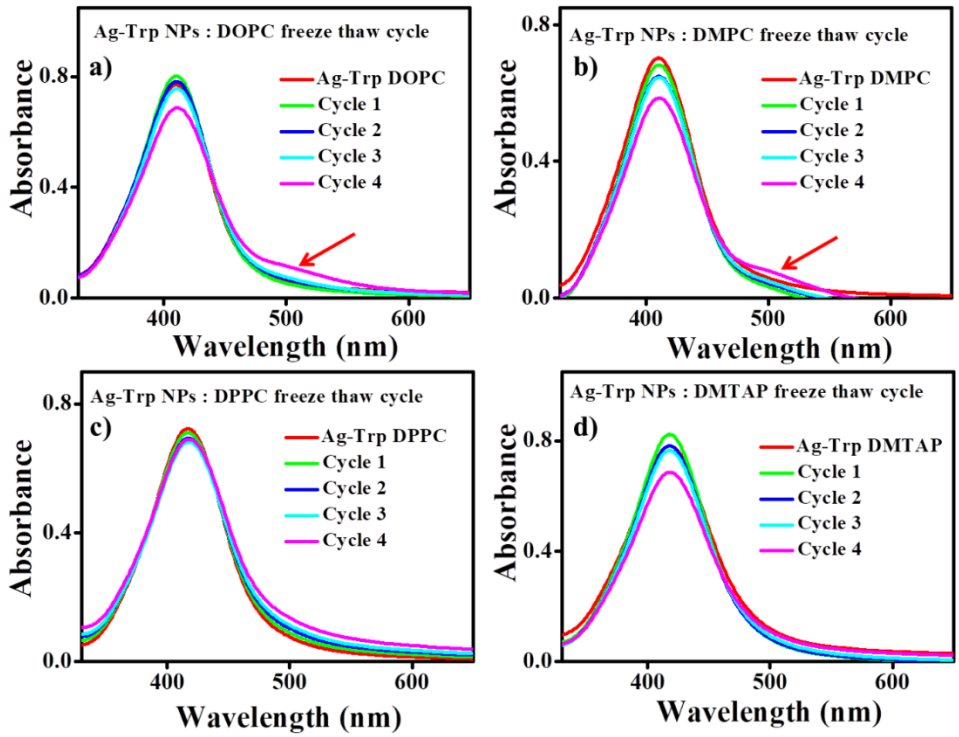

Figure 4.14 *UV-Visible absorption spectra of DOPC (a), DMPC (b), DPPC (c), and DMPC/DMTAP (d) lipid coated Ag-Trp NPs against freeze-thaw cycles.*

Next, we studied the kinetics of the stability of lipid coated Ag-Tyr and Ag-Trp NPs as control and against acidic pH (pH ~ 5) and 150 mM NaCl (physiological salt concentration).

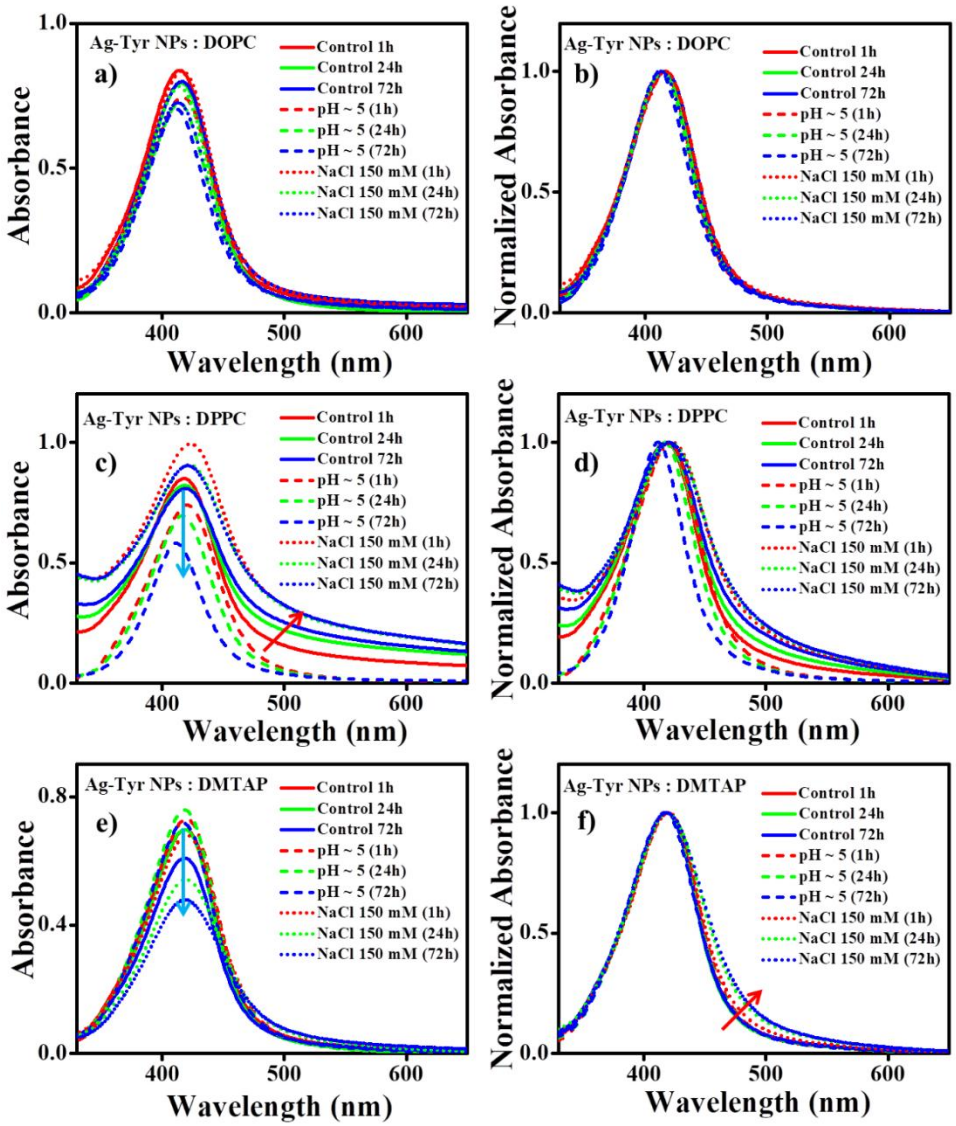

Figure 4.15 *UV-Visible (a, c, e) and normalized UV-Visible (b, d, f) absorption spectra of kinetics of DOPC (a,b), DPPC (c,d), and DMPC/DMTAP (e-f) lipid coated Ag-Tyr NPs as control and against acidic pH (pH ~ 5) and 150 mM NaCl concentration.*

Both the UV-Visible and normalized UV-Visible spectra revealed that the DOPC lipid coated Ag-Tyr NPs are stable as control and also in presence of acidic pH and salt concentration after 72 hours (**Figure 4.15a, b**).

Interestingly, the DPPC lipid coated Ag-Tyr NPs underwent aggregation with time (peak broadened at longer wavelength as indicated by red arrow) which indicates the DPPC lipid coated Ag-Tyr NPs are not so much stable with time (**Figure 4.15c, d**). Although at pH ~ 5, the DPPC lipid coated Ag-Tyr NPs did not undergo aggregation (no peak broadening) but Ag^+ ion dissolution happened with time as both the decrement of O.D. and blue shift of SPR peak was observed (as indicated by light blue arrow) (**Figure 4.15c, d**). Similar to our previous observation, in presence of salt, the O.D. value increases along with the broadening of SPR peak which suggests the aggregation of DPPC lipid coated Ag-Tyr NPs. For positively charged DMPC/DMTAP lipid coated Ag-Tyr NPs, marginal Ag^+ ion dissolution was observed (O.D. decreases marginally) with time (**Figure 4.15e, f**). But in presence of salt concentration, both the aggregation and Ag^+ ion dissolution happened as both the peak broadening and O.D. decrement took place (**Figure 4.15e, f**). Unlike the DOPC coated Ag-Tyr NPs, the DOPC coated Ag-Trp NPs was not so much stable with time (secondary peak generated at longer wavelength with the decrement of O.D) (**Figure 4.16a, b**) which may be due to the less coating of lipid around Ag-Trp NPs in presence of DOPC lipid vesicles as discussed above. We found that DPPC coated Ag-Trp NPs also underwent aggregation as control and in presence of salt concentration and Ag^+ ion dissolution at pH ~5 with time (**Figure 4.16c, d**). Similar phenomenon was observed in case of DMPC/DMTAP lipid coated Ag-Trp NPs like DMPC/DMTAP lipid coated Ag-Tyr NPs (**Figure 4.16e, f**). Although some aggregation and Ag^+ ion dissolution happened in case of lipid coated Ag-Tyr and Ag-Trp NPs, the quantity is very less compared to native Ag-Tyr and Ag-Trp NPs.

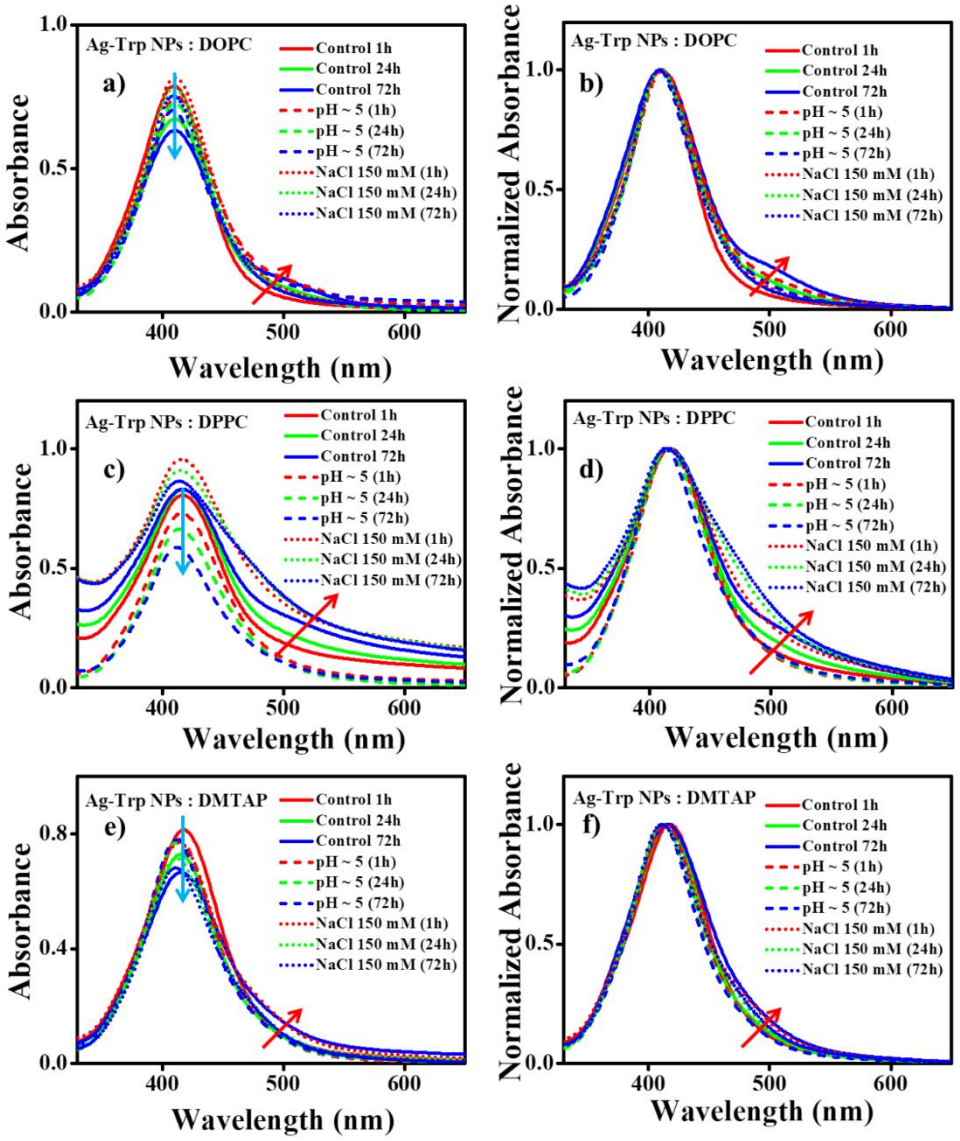

Figure 4.16 *UV-Visible (a, c, e) and normalized UV-Visible (b, d, f) absorption spectra of kinetics of DOPC (a, b), DPPC (c, d), and DMPC/DMTAP (e-f) lipid coated Ag-Trp NPs as control and against acidic pH (pH ~5) and 150 mM NaCl concentration.*

Now the question arises whether the excess liposomes give the stability to the lipid coated Ag-Tyr and Ag-Trp NPs against external stimuli. To answer this question, we centrifuged all the lipid-nanoparticle mixture to remove the excess lipids which may affect the stability of lipid coated Ag-Tyr and Ag-Trp NPs. In case of DOPC coated Ag-Tyr NPs, the Ag-Tyr NPs was

found to be stable as control and in the presence of acidic pH (pH ~5) after 36 h (no shift and broadening in SPR peak and negligible decrement in O.D (**Figure 4.17a, b**). But, in presence of 150 mM NaCl concentration, the percentage of O.D. decrement was 10.7 % and 19.7 % after 1h and 36h respectively (**Figure 4.17a**). This data suggests that excess liposomes affect the stability of DOPC coated Ag-Tyr NPs against high salt concentration.

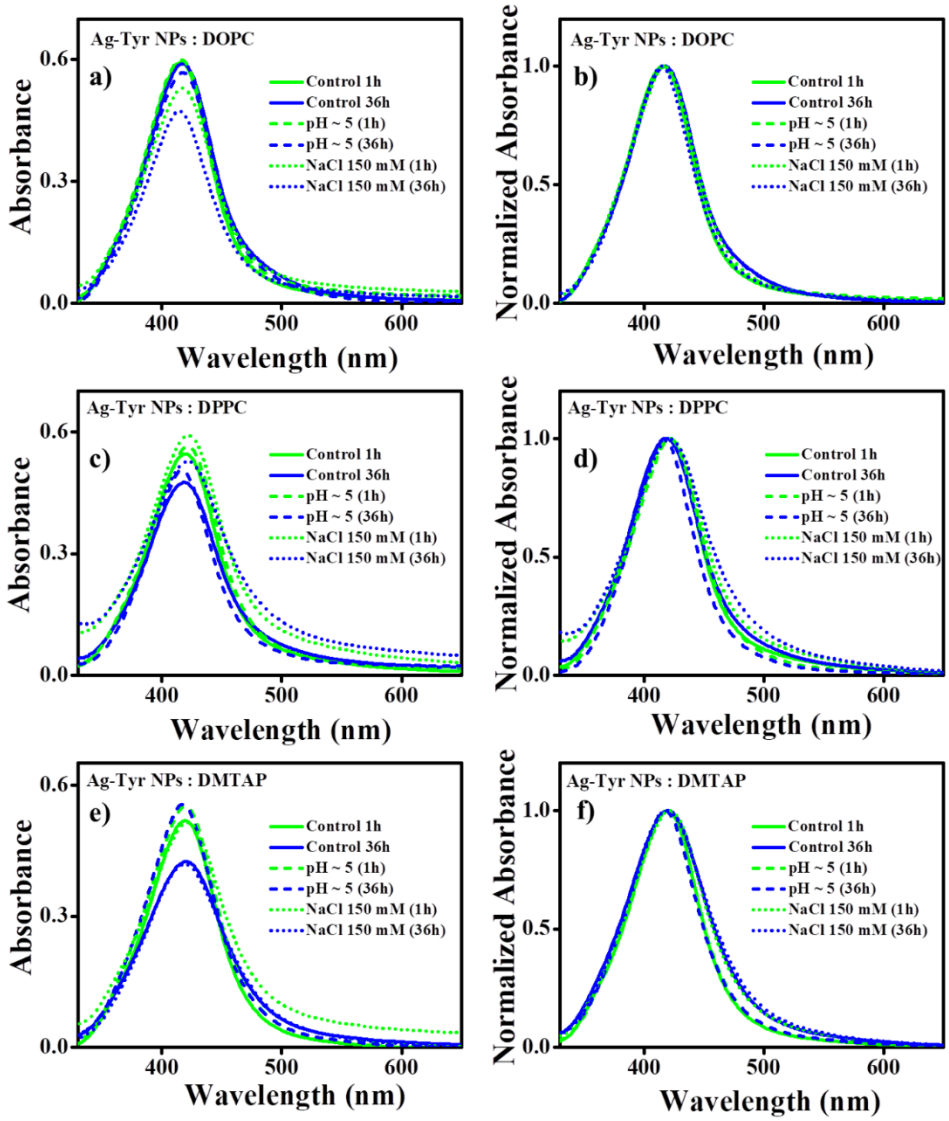

Figure 4.17 *UV-Visible (a, c, e) and normalized UV-Visible (b, d, f) absorption spectra of kinetics of DOPC (a, b), DPPC (c, d), and DMPC/DMTAP (e-f) lipid coated Ag-Tyr NPs as control and against acidic pH (pH ~5) and 150 mM NaCl concentration after removing the extra lipids through centrifugation of lipid-nanoparticle mixture.*

For DPPC lipid coated Ag-Tyr NPs, the decrement in O.D was observed for both native DPPC lipid coated nanoparticles and in presence of salt after 36h (**Figure 4.17c, d**). However, the broadening of the SPR peak indicates the slight aggregation of DPPC lipid coated Ag-Tyr NPs as observed in case of non-centrifuge also. Similar behaviour was also found for positively charged DMPC/DMTAP lipid vesicle (**Figure 4.17e, f**). Interestingly, the DOPC lipid coated Ag-Trp NPs underwent aggregation along with the Ag^+ ion dissolution (solution almost become colorless) after centrifugation as the O.D. value significantly reduced as well the SPR peak was more broadened (**Figure 4.18a, b**). Previously, we mentioned that the Ag-Trp NPs may form partial lipid coating around the NPs in presence of DOPC lipid vesicles. It is possible that during centrifuging the mixture, the partial lipid coated nanoparticle come closes and induce aggregation and Ag^+ ion dissolution of NPs (It is worthy to mention that blank Ag-Trp NPs do not undergo aggregation after centrifugation).

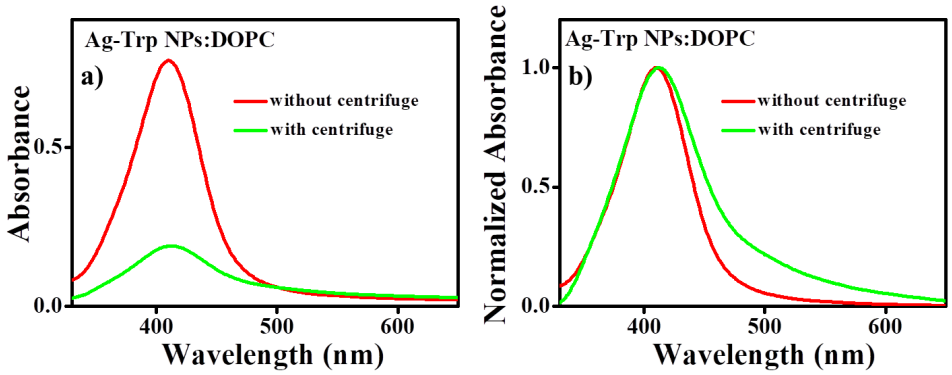

Figure 4.18 *UV-Visible (a) and normalized UV-Visible (b) absorption spectra of DOPC (a, b) lipid coated Ag-Trp NPs before and after centrifugation of lipid-nanoparticle mixture.*

The native DPPC lipid coated Ag-Trp NPs underwent aggregation with time as the SPR peak was broadened in longer wavelength (**Figure 4.19a, b**). In both the presence of acidic pH and salt concentration, the decrement of O.D. was observed although the SPR peak was broadened in case of salt concentration only (**Figure 4.19a, b**). So, aggregation and dissolution of

Ag^+ ion happened for DPPC lipid coated Ag-Trp NPs in presence of acidic pH and salt concentration with time. The DMPC/DMTAP lipid coated Ag-Trp NPs itself underwent aggregation with time (SPR peak was broadened at longer wavelength (**Figure 4.19c, d**). Although the decrement of O.D. of DMPC/DMTAP coated Ag-Trp NPs at acidic pH and salt concentration is more compared to native DMPC/DMTAP lipid coated Ag-Trp NPs with time, the aggregation was more in case of native DMPC/DMTAP lipid coated Ag-Trp NPs (more broadening in SPR peak) (**Figure 4.19c, d**). So, we conclude that the excess liposome gives more stability to the Ag-Tyr and Ag-Trp NPs against external stimulis. But after removing the excess liposome also, the lipid coated Ag-Tyr NPs and Ag-Trp NPs (expect DOPC for Ag-Trp NPs) give far more better stability than native Ag-Tyr and Ag-Trp NPs with time.

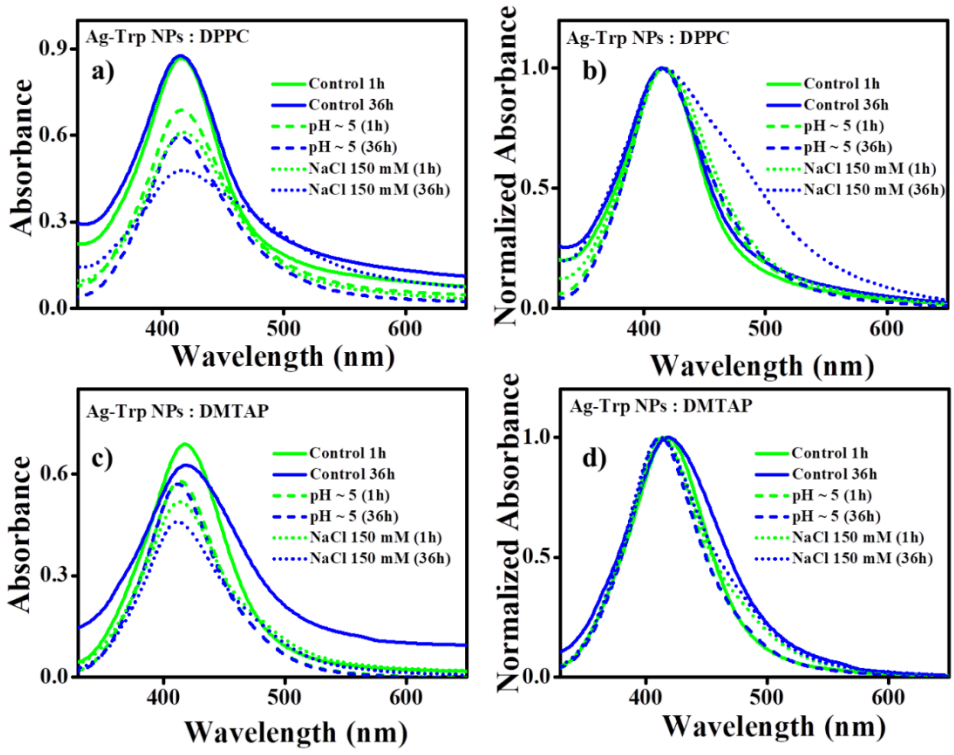

Figure 4.19 *UV-Visible (a, c) and normalized UV-Visible (b, d) absorption spectra of kinetics of DPPC (a-b), and DMPC/DMTAP (c-d) lipid coated Ag-Trp NPs as control and against acidic pH (pH ~ 5) and 150 mM NaCl Concentration after removing the extra lipids through centrifugation of lipid-nanoparticle mixture.*

4.3 Conclusion

In summary, we have successfully synthesized tyrosine and tryptophan functionalized silver nanoparticles (Ag-Tyr and Ag-Trp NPs) and investigated their interaction with different charged and phase state lipid vesicles to prove the dependency of lipid corona on surface ligand and metallic core. The lipid coated Ag-Tyr and Ag-Trp NPs (lipid corona) were found to prevent aggregation, surface oxidation and Ag^+ ion dissolution against harsh external stimuli (acidic pH, high NaCl concentration, and freeze-thaw cycles). We found that lipid corona and lipid-induced aggregation predominantly depends on the surface ligands irrespective of the metallic core as aromatic amino acid functionalized both the gold and silver nanoparticles showed similar interaction with lipid vesicles. The excellent stability of all the different lipid corona around the Ag-Tyr and Ag-Trp NPs against external stimuli over native Ag NPs proves the striking advantage of the lipid corona. The zwitterionic lipid coating around the Ag NPs have greater impact to impede the aggregation and Ag^+ ion dissolution of Ag NPs than positively charged lipid coated Ag NPs. The DOPC lipid coated Ag-Tyr NPs is more superior than all other lipid coated Ag-Tyr and Ag-Trp NPs. All of these studies will help researchers to engineer suitable lipid coated nanoparticles for various biomedical and commercial applications.

4.4 References

[1] Olenick L. L., Troiano J. M., Vartanian A. *et al.* (2018), Lipid Corona Formation from Nanoparticle Interactions with Bilayers, Chem 4, 2709−2723 (DOI: 10.1016/j.chempr.2018.09.018)

[2] Zhang X., Pandiakumar A. K., Hamers R. J. *et al.* (2018), Quantification of Lipid Corona Formation on Colloidal Nanoparticles from Lipid Vesicles, Anal. Chem. 90, 14387−14394 (DOI: 10.1021/acs.analchem.8b03911)

[3] Bornholdt Z. A., Noda T., Abelson D. M. *et al.* (2013), Structural Rearrangement of Ebola Virus VP40 Begets Multiple Functions in the Virus Life Cycle, Cell 154, 763-774 (DOI: 10.1016/j.cell.2013.07.015)

[4] Dessen A., Volchkov V., Dolnik O. *et al.* (2000), Crystal Structure of the Matrix Protein VP40 from Ebola Virus, EMBO J. 19, 4228-4236 (DOI: 10.1093/emboj/19.16.4228)

[5] Chetwynd A. J., Lynch I. (2020), The Rise of the Nanomaterial Metabolite Corona, and Emergence of the Complete Corona, Environ. Sci.: Nano 7, 1041−1060 (DOI: 10.1039/c9en00938h)

[6] Bahrami A. H., Raatz M., Agudo-Canalejo J. *et al.* (2014), Wrapping of Nanoparticles by Membranes, Adv. Colloid Interface Sci. 208, 214−224 (DOI: 10.1016/j.cis.2014.02.012)

[7] Zhang S., Gao H., Bao G. (2015), Physical Principles of Nanoparticle Cellular Endocytosis, ACS Nano 9, 8655−8671 (DOI: 10.1021/acsnano.5b03184)

[8] Xu F., Bandara A., Akiyama H. *et al.* (2018), Membrane Wrapped Nanoparticles Probe Divergent Roles of GM3 and Phosphatidylserine in Lipid-Mediated Viral Entry Pathways, Proc. Natl. Acad. Sci. U.S.A. 115, E9041−E9050 (DOI: 10.1073/pnas.1804292115)

[9] Mendozza M., Caselli L., Salvatore A. *et al.* (2019), Nanoparticles and Organized Lipid Assemblies: from Interaction to Design of Hybrid Soft Devices, Soft Matter 15, 8951−8970 (DOI: 10.1039/c9sm01601e)

[10] Yu X., Feizpour A., Ramirez N.-G. P. *et al.* (2014), Glycosphingolipid-Functionalized Nanoparticles Recapitulate CD169-Dependent HIV-1 Uptake and Trafficking in Dendritic Cells, Nat. Commun. 5, 4136 (DOI: 10.1038/ncomms5136)

[11] Zuraw-Weston S., Wood D. A., Torres I. K. *et al.* (2019), Nanoparticles Binding to Lipid Membranes: from Vesicle-Based Gels to Vesicle Tubulation and Destruction, Nanoscale 11, 18464−18474 (DOI: 10.1039/c9nr06570a)

[12] Xu F., Reiser M., Yu X. *et al.* (2016), Lipid-Mediated Targeting with Membrane-Wrapped Nanoparticles in the Presence of Corona Formation, ACS Nano 10, 1189−1200 (DOI: 10.1021/acsnano.5b06501)

[13] Yang J. A., Murphy C. J. (2012), Evidence for Patchy Lipid Layers on Gold Nanoparticle Surfaces, Langmuir 28, 5404−5416 (DOI: 10.1021/la300325p)

[14] Francia V., Schiffelers R. M., Cullis P. R. *et al.* (2020), The Biomolecular Corona of Lipid Nanoparticles for Gene Therapy, Bioconjugate Chem. 31, 2046-2059 (DOI: 10.1021/acs.bioconjchem.0c00366)

[15] Raesch S. S., Tenzer S., Storck W. *et al.* (2015), Proteomic and Lipidomic Analysis of Nanoparticle Corona upon Contact with Lung Surfactant Reveals Differences in Protein, but Not Lipid Composition, ACS Nano 9, 11872−11885 (DOI: 10.1021/acsnano.5b04215)

[16] Kapralov A. A., Feng W. H., Amoscato A. A. *et al.* (2012), Adsorption of Surfactant Lipids by Single-Walled Carbon Nanotubes in Mouse Lung upon Pharyngeal Aspiration, ACS Nano 6, 4147−4156 (DOI: 10.1021/nn300626q)

[17] Hu Q., Bai X., Hu G., *et al.* (2017), Unveiling the Molecular Structure of Pulmonary Surfactant Corona on Nanoparticles, ACS Nano 11, 6832−6842 (DOI: 10.1021/acsnano.7b01873)

[18] Hu G., Jiao B., Shi X. *et al.* (2013), Physicochemical Properties of Nanoparticles Regulate Translocation across Pulmonary Surfactant

Monolayer and Formation of Lipoprotein Corona, ACS Nano 7, 10525−10533 (DOI: 10.1021/nn4054683)

[19] Lima T., Bernfur K., Vilanova M. *et al.* (2020), Understanding the Lipid and Protein Corona Formation on Different Sized Polymeric Nanoparticles, Sci. Rep. 10, 1129 (DOI: 10.1038/s41598-020-57943-6)

[20] Maity A., De S. K., Chakraborty A. (2021), Interaction of Aromatic Amino Acid-Functionalized Gold Nanoparticles with Lipid Bilayers: Insight into the Emergence of Novel Lipid Corona Formation, J. Phys. Chem. B 125, 2113−2123 (DOI: 10.1021/acs.jpcb.0c10079)

[21] Mandal T., Konduru N. V., Ramazani A. *et al.* (2018), Effect of Surface Charge and Hydrophobicity on Phospholipid-Nanoparticle Corona Formation: A Molecular Dynamics Simulation Study, Colloid Interface Sci. Commun. 25, 7−11 (DOI: 10.1016/j.colcom.2018.04.008)

[22] Maity A., De S. K., Bagchi D. *et al.* (2022), Mechanistic Pathway of Lipid Phase-Dependent Lipid Corona Formation on Phenylalanine-Functionalized Gold Nanoparticles: A Combined Experimental and Molecular Dynamics Simulation Study, J. Phys. Chem. B 126, 2241−2255 (DOI: 10.1021/acs.jpcb.2c00356)

[23] Luoma S.N., Ho Y., Bryan G. (1995), Fate, Bioavailability and Toxicity of Silver in Estuarine Environments, Mar. Pollut. Bull. 31, 44–54 (DOI: 10.1016/0025-326X(95)00081-W)

[24] Ratte H.T. (1999), Bioaccumulation and Toxicity of Silver Compounds: A Review, Environ. Toxicol. Chem. 18, 89–108 (DOI: 10.1002/etc.5620180112)

[25] Kim K.T., Truong L., Wehmas L. *et al.* (2013), Silver Nanoparticle Toxicity in the Embryonic Zebrafish is Governed by Particle Dispersion and Ionic Environment, Nanotechnology 24, 957–4484 (DOI: 10.1088/0957-4484/24/11/115101)

[26] Braydich-Stolle L., Hussain S., Schlager J. J. *et al.* (2005), In Vitro Cytotoxicity of Nanoparticles in Mammalian Germline Stem Cells, Toxicol. Sci. 88, 412–419 (DOI: 10.1093/toxsci/kfi256)

[27] Van Aerle R., Lange A., Moorhouse A. *et al.* (2013), Molecular Mechanisms of Toxicity of Silver Nanoparticles in Zebrafish Embryos, Environ. Sci. Technol. 47, 8005–8014 (DOI: 10.1021/es401758d)

[28] Hussain S., Hess K., Gearhart J. *et al.* (2005), In Vitro Toxicity of Nanoparticles in BRL 3A Rat Liver Cells, Toxicol. In Vitro 19, 975–983 (DOI: 10.1016/j.tiv.2005.06.034)

[29] Park M.V., Neigh A. M., Vermeulen J. P. *et al.* (2011), The effect of Particle Size on the Cytotoxicity, Inflammation, Developmental Toxicity and Genotoxicity of Silver Nanoparticles, Biomaterials 32, 9810–9817 (DOI: 10.1016/j.biomaterials.2011.08.085)

[30] Yang X., Gondikas A. P., Marinakos S. M. *et al. (2012),* Mechanism of Silver Nanoparticle Toxicity is Dependent on Dissolved Silver and Surface Coating in Caenorhabditis Elegans, Environ. Sci. Technol. 46, 1119–1127 (DOI: 10.1021/es202417t)

[31] Gorka D. E., Osterberg J. S., Gwin C. A. *et al.* (2015), Reducing Environmental Toxicity of Silver Nanoparticles through Shape Control, Environ. Sci. Technol. 49, 10093–10098 (DOI: 10.1021/acs.est.5b01711)

[32] George S., Lin S., Ji Z. *et al.* (2012), Surface Defects on Plate-Shaped Silver Nanoparticles Contribute to Its Hazard Potential in a Fish Fill Cell Line and Zebrafish Embryos, ACS Nano 6, 3745–3759 (DOI: 10.1021/nn204671v)

[33] Cho Y. M., Mizuta Y., Akagi J. I. *et al.* (2018), Size-Dependent Acute Toxicity of Silver Nanoparticles in Mice, J. Toxicol. Pathol. 31, 73–80 (DOI: 10.1293/tox.2017-0043)

[34] Tree-Udom T., Seemork J., Shigyou K. *et al.* (2015), Shape Effect on Particle-Lipid Bilayer Membrane Association, Cellular uptake, and Cytotoxicity, ACS Appl. Mater. Interfaces 7, 23993–24000 (DOI: 10.1021/acsami.5b06781)

[35] Moon J., Kwak J. I., An Y. -J. (2019), The Effects of Silver Nanomaterial Shape and Size on Toxicity to Caenorhabditis Elegans in Soil Media, Chemosphere 215, 50–56 (DOI: 10.1016/j.chemosphere.2018.09.177)

[36] Li Y., Kroger M., Liu W. K. (2015), Shape effect in Cellular Uptake of PEGylated Nanoparticles: Comparison between Sphere, Rod, Cube and Disk, Nanoscale 7, 16631–16646 (DOI: 10.1039/c5nr02970h)

[37] Bar-Ilan O., Albrecht R. M., Fako V. E. *et al.* (2009), Toxicity Assessments of Multisized Gold and Silver Nanoparticles in Zebrafish Embryos, Small 5, 1897–1910 (DOI: 10.1002/smll.200801716)

[38] Liu H., Wang X., Wu Y. *et al.* (2019), Toxicity Responses of Different Organs of Zebrafish (Danio Rerio) to Silver Nanoparticles with Different Particle Sizes and Surface Coatings, Environ. Pollut. 246, 414–422 (DOI: 10.1016/j.envpol.2018.12.034)

[39] Lee K. J., Browning L. M., Nallathamby P. D. *et al.* (2012), In Vivo Quantitative Study of Sized-Dependent Transport and Toxicity of Single Silver Nanoparticles using Zebrafish Embryos, Chem. Res. Toxicol. 25, 1029–1046 (DOI: 10.1021/tx300021u)

[40] Powers C. M., Slotkin T. A., Seidler F. J. *et al.* (2011), Silver Nanoparticles Alter Zebrafish Development and Larval Behavior: Distinct Roles for Particle Size, Coating and Composition, Neurotoxicol. Teratol. 33, 708–714 (DOI: 10.1016/j.ntt.2011.02.002)

[41] Huang T., Xu X.-H. N. (2010), Synthesis and Characterization of Tunable Rainbow Colored Colloidal Silver Nanoparticles Using Single-

Nanoparticle Plasmonic Microscopy and Spectroscopy, J. Mater. Chem. 20, 9867−9876 (DOI: 10.1039/c0jm01990a)

[42] Lee S. H., Jun B. H. (2019), Silver Nanoparticles: Synthesis and Application for Nanomedicine, Int. J. Mol. Sci. 20, 865 (DOI: 10.3390/ijms20040865)

[43] Luo C., Zhang Y., Zeng X. *et al.* (2005), The Role of Poly(Ethylene Glycol) in the Formation of Silver Nanoparticles, J. Colloid Interface Sci. 288, 444−448 (DOI: 10.1016/j.jcis.2005.03.005)

[44] Stevenson A. P. Z., Blanco Bea D., Civit S. *et al.* (2012), Three Strategies to Stabilise Nearly Monodispersed Silver Nanoparticles in Aqueous Solution, Nanoscale Res. Lett. 7, 151 (DOI: 10.1186/1556-276X-7-151)

[45] Sanedrin R. G., Huang L., Jang J.-W. *et al.* (2008), Polyethylene Glycol as a Novel Resist and Sacrificial Material for Generating Positive and Negative Nanostructures, Small 4, 920−924 (DOI: 10.1002/smll.200701089)

[46] Liu C., Leng W., Vikesland P. J. (2018), Controlled Evaluation of the Impacts of Surface Coatings on Silver Nanoparticle Dissolution Rates, Environ. Sci. Technol. 52, 2726−2734 (DOI: 10.1021/acs.est.7b05622)

[47] Shkilnyy A., Soucé M., Dubois P. *et al.* (2009), Poly(ethylene Glycol)-Stabilized Silver Nanoparticles for Bioanalytical Applications of SERS Spectroscopy, Analyst 134, 1868−1872 (DOI: 10.1039/b905694g)

[48] Cunningham B., Engstrom A. E., Harper B. J. *et al.* (2021), Silver Nanoparticles Stable to Oxidation and Silver Ion Release Show Size-Dependent Toxicity in Vivo, Nanomaterials 11, 1516 (DOI: 10.3390/nano11061516)

[49] Miesen T. J., Engstrom A. M., Frost D. C. *et al.* (2020), A Hybrid Lipid Membrane Coating “Shape-Lock” Silver Nanoparticles to Prevent Surface Oxidation and Silver Ion Dissolution, RSC Adv. 10, 15677 (DOI: 10.1039/d0ra01727b)

[50] Karunamuni R., Naha P. C., Lau K. C. *et al.* (2016), Development of Silica-Encapsulated Silver Nanoparticles as Contrast Agents Intended for Dual-Energy Mammography, Eur. Radiol. 26, 3301−3309 (DOI: 10.1007/s00330-015-4152-y)

[51] Bonventre J. A., Pryor J. B., Harper B. J. *et al.* (2014), The Impact of Aminated Surface Ligands and Silica Shells on the Stability, Uptake, and Toxicity of Engineered Silver Nanoparticles, J. Nanopart. Res. 16, 2761 (DOI: 10.1007/s11051-014-2761-z)

[52] Selvakannan P. R., Ramanathan R., Plowman B. J. *et al.* (2013), Probing the Effect of Charge Transfer Enhancement in off Resonance Mode SERS via Conjugation of the Probe Dye between Silver Nanoparticles and Metal Substrates, Phys. Chem. Chem. Phys. 15, 12920−12929 (DOI: 10.1039/c3cp51646f)

[53] Mukha I., Vityuk N., Severynovska O. *et al.* (2016), The pH-Dependent Stucture and Properties of Au and Ag Nanoparticles Produced by Tryptophan Reduction. Nanoscale Res. Lett. 11, No. 101 (DOI: 10.1186/s11671-016-1318-8)

[54] Chuang C.-H., Chen Y.-T. (2009), Raman Scattering of L-Tryptophan Enhanced by Surface Plasmon of Silver Nanoparticles: Vibrational Assignment and Structural Determination, J. Raman Spectrosc. 40, 150−156 (DOI: 10.1002/jrs.2097)

[55] Wimuktiwan P., Shiowatana J., Siripinyanond A. (2015), Investigation of Silver Nanoparticles and Plasma Protein Association Using Flow Field-Flow Fractionation Coupled with Inductively Coupled Plasma Mass

Spectrometry (FlFFF-ICP-MS), J. Anal. At. Spectrom. 30, 245−253 (DOI: 10.1039/c4ja00225c)

Chapter 5

Insight into the Lysozyme Induced Aggregation of Aromatic Amino Acid Functionalized Gold Nanoparticles: Impact of Protein Binding and Lipid Corona on the Aggregation Phenomena

5.1 Introduction

The utilization of tailored nanoparticles in biomedical applications has always been an exciting prospect in nano-bio research for the nano-science community. Recently, gold nanoparticles (Au NPs) because of their small size, ease of functionalization by surface ligands, high volume to mass ratio, and low toxicity *[1-4]* have gained tremendous applications in optics, bio-sensing, medical science, genetics, and drug encapsulation *[1-12]*. However, the functionality of Au NPs in biological environments as well as their impacts on human health and the environment are always under questions. Normally, when Au NPs come into contact with biological fluids, the biomolecules particularly proteins and lipids rapidly adsorb to the surface of the NPs *[13-16]* and govern the physicochemical properties of Au NPs *[17-21]*. The interaction of Au NPs with proteins is always a complex process due to the large variety of protein molecules available in the biological systems. Protein molecules coat the NPs forming a protein corona in the biological environment. The stable complexes which are formed upon the interaction of Au NPs with proteins may modify the structure of proteins *[22-27]*. Previous studies reported that the interaction of Au NPs with proteins may induce the aggregation of the either Au NPs or the protein, or both [28-33]. Apart from the biological standpoint of native surface functionalized Au NPs functions in biological media, the protein mediated agglomerates have profound applications in drug delivery

[34,35], photothermal therapy *[36]*, and biosensing *[37-40]*. But the precipitation of the Au NPs in presence of certain proteins diminishes the Au NPs functions completely and thus should be avoided. Therefore, it is utmost important to know the exact mechanistic pathway of the formation of stable protein bound Au NPs and protein-induced nanoparticles aggregates/precipitation.

Among all the proteins, Lysozyme (Lyz) is often chosen as model protein to study the interaction with nanoparticles because it is a small globular protein having antiviral, antifungal, antitumor, and immune modulatory properties *[41]*. The interaction of this positively charged protein with negatively charged silica nanoparticles and various surface functionalized Au NPs was extensively investigated and several mechanisms have been proposed *[42-49]*. Electrostatic bridging by lysozyme molecules leads to the aggregation of the particles at physiological pH. Using various spectroscopic and microscopic approaches, researchers discovered that surface functionalization, size, and concentration of the Au NPs, pH, and ionic strength of the solution play important roles in the aggregation of the Au NPs and conformational changes and aggregation of lysozyme protein *[30,33,47-49]*. Neupane and co-workers found that the protein's native structure retained upon interaction with Au NPs but electrostatic interactions between the Au NPs and T4 Lysozyme (T4L) trigger the bridging of the two nanoparticles, eventually leading to the formation of aggregates. So far, lysozyme induced aggregation of nanoparticle is concerned, all the preceding studies stressed mostly upon Au NPs properties, pH, and ionic strength of the medium. However, there is possibility that aggregation of nanoparticles depends on the protein concentration and the related mechanism of aggregation is different at different protein concentration. Previously, Link and co-workers investigated different interaction pathways between gold nanorods and bovine serum albumin depending on the protein concentration. They reported that low protein concentration can induce aggregation via

unfolding while stable protein corona was formed at high protein concentration *[50]*. Further, very little effort has been put to prevent the aggregation/precipitation of Au NPs in presence of lysozyme protein. The stability of negatively charged nanoparticles is a crucial challenge in presence of lysozyme as most of the studies report aggregation/precipitation happens when negatively charged nanoparticles are allowed to interact with the positively charged lysozyme protein. The Au NPs coated with proteins (HSA, BSA), various thiol-containing ligands, and aptamer (single-strand DNAs) even failed to inhibit lysozyme-induced Au NPs aggregation at physiological pH *[30,33,41]*. A protein chemical modification was also applied to prevent the aggregation of Au NPs *[33]*. According to other report, PEG functionalized Au NPs suppressed lysozyme driven NPs aggregation when the coating of poly(ethylene glycol) (PEG) was over the threshold concentration (above 1 μM) *[29]*. It was reported that both the neutral and positively charged polymer coating around the Au NPs prevented the aggregation/precipitation of the Au NPs while the negative polymer coatings either led stable protein corona or aggregates *[32]*.

Apart from the proteins and polymers, lipid molecules can also coat the Au NPs to form the lipid corona *[51-57]*. Previously, our group reported that when phenylalanine and tyrosine functionalized gold nanoparticles interact with zwitterionic and positively charged lipid vesicles forming lipid corona which impart stability towards nanoparticle against external stimuli *[56,57]*. The lipid molecules depending on their phase transition temperature also form hard and soft corona around the phenylalanine functionalized gold nanoparticles in presence of different zwitterionic lipid vesicles *[57]*. It is not clear whether lipid coated nanoparticles (lipid corona) interact with proteins in the same way that native surface ligand functionalised Au NPs do. If they at all interact, what is the protein's conformational stability? Moreover, there is a possibility that the lipid corona can impede the protein-induced aggregation of Au NPs. There is a substantial research gap in the existing literature regarding how these lipid-coated molecules will interact

with protein molecules. Keeping all of these in mind, **(i)** we have conducted a detailed study on the interaction of aromatic amino acids (phenylalanine and tyrosine) functionalized gold nanoparticles (Au-AA NPs) with lysozyme (by varying the ratio of Au NPs to lysozyme molecules) by using different spectroscopic (UV-Visible, Fluorescence, Dynamic Light Scattering, and Circular Dichroism) and microscopic (Confocal Laser Scanning Microscopy and Scanning Electron Microscopy) techniques. We also compared all the results with conventional citrate functionalized gold nanoparticles to prove the uniqueness and superiority of the Au-AA NPs over Au-Cit NPs. **(ii)** Next, we coated both the amino acids and citrate functionalized gold nanoparticles with serum proteins (Bovine Serum Albumin, Human Serum Albumin) and thiol-containing small peptide (Glutathione) and studied their ability to inhibit the Au NPs aggregation in presence of different concentration of lysozymes. **(iii)** Finally, we investigated the interaction of the different lipid coated phenylalanine functionalized nanoparticle with lysozyme (by varying the ratio of Au NPs to lysozyme molecules) at physiological pH. We first coated the amino acid functionalized gold nanoparticles by using positively charged lipid (1,2-dimyristoyl-3-trimethylammonium-propane (chloride salt) (DMTAP), and two different zwitterionic lipids of different phase transition temperatures namely, 1,2-dioleoyl-sn-glycero-3-phosphocholine (DOPC, T_m = -20 °C), 1,2-dipalmitoyl-sn-glycero-3-phosphocholine (DPPC, T_m = 41 °C). As mentioned earlier that lipid molecules may form hard and soft corona depending on the phase transition temperature. Therefore, it is expected that hard and soft lipid corona will display different interaction towards lysozyme induced aggregation. In the present manuscript, apart from protein concentration dependent aggregation of aromatic amino acid functionalized nanoparticles, we attempted to unravel how hard and soft lipid corona as well as protein binding plays significant roles in resisting the aggregation of the nanoparticles.

5.2 Results and Discussion

We have summarized the results in a tabular form (**Table 5.1**) for the readers for an easy understanding of the aggregation phenomena of different nanoparticles in presence of different concentrations of lysozyme.

System	Aggregation	Aggregates Size (nm)	Reversibility of the aggregates after NaOH addition
Au-Phe NPs: Lysozyme (1:25)	**yes**	**120-130**	**No**
Au-Tyr NPs: Lysozyme (1:25)	**yes**	**150-160**	**No**
Au-Cit NPs: Lysozyme (1:25)	**yes**	**180-190**	**No**
Au-Phe NPs: Lysozyme (1:1000)	**yes**	**1000-1200**	**Yes**
Au-Tyr NPs: Lysozyme (1:1000)	**yes**	**900-1100**	**Yes**
Au-Cit NPs: Lysozyme (1:1000)	**yes**	**1400-1500**	**Partial**

Table 5.1 *The Aggregation, aggregated size, and reversibility of aggregates of Au-Phe, Au-Tyr, and Au-Cit NPs after the addition of NaOH at low (ratio 1:25) and high (ratio 1:1000) concentrations of lysozyme.*

5.2.1 Lysozyme Induced Aggregation of the Au NPs:

At first, we investigated the interaction of lysozyme with gold nanoparticles functionalized by citrate molecules (Au-Cit NPs) and aromatic amino acids (Au-AA NPs) namely phenylalanine and tyrosine (Au-Phe and Au-Tyr NPs) at physiological pH. The normalized UV-Visible spectra (**Figure 5.1a**) showed SPR peak at ~ 520 nm for Au-AA and Au-Cit NPs, indicating the diameter of the Au NPs are in the range 13-16 nm *[58]*. The zeta potential of Au-Phe NPs, Au-Tyr NPs, and Au-Cit NPs was -33 mV, -23 mV, -35 mV respectively which implies that all the Au NPs were negatively charged (**Figure 5.1b**).

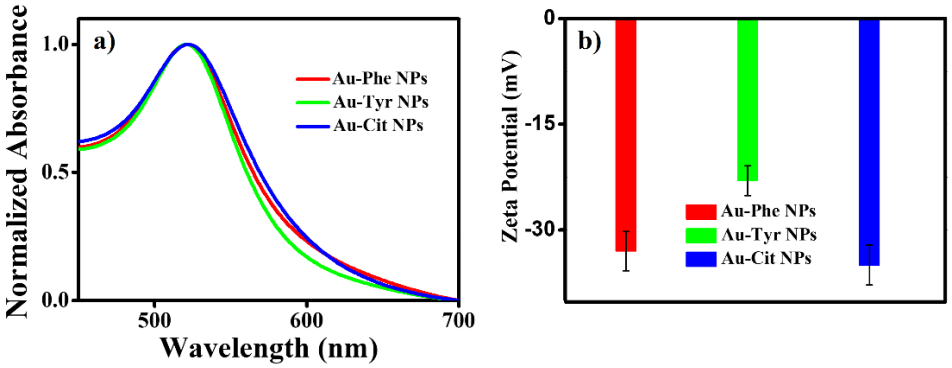

Figure 5.1 *Normalized UV-Visible spectra (a), and Zeta potential measurements (b) of Au-Phe, Au-Tyr, and Au-Cit NPs.*

Fixed concentration of Au-AA and Au-Cit NPs (4 nM) was incubated with different concentrations of lysozyme (20 nM to 8 µM) for 2 h at room temperature. The Au NPs-lysozyme interaction was monitored through UV-Visible, fluorescence spectroscopy, and DLS measurements as a function of the number ratio of Au NPs/lysozyme (see Experimental Methods and **Table 5.2** for detailed calculation).

Concentration of Au NPs (nM)	Number of Au NPs / mL	Concentration of lysozyme (µM)	Number of lysozymes / mL	Number ratio of Au NPs: Lysozymes
4	2.40×10^{12}	0.02	1.2×10^{13}	1:5
4	2.40×10^{12}	0.1	6.0×10^{13}	1:25
4	2.40×10^{12}	0.2	1.2×10^{14}	1:50
4	2.40×10^{12}	0.4	2.4×10^{14}	1:100
4	2.40×10^{12}	1	6.0×10^{14}	1:250
4	2.40×10^{12}	2	1.2×10^{15}	1:500
4	2.40×10^{12}	4	2.4×10^{15}	1:1000
4	2.40×10^{12}	8	4.8×10^{15}	1:2000

Table 5.2 *Calculation of the ratio of number of Au NPs to the number of lysozyme molecules per mL.*

The visual images revealed a change in color from wine red to violet-purple upon interaction of Au-AA and Au-Cit NPs with lysozyme indicating that all of Au NPs underwent aggregation over a wide range of Au NPs/lysozyme ratios ranging from 1:25 to 1:2000 (**Figure 5.2a, c, e**).

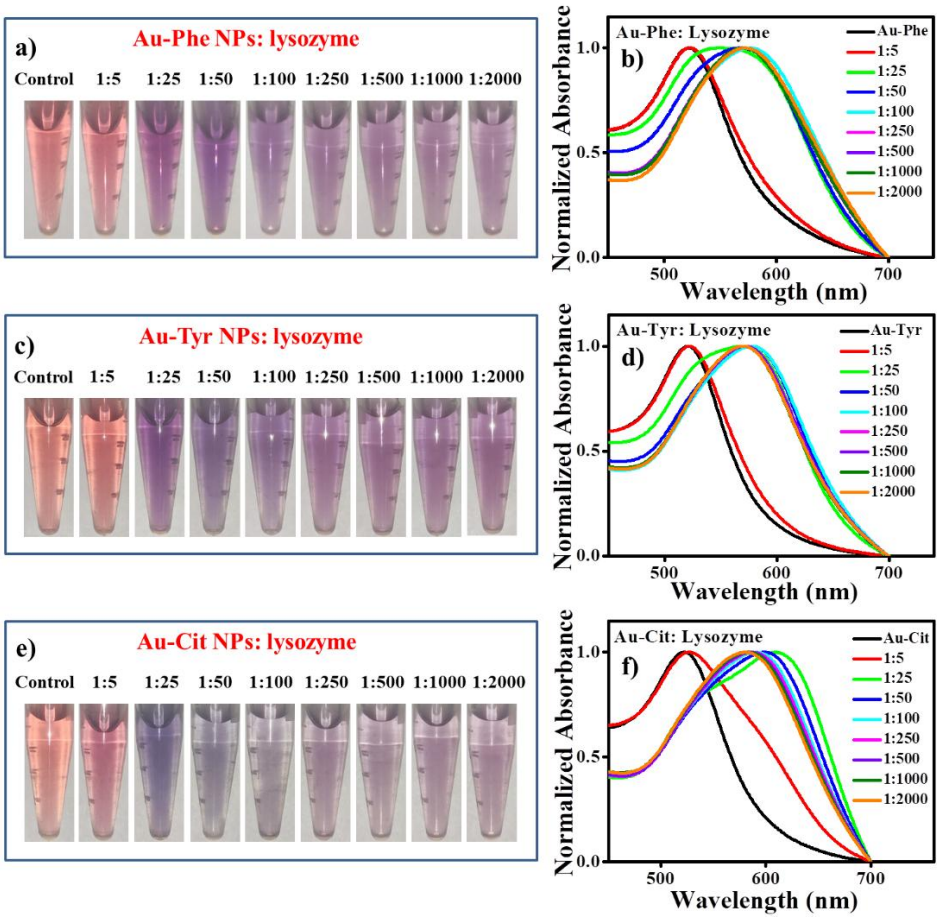

Figure 5.2 *Photographs (a, c, e) and UV-Visible spectra (b, d, f) of the Au-Phe (a, b), Au-Tyr (c, d), and Au-Cit (e, f) NPs at different Au NPs/lysozyme ratios.*

Further, overnight incubation (data not shown) led to the precipitation out of Au-AA and Au-Cit NPs ranging from number ratio 1:50 to 1:2000 as visible dark pellets. Although for number ratio 1:25, the aggregation was observed, however; no pellet formation took place for any of the three Au NPs. The UV-Visible spectra revealed that the SPR peak of Au-AA and Au-Cit NPs was red shifted for all Au NPs/lysozyme ratios ranging from 1:25 to 1:2000 with a new broadened peak appearing at a longer wavelength (**Figure 5.2b, d, f**). All these findings imply that negatively charged Au-AA and Au-Cit NPs undergo aggregation in presence of positively charged lysozyme protein over a wide Au NPs/lysozyme ratio.

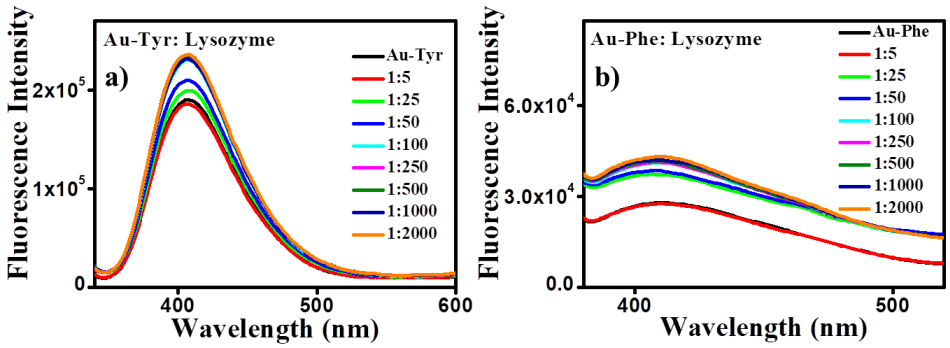

Figure 5.3 *Fluorescence spectra of the Au-Tyr NPs (a) and Au-Phe NPs (b) at different Au NPs/lysozyme ratios. The excitation wavelength for Au-AA NPs and Au-AA NPs/lysozyme system was 330 nm.*

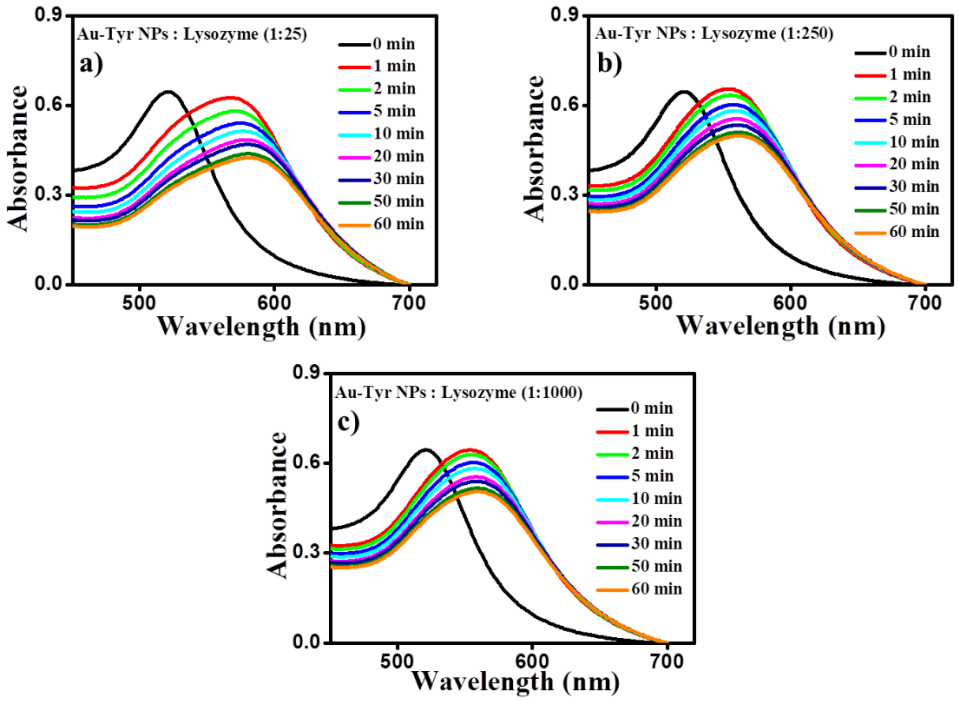

Figure 5.4 *Kinetics of the aggregation of the Au-Tyr NPs (a-c) at three different Au NPs/lysozyme ratios (1:25, 1:250, and 1:1000).*

The steady-state fluorescence spectra for Au-Tyr and Au-Phe NPs also revealed that the fluorescence intensity increased with the aggregation of Au-AA NPs (**Figure 5.3a, b**). The increment in the fluorescence intensity could be attributed to the enhanced local concentration followed by aggregation-induced emission of the amino acid upon the aggregation of

nanoparticles *[56]*. The kinetics of the aggregation of Au NPs at three different number ratios (1:25, 1:250, and 1:1000) revealed that regardless of different Au NPs/lysozyme ratios, Au NPs underwent aggregation immediately upon the addition of the lysozyme protein (**Figure 5.4, 5.5, and 5.6**). Although the spectroscopic measurements shred evidence on the aggregation of the Au NPs at various lysozyme concentrations, however, our study is not conclusive about the mechanism of aggregates formation.

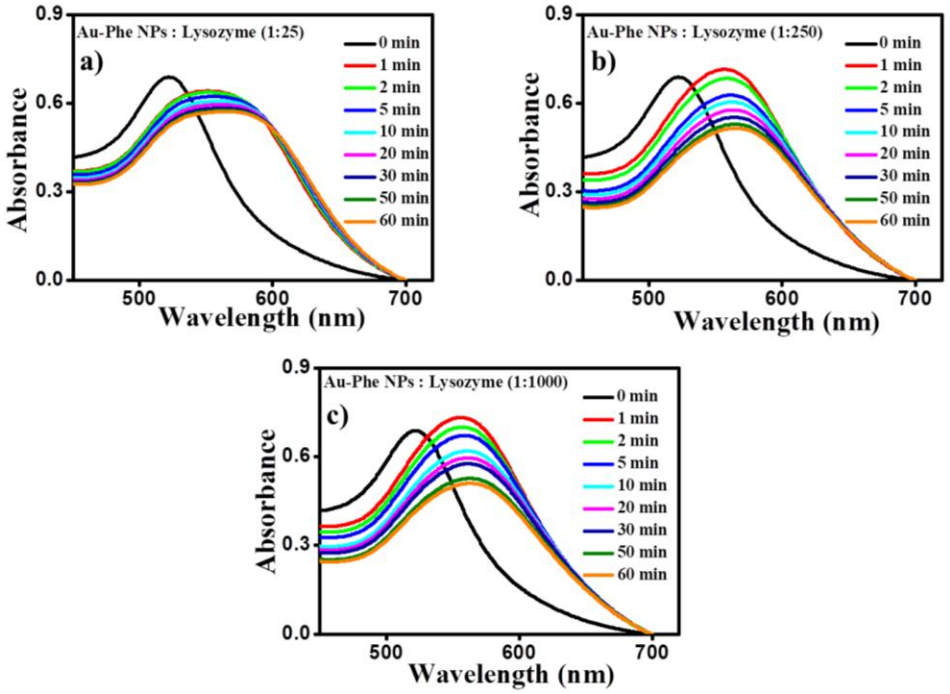

Figure 5.5 *Kinetics of the aggregation of the Au-Phe NPs (a-c) at three different Au NPs/lysozyme ratios (1:25, 1:250, and 1:1000).*

We, therefore, conducted DLS measurements to estimate the average particle size of Au-AA and Au-Cit NPs aggregates at various lysozyme concentrations after 2 hours incubation. The DLS measurement estimated hydrodynamic diameter of the Au-Phe, Au-Tyr and Au-Cit NPs was around 24.2 ± 0.4, 25 ± 0.2, and 16.2 ± 0.5 respectively and that of native lysozyme was 4.38 ± 0.2 nm (**Figure 5.7**).

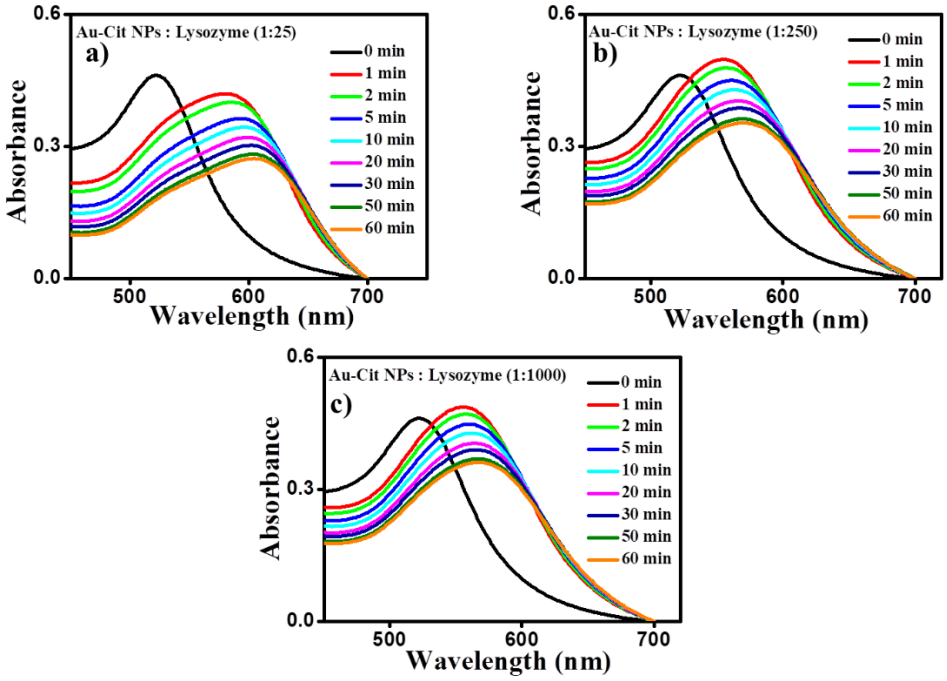

Figure 5.6 *Kinetics of the aggregation of the Au-Cit NPs (a-c) at three different Au NPs/lysozyme ratios (1:25, 1:250, and 1:1000).*

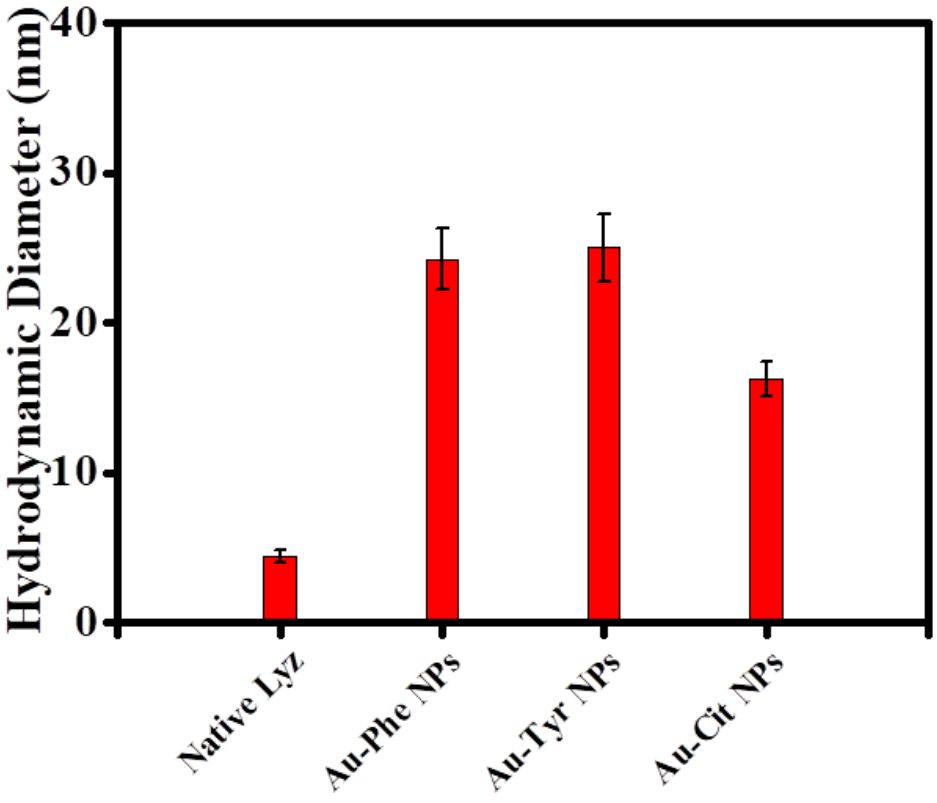

Figure 5.7 *Hydrodynamic diameter of native lysozyme, Au-Phe NPs, Au-Tyr NPs, and Au-Cit NPs.*

At a low lysozyme concentration [Au NPs/lysozyme (1:25)], the average particle size of the Au-AA and Au-Cit NPs was increased to 120-200 nm, whereas at higher lysozyme concentrations [Au NPs/lysozyme (1:100 to 1:2000)], the average particle size of Au NPs was increased to 1000 nm (**Figure 5.8a, 5.9a, and 5.10a**). We next estimated the diameter of Au-AA and Au-Cit NPs at different time with respect to low and high lysozyme concentrations [Au NPs/lysozyme (1:25 and 1:1000)] to quantify the aggregation kinetics.

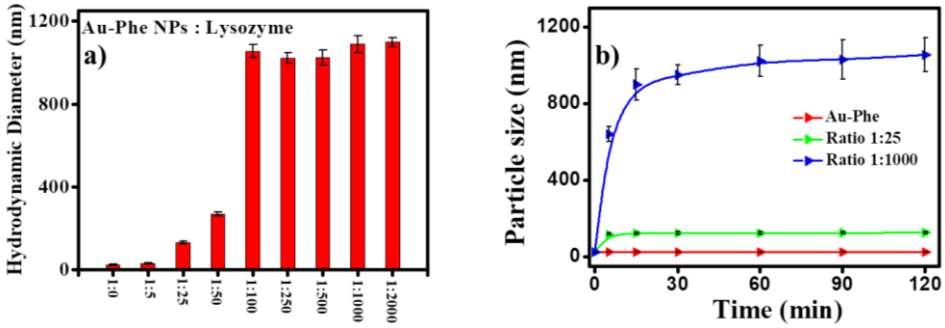

Figure 5.8 *Hydrodynamic diameter (a) of the Au-Phe NPs at different Au NPs/lysozyme ratio. The change in hydrodynamic diameter (b) of the Au-Phe NPs with time as control and at two different Au NPs/lysozyme ratios (1:25 and 1:1000).*

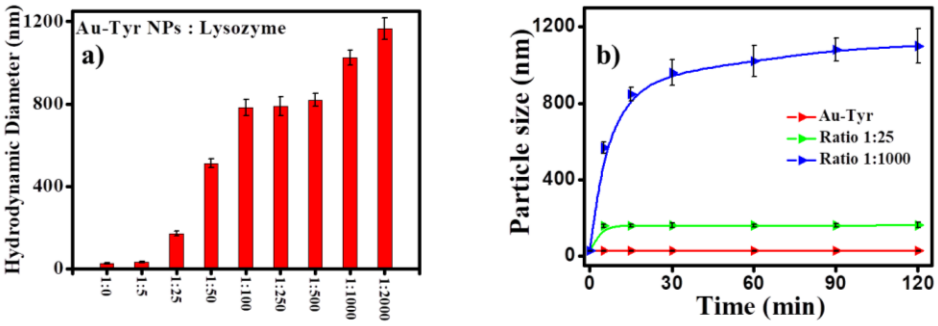

Figure 5.9 *Hydrodynamic diameter (a) of the Au-Tyr NPs at different Au NPs/lysozyme ratio. The change in hydrodynamic diameter (b) of the Au-Tyr NPs with time as control and at two different Au NPs/lysozyme ratios (1:25 and 1:1000).*

At a low lysozyme concentration [Au NPs/lysozyme (1:25)], the increment in average diameter of Au NPs became saturated within 5 minutes, while at high lysozyme concentration [Au NPs/lysozyme (1:1000)], the average diameter of Au NPs was continuously increased with time (**Figure 5.8b, 5.9b, and 5.10b**). The DLS measurement primarily indicates that the aggregation mechanism at low concentration of lysozyme is different from that at high lysozyme concentration.

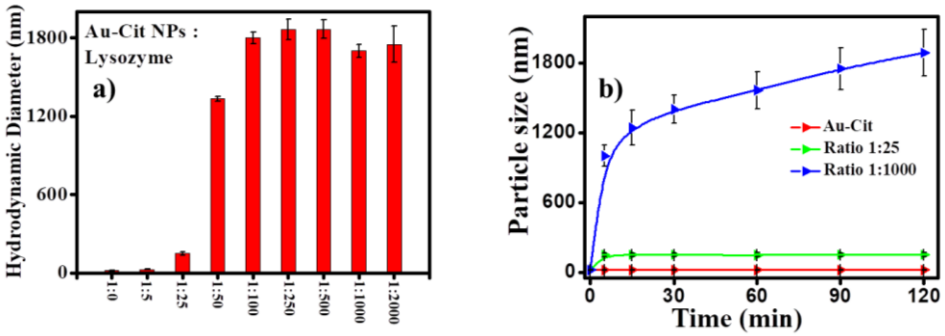

Figure 5.10 *Hydrodynamic diameter (a) of the Au-Cit NPs at different Au NPs/lysozyme ratio. The change in hydrodynamic diameter (b) of the Au-Cit NPs with time as control and at two different Au NPs/lysozyme ratios (1:25 and 1:1000).*

5.2.2 Effect of NaOH on the Reversibility of the Aggregates of Au NPs:

To investigate whether Au NPs aggregates were reversible in presence of NaOH, we used three different Au NPs/lysozyme ratios (1:25, 1:250, and 1:1000) and for each of the ratio, four time intervals for incubation (30 min, 2 h, 5 h, and 24 h) were set. The formation of aggregates and their reversibility were checked through UV-Visible spectroscopy and DLS measurements. We added required volume of 1 M NaOH to the lysozyme induced Au NPs aggregates and adjusted the pH of solution to pH~12 (above the pI of lysozyme) and monitored time to time through UV-Visible spectroscopy. Interestingly, for the Au-Phe and Au-Tyr NPs, at high lysozyme concentrations [Au-AA NPs/lysozyme (1:250 and 1:1000)], the aggregation became reversible upon the addition of NaOH to the formed aggregates (**Figure 5.11a, b**). The visual color of the sample (Au-AA NPs)

changed from violet-purple to red (**Figure 5.12 and 5.13**) even after 24 h. The UV-Visible spectra also showed the reversibility of Au-AA NPs aggregates as the absorbance for the Au-AA NPs again reverse back fully along with the blue shift in the SPR peak towards the native Au-AA NPs (**Figure 5.11d, e**). The 10-15 nm red shift in the SPR peak of Au-AA NPs upon reversibility in presence of NaOH compared to the native NPs (Au-AA NPs without any lysozyme) suggests us that stable protein corona might have been present after the addition of NaOH (**Figure 5.11d, e**).

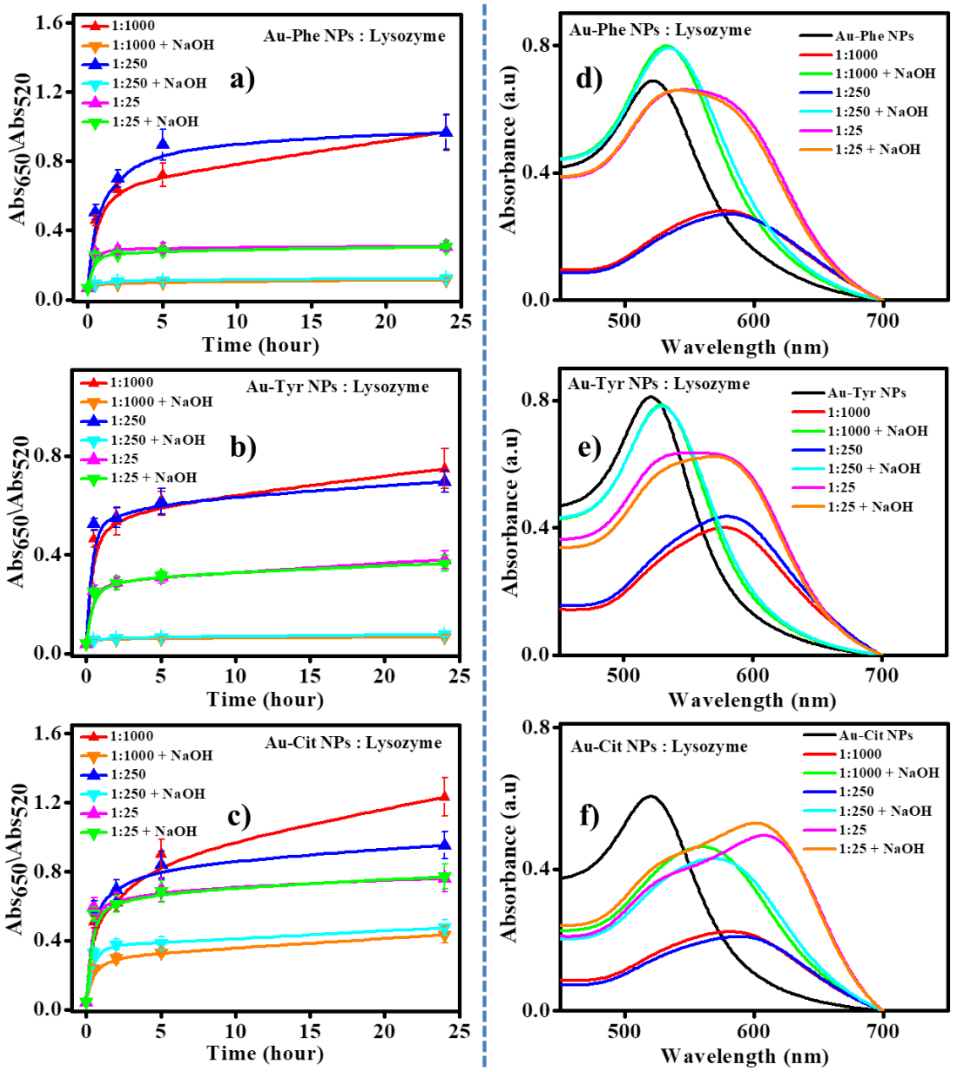

Figure 5.11 *Aggregates and Non-aggregates formation of the Au-Phe (a), Au-Tyr (b), and Au-Cit NPs (c) as control and after the addition of NaOH to the aggregates respectively with time at three different Au NPs/lysozyme ratio 1:25, 1:250, and 1:1000. The UV-*

Visible spectra of the Au-Phe (d), Au-Tyr (e), and Au-Cit (f) NPs as control and after the addition of NaOH to the aggregates respectively after a certain time (2 hour) at Au NPs/lysozyme ratio 1:25, 1:250, and 1:1000.

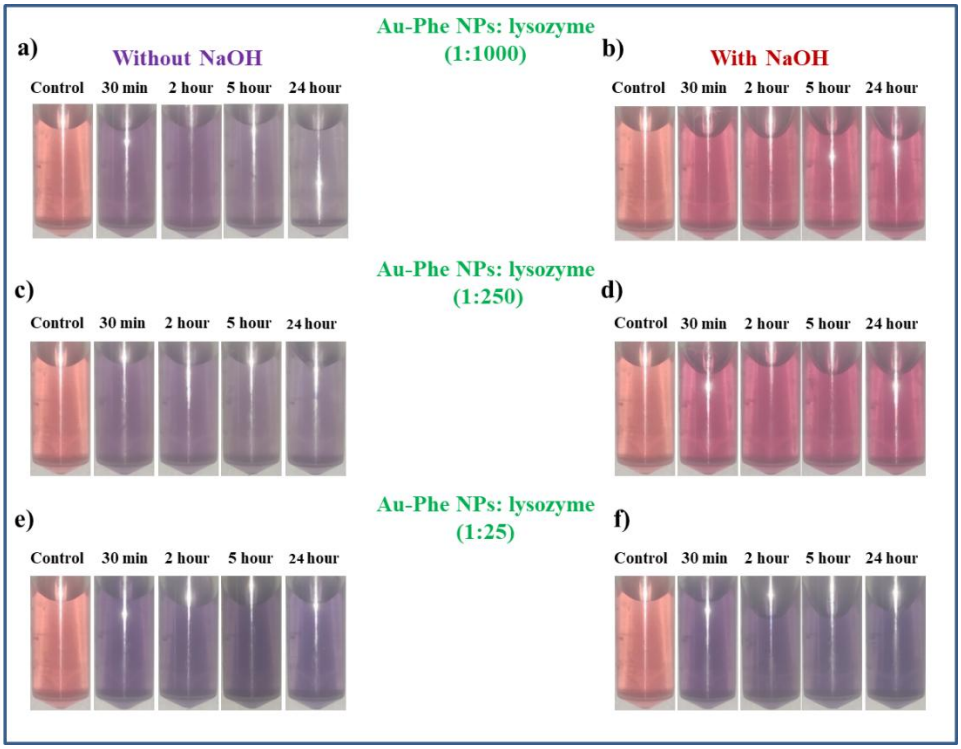

Figure 5.12 *Photograph of the Au-Phe NPs in the absence (a, c, e) and presence (b,d,f) of NaOH at Au-Phe NPs/lysozyme ratio 1:1000 (a, b), 1:250 (c, d), and 1:25 (e, f).*

The DLS data also supported the reversibility of the Au-AA NPs in presence of NaOH. The average diameter of the Au NPs was decreased form 1000 nm to 75 nm (**Figure 5.14a and 5.15a**). Surprisingly, we did not observe any reversibility of the aggregation (**Figure 5.11a-f, 5.12, 5.13, 5.14b, 5.15b, and 5.16**) for Au-AA and Au-Cit NPs at low lysozyme concentration [Au NPs/lysozyme (1:25)]. Even prolong incubation of aggregated Au NPs with NaOH did not help to reverse back to smaller size. Furthermore, after the addition of NaOH, the aggregation of the Au-Cit NPs was partially reversible at high lysozyme concentrations [Au NPs/lysozyme (1:250 and 1:1000)] (**Figure 5.11c, f and 5.16**). The reversibility of Au-Phe and Au-Tyr NPs aggregation at high lysozyme concentrations [Au NPs/lysozyme (1:250 and 1:1000)] indicates that the aggregation mechanism of Au NPs at

low and high lysozyme concentrations [Au NPs/lysozyme (1:25 and 1:1000)] is different.

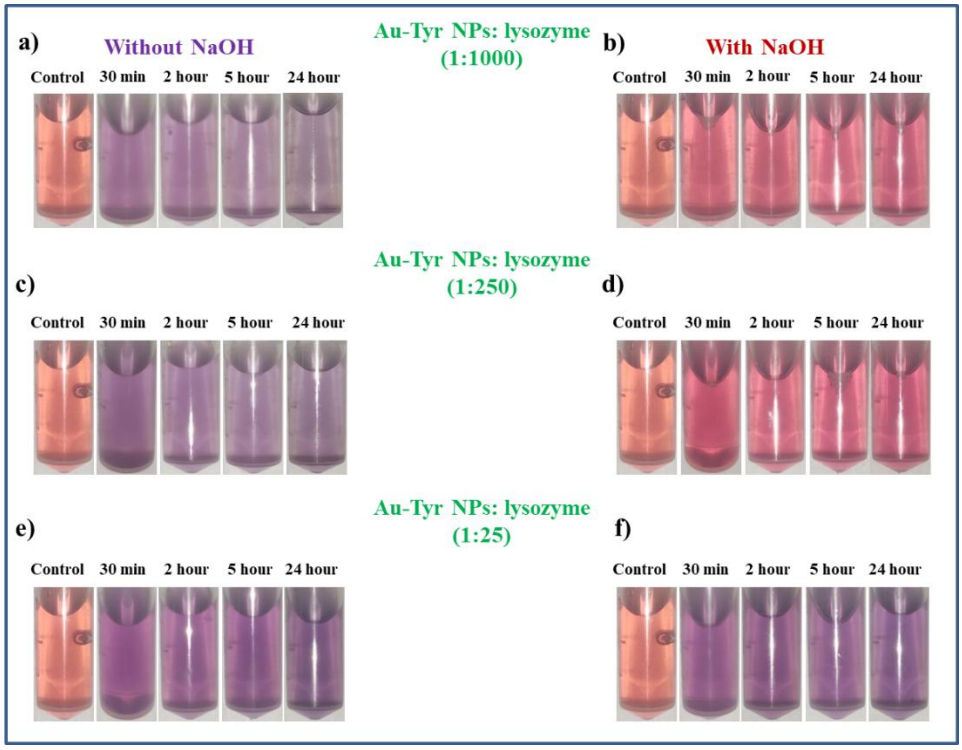

Figure 5.13 *Photograph of the Au-Tyr NPs in the absence (a, c, e) and presence (b, d, f) of NaOH at Au-Tyr NPs/lysozyme ratio 1:1000 (a, b), 1:250 (c, d), and 1:25 (e, f).*

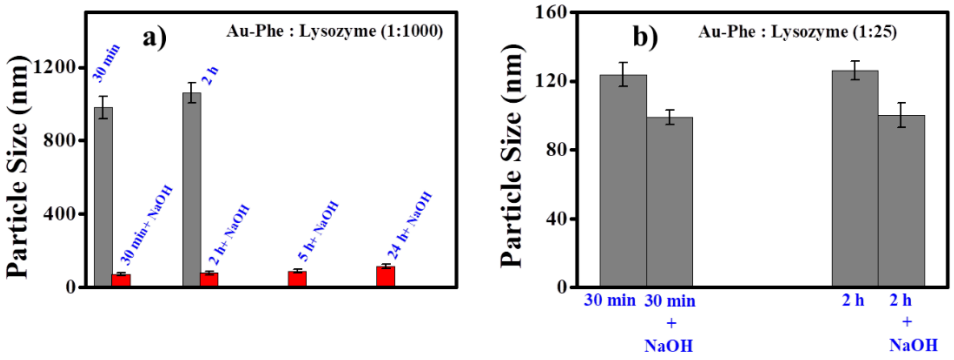

Figure 5.14 *Change in hydrodynamic diameter of the Au-Phe NPs in absence and presence of NaOH at Au NPs/lysozyme ratio 1:1000 (a) and 1:25 (b). We could not measure the hydrodynamic diameter of the Au-Phe NPs at 5 h and 24 h at ratio 1:1000 due to the large aggregated structure of higher PDI value (>0.4).*

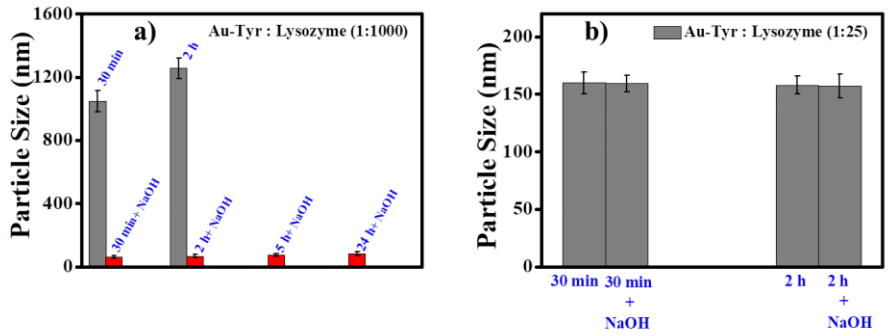

Figure 5.15 *Change in hydrodynamic diameter of the Au-Tyr NPs in absence and presence of NaOH at Au NPs/lysozyme ratio 1:1000 (a) and 1:25 (b). We could not measure the hydrodynamic diameter of the Au-Tyr NPs at 5 h and 24 h at ratio 1:1000 due to the large aggregated structure of higher PDI value (>0.4).*

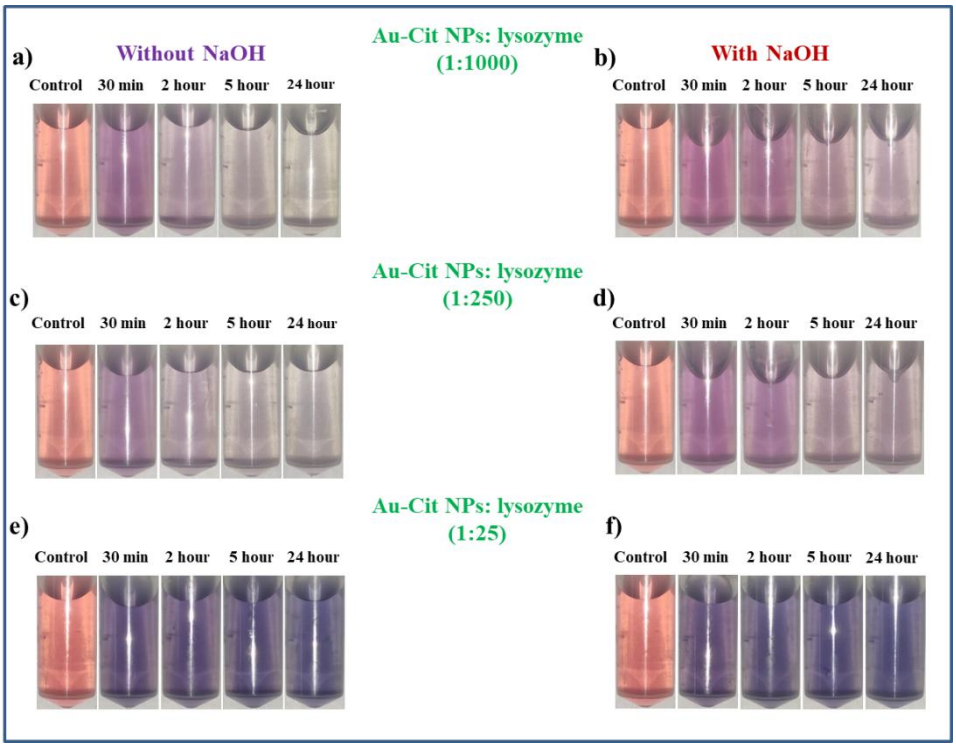

Figure 5.16 *Photograph of the Au-Cit NPs in the absence (a, c, e) and presence (b, d, f) of NaOH at Au-Cit NPs/lysozyme ratio 1:1000 (a, b), 1:250 (c, d), and 1:25 (e, f).*

To the best of our knowledge, this is the first report of lysozyme-induced Au NPs aggregation which is reversible upon addition of NaOH. Driskell and co-workers previously reported the reversibility of the Au Cit NPs and IgG antibody aggregates upon the increment in solution pH *[59]*. The

irreversibility of Au-Cit NP aggregates at any Au NPs/lysozyme ratio emphasises the uniqueness of the Au-Phe and Au-Tyr NPs.

5.2.3 Influence of solution pH on the formation and stability of the Lyz bound Au Phe, Au Tyr, and Au Cit NPs:

Following the investigation of the reversibility of Au NPs aggregation, we were keen to study the interaction of Au NPs and lysozyme molecules at pH 12 (above the pI of the lysozyme). The visual images (**Figure 5.17**) showed that Au-AA and Au-Cit NPs were stable at all the concentrations of lysozyme at pH ~ 12.

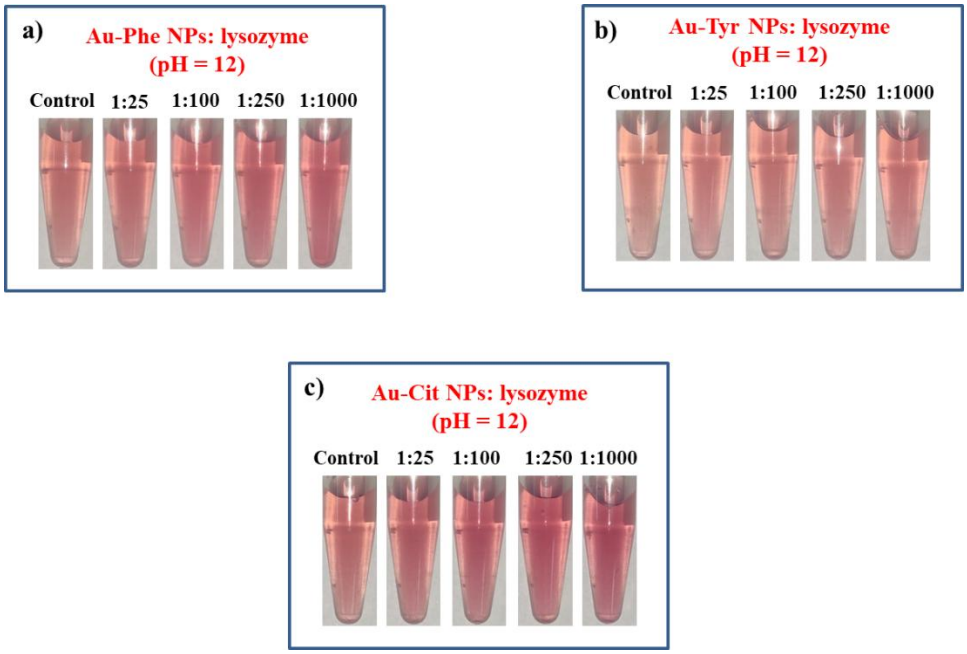

Figure 5.17 *Photograph of the Au-Phe (a), Au-Tyr (b), and Au-Cit (c) NPs at different Au NPs/lysozyme ratio at pH ~ 12.*

The UV-Visible spectra revealed that the SPR peak of all the Au NPs were slightly red shifted ~ 5 nm at Au NPs/lysozyme ratios 1:250 and 1:1000, indicating the formation of stable lysozyme bound Au NPs systems (**Figure 5.18a, c, e**).These systems were found to undergo aggregation as the pH decreased from pH ~ 12 to pH ~ 8 (**Figure 5.18b, d, f**). Interestingly, it was observed that lysozyme bound Au NPs systems where the lysozyme

concentration is low [Au NPs/lysozyme (1:25)] remained stable upon decreasing the pH from pH ~ 12 to pH ~ 7 (**Figure 5.18b, d, f**).

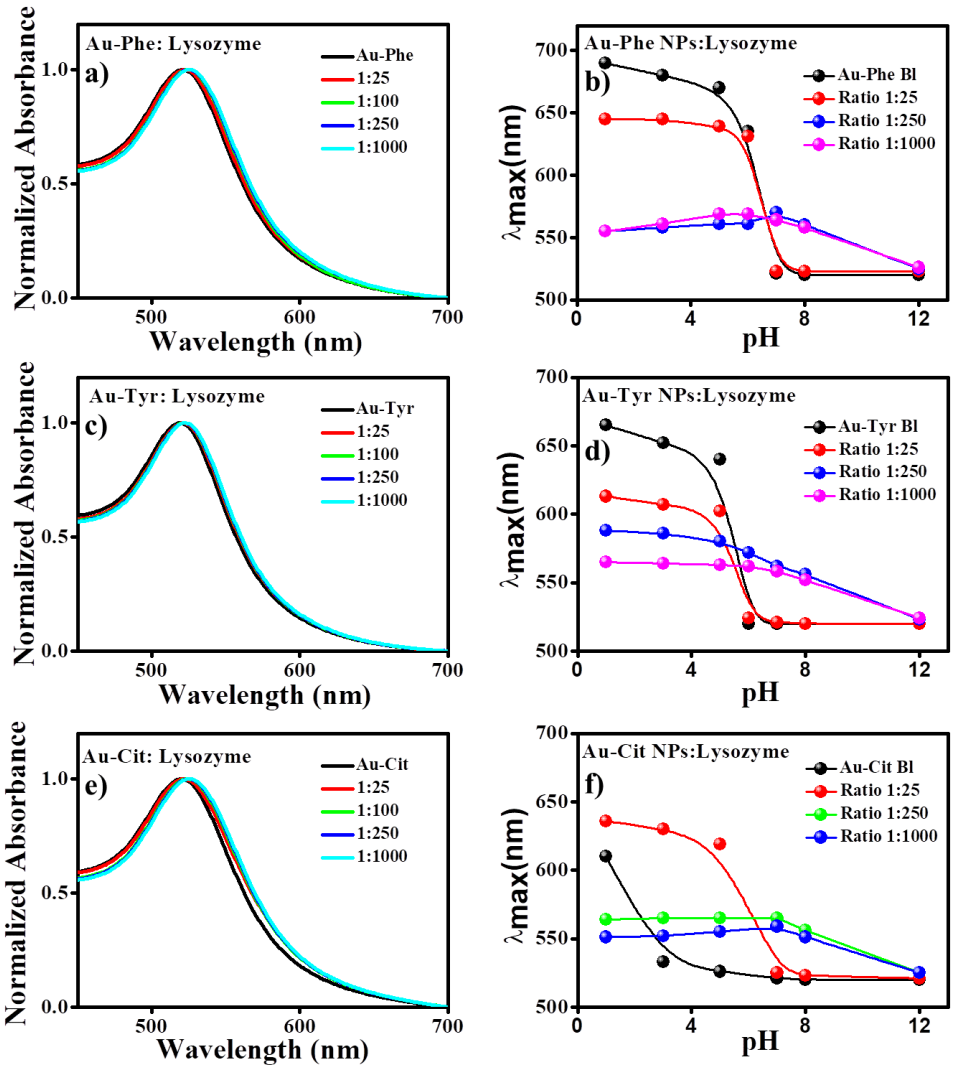

Figure 5.18 *UV-Visible spectra (a, c, e) of the Au NPs interaction with different concentrations of lysozyme at pH ~ 12. pH dependent stability of the native Au NPs and Lyz bound Au NPs (b, d, f) formed at pH ~ 12 at different number ratio of 1:25, 1:250, and :1000.*

This observation is in contradiction to our previous finding, where we observed that Au-AA and Au-Cit NPs at pH 7.4 undergo aggregation at low lysozyme concentration [Au NPs/lysozyme (1:25)] and this aggregation was not reversible upon increasing the pH of the system to pH ~ 12. Now, we have theoretically estimated the number of lysozyme molecules needed

to fully coat the Au-AA and Au-Cit NPs for formation of compact protein monolayer. The size of the lysozyme molecule is 4.5 × 3.5 × 3.5 nm^3 *[33]*. The DLS measurement determined that the hydrodynamic diameter of the Au-Phe, Au-Tyr and Au-Cit NPs were 24.2 ± 0.4, 25 ± 0.2, and 16.2 ± 0.5 nm respectively and that of native lysozyme was 4.38 ± 0.2 nm. This computes that an average of 93, 100, and 52 lysozyme molecules are needed to fully coat the Au-Phe, Au-Tyr, and Au-Cit NPs respectively to complete a compact protein monolayer. Therefore, the lysozyme is in sub-monolayer concentration in the Au NPs/lysozyme ratio 1:25, while lysozyme is in excess concentration in Au NPs/lysozyme ratio 1:250 and 1:1000. So, the ratio 1:25 is lower than the necessary to obtain a complete protein layer around the nanoparticle. Futher, our observations clearly indicates two different mechanisms of interaction of lysozyme with Au NPs when lysozyme is in excess and sub-monolayer concentrations.

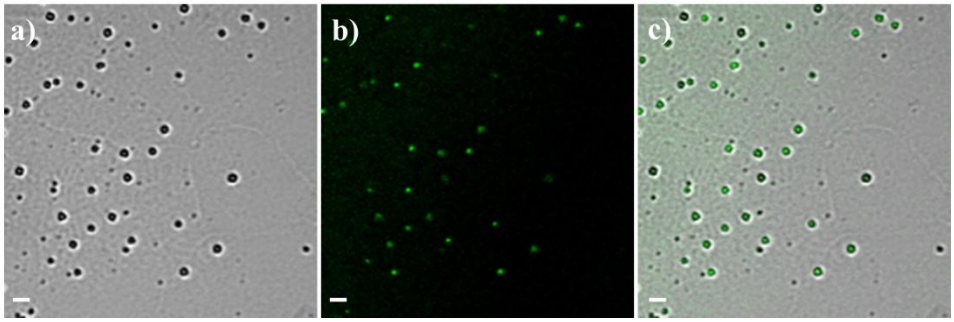

Figure 5.19 *Bright field, fluorescence, and merged images (a-c) of the native lysozyme protein (without Au NPs). Scale bar = 2 µm.*

5.2.4 Confocal Laser Scanning Microscopy (CLSM) and Field Emission Scanning Electron Microscopy (FESEM) images of Au NPs at two different Au NPs/ lysozyme ratio [Au NPs/lysozyme (1:25 and 1:1000)]:

After the spectroscopic investigation of the Au-AA and Au-Cit NPs aggregates formation in presence of low and high lysozyme concentrations, we tried to visualize these aggregates through CLSM and FESEM imaging techniques. For CLSM imaging, Thioflavin T dye was used to probe the

assembly of protein and amino acids. **Figure 5.19a-c** revealed uniform spherical shape for native lysozyme molecules (without Au NPs) at physiological pH *[60]*.

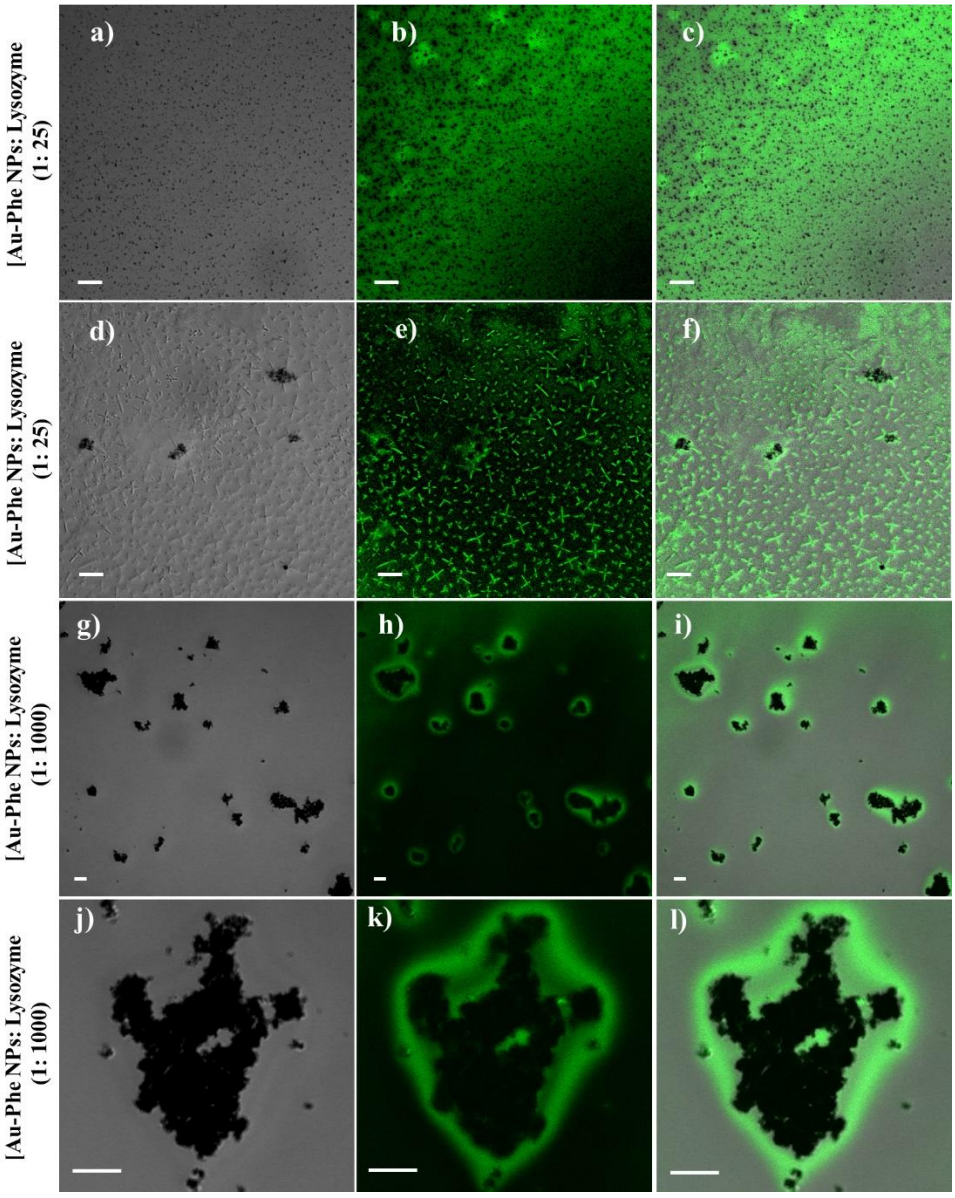

Figure 5.20 *CLSM images of the Au-Phe NPs in presence of low and high concentration of lysozyme using Thioflavin T as a probe for protein and amino acid. Bright field, fluorescence, and merged images of the protein induces Au-Phe NPs aggregates at low [Au NPs/lysozyme (1:25)] (a-f) and high lysozyme concentration [Au NPs/lysozyme (1:1000)] (g-l). Scale bar = 2 µm. Images a-f belong to the same sample, however, the images were taken at different positions of the immobilized sample on the cover slide*.

Images a-c showed the small aggregates of the Au-Phe NPs and d-f showed the small nanofibril aggregates of the amino acid (phenylalanine) assembly which was displaced from the Au-Phe NPs in presence of low lysozyme concentration [Au-Phe NPs/lysozyme (1:25)]. Images g-i showed the large aggregates of Au-Phe NPs along with the aggregates of protein molecules on the surface of aggregated Au-Phe NPs and j-l showed only one Au-Phe NPs aggregates at high lysozyme concentration [Au-Phe NPs/lysozyme (1:1000)].

At low lysozyme concentration [Au NPs/lysozyme (1:25)], the Au-AA NPs formed small aggregates of the Au NPs (**Figure 5.20a-c and 5.21a-c**) along with some distinct small nanofibrils of the amino acids assembly (**Figure 5.20d-f and 5.21d-f**).

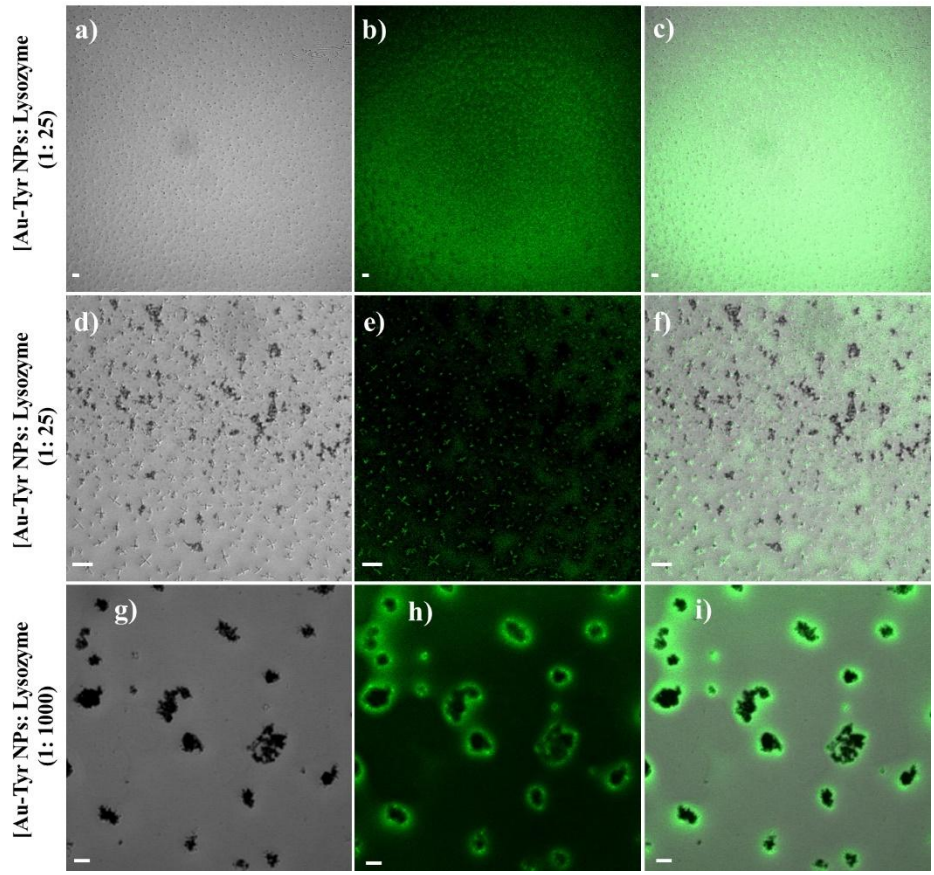

Figure 5.21 *CLSM images of the Au-Tyr NPs in presence of low and high concentration of lysozyme using Thioflavin T as a probe for protein. Bright field, fluorescence, and merged images of the protein induces Au-Tyr NPs aggregates at low [Au NPs/lysozyme (1:25)] (a-f) and high lysozyme concentration [Au NPs/lysozyme (1:1000)] (g-i). Scale bar = 2 µm.*

These nano fibril aggregates of amino acids were distinctly different from the large fibrilar aggregates of the lysozyme protein (**Figure 5.22a-c**). Interestingly, at high lysozyme concentration [Au NPs/lysozyme (1:1000)], larger aggregates of the Au-AA NPs were observed along with the thick coating of the aggregated proteins (**Figure 5.20g-l and 5.21g-i**). These results imply that at low lysozyme concentration surface ligands (amino acids in the present case) are decoated leading to the aggregates formation. On the other hand, at high lysozyme concentration, the protein molecules also aggregated on the surface of the aggregated Au-AA NPs. For the Au-Cit NPs, at low lysozyme concentration [Au-Cit NPs /lysozyme (1:25)], some protein molecules remained intact on the surface of the aggregated Au-Cit NPs (**Figure 5.23a-c**). Moreover, at high lysozyme concentration [Au NPs/lysozyme (1:1000)], the Au-Cit NPs formed larger aggregates although no coating of the protein aggregates was spotted (**Figure 5.23d-f**).

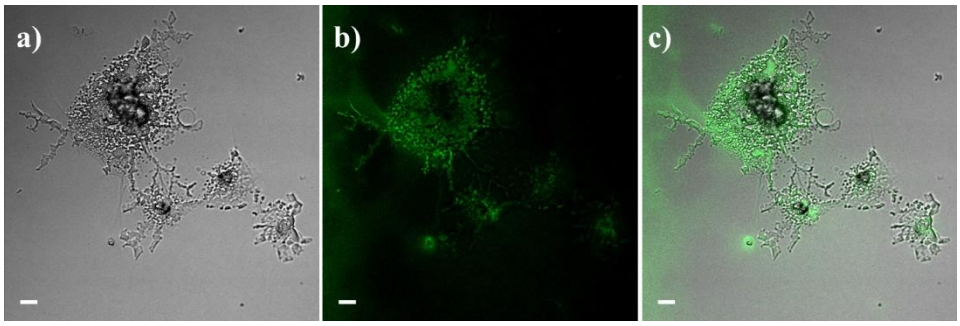

Figure 5.22 *Bright field, fluorescence, and merged images (a-c) of the lysozyme aggregates at acidic pH (pH ~2). Scale bar = 2 µm.*

We further employed FESEM imaging techniques to visualize the Au NPs aggregates at low [Au NPs/lysozyme (1:25)] and high [Au NPs/lysozyme (1:1000)] lysozyme concentrations. The FESEM images rules out any dye induced aggregation of the proteins. The **Figure 5.24a** showed the presence of small aggregates of Au-Phe NPs along with small nanofibrils (**Figure 5.24b**) at low lysozyme concentration. Interestingly, at high lysozyme concentration, the Au-Phe NPs formed larger aggregates along with the

aggregates of protein on the aggregated Au NPs surface (**Figure 5.24c, d**). This observation supports well with our CLSM images.

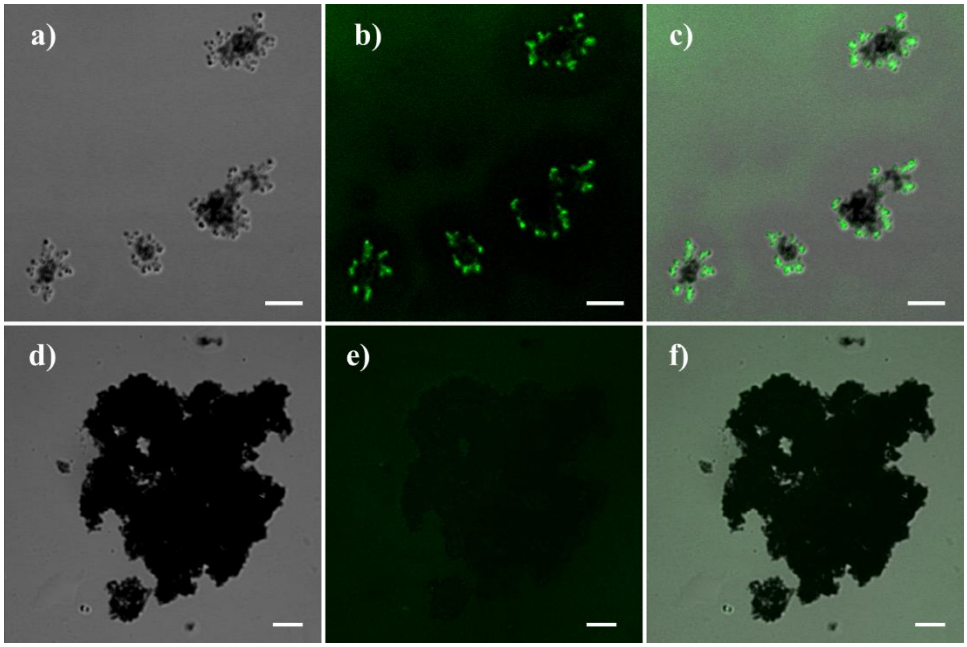

Figure 5.23 *CLSM images of the Au-Cit NPs in presence of low and high concentration of lysozyme using Thioflavin T as a probe for protein. Bright field, fluorescence, and merged images of the protein induces Au-Cit NPs aggregates at low [Au NPs/lysozyme (1:25)] (a-c) and high lysozyme concentration [Au NPs/lysozyme (1:1000)] (d-f). Scale bar = 2 µm.*

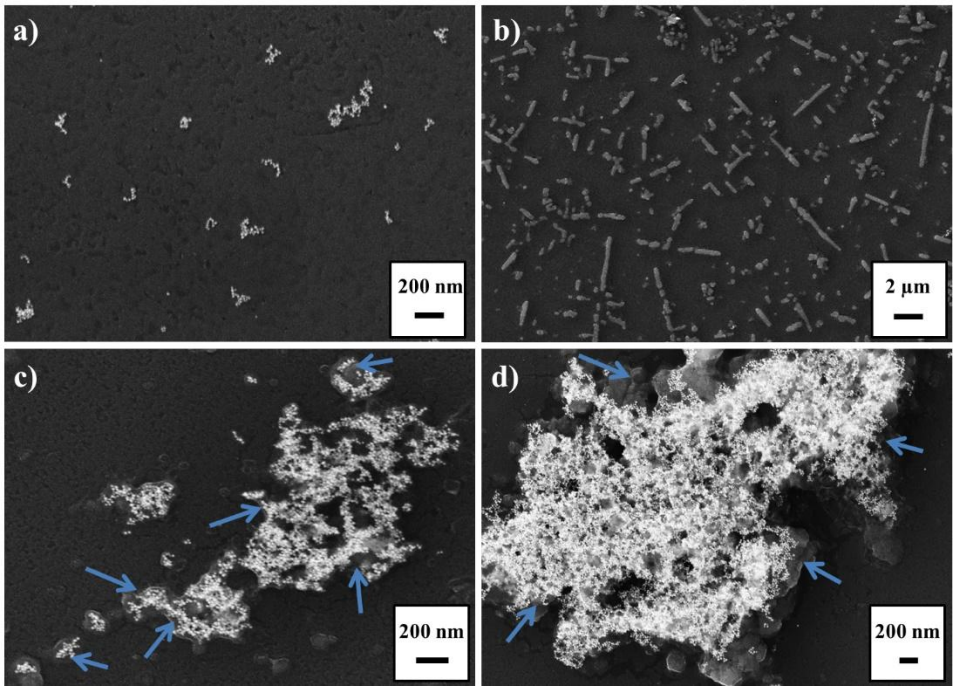

Figure 5.24 *FESEM images of the Au-Phe NPs at low [Au-Phe NPs/lysozyme (1:25)] (a-b) and high lysozyme concentration [Au-Phe NPs/lysozyme (1:1000)] (c-d). Images a showed the small aggregates of the Au-Phe NPs and b showed the small nanofibril aggregates of the amino acid (phenylalanine) assembly which was displaced from the Au-Phe NPs in presence of low lysozyme concentration [Au-Phe NPs/lysozyme (1:25)]. Images c and d showed the large aggregate of Au-Phe NPs along with the aggregates of protein molecules on the surface of aggregated Au-Phe NPs at high lysozyme concentration [Au-Phe NPs/lysozyme (1:1000)].*

5.2.5 Influence of bound proteins and small peptides on the surface of Au NPs on the lysozyme-induced aggregation of Au NPs:

First, we bound BSA (Bovine Serum Albumin) and HSA (Human Serum Albumin) serum albumin proteins on the surface of amino acid and citrate functionalized gold nanoparticles. We also used a small thiol containing tripeptide namely Glutathione (GSH) to stabilise the surface of the Au NPs.

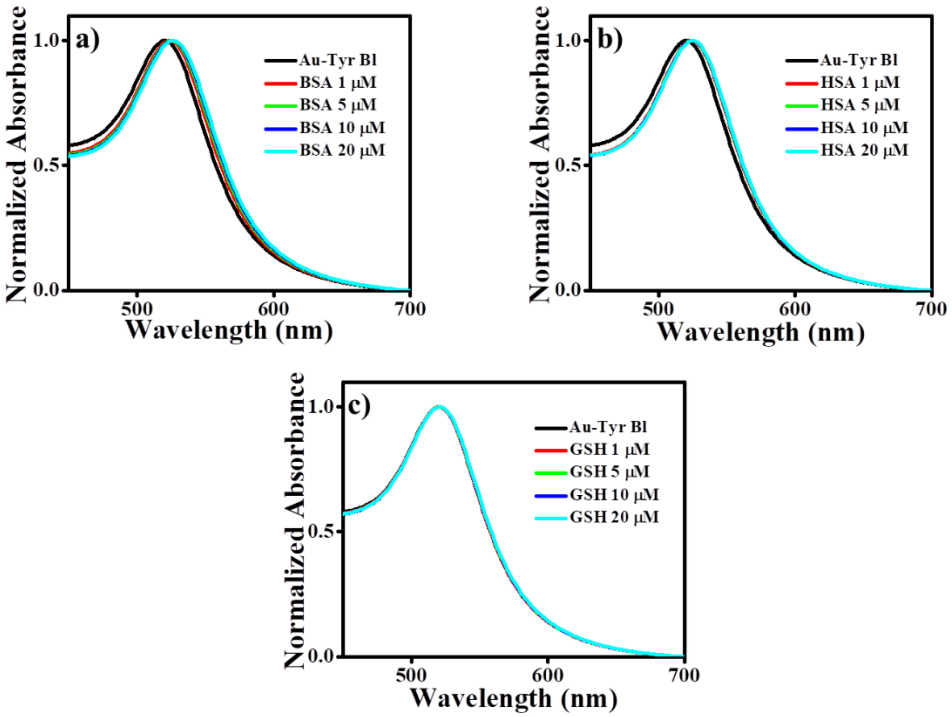

Figure 5.25 *Normalized UV-vis absorption spectra of the Au-Tyr NPs in presence of different concentration (1-20 μM) of BSA (a), HSA (b), and GSH (c).*

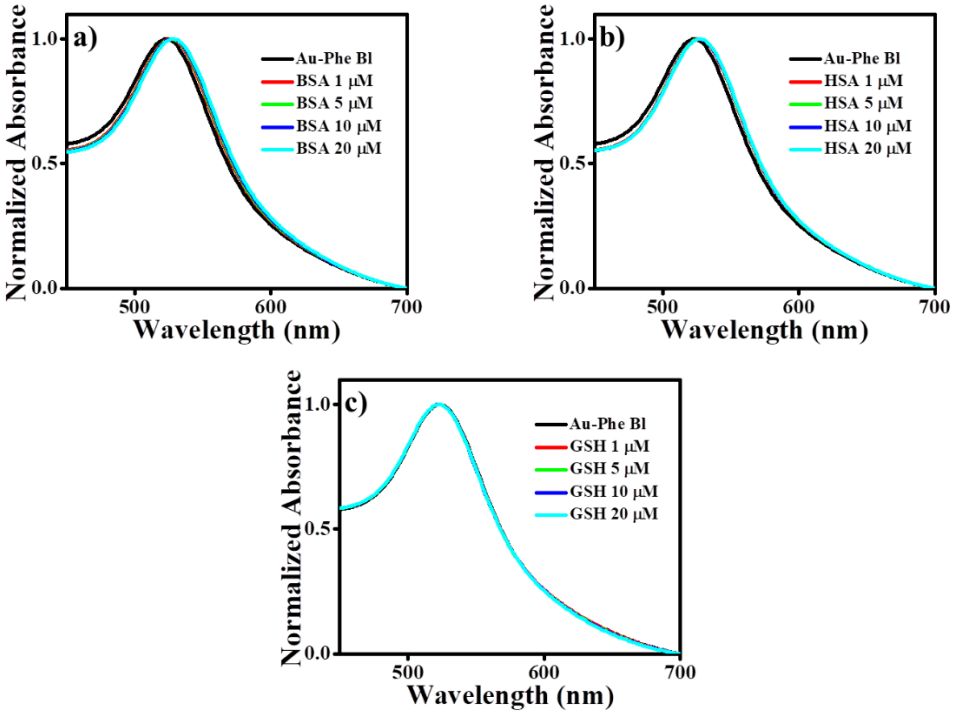

Figure 5.26 *Normalized UV-vis absorption spectra of the Au-Phe NPs in presence of different concentration (1-20 µM) of BSA (a), HSA (b), and GSH (c).*

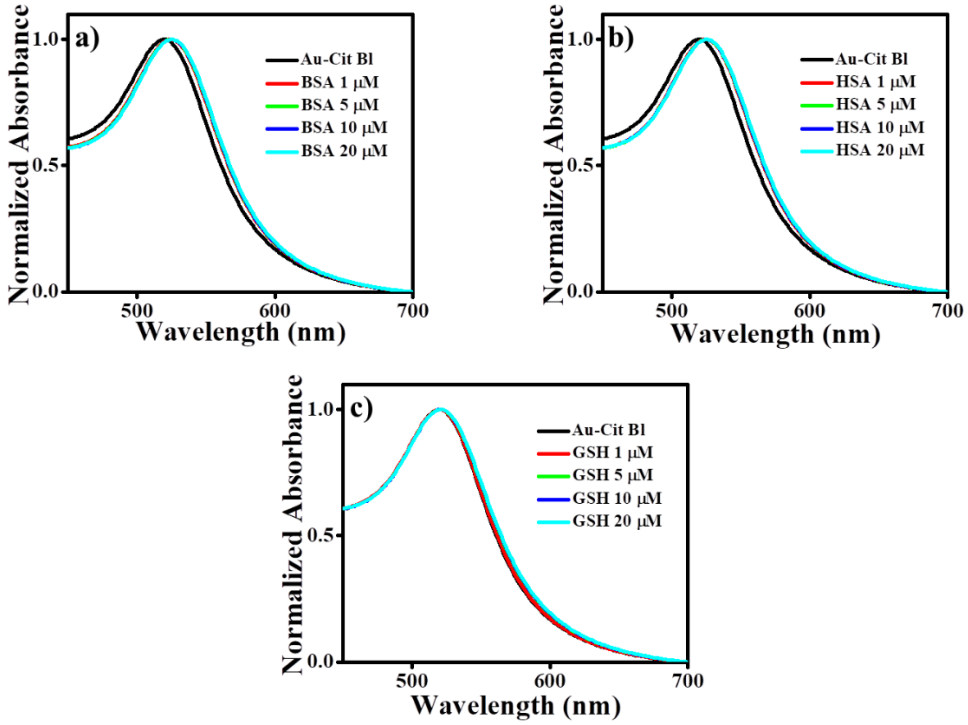

Figure 5.27 *Normalized UV-vis absorption spectra of the Au-Cit NPs in presence of different concentration (1-20 µM) of BSA (a), HSA (b), and GSH (c).*

The UV-Visible spectra revealed a ~ 5 nm red shift in the SPR peak for Au-AA and Au-Cit NPs in the presence of different concentrations (1-20 µM) of BSA and HSA protein indicating that these proteins coated the surface of the Au NPs (**Figure 5.25a-b, 5.26a-b, and 5.27a-b)** *[61]*. However, the SPR peak of the Au-AA and Au-Cit NPs was slightly broadened in presence of different glutathione concentrations (1-20 µM) (**Figure 5.25c, 5.26c, and 5.27c)** *[62]*.

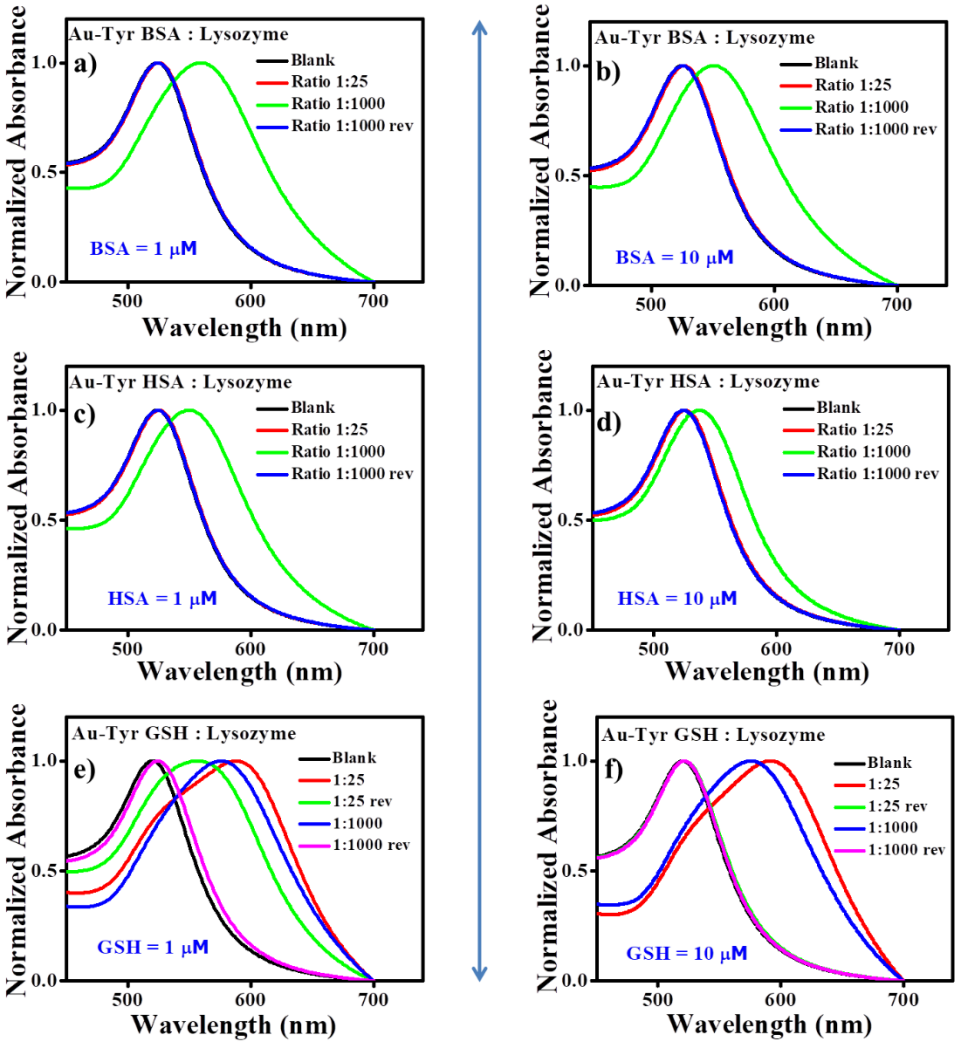

Figure 5.28 *UV-Visible spectra of the BSA (a, b), HSA (c, d), and glutathione (e, f) coated Au-Tyr NPs in presence of low and high concentrations of lysozyme.*

We, next, allowed BSA, HSA, and GSH (1 and 10 µM) bound Au-AA and Au-Cit NPs to interact with low and high concentrations of lysozymes [Au

NPs/lysozyme (1:25 and 1:1000)]. We found that the BSA and HSA coated Au-AA and Au-Cit NPs were stable at low lysozyme concentration [Au NPs/lysozyme (1:25)] (**Figure 5.28a-d, 5.29a-d, and 5.30a-d**). But, when the concentration of lysozyme is higher [Au NPs/lysozyme (1:1000)], the Au-AA and Au-Cit NPs aggregated again indicating that the BSA and HSA coating around the Au NPs failed to prevent aggregation at high lysozyme concentration (**Figure 5.28a-d, 5.29a-d, and 5.30a-d**).

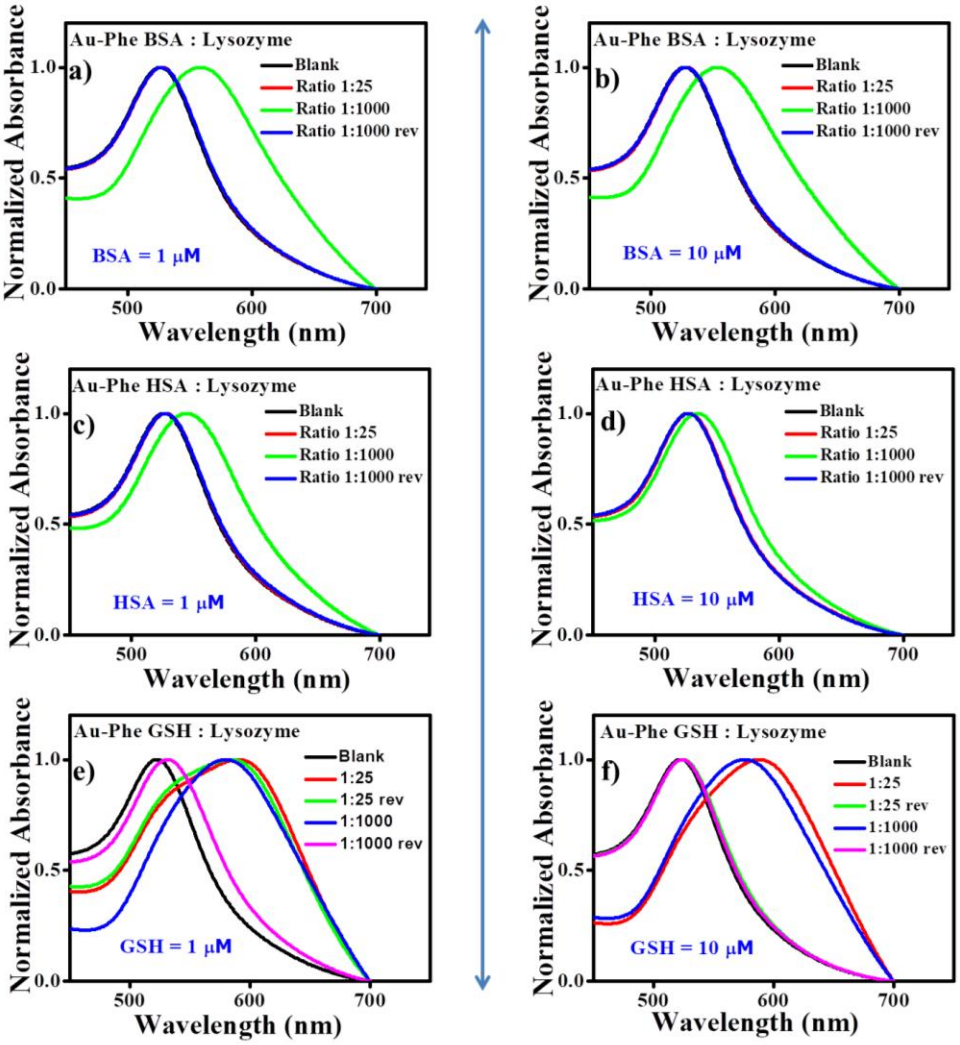

Figure 5.29 *UV-visible spectra of the BSA (a, b), HSA (c, d), and glutathione (e, f) coated Au-Phe NPs in presence of low and high concentrations of lysozyme.*

Further, resistance towards aggregation is higher for HSA coated Au NPs than for BSA coated nanoparticles. The degree of resistance is much higher

at high concentrations (10 µM) proteins than at low concentration (1 µM). We would like to mention that we did not observe any precipitation for BSA and HSA coated Au-AA and Au-Cit NPs in presence of high concentration of lysozyme [Au NPs/lysozyme (1:1000)] like the native Au NPs. Interestingly, unlike native Au-Cit NPs, the aggregation of BSA and HSA coated Au-Cit NPs, as well as BSA and HSA coated Au-Phe and Au-Tyr NPs, was reversible at high lysozyme concentrations. We already mentioned that the ratio 1:25 is too low for the formation of complete monolayer of lysozyme protein around the Au NPs. However, the native Au NPs underwent aggregation at ratio 1:25 because the less number of lysozyme proteins can access the native Au NPs surface to decoat the surface ligands. But the albumin coated Au NPs did not undergo aggregation. As there is coating of albumins on the surface of the Au NPs, these less number of lysozyme molecules cannot access the native Au NPs surface to cause the aggregation. But in case of high lysozyme concentration, the more number of lysozyme molecules was able to access the Au NPs surface via an exchange with albumins (dynamic corona). Previously, Neupane et al. showed the aggregation of BSA coated Au-Cit NPs at Au-Cit NPs/lysozyme ratio 1:200. They reported that lysozyme protein molecules access the native Au NPs surface via the dynamic protein corona between lysozyme and BSA *[30]*. In the present scenario, for the ratio 1:1000, lysozyme concentration was 4 µM which is greater than 1 µM concentration of albumins and less than 10 µM concentrations of albumins. That is why when more number of albumin protein molecules was present on the Au NPs surface, the lysozyme molecules could not fully displace the albumin proteins to access the native Au NPs surface and less aggregation was happened at higher albumin concentrations. At glutathione concentrations of 1 and 10 µM, all Au NPs aggregated at both high and low lysozyme concentrations [Au NPs/lysozyme (1:25 and 1:1000)] (**Figure 5.28e-f, 5.29e-f, 5.30e-f)**. But, at 1 µM glutathione concentration, the aggregation of all the Au NPs was irreversible in presence of NaOH at Au

NPs/lysozyme ratio 1:25 whereas the aggregation was reversible at high lysozyme concentrations [Au NPs/lysozyme (1:1000)]. Surprisingly, at 10 µM glutathione concentrations, all Au NPs aggregation was reversible at both high and low concentrations of lysozyme.

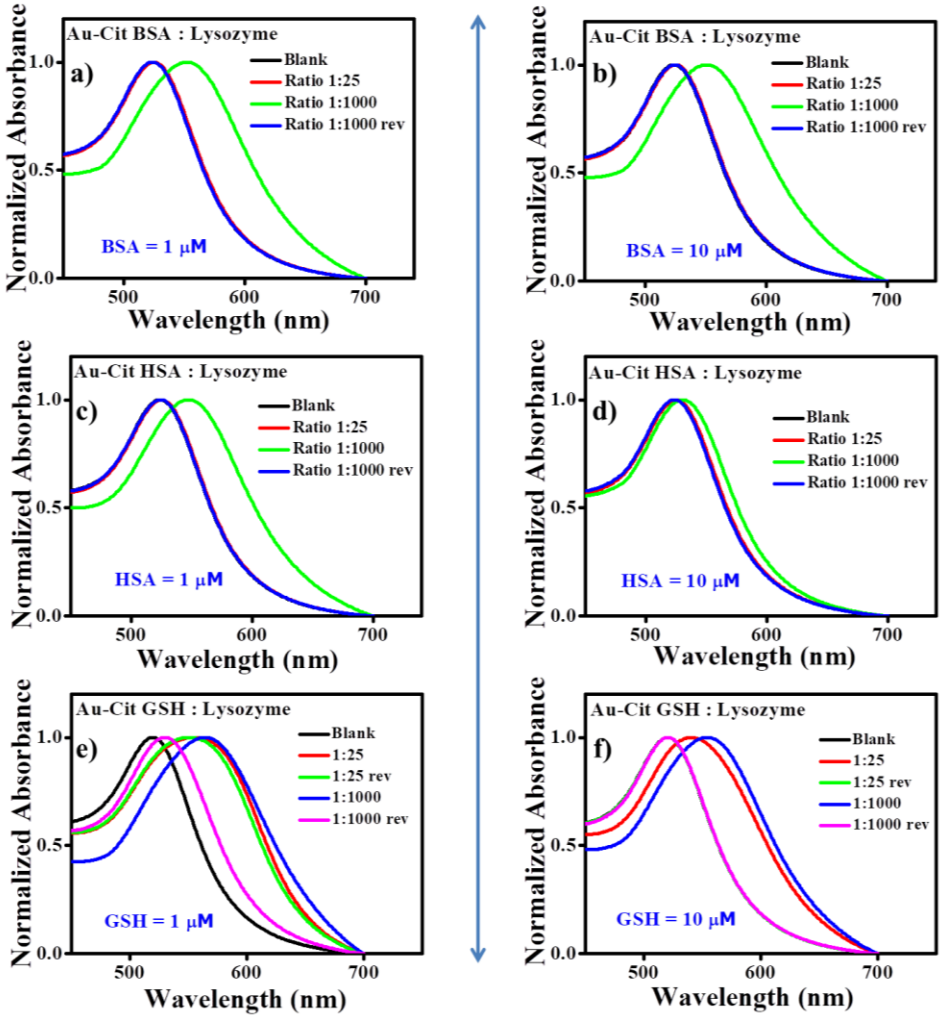

Figure 5.30 *UV-visible spectra of the BSA (a, b), HSA (c, d), and glutathione (e, f) coated Au-Cit NPs in presence of low and high concentrations of lysozyme.*

GSH binding on the Au NPs surface leads to a completely different system as GSH is very small molecule in comparison to albumins and also GSH is endowed of mercapto group. It is very much likely that GSH displaces the surface ligands to form a completely new and stable system. As the Au-AA and Au-Cit NPs showed almost similar behaviour at low GSH concentration

(1 µM), it suggests that GSH at this concentration was unable to displace the surface ligands. However, at higher concentration of GSH (10 µM), there is possibility that GSH removed the surface ligands and formed complete new system. But, it is very hard to determine the number of surface ligands displacement from the Au NPs surface quantitatively. As GSH already displaces the surface ligands at concentration 10 µM, there is no possibility of aggregation through surface displacement (due to the presence of mercapto group) at ratio 1:25. So, the aggregation happens through different mechanism. At low concentration of lysozyme (ratio 1:25), a single lysozyme molecule is in direct contact and electrostatically crosslinks two Au NPs. Because of this, when we added NaOH, electrostatic interaction become weakened and the Au NPs aggregation was reversed back.

5.2.6 Influence of lipid corona on the interaction of Au-Phe NPs with lysozyme:

As the protein corona failed to inhibit the aggregation of the Au NPs at high lysozyme concentration, we looked for an alternative system that can prevent aggregation of Au NPs at high lysozyme concentration. Recently, we have demonstrated that lipid corona on the amino acids (Phenylalanine) functionalized gold nanoparticles (Au-Phe NPs) are effective to prevent the aggregation of Au-Phe NPs against high salt concentration, pH, and freeze-thaw cycles [56, 57]. The literature also seeks the study on how these lipid coated Au-Phe NPs interact with positively charged lysozyme protein. In order to do this, we systematically coated the Au-Phe NPs with different surface charged (zwitterionic and positively) lipid molecules by using our previously reported method [*56, 57*]. Among the zwitterionic lipids, we used two lipids of different phase transition temperatures namely, 1,2-dioleoyl-sn-glycero-3-phosphocholine (DOPC, T_m = −20 °C), 1,2-dipalmitoyl-sn-glycero-3-phosphocholine (DPPC, T_m = 41 °C). The lipid coating around all the Au-Phe NPs was confirmed by the slight red shift (~

5-7 nm) of SPR peak of the Au-Phe NPs in presence of different zwitterionic and positively charged lipid vesicles (**Figure 5.31a**).

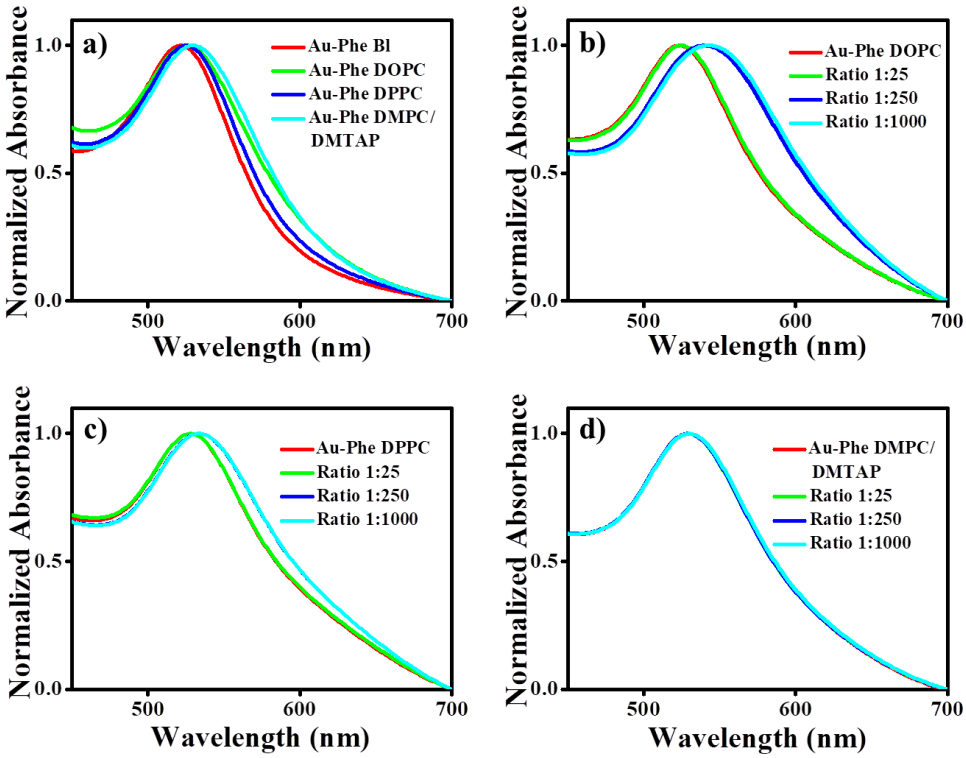

Figure 5.31 *UV-Visible spectra of the Au-Phe NPs (a) in presence of DOPC, DPPC, and DMPC/DMTAP lipid vesicles and DOPC (b), DPPC (c), and DMPC/DMTAP (d) lipid coated Au-Phe NPs in presence of different concentration of lysozyme after incubating 2 hour.*

At low lysozyme concentration [Au-Phe NPs/lysozyme (1:25)], all the different surface charged lipid coated Au-Phe NPs remained stable indicating the lipid coating around the Au-Phe NPs prevents the surface ligand decoating from the Au NPs surface (**Figure 5.31b-d**). Interestingly, the DOPC lipid coated Au-Phe NPs underwent aggregation than DPPC coated Au-Phe NPs at high lysozyme concentration [Au-Phe NPs/lysozyme (1:250 and 1:1000)] (**Figure 5.31b, c**). The UV-Visible spectra showed a ~ 8-10 nm SPR peak shift for the DPPC coated Au-Phe NPs at high concentration of lysozyme [Au-Phe NPs/lysozyme (1:250 and 1:1000)] which may be due to the adsorption of the lysozyme molecules on the lipid

coated Au-Phe NPs surface (**Figure 5.31c**). But, for the DOPC coated Au-Phe NPs, ~ 20-25 nm SPR peak shift was observed implying the aggregation of the Au-Phe NPs (**Figure 5.31b**). Moreover, the positively charged lipid coated Au-Phe NPs did not undergo any aggregation at high concentration of lysozyme [Au-PheNPs/lysozyme (1:250 and 1:1000)] which may be due to the strong charged repulsion of the positively charged lipid molecules and positively charged lysozyme molecules (**Figure 5.31d**). Although both the DOPC and DPPC lipid is zwitterionic, these two lipid coated Au-Phe NPs showed distinct behaviour in presence of high lysozyme concentration. We previously reported that DOPC and DPPC lipid formed soft and hard lipid corona respectively on the surface of phenylalanine functionalized gold nanoparticles *[57]*. Due to the soft nature of the DOPC lipid bilayer, the adsorbed lysozyme molecules can access the native Au-Phe NPs to prompt the aggregation of Au-Phe NPs. But, in case of DPPC lipid coated Au-Phe NPs, the adsorbed lysozyme molecule can not access the native Au-Phe NPs surface due to the hard nature of the DPPC lipid bilayer. To the best of our knowledge, this is the first report of the impact of hard and soft lipid corona in the interaction with protein. This study will help the nano-researchers for engineering the suitable nanomaterials for biomedical applications.

5.2.7 Possible mechanistic pathway of interaction between different Au NPs and lysozyme:

After analyzing all the results of our above experiments, we are now in a position to draw a mechanistic pathway of interaction between different Au NPs (Au-AA and Au-Cit NPs) and lysozyme depending on the protein concentrations. It is well-known that lysozyme carries global positive charge at physiological pH as the pI of the lysozyme is 11.35. Therefore, one may expect stronger interaction between lysozyme and the negatively charged citrate and amino acids (Phe and Tyr) functionalized gold nanoparticles irrespective of the protein concentration. Following distinctly

different aggregation phenomena at low and high lysozyme concentration, we propose two different mechanisms of interaction at low and high concentration of lysozyme. At low lysozyme concentration [Au NPs/lysozyme (1:25)], at physiological pH, the lysozyme molecules adsorb on the Au NPs surface through strong electrostatic interaction between negative COO^- group of the Au NPs and positive lysine residue of the lysozyme protein. Based on our calculations, as the ratio 1:25 is very low to complete a compact monolayer around the Au NPs, the less number of adsorbed lysozyme molecules cannot fully covered the Au NPs surface. The adsorbed lysozyme molecules decoat the surface ligands (citrate, amino acids) from the Au NPs surface. The displacement of capping agent from Au NPs surface (citrate, Tyr, Phe) would allow lysozyme to directly interact and form hard corona over time on the Au NPs surface thus preventing the Au NPs aggregation with time.

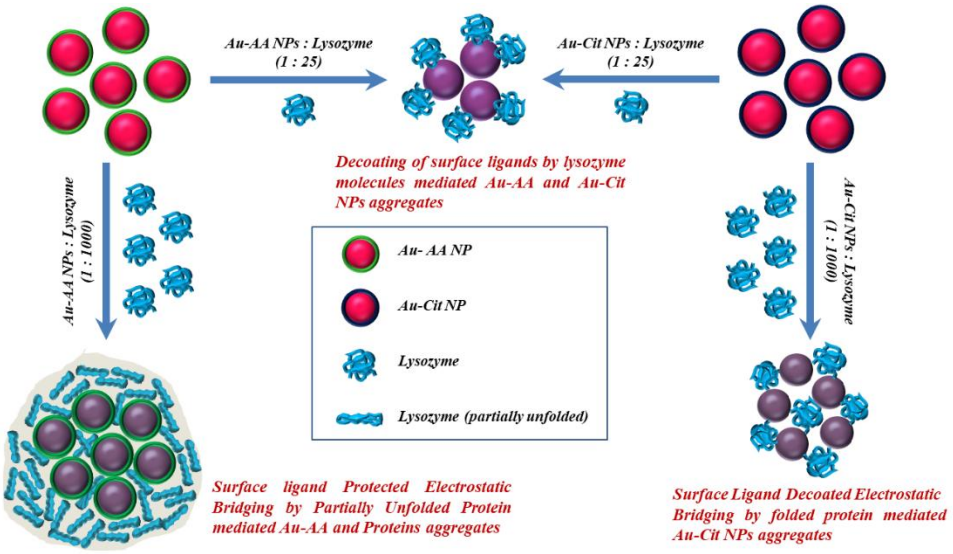

Scheme 5.1 *Schematic representation of the aggregation mechanism of Au-AA and Au-Cit NPs at low [Au NPs/lysozyme (1:25)] and high concentration [Au NPs/lysozyme (1:1000)] of lysozyme. At low lysozyme concentration [Au NPs/lysozyme (1:25)], decoating of the surface ligands by lysozyme molecules triggers the aggregation of the Au-AA and Au-Cit NPs. At high lysozyme concentration [Au-AA NPs/lysozyme (1:1000)], the Au-AA NPs form aggregates keeping the surface ligand protected. But partial unfolding of the lysozyme molecules during electrostatic bridging influences the protein aggregation on the*

aggregated Au-AA NPs surface. But for the Au-Cit NPs, the surface ligands are decoated during the electrostatic bridging which triggers the aggregation of the Au-Cit NPs at high lysozyme concentration [Au-Cit NPs/lysozyme (1:1000)]. Schematics are not drawn to scale.

However, based on our experimental results, the aggregation mechanism seems to be different at higher concentration from that at lower concentration of lysozyme. The reversibility experiment implies that the amino acid functionalized Au NPs interact differently from that of citrate capped Au NPs at high lysozyme concentration. We have used the plasmon ruler equation to estimate the interparticle separation from an experimentally observed plasmon shift *[33]*.

$$\frac{\Delta\lambda}{\lambda_0} \approx 0.18 \exp\{\frac{-(s/D)}{0.23}\}$$

Where $\frac{\Delta\lambda}{\lambda_0}$ is the fractional plasmon shift, s is the interparticle edge-to-edge separation, and D is the nanoparticle diameter.

This equation was used to estimate the interparticle distance of lysozyme bound Au NPs surface (formed at pH 12) in the pH range where they start to aggregate (pH<pI). At pH < 10, the plasmon shift observed for the lysozyme bound Au NPs surface is in the range of 27-30 nm which gives an interparticle separation of ~ 6.5 nm for Au-AA NPs and ~ 3.5 nm for Au-Cit NPs. So, at high lysozyme concentration, the Au-AA NPs is first fully coated by lysozyme protein layer electrostatically followed by crosslinking through lysozyme-lysozyme electrostatic bridging interactions where lysozymes are immobilized on aggregated Au-AA NPs. Now, the lysozyme protein have to be unfolded to crosslink another lysozyme coated Au-AA NPs leading to the aggregation of both Au-AA NPs and lysozyme proteins. But, for the Au-Cit NPs, it did not happen as the separation is less. In case of Au-Cit NPs, lysozyme serves as a bridge to bring the Au NPs at close proximity, eventually leading to the aggregation of Au NPs. Thus in case of Au-Cit NPs, unfolding of lysozyme protein is not necessary to take place.

During electrostatic bridging, weakly adsorbed citrate ligands are decoated from the Au NPs surface. The CD spectroscopy also revealed that the lysozyme protein structure (at higher concentration) remains intact for the Au-Cit NPs but not for Au-AA NPs (**Figure 5.32**).

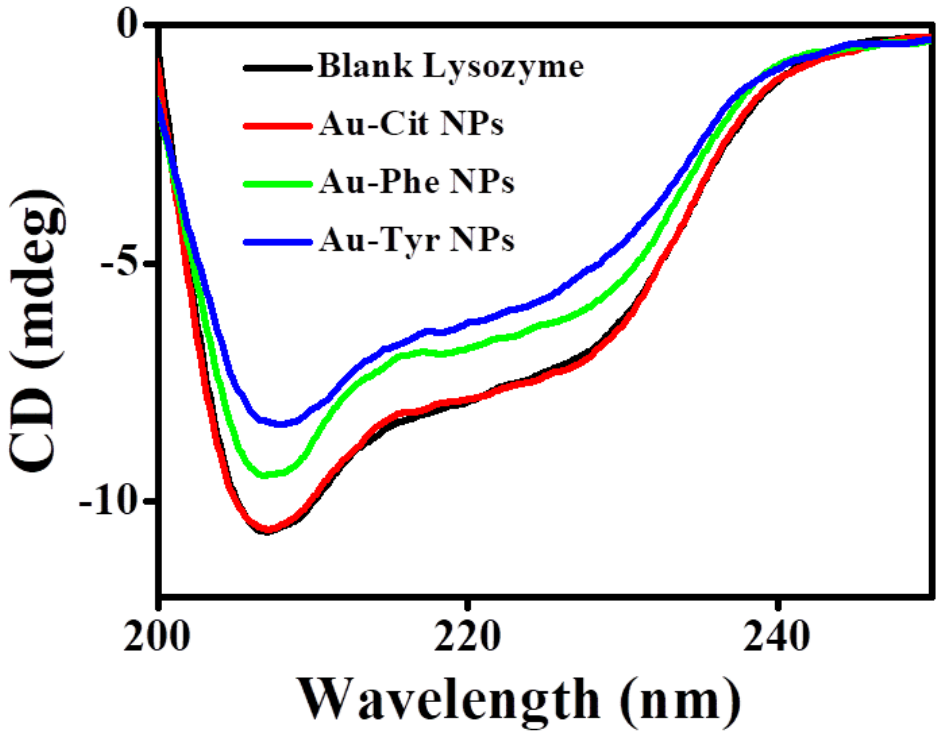

Figure 5.32 *CD spectra of lysozyme in presence of Au-AA and Au-Cit NPs at ratio [Au NPs: Lysozyme (1:1000)].*

In our previous paper, we reported that amino acids formed a thick coating of around ~ 6 nm around the Au NPs surface [57]. It was also well-known that citrate molecules are weakly adsorbed on the Au NPs surface and formed a coating of around ~1 nm. Previously, Neupane et al. reported that if the negative coatings is thick and stable enough, the Au NPs form agglomerates along with the protein aggregates *[32]*. But if the ligands are weakly adsorbed, decoating of the surface ligands takes place. So, this conjecture collaborates well with our present findings. Therefore, we propose "surface ligand protected electrostatic bridging by partially unfolded protein" mechanism for the amino acid functionalized Au NPs and

"Surface ligand decoated electrostatic bridging by folded protein" mechanism for Au-Cit NPs at high lysozyme concentration [Au NPs/lysozyme (1:250 and 1:1000)]. We have depicted the whole mechanism in **Scheme 5.1**.

5.3 Conclusion

In summary, we investigated the aggregation mechanism of Au-AA and Au-Cit NPs in the presence of different concentrations (low and high) of globular lysozyme protein. The impact of protein binding and lipid corona on lysozyme-induced Au NPs aggregation has been thoroughly discussed. Therefore, we draw the following fascinating conclusions from our studies.

i) All the Au NPs (Au-Cit, Au-Phe, and Au-Tyr) at physiological pH underwent aggregation at wide range of Au NPs/lysozyme ratio (1:25 to 1: 2000). At low lysozyme concentration [Au NPs/lysozyme (1:25)], the Au NPs formed small aggregates and the large aggregates were found at high concentration [Au NPs/lysozyme (1:100 - 1:2000)]**.**

(ii) The aggregation of all the three Au NPs was found to be irreversible in presence of NaOH at low lysozyme concentration [Au NPs/lysozyme (1:25)]. Interestingly, at high lysozyme concentrations [Au NPs/lysozyme (1:250 and 1:1000)], aggregation was reversible for amino acid functionalized gold nanoparticles (Au-Phe and Au-Tyr NPs), but not for Au-Cit NPs.

(iii) All the Au NPs when coated by globular protein such as BSA and HSA were found to offer resistance towards aggregation at low lysozyme concentration [Au NPs/lysozyme (1:25)]. However, higher lysozyme concentration caused the aggregation which was found to be reversible in presence of NaOH.

(iv) All the lipid coated Au-Phe NPs prevented the aggregation of Au NPs at low lysozyme concentration [Au-Phe NPs/lysozyme (1:25)].

Interestingly, the DOPC lipid coated Au-Phe NPs underwent aggregation at high lysozyme concentration [Au-Phe NPs/lysozyme (1:250 and 1:1000)], whereas the DPPC lipid coated Au-Phe NPs did not. This observation affirms the effectiveness of soft and hard lipid corona to impede the protein induced Au NPs aggregation.

(v) We have proposed two mechanisms for aggregation of Au NPs at two different protein concentrations. At low lysozyme concentration [Au NPs/lysozyme (1:25)], decoating of surface ligands by lysozyme molecules mediated Au-AA and Au-Cit NPs aggregation was proposed. "Surface ligand decoated electrostatic bridging by folded protein" and "surface ligand protected electrostatic bridging by partially unfolded protein" mechanism was proposed for Au-Cit NPs and Au-AA NPs respectively at high lysozyme concentrations [Au NPs/lysozyme (1:250 and 1:1000)].

5.4 References

[1] Alkilany A. M., Lohse S. E., Murphy C. J. (2013), The Gold Standard: Gold Nanoparticle Libraries to Understand the Nano-Bio Interface, Acc. Chem. Res. 46, 650−661 (DOI: 10.1021/ar300015b)

[2] Dykman L., Khlebtsov N. (2012), Gold Nanoparticles in Biomedical Applications: Recent Advances and Perspectives, Chem. Soc. Rev. 41, 2256−2282 (DOI: 10.1039/C1CS15166E)

[3] Yeh Y.-C., Creran B., Rotello V. M. (2012), Gold Nanoparticles: Preparation, Properties, and Applications in Bionanotechnology, Nanoscale 4, 1871−1880 (DOI: 10.1039/C1NR11188D)

[4] Tiwari M. P., Vig K., Dennis A. V. *et al.* (2011), Functionalized Gold Nanoparticles and Their Biomedical Applications, Nanomaterials 1, 31−63 (DOI: 10.3390/nano1010031)

[5] Xiao T., Qin J., Peng C. *et al.* (2020), A Dendrimer Based Dual Radiodense Element-Containing Nanoplatform for Targeted Enhanced Tumor Computed Tomography Imaging, Langmuir 36, 3096−3103 (DOI: 10.1021/acs.langmuir.0c00451)

[6] Kundu S., Mukherjee D., Maiti T. K. *et al.* (2019), Highly Luminescent Thermoresponsive Green Emitting Gold Nanoclusters for Intracellular Nanothermometry and Cellular Imaging: a Dual Function Optical Probe, ACS Appl. Bio Mater. 2, 2078-2091 (DOI: 10.1021/acsabm.9b00107)

[7] Dreaden E. C., Alkilany A. M., Huang X. *et al.* (2012), The Golden Age: Gold Nanoparticles for Biomedicine, Chem. Soc. Rev. 41, 2740−2779 (DOI: 10.1039/C1CS15237H)

[8] Ghosh P., Han G., De M. *et al.* (2008), Gold Nanoparticles in Delivery Applications, Adv. Drug Delivery Rev. 60, 1307−1315 (DOI: 10.1016/j.addr.2008.03.016)

[9] Giljohann D. A., Seferos D. S., Daniel W. L. *et al.* (2010), Gold Nanoparticles for Biology and Medicine, Angew. Chem. Int. Ed. 49, 3280−3294 (DOI: 10.1002/anie.200904359)

[10] De M., Ghosh P. S., Rotello V. M. (2008), Applications of Nanoparticles in Biology, Adv. Mater. 20, 4225−4241 (DOI: 10.1002/adma.200703183)

[11] Pissuwan D., Niidome T., Cortie M. B. (2011), The Forthcoming Applications of Gold Nanoparticles in Drug and Gene Delivery Systems, J. Controlled Release 149, 65−71 (DOI: 10.1016/j.jconrel.2009.12.006)

[12] Pyne A., Nandi S., Ghosh M. *et al.* (2020), Denaturant-Mediated Modulation of the Formation and Drug Encapsulation Responses of Gold Nanoparticles, Langmuir 36, 7634-7647 (DOI: 10.1021/acs.langmuir.0c01293)

[13] Tenzer S., Docter D., Rosfa S. *et al.* (2011), Nanoparticle Size is a Critical Physicochemical Determinant of the Human Blood Plasma Corona: a Comprehensive Quantitative Proteomic Analysis, ACS Nano 5, 7155−7167 (DOI: 10.1021/nn201950e)

[14] Nel A. E., Mädler L., Velegol D. *et al.* (2009), Understanding Biophysicochemical Interactions at the Nano−Bio Interface, Nat. Mater. 8, 543−557 (DOI: 10.1038/nmat2442)

[15] Lynch I., Dawson K. A. (2008), Protein-Nanoparticle Interactions, Nano Today 3, 40−47 (DOI: 10.1016/S1748-0132(08)70014-8)

[16] Cedervall T., Lynch I., Lindman S. *et al.* (2007), Understanding the Nanoparticle-Protein Corona Using Methods to Quantify Exchange Rates and Affinities of Proteins for Nanoparticles, Proc. Natl. Acad. Sci. U.S.A. 104, 2050−2055 (DOI: 10.1073/pnas.0608582104)

[17] Monopoli M. P., Åberg C., Salvati A. *et al.* (2012), Biomolecular Coronas Provide the Biological Identity of Nanosized Materials, Nat. Nanotechnol. 7, 779−786 (DOI: 10.1038/nnano.2012.207)

[18] Aggarwal P., Hall J. B., McLeland C. B. *et al.* (2009), Nanoparticle Interaction with Plasma Proteins as It Relates to Particle Biodistribution, Biocompatibility and Therapeutic Efficacy, Adv. Drug Deliv. Rev. 61, 428−437 (DOI: 10.1016/j.addr.2009.03.009)

[19] Walkey C. D., Chan W. C. W. (2012), Understanding and Controlling the Interaction of Nanomaterials with Proteins in a Physiological Environment, Chem. Soc. Rev. 41, 2780−2799 (DOI: 10.1039/C1CS15233E)

[20] Walczyk D., Bombelli F. B., Monopoli M. P. *et al.* (2010), What the Cell “sees” in Bionanoscience, J. Am. Chem. Soc. 132, 5761−5768 (DOI: 10.1021/ja910675v)

[21] Deng Z. J., Liang M., Monteiro M. *et al.* (2011), Nanoparticle-Induced Unfolding of Fibrinogen Promotes Mac-1 Receptor Activation and Inflammation, Nat. Nanotechnol. 6, 39−44 (DOI: 10.1038/nnano.2010.250)

[22] Canaveras F., Madueno R., Sevilla J. M. *et al.* (2012), Role of the Functionalization of the Gold Nanoparticle Surface on the Formation of Bioconjugates with Human Serum Albumin, J. Phys. Chem. C 116, 10430−10437 (DOI: 10.1021/jp3021497)

[23] Brewer S. H., Glomm W. R., Johnson M. C. *et al.* (2005), Probing BSA Binding to Citrate-Coated Gold Nanoparticles and Surfaces, Langmuir 21, 9303−9307 (DOI: 10.1021/la050588t)

[24] Shang L., Wang Y., Jiang J. *et al.* (2007), pH-Dependent Protein Conformational Changes in Albumin: Gold Nanoparticle Bioconjugates: A Spectroscopic Study, Langmuir 23, 2714−2721 (DOI: 10.1021/la062064e)

[25] Kim Y., Ko S. M., Nam, J.-M. (2016), Protein−Nanoparticle Interaction-Induced Changes in Protein Structure and Aggregation, Chem. - Asian J. 11, 1869−1877 (DOI: 10.1002/asia.201600236)

[26] Jiang X., Jiang J., Jin Y. *et al.* (2005), Effect of Colloidal Gold Size on the Conformational Changes of Adsorbed Cytochrome c: Probing by Circular Dichroism, UV-Visible, and Infrared Spectroscopy, Biomacromolecules 6, 46−53 (DOI: 10.1021/bm049744l)

[27] James A. E., Driskell J. D. (2013), Monitoring Gold Nanoparticle Conjugation and Analysis of Biomolecular Binding with Nanoparticle Tracking Analysis (NTA) and Dynamic Light Scattering (DLS), Analyst 138, 1212−1218 (DOI: 10.1039/c2an36467k)

[28] Dominguez-Medina S., Kisley L., Tauzin L. J. *et al.* (2016), Adsorption and Unfolding of a Single Protein Triggers Nanoparticle Aggregation, ACS Nano 10, 2103−2112 (DOI: 10.1021/acsnano.5b06439)

[29] Zhang D., Neumann O., Wang H. *et al.* (2009), Gold Nanoparticles Can Induce the Formation of Protein-based Aggregates at Physiological pH, Nano Lett. 9, 666−671 (DOI: 10.1021/nl803054h)

[30] Neupane S., Pan Y., Takalkar S. *et al.* (2017), Probing the Aggregation Mechanism of Gold Nanoparticles Triggered by a Globular Protein, J. Phys. Chem. C 121, 1377−1386 (DOI: 10.1021/acs.jpcc.6b11963)

[31] Zhang S., Moustafa Y., Huo Q. (2014) Different Interaction Modes of Biomolecules with Citrate-Capped Gold Nanoparticles, ACS Appl. Mater. Interfaces 6, 21184−21192 (DOI: 10.1021/am506112u)

[32] Neupane S., Pan Y., Li H. *et al.* (2018), Engineering Protein−Gold Nanoparticle/Nanorod Complexation Via Surface Modification for Protein Immobilization and Potential Therapeutic Applications, ACS Appl. Nano Mater. 1, 4053−4063 (DOI: 10.1021/acsanm.8b00839)

[33] Cardenas B., Sa´ nchez-Obrero G., Maduen˜o R. *et al.* (2014), Influence of the Global Charge of the´Protein on the Stability of Lysozyme – AuNP Bioconjugates, J. Phys. Chem. C 118, 22274−22283 (DOI: 10.1021/jp505301h)

[34] Khandelia R., Jaiswal A. Ghosh S. S. *et al.* (2013), Gold Nanoparticle−Protein Agglomerates as Versatile Nanocarriers for Drug Delivery, *Small 9*, 3494−3505 (DOI: 10.1002/smll.201203095)

[35] Cheng Y., Samia A. C., Meyers J. D. *et al.* (2008), Highly Efficient Drug Delivery with Gold Nanoparticle Vectors for in vivo Photodynamic Therapy of Cancer, J. Am. Chem. Soc. 130, 10643−10647 (DOI: 10.1021/ja801631c)

[36] Nam J., Won N., Jin H. *et al.* (2009), pH-Induced Aggregation of Gold Nanoparticles for Photothermal Cancer Therapy, J. Am. Chem. Soc. 131, 13639−13645 (DOI: 10.1021/ja902062j)

[37] Saha K., Agasti S. S., Kim C. *et al.* (2012), Gold Nanoparticles in Chemical and Biological Sensing, Chem. Rev. 112, 2739−2779 (DOI: 10.1021/cr2001178)

[38] Zhao W., Lam J. C. F., Chiuman W. *et al.* (2008), Enzymatic Cleavage of Nucleic Acids on Gold Nanoparticles: A Generic Platform for Facile Colorimetric Biosensors, Small 4, 810−816 (DOI: 10.1002/smll.200700757)

[39] Lee J. H., Wang Z., Liu J. *et al.* (2008), Highly Sensitive and Selective Colorimetric Sensors for Uranyl (UO22+): Development and Comparison of Labeled and Label-Free DNAzyme-Gold Nanoparticle Systems, J. Am. Chem. Soc. 130, 14217−14226 (DOI: 10.1021/ja803607z)

[40] Liu J., Lu Y. (2006), Preparation of Aptamer-Linked Gold Nanoparticle Purple Aggregates for Colorimetric Sensing of Analytes, Nat. Protoc. 1, 246−252 (DOI: 10.1038/nprot.2006.38)

[41] Samaranayake Y. H., Samaranayake L. P., Pow E. H. N. *et al.* (2001), Antifungal Effects of Lysozyme and Lactoferrin against Genetically Similar, Sequential Candida Albicans Isolates from a Human Immunodeficiency Virus-Infected Southern Chinese Cohort, J. Clin. Microbiol. 39, 3296−3302 (DOI: 10.1128/JCM.39.9.3296-3302.2001)

[42] Bharti B., Meissner J., Findenegg G. H. (2011), Aggregation of Silica Nanoparticles Directed by Adsorption of Lysozyme, Langmuir 27, 9823−9833 (DOI: 10.1021/la201898v)

[43] Kumar S., Aswal V. K., Callow P. (2014), pH-Dependent Interaction and Resultant Structures of Silica Nanoparticles and Lysozyme Protein, Langmuir 30, 1588−1598 (DOI: 10.1021/la403896h)

[44] Vertegel A. A., Siegel R. W., Dordick J. S. (2004), Silica Nanoparticle Size Influences the Structure and Enzymatic Activity of Adsorbed Lysozyme, Langmuir 20, 6800−6807 (DOI: 10.1021/la0497200)

[45] Bharti B., Meissner J., Klapp S. H. L. *et al.* (2014), Bridging Interactions of Proteins with Silica Nanoparticles: The Influence of pH, Ionic Strength and Protein Concentration, Soft Matter 10, 718–728 (DOI: 10.1039/C3SM52401A)

[46] Galdino F. E., Picco A. S., Sforca M. L. *et al.* (2020), Effect of Particle Functionalization and Solution Properties on the Adsorption of Bovine Serum Albumin and Lysozyme onto Silica Nanoparticles, Colloids Surf., B 186, 110677 (DOI: 10.1016/j.colsurfb.2019.110677)

[47] Mishra K., Das, P. K. (2019), Thermodynamics of Adsorption of Lysozyme on Gold Nanoparticles from Second Harmonic Light Scattering, Phys. Chem. Chem. Phys. 21, 7675−7684 (DOI: 10.1039/C8CP07299J)

[48] Chen Y.-M., Yu C.-J., Cheng T.-L. *et al.* (2008), Colorimetric Detection of Lysozyme Based on Electrostatic Interaction with Human Serum Albumin-Modified Gold Nanoparticles, Langmuir 24, 3654−3660 (DOI: 10.1021/la7034642)

[49] Gomes A., Carnerero J. M., Jimenez-Ruiz A. *et al.* (2021), Lysozyme–AuNPs Interactions: Determination of Binding Free Energy, Nanomaterials 11, 2139 (DOI: 10.3390/nano11082139)

[50] Dominguez-Medina S., Kisley L., Tauzin L. J. *et al.* (2016), Adsorption and Unfolding of a Single Protein Triggers Nanoparticle Aggregation, ACS Nano 10, 2103−2112 (DOI: 10.1021/acsnano.5b06439)

[51] Olenick L. L., Troiano J. M., Vartanian A. *et al.* (2018), Lipid Corona Formation from Nanoparticle Interactions with Bilayers, Chem 4, 2709−2723 (DOI: 10.1016/j.chempr.2018.09.018)

[52] Zhang X., Pandiakumar A. K., Hamers R. J. *et al.* (2018), Quantification of Lipid Corona Formation on Colloidal Nanoparticles from Lipid Vesicles, Anal. Chem. 90, 14387−14394 (DOI: 10.1021/acs.analchem.8b03911)

[53] Yang J. A., Murphy C. J. (2012), Evidence for Patchy Lipid Layers on Gold Nanoparticle Surfaces, Langmuir 28, 5404−5416 (DOI: 10.1021/la300325p)

[54] Mandal T., Konduru N. V., Ramazani A. *et al.* (2018), Effect of Surface Charge and Hydrophobicity on Phospholipid-Nanoparticle Corona Formation: A Molecular Dynamics Simulation Study, Colloid Interface Sci. Commun. 25, 7−11 (DOI: 10.1016/j.colcom.2018.04.008)

[55] Lima T., Bernfur K., Vilanova M. *et al.* (2020), Understanding the Lipid and Protein Corona Formation on Different Sized Polymeric Nanoparticles, Sci. Rep. 10, 1129 (DOI: 10.1038/s41598-020-57943-6)

[56] Maity A., De S. K., Chakraborty A. (2021), Interaction of Aromatic Amino Acid-Functionalized Gold Nanoparticles with Lipid Bilayers: Insight into the Emergence of Novel Lipid Corona Formation, J. Phys. Chem. B 125, 2113−2123 (DOI: 10.1021/acs.jpcb.0c10079)

[57] Maity A., De S. K., Bagchi D. *et al.* (2022), Mechanistic Pathway of Lipid Phase-Dependent Lipid Corona Formation on Phenylalanine-Functionalized Gold Nanoparticles: A Combined Experimental and Molecular Dynamics Simulation Study, J. Phys. Chem. B 126, 2241-2255 (DOI: 10.1021/acs.jpcb.2c00356)

[58] Haiss W., Thanh N. T., Aveyard J. *et al.* (2007), Determination of Size and Concentration of Gold Nanoparticles from UV− Vis Spectra, Anal. Chem. 79, 4215-4221 (DOI: 10.1021/ac0702084)

[59] Okyem S., Awotunde O., Ogunlusi T. *et al.* (2021), Probing the Mechanism of Antibody-Triggered Aggregation of Gold Nanoparticles, Langmuir 37, 2993-3000 (DOI: 10.1021/acs.langmuir.1c00100)

[60] Sindhu A., Varma R. S., Venkatesu P. (2022), Cholinium-Based Ionic Liquids Attenuate the Amyloid Fibril Formation of Lysozyme: A Greener

Concept of Antiamyloidogenic Ionic Liquids, ACS Sustainable Chem. Eng. 10, 9242−9253 (DOI: 10.1021/acssuschemeng.2c02963)

[61] Wu R., Peng H., Zhu J. J. *et al.* (2020), Attaching DNA to Gold Nanoparticles with a Protein Corona, Front. Chem. 8, 121 (DOI: 10.3389/fchem.2020.00121)

[62] Kanwa N., Patnaik A., De S. K. *et al.* (2019), Effect of Surface Ligand and Temperature on Lipid Vesicle−Gold Nanoparticle Interaction: A Spectroscopic Investigation, Langmuir 35, 1008−1020 (DOI: 10.1021/acs.langmuir.8b03673)

Chapter 6

Materials, Methods, and Instrumentation

6.1 Materials

Chapter 2

Gold (III) chloride hydrate ($HAuCl_4 \cdot xH_2O$), three aromatic amino acids, namely phenylalanine (Phe), tyrosine (Tyr), tryptophan (Trp), and 4-(2-hydroxyetyl)-1-piperazineethanesulfonic acid (HEPES) were purchased from Sigma-Aldrich. All of the phospholipids, namely, 1,2-dimyristoyl-sn-glycero-3-phosphocholine (DMPC), 1,2-dimyristoyl-sn-glycero-3-phospho-(1′-rac-glycerol) (sodium salt) (DMPG), 1,2-dimyristoyl-3-trimethylammonium-propane (chloride salt) (DMTAP), and 1,2-dimyristoyl-sn-glycero-3-phosphoethanolamine-N-(lissamine rhodamine B sulfonyl) (ammonium salt) (Liss Rhod PE) were purchased from Avanti Polar Lipids. Sodium hydroxide (NaOH) and Milli-Q water were obtained from Merck. All of the chemicals were used as received without further purification. Milli-Q water was used to prepare all of the solutions. All the glassware was kept overnight with freshly prepared 3:1 HCl/HNO_3 (aqua regia) and cleaned thoroughly with Milli-Q water before any experiments.

Chapter 3

All the zwitterionic phospholipids, namely, DOPC (1,2-dioleoyl-sn-glycero-3-phosphocholine), DLPC (1,2-dilauroyl-sn-glycero-3-phosphocholine), DMPC (1,2-dimyristoyl-snglycero-3-phosphocholine), DPPC (1,2-dipalmitoyl-sn-glycero-3-phosphocholine), and 1,2-dimyristoyl-sn-glycero-3-phosphoethanolamine-N-(lissamine rhodamine B sulfonyl) (ammonium salt) (Liss Rhod PE) were purchased from Avanti polar lipids. Gold (III) chloride hydrate ($HAuCl_4 \cdot xH_2O$), phenylalanine

(Phe), Cholesterol, and 4-(2-hydroxyetyl)-1-piperazineethanesulfonic acid (HEPES) were purchased from Sigma-Aldrich. Sodium hydroxide (NaOH) and Milli-Q water were obtained from Merck. All the chemicals were used as received without further purification. Milli-Q water was used to prepare all the solutions. All the glassware was kept in freshly prepared aqua regia (3:1 HCl/HNO_3) overnight and washed thoroughly with Milli-Q water before doing any experiments.

Chapter 4

All of the three zwitterionic phospholipids, namely, 1,2-dioleoyl-sn-glycero-3-phosphocholine (DOPC), 1,2-dimyristoyl-sn-glycero-3-phosphocholine (DMPC), and 1,2-dipalmitoyl-sn-glycero-3-phosphocholine (DPPC) and two charged lipids 1,2-dimyristoylsn-glycero-3-phospho-(1′-rac-glycerol) (sodium salt) (DMPG), and 1,2-dimyristoyl-3-trimethylammonium-propane (chloride salt) (DMTAP) were purchased from Avanti Polar Lipids. Phenylalanine, tryptophan, and tyrosine amino acids and HEPES (4-(2-hydroxyetyl)-1-piperazineethanesulfonic acid were purchased from Sisco Research Laboratories. Sodium hydroxide (NaOH), sodium chloride (NaCl), and silver nitrate ($AgNO_3$) were purchased from Merck. All the chemicals were used as received from the manufacturer. Milli-Q water was used to prepare all the solutions for the experiment.

Chapter 5

All the phospholipids namely, 1,2-dioleoyl-sn-glycero-3-phosphocholine (DOPC), 1,2-dimyristoyl-sn-glycero-3-phosphocholine (DMPC), 1,2-dipalmitoyl-sn-glycero-3-phosphocholine (DPPC), and 1,2-dimyristoyl-3-trimethylammonium-propane (chloride salt) (DMTAP), were purchased from Avanti Polar Lipids. Bovine Serum Albumin (BSA), Human Serum Albumin (HSA), and Gold (III) chloride hydrate (HAuCl4·xH2O) were purchased from Sigma-Aldrich. Phenylalanine, Tyrosine, Glutathione Reduced (GSH), and Lysozyme (3x cryst) ex. Egg white were obtained

from Sisco Research Laboratories. Sodium hydroxide (NaOH), tri-sodium citrate dihydrate, di-sodium hydrogen phosphate anhydrous, sodium dihydrogen phosphate monohydrate, and sodium chloride were purchased from Merck. Milli-Q water was used to prepare all the solutions. All the chemicals were used as received without further purification.

6.2 Methods

Chapter 2

6.2.1 Synthesis of the Aromatic Amino Acid-Functionalized Gold Nanoparticles (Au-AA NPs):

We synthesized Au-AA NPs following previously reported in situ green synthesis protocol with slight modification *[1]*. Briefly, 0.125 mL of chloroauric acid solution of 30 mM was taken in 3.875 mL of Milli-Q water and the solution was gently stirred for a few minutes at room temperature. Then, 1 mL of freshly prepared 5 mM individual aromatic amino acid solution was added to the previous solution followed by the instantaneous addition of freshly prepared 100 μL of 1 M NaOH solution for an additional 5-6 h under vigorous stirring. The colorless solution slowly turned into a ruby red color indicating the formation of Au NPs.

6.2.2 Preparation of the Lipid Vesicles:

Thin-film hydration method was employed to prepare lipid vesicles of different compositions (DMPC, DMPC/DMPG, and DMPC/DMTAP). The DMPC/DMPG and DMPC/DMTAP lipid vesicles were prepared by taking a fixed ratio (7:3) of zwitterionic and charged lipid. The required amount of lipids was dissolved in a mixture of chloroform and ethanol to achieve a homogeneous mixture, and then the solvents were evaporated completely in a rotary evaporator under gentle conditions (P = 200 mbar, T = 30 °C). The formed dry lipid film was kept under a high vacuum overnight to remove any residual solvent from the flask. The film was hydrated with a

preheated 10 mM HEPES buffer (pH ~ 7.40) solution, vortexed, and stirred for 1 h above the phase transition of the respective lipid to a milky solution. The vesicles were extruded (using Avanti mini extruder) several times through 100 nm track-etched polycarbonate membranes to yield monodispersed small unilamellar vesicles (SUV). For confocal microscopy imaging, 1 mol % Liss Rhod PE was mixed with the required amount of lipid vesicles, and the lipid vesicle solution was passed through a 1 μm polycarbonate membrane, whereas for atomic force microscopy imaging 0.1 μm polycarbonate membrane was used.

6.2.3 Preparation of Lipid Vesicles-Nanoparticle Mixture:

To study the interaction of Au-AA NPs with the lipid vesicles at physiological pH, we varied the ratio of the number of nanoparticles to the number of lipid vesicles per ml (from 2:1 to 80:1). For this purpose, we varied the concentration of the lipid at a fixed concentration of Au-AA NPs (20 nM) to get the desired ratio of the number of NPs to the number of lipid vesicles per milliliter (**see below for calculation**). Then, 500 μL of fixed Au NP solution was placed in each 1.5 mL Eppendorf tubes; then different concentrations of 500 μL lipid vesicles were added in each Au-AA NPs solution and kept overnight to reach the equilibrium.

We calculated the number of liposomes per ml for a known concentration of lipids by using the following methodology *[2]*. The total number of lipid molecules per lipid vesicles was calculated as:

$$N_{tot} = \frac{\left[4\pi\left(\frac{d}{2}\right)^2 + 4\pi\left(\frac{d}{2} - h\right)^2\right]}{a}$$

d is the diameter of the small unilamellar vesicle (SUV). Our group had already reported that the size of the SUV is around 100 nm. h is the thickness of the lipid bilayer and was taken as 4.45 nm. And, a is the average area per lipid molecule was taken as 0.59 nm^2. Putting all these values in the equation,

$$N_{tot} = \frac{\left[4\pi\left(\frac{100}{2}\right)^2 + 4\pi\left(\frac{100}{2} - 4.45\right)^2\right]}{0.59}$$

$$= 97{,}389.01$$

Now, the following equation was used for the calculation of liposomes per mL (N_{lipo}) for a known concentration of lipids.

$$N_{lipo} = \frac{M_{lipid} \times N_A}{N_{tot} \times 1000}$$

M_{lipid} is the molar concentrations of lipids, N_A is the Avogadro number and the value is 6.023×10^{23} and N_{tot} is the total number of lipid molecules per lipid vesicle.

Here, to calculate the number ratios of Au-AA NPs: lipid vesicles or liposomes, we had fixed the concentration of Au-AA NPs (20 nM) and systematically varied the concentration of lipids. In 0.5 mL of each Au-AA NPs solution, 0.5 mL different concentrations of lipids were added in an Eppendorf.

Now, 0.5 mL of 20 nM Au-AA NPs solutions will have 6.023×10^{12} Au-AA NPs.

The **Table 2.1** shows all the number ratio of AuNPs: lipid vesicles or liposomes per mL with the variation of lipid concentration in a fixed concentration of Au-AA NPs solution.

6.2.4 Freeze-Thaw Cycle:

For the freeze-thaw cycles, the Au-AA NPs and lipid mixture were frozen after equilibrium in liquid nitrogen (temperature: -196 °C) and then thawed at room temperature.

6.2.5 Synthesis of Phenylalanine functionalized gold nanoparticles:

We followed an in situ green synthesis method to synthesize the phenylalanine functionalized gold nanoparticles (Au-Phe NPs) *[3]*. At first, 7.750 mL of Milli-Q water was added in 0.250 mL of 30 mM chloroauric acid solution and the solution was gently stirred for few minutes at room temperature. Then, 2 mL of freshly prepared 5 mM phenylalanine solution was added to the previous solution followed by the instantaneous addition of 0.2 mL of 1 M NaOH solution. The solution was kept under vigorous stirring for an additional 6-7 hr. The formation of colloidal stable Au-Phe NPs was confirmed as the colorless solution slowly turned into a ruby red solution.

6.2.6 Preparation of the lipid vesicle and Au-Phe NPs mixture:

To study the interaction of Au-Phe NPs with different zwitterionic lipid vesicles, we took two different ratios of the number of nanoparticles to the number of lipid vesicles per mL (2:1 and 80:1). To calculate the number ratio, we took two different concentrations of lipid (0.4 mM and 0.0125 mM) at a fixed concentration of the Au-Phe NPs (20 nM). Then, 500 μL of fixed Au-Phe NPs solution was placed in each 1.5 mL Eppendorf tubes, then two different concentrations of 500 μL lipid vesicles were added in each Au-Phe NPs solution and kept overnight to reach the equilibrium.

6.2.7 Simulation Methods:

All simulations and analyses were performed using the GROMACS-2018 simulation package *[4-6]*. Potential parameters for phenylalanine and lipids were taken directly from the "MARTINI" coarse-grained (CG) force field (FF), which lumps a few (three or four) heavy atoms into each CG bead *[7-9]*. Coordinates and potential parameters for the 12 nm-sized spherical Au particle were obtained from the CHARMM-GUI website *[10]*. All-atom Au

atoms were converted to CG Au beads by 1-to-1 mapping, and the bead type "C5" (ε = 3.5 kJ/mol and σ = 0.47 nm, no charge; hydrophobic) was assigned for Au beads interacting with phenylalanine, lipids, and water, which has successfully reproduced experimental results regarding the structure and dynamics of Au particles and their interactions with lipid membranes *[11,12]*. A mixture of an Au particle and phenylalanine molecules were equilibrated, leading to the adsorption of 1,443 phenylalanine molecules onto the surface of Au particle, called the "Au-Phe" particle. A temperature of 293 K, which is slightly lower than the phase-transition temperature of the CG 1,2-dipalmitoyl-sn-glycero-3-phosphocholine (DPPC) bilayer (295 K) *[13]*, and a pressure of 1 bar were maintained by applying a velocity-rescale thermostat *[14]* and Parrinello-Rahman barostat *[15]* in an NPT ensemble. Note that Marrink et al.'s simulations captured the gel phase of CG DPPC bilayer below the phase-transition temperature of 295 K *[13]*. However, it has been experimentally known that the phase-transition temperature decreases as the liposome size decreases *[16]*, and thus only qualitative comparison for phase behaviour can be achieved in this work. The Lennard-Jones and Coulomb potentials were smoothly shifted to zero between 0.9 and 1.2 nm and between 0 and 1.2 nm, respectively. The LINCS algorithm was used to constrain the bond lengths *[17,18]*. Simulations were performed for 100 ns with a time step of 20 fs on computational facilities supported by the National Institute of Supercomputing and Networking/Korea Institute of Science and Technology Information with supercomputing resources including technical support (KSC-2020-CRE-095).

6.2.8 Simulations of a single Au-Phe particle and lipids:

A single Au-Phe particle was randomly mixed with 3,200 1,2-dipalmitoyl-sn-glycero-3-phosphocholine (DPPC) or 2,900 1,2-dioleoyl-sn-glycero-3-phosphocholine (DOPC) lipids and then solvated with ~79,000 water molecules (representing ~316,000 real water molecules) in a periodic box

of size 24 nm per side. Note that in simulations the thickness of the amino-acid coating is less than 1 nm, and hence the diameter of Au-Phe NP is ~13 nm, which is much smaller than the experimental NP-diameter of 24-26 nm with the coating thickness of ~6 nm. Therefore, ~3,000 lipids per nanoparticle were used instead of 48,964 lipids for the high lipid concentration.

6.2.9 Simulations of eight Au-Phe particles and lipids:

Eight Au-Phe particles, which were positioned with a distance of 2.5 nm between neighboring particles, were randomly mixed with 4,000 DPPC or DOPC lipids and then solvated with ~310,000 water molecules (representing ~1,240,000 real water molecules) in a periodic box of size 37 nm per side. Note that although ~1,000 lipids per nanoparticle are required to mimic the experimental condition of low lipid concentration, here 500 lipids per nanoparticle were simulated to avoid the crowding problem of lipids because eight nanoparticles are quite tightly positioned in the simulation box.

6.2.10 Freeze-Thaw Cycles:

For the freeze-thaw cycles, we adopted two different freezing protocols. One was that the Au-Phe NPs and different lipid mixtures after equilibrium were frozen in liquid nitrogen (-196 ℃) and then thawed at room temperature (RT). Another one was that the Au-Phe NPs and different lipid mixtures after equilibrium were frozen in Refrigerator (-12 ℃) and then thawed at RT.

Chapter 4

6.2.11 Synthesis of Amino Acid Functionalized Silver Nanoparticles (Ag-AA NPs):

With the use of three distinct aromatic amino acids (AA) and NaOH, we tried to synthesize the Ag-AA NPs in situ, by altering the AA and NaOH

concentrations. We primarily optimize the size variation of Ag NPs functionalized with AA. To synthesize colloidal and stable AA functionalized Ag NPs, we use two distinct AA concentrations of 1 mM and 0.5 mM as well as altering the concentration of NaOH from 2 mM to 10 mM.

To synthesize the Ag NPs, we first mixed 8.75 mL of Milli-Q water with 250 µL of 30 mM aqueous silver nitrate solution. The 9 mL solution underwent continuous stirring for 30 minutes at 80 °C. The necessary quantity of AA solution at a particular concentration was then added to it, followed by the addition of NaOH at a particular concentration. The entire solution was then left at 80 °C for 2 hours while being constantly stirred. As colloidal Ag NPs developed, the colour of the solution changed from colourless to yellow.

6.2.12 Calculation of Ag NPs concentration:

The concentration of the synthesized Ag NPs was calculated by previously reported method by Siripinyanond et al. *[19]*. Our TEM images revealed that Ag NPs were spherical in shape. The number of silver atoms was calculated by considering that the volume ratio of silver atom to Ag NPs is 74.1% in the cubic structure. We know that the radius of silver atom is 0.144 nm, and hence its volume is 0.0125 nm^3. Now, for Ag NPs with the diameter of d nm, its volume is $(\pi/6)d^3$ nm^3. Thus, the number of silver atoms (N) present in each Ag NPs is equal to $\frac{74.1}{100} \times \frac{\pi}{6} d^3 \times \frac{1}{0.0125}$ which is ~ 31 d^3. Now, the concentration of the Ag NPs was calculated by the below following equation:

Concentration of the Ag NPs = $\frac{N_{total}}{NVN_A}$

Where N_{total} is the total number of silver atoms added to the reaction solution, N is the number of silver atoms present in each nanoparticle, V is the volume of the reaction solution in liters, N_A is the Avogadro's Number.

In our experiment, we took the $AgNO_3$ concentration in solution 0.75 mM and total volume of the reaction solution was 10 mL or 0.01 L. So, the total number of silver atoms added to the reaction solution was $0.75 \times 10^{-3} \times 6.023 \times 10^{23}$

Now, from our HR-TEM experiment, the average size of the Ag-Tyr and Ag-Trp NPs were ~ 22 and ~24 nm respectively. So, for calculation, we took the average size of Ag NPs was 23 nm (d = 23 nm).

The concentration of the Ag NPs = $\frac{0.75 \times 10^{-3} \times 6.023 \times 10^{23}}{31 \times (23)^3 \times 0.01 \times 6.023 \times 10^{23}} =$ 1.988×10^{-7} M ~ 200 nM.

Then, the solution was diluted 10 times with the 10 mM HEPES buffer to get the desired experimental concentration of Ag NPs (20 nM).

6.2.13 Preparation of Lipid Vesicles:

Three zwitterionic lipid vesicles DOPC, DMPC, DPPC and two charged lipids DMPC/DMTAP and DMPC/DMPG was prepared by rapid ethanol injection method *[20]*. For charged lipids, we used 7:3 ratio of neutral to charged lipids. Briefly, the required amount of HEPES buffer solution (10 mM) was heated on a round bottom flask for 1 h above the phase transition temperature of respective lipids. Then, the required amount of ethanolic solution of lipid was rapidly injected in the preheated solution. After 1 h, the solution was cooled at room temperature for further use. The final concentration of all lipids was 0.8 mM and the added ethanol volume was less than 1% of the total solution.

6.2.14 Preparation of lipid vesicle-Ag NPs mixture:

We investigated the formation of lipid corona and lipid-induced aggregates around Ag NPs at different number ratio of the number of nanoparticles to the number of lipid vesicles per mL (1:1 to 1:80). To calculate the number ratio, the concentration of Ag-NPs was fixed (20 nM) and the concentration of lipid was varied from 0.8 mM to 0.0125 mM (see **Table 4.3**). Briefly, 500 µL of Ag-NPs was placed in Eppendrof tube and then 500 µL of different concentration of lipid was added to it and the mixture was incubated for 10 h at 30 °C.

6.2.15 Effect of the lipid corona on the aggregation of Ag-NPs and Ag^+ ion dissolution against external stimuli: We took 1:2 number ratio to study the effect of lipid corona on the aggregation of Ag NPs and Ag^+ dissolution against external stimuli i.e pH, high NaCl concentration, freeze thaw cycles. To remove all the excess lipids, the lipid-NPs was centrifuged and again re-dispersed with buffer solution.

Chapter 5

6.2.16 Synthesis of Aromatic Amino Acid-Functionalized Gold Nanoparticles (Au-AA NPs):

We synthesized Au-AA NPs following our previously reported method with slight modification *[1,3]*. At first, 0.625 mL of chloroauric acid solution of 30 mM was taken in 19.375 mL of Milli-Q water and the solution was stirred for 30 minutes at 80 °C. Then, 5 mL of freshly prepared 5 mM individual amino acids solution was added to the previously heated solution followed by the addition of 500 µL of 1 M NaOH solution for an additional 2 h under vigorous stirring. The colorless solution turned into a ruby red color indicating the formation of Au NPs. The synthesized Au NPs was centrifuged to remove the excess amino acids and then re-dispersed into 10 mM (NaCl concentration = 1 mM) phosphate buffer solutions (pH = 7.4) to get the desired Au NPs solution for experiment.

6.2.17 Synthesis of Citrate Functionalized Gold Nanoparticles (Au-Cit NPs):

The citrate functionalized gold nanoparticles were synthesized following our previously reported method with slight modification *[21]*. Briefly, 0.416 mL of chloroauric acid solution of 30 mM was taken in 23.844 mL of Milli-Q water and the solution was stirred for 30 minutes at 80 ℃. Then, 0.740 mL of 68 mM tri-sodium citrate dihydrate solution was added under vigorous stirring for an additional 2 h. The formation of colloidal Au-Cit NPs was confirmed as the colorless solution slowly turned into ruby red solutions. The synthesized Au-Cit NPs was centrifuged to remove the excess citrate molecules and then re-dispersed into 10 mM (NaCl concentration = 1 mM) phosphate buffer solutions (pH = 7.4).

6.2.18 Preparation of Au NPs and lysozyme mixture:

To investigate the interaction of the Au NPs and lysozyme at physiological pH (7.4), we varied a wide ratio of the number of nanoparticles to the number of lysozymes per mL (from 1:5 to 1:2000). For this purpose, we varied the concentration of the lysozyme at a fixed concentration of Au NPs (4 nM) to get the desired ratio of the number of NPs to the number of lysozyme molecules per mL (see **Table 5.2**). Then, 500 μL of fixed Au NPs solution was placed in each 1.5 mL Eppendorf tubes; then different concentrations of 500 μL lysozyme were added in each Au NPs solution and kept 2 h to reach the equilibrium.

To study the interaction of Au NPs and lysozyme at pH 12 (above the pI of the lysozyme), we took fixed concentration of Au NPs and added NaOH, then different concentrations of lysozymes were mixed and equilibrated for 2 h.

6.2.19 Binding of proteins and peptides on the surface of the Au NPs:

We took two Serum Albumin Proteins (BSA and HSA) and a small tri-peptide Glutathione (GSH) to bind on the Au NPs surface. To accomplish this, we varied the concentration of BSA, HSA, and GSH (1 to 20 μM). To study the interaction of these protein and tri-peptide coated Au NPs with the lysozyme, we first centrifuge the mixture to remove the excess proteins and tri-peptides. Then, we mixed required lysozyme concentration to achieve the desired ratio to the number of Au NPs to the number of lysozymes.

6.2.10 Formation of the lipid corona on the surface of the Au-AA NPs:

The lipid corona on the surface of the amino acid (phenylalanine) functionalized gold nanoparticles was formed following our previously reported protocol *[22,23]*. Briefly, at a fixed concentration (20 nM) of the Au-AA NPs, 0.4 mM of zwitterionic (DOPC and DPPC), and positively charged lipid vesicles was added and equilibrated for 2 h. After that, the mixture was centrifuged to remove the excess liposomes from the solution. Then, we mixed required lysozyme concentration to achieve the desired ratio to the number of Au NPs to the number of lysozymes.

6.3 Instrumentation

6.3.1 Steady-State Measurements:

All the UV-visible absorption spectra were recorded using a Varian UV-Visible spectrophotometer (Cary 100 Bio). All of the fluorescence spectra were recorded using a Fluoromax-4p spectrofluorometer from Horiba JobinYvon (model: FM-100). The absorption and emission spectra were corrected for the spectral sensitivity of the instrument. All of the absorption and fluorescence emission spectra were analyzed using Origin Pro 8.1 software.

6.3.2 DLS and Zeta Potential Measurements:

DLS of the all-synthesized NPs and all the mixture was measured by using a Nano Plus particle size analyzer (NanoPlus-3 model). The zeta potential of each synthesized NPs was also measured by using a Nano Plus particle size analyzer (NanoPlus-3 model). Each sample was measured three times for better reproducibility of the result.

6.3.3 Confocal Laser Scanning Microscopy (CLSM):

We used a confocal microscope from OLYMPUS, model IX-83 for the confocal imaging of samples. A Multiline Ar laser (gas laser) with an excitation wavelength of 405 and 559 nm was used to visualize both the morphological changes of the Au-AA NPs, lipid vesicles, and their binary mixtures. An excitation wavelength of 448 nm was used to visualize both the morphological changes of the Au NPs and lysozymes in their binary mixtures. An aliquot of the sample was immobilized on a clean cover slide by spin coating at 750 rpm for 3 min. Then, it was fixed by a glass slide in a sandwich manner by using transparent nail polish before imaging. ImageJ software was used to process all of the images with linear adjustments of brightness and contrast. All imaging studies were performed at room temperature.

6.3.4 High Resolution-Transmission Electron Microscopy (HR-TEM):

HR-TEM images were taken using a field emission gun transmission electron microscope (model:Tecnai G2, F30) with an acceleration voltage of 300 kV. A small amount of the concentrated sample was dropped onto a carbon-coated copper grid and allowed to sit for about 1 h. The excess sample was wicked off by the use of Whatman filter paper. The grid was wicked dry and washed two times with water for 10 min each. The grid was placed under an IR lamp for 1 h and then overnight at RT for drying.

6.3.5 Atomic Force Microscopy (AFM):

For AFM imaging, all of the samples were incubated for 12 h to reach equilibrium. The samples were then drop-casted on mica substrates and dried under a vacuum. The images were recorded using Smart Scan software (model park NX10) in a tapping mode at a scan frequency of 0.65-1.0 Hz.

6.3.6 Field Emission Scanning Electron Microscopy (FESEM):

Field emission scanning electron microscopy study was performed by using a ZEISS Supra55 field emission scanning electron microscope. An aliquot of the sample was then drop-cast on glass slides and dried under vacuum.

6.3.7 Circular Dichroism (CD) Spectroscopy Measurements:

CD spectra of all the samples were recorded on a JASCO J-815CD spectropolarimeter using a quartz cell of 1 mm path length with a scan range of 190-260 nm. Scans were recorded with a slit width of 1 mm and speed of 50 nm/min.

6.4 References

[1] Kim D. Y., Kim M., Shinde S. *et al.* (2019), Temperature Dependent Synthesis of Tryptophan-Functionalized Gold Nanoparticles and Their Application in Imaging Human Neuronal Cells, ACS Sustain. Chem. Eng. 5, 7678-7689 (DOI: 10.1021/acssuschemeng.7b01101)

[2] Das A., Adhikari C., Chakraborty A. (2016), Lipoplex-Mediated Deintercalation of Doxorubicin from Calf Thymus DNA–Doxorubicin Complex, Langmuir 32, 8889-8899 (DOI: 10.1021/acs.langmuir.6b01860)

[3] De S. K., Maity A., Chakraborty A. (2021), Underlying Mechanisms for the Modulation of Self-Assembly and the Intrinsic Fluorescent Properties

of Amino Acid-Functionalized Gold Nanoparticles, Langmuir 37, 5022-5033 (DOI: 10.1021/acs.langmuir.1c00431)

[4] Hess B., Kutzner C., van der Spoel D. *et al.* (2008), GROMACS 4: Algorithms for Highly Efficient, Load-Balanced, and Scalable Molecular Simulation, J. Chem. Theory Comput. 4, 435-447 (DOI: 10.1021/ct700301q)

[5] Lindahl E., Hess B., van der Spoel D. (2001), GROMACS 3.0: a Package for Molecular Simulation and Trajectory Analysis, J. Mol. Model. 7, 306-317 (DOI: 10.1007/s008940100045)

[6] Van Der Spoel D., Lindahl E., Hess B. *et al.* (2005), GROMACS: Fast, flexible, and Free, J. Comput. Chem. 26, 1701-1718 (DOI: 10.1002/jcc.20291)

[7] Marrink S. J., de Vries A. H., Mark A. E. (2004), Coarse Grained Model for Semiquantitative Lipid Simulations, J. Phys. Chem. B 108, 750-760 (DOI: 10.1021/jp036508g)

[8] Marrink S. J., Risselada H. J., Yefimov S. *et al.* (2007), The MARTINI Force Field: Coarse Grained Model for Biomolecular Simulations, J. Phys. Chem. B 111, 7812-7824 (DOI: 10.1021/jp071097f)

[9] Monticelli L., Kandasamy S. K., Periole X. *et al.* (2008), The MARTINI Coarse-Grained Force Field: Extension to Proteins, J. Chem. Theory Comput. 4, 819-834 (DOI: 10.1021/ct700324x)

[10] Jo S., Kim T., Iyer V. G. *et al.* (2008), CHARMM-GUI: A Web-Based Graphical User Interface for CHARMM, J. Comput. Chem. 29, 1859-1865 (DOI: 10.1002/jcc.20945)

[11] Lin J., Zhang H., Chen Z. *et al.* (2010), Penetration of Lipid Membranes by Gold Nanoparticles: Insights into Cellular Uptake, Cytotoxicity, and Their Relationship, ACS Nano 4, 5421-5429 (DOI: 10.1021/nn1010792)

[12] Lunnoo T., Assawakhajornsak J., Puangmali T. (2019), In Silico Study of Gold Nanoparticle Uptake into a Mammalian Cell: Interplay of Size,

Shape, Surface Charge, and Aggregation, J. Phys. Chem. C 123, 3801-3810 (DOI: 10.1021/acs.jpcc.8b07616)

[13] Marrink S. J., Risselada J., Mark A. E. (2005), Simulation of Gel Phase Formation and Melting in Lipid Bilayers Using a Coarse Grained Model, Chem. Phys. Lipids 135, 223-244 (DOI: 10.1016/j.chemphyslip.2005.03.001)

[14] Bussi G., Donadio D., Parrinello M. (2007), Canonical Sampling Through Velocity Rescaling, J. Chem. Phys. 126, 014101-014101 (DOI: 10.1063/1.2408420)

[15] Parrinello M., Rahman A. (1981), Polymorphic Transitions in Single Crystals: A New Molecular Dynamics Method, J. Appl. Phys. 52, 7182-7190 (DOI: 10.1063/1.328693)

[16] Koynova R., Caffrey M. (1998), Phases and Phase Transitions of the Phosphatidylcholines, Biochim. Biophys. Acta-Rev. Biomembr. 1376, 91-145 (DOI: 10.1016/s0304-4157(98)00006-9)

[17] Hess B., Bekker H., Berendsen H. J. C. *et al.* (1997), LINCS: A Linear Constraint Solver for Molecular Simulations, J. Comput. Chem. 18, 1463-1472 (DOI: 10.1002/(sici)1096-987x(199709)18:12<1463::aid-jcc4>3.0.co;2-h)

[18] Hess B. (2008), P-LINCS. A Parallel Linear Constraint Solver for Molecular Simulation, J. Chem. Theory Comput. 4, 116-122 (DOI: 10.1021/ct700200b)

[19] Wimuktiwan P., Shiowatana J., Siripinyanond A. (2015), Investigation of Silver Nanoparticles and Plasma Protein Association Using Flow Field-Flow Fractionation Coupled with Inductively Coupled Plasma Mass Spectrometry (FlFFF-ICP-MS), J. Anal. At. Spectrom. 30, 245-253 (DOI: 10.1039/c4ja00225c)

[20] Maity A., Bagchi D., De S. K. *et al.* (2023), Insight into the Lysozyme-Induced Aggregation of Aromatic Amino Acid-Functionalized Gold Nanoparticles: Impact of the Protein Conjugation and Lipid Corona on the

Aggregation Phenomena, Langmuir 39, 4881-4894 (DOI: 10.1021/acs.langmuir.2c03077)

[21] Kanwa N., Patnaik A., De S. K. *et al.* (2019), Effect of Surface Ligand and Temperature on Lipid Vesicle−Gold Nanoparticle Interaction: A Spectroscopic Investigation, Langmuir 35, 1008-1020 (DOI: 10.1021/acs.langmuir.8b03673)

[22] Maity A., De S. K., Chakraborty A. (2021), Interaction of Aromatic Amino Acid-Functionalized Gold Nanoparticles with Lipid Bilayers: Insight into the Emergence of Novel Lipid Corona Formation, J. Phys. Chem. B 125, 2113-2123 (DOI: 10.1021/acs.jpcb.0c10079)

[23] Maity A., De S. K., Bagchi D. *et al.* (2022), Mechanistic Pathway of Lipid Phase-Dependent Lipid Corona Formation on Phenylalanine-Functionalized Gold Nanoparticles: A Combined Experimental and Molecular Dynamics Simulation Study, J. Phys. Chem. B 126, 2241-2255 (DOI: 10.1021/acs.jpcb.2c00356)

Chapter 7

Conclusion and Future Aspects

7.1 Conclusion

In this thesis, we shed light on the physical interactions leading to novel lipid corona formation around nanoparticles (NPs) and its impact on the interaction with protein. Our study reveals that aromatic amino acids (building blocks of protein) functionalized nanoparticles have intrinsic ability to drag the lipid molecules away from the membrane to form a lipid coating i.e., “lipid corona” around themselves. The formation of the lipid corona depends on both the surface charge of NPs and lipid vesicles. Also, the concentration of lipid plays a crucial role in lipid corona formation. At high lipid concentration i.e., when the number of nanoparticles is almost equal to the number of lipid vesicles, NPs form a stable lipid corona. Stable lipid corona refers to a durable and organized coating of lipids surrounding a nanoparticle, which persists without significant disruption under physiological conditions over time. But the same NPs undergo lipid-induced aggregation at low lipid concentration i.e., when the number of nanoparticles is significantly higher than the number of lipid vesicles in the solution. Lipid-induced aggregation or corona formation of NPs also depends on the phase state of the lipid, area per lipid head group, and the buffer medium. Surface ligands on the nanoparticle surface predominantly account for the lipid corona formation rather than the metallic NPs core. Lipid coated NPs offer excellent stability against external stimuli like pH, high salt concentration, several freeze-thaw cycles. The lipid corona around the NPs also inhibits the metal ion oxidation and dissolution of Ag NPs. Based on the stability, for the first time, we also classified the lipid corona as “hard” and “soft” lipid corona. The concept of "hard" and "soft" lipid coronas is distinct from that of protein coronas. A hard lipid corona

comprises lipids that are tightly bound to the nanoparticles surface and remain associated even after multiple centrifugation steps, freeze-thaw cycles, or exposure to harsh conditions. This robust attachment helps preserve nanoparticle stability and prevents concentration loss or aggregation. In contrast, a soft lipid corona is characterized by a leaky lipid layer that is more susceptible to disruption under similar conditions, potentially leading to nanoparticle dissolution or aggregation.

Protein induced nanoparticle aggregation is a concern to nano-researchers for the application of NPs in biomedical aggregation. Different charged and phase state lipid-coated NPs are suitable candidates to inhibit the aggregation of NPs in presence of protein. We discussed how a hard lipid corona maintains structural integrity, allowing proteins to adsorb only on the lipid surface without directly accessing the nanoparticle core. Conversely, a soft lipid corona permits protein penetration through the lipid layer, enabling direct interaction with the nanoparticle surface and potentially modifying its physicochemical characteristics.

In a nutshell our research not only provides physical insights into lipid corona formation, but it also develops smart nanoparticles that minimize protein adsorption for future biomedical applications.

7.2 Future Aspects

The lipid corona is a recently developing field relative to protein corona. In future, the influence of aliphatic amino acids on lipid corona formation could be discussed. The other important topic for investigation is how these lipids coated NPs will affect the protein corona formation and vice-versa. The properties of the lipid corona can also be modulated by varying the composition of the lipid components. The quantification and mechanism of these lipid-coated NPs cellular uptake will open a new direction to nano-researcher for the application of NPs in catalysis, drug delivery, and photo thermal therapy inside cellular environment.